



University of Sheffield

New Thermally Reversible Thermoplastic Polyurethanes

Simon Andrew Fawcett

A thesis submitted in partial fulfilment of the requirements for the degree of Doctor of

Philosophy

The University of Sheffield

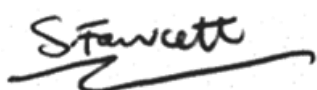
Faculty of Science

Department of Chemistry

January 2023

Declaration

I, Simon Fawcett, confirm that the Thesis is my own work. I am aware of the University's Guidance on the Use of Unfair Means (www.sheffield.ac.uk/ssid/unfair-means). This work has not been previously presented for an award at this, or any other, university. All the work is the original work of the author, except where acknowledged.



Signature:

Simon Andrew Fawcett

January 2023

- DMA data in Chapters 3, 4 and 5 was obtained by Nicholas Hawkins (University of Oxford)
- Tensile testing data in Chapters 3, 4 and 5 was obtained by Jennifer Hughes (Natural Materials Lab, University of Sheffield)
- Adhesion data in Chapters 4 and 5 was obtained by Jonathan Gregg (Scott Bader/ University of Sheffield)

To my dad,

The world's best trainer

Acknowledgements

My PhD could be viewed as 4 years of glue-themed puns, I've made a rule to not stick any in here, but I'm not too sure how well I'll adhere to it. Sorry to all those who have suffered them.

Firstly, I'd like to thank my supervisor, Professor Andrew Slark, for your constant guidance, knowledge and support. I am extremely grateful for such a wonderful opportunity. Thanks to the UKRI for the funding and to Joe Gaunt who passed my late CDT application onto Andrew, whose email I received while being hospitalised by an 18" pizza. Thank you to the CDT, I have made some amazing friends, despite their judgement of how I eat cereal, I am glad to have met all of you. Also, thanks to the support staff who keep the department running. Thanks to Wayne Hayes and Lewis Hart at the University of Reading for providing the bisureadiol.

A big thank you to rest of the Slark group, it has been an adventure, from purchasing our first beaker as a new group, to smashing more than my fair share of flange lids. Thanks to James for your guidance and advice, Devanshi for your support, Jenny for all your help, Neil for always being canny and Tom and Reuben for creating a positive office atmosphere. A massive thank you to Jonny who always makes me laugh and for co-founding the jamborees which were my highlight of living in Sheffield. Thank you to Xander, we have climbed both a literal and metaphorical mountain together, I wouldn't have wanted to do it with anyone else. I could not have wished for a better group of people to be by my side these past 4 years.

An enormous thank you to my family, Mum, Dad, Petes, Emma, Helena and Milly. Thanks Mum for always being there to chat and listen. Special thanks Dad for all your encouragement. Thanks Petes for convincing me to take A-level Chemistry by falsely promising me help with homework. Thank you also Christine, Peter and Rose for all your support.

My biggest thanks go to my amazing girlfriend Anna who is equally if not more deserving of a PhD, enduring 4 years of constant glue talk (puns) and being the only non-scientist in a room. I couldn't have managed this without you, your consistent support and encouragement has had such a positive and invaluable impact on my life. I can't wait for our next adventure.

I would not be here without the help of everyone mentioned (even those not named – space is tight!), I believe you are a product of your environment and so anything good I have done is a reflection of those around me. That also means if there are any typos, don't blame me.

Abstract

Traditional reactive polyurethane adhesives are versatile materials with a range of mechanical properties. However, they are irreversibly crosslinked preventing separation of substrates at end-of-life for reuse or recycling, causing negative environmental impacts. Therefore, reversible adhesives are of interest in the drive towards a circular economy. Thermoplastic polyurethanes (TPUs) display a physical response to temperature (solid at ambient, fluid with heat), but the strong intermolecular hydrogen bonding persists in the melt phase causing highly viscous fluids and processing challenges. To overcome these issues, the structure-property relationships of new TPUs were investigated with the aim of exploring potential copolymers as reversible adhesives.

Initially, model copolymers were made without chain extenders using semi-crystalline polyols. Polyol molecular weight influenced the crystallinity, degree of physical interactions and molecular weight of the TPU. Branching in chain extenders hinders hard segment association leading to mechanically poor copolymers, whereas urea functionality affords enhanced mechanical performance but lower sensitivity to thermal stimulus, retaining high melt viscosity. Therefore, physical interactions alone do not seem viable for reversible adhesion.

Reversible covalent bonds were incorporated along TPU copolymer backbones *via* Diels-Alder (DA) cycloadducts from the copolymerisation of functional PU prepolymers made from semi-crystalline and amorphous polyols. All copolymers displayed substantial change in physical state as a response to temperature with dynamic and reversible M_n (typically changing from 6 to > 25 kDa). Material properties were revealed as heavily dependent on constituent prepolymers and starting polyols, with semi-crystalline materials showing greater stiffness

and amorphous materials greater flexibility. Therefore, final studies were conducted using blends of different prepolymers, making linear TPUs that contain DA cycloadducts. TPUs were synthesised showing phase separation without chain extender and highly tuneable properties. Several materials throughout these studies show promise in the application of thermally reversible adhesives differentiating between high mechanical properties and low melt viscosity.

Table of Contents

Declaration	i
Acknowledgements.....	iii
Abstract.....	iv
Table of Contents	vi
List of Figures.....	ix
List of Tables.....	xix
List of Schemes	xxii
List of Abbreviations	xxiii
Conferences	xxvi
1 Introduction	1
1.1 Step-growth polymerisation.....	2
1.2 Brief history of polyurethanes.....	4
1.3 The urethane reaction.....	4
1.4 Polyurethane composition	7
1.4.1 <i>Soft segment</i>	7
1.4.2 <i>Hard segment - diisocyanates</i>	10
1.4.3 <i>Hard segment – chain extenders</i>	12
1.5 Morphology of thermoplastic polyurethanes.....	13
1.5.1 <i>Effects of the soft segment</i>	16
1.5.2 <i>Effects of the hard segment</i>	20
1.6 The Diels-Alder reaction	27
1.7 Adhesives and adhesion	31
1.7.1 <i>Traditional polyurethane adhesives</i>	35
1.7.2 <i>Thermoplastic polyurethanes as adhesives</i>	37
1.7.3 <i>Recycling and life cycle analysis</i>	39
1.8 References.....	42
2 Thermoplastic polyurethanes from copolymerisation without chain extenders	50
2.1 Introduction.....	51
2.2 Results and Discussion	53
2.2.1 <i>Synthesis of Thermoplastic Polyurethanes</i>	53
2.2.2 <i>Effect of polymerisation process on polymer properties</i>	57
2.2.3 <i>Effect of PCL molecular weight on TPU copolymer properties</i>	65
2.3 Conclusion	73
2.4 Experimental	74

2.4.1	<i>Materials</i>	74
2.4.2	<i>Instrumental methods</i>	74
2.4.3	<i>General synthesis of PCL-MDI copolymers via bulk polymerisation</i>	75
2.4.4	<i>General synthesis of PCL-MDI copolymers via solution polymerisation</i>	76
2.5	References.....	77
3	Synthesis and characterisation of thermoplastic polyurethanes with different chain extenders	79
3.1	Introduction.....	80
3.2	Results and discussion.....	83
3.2.1	<i>Synthesis of copolymers and molecular architecture</i>	83
3.2.2	<i>Thermal Properties</i>	87
3.2.3	<i>Rheology</i>	91
3.2.4	<i>Mechanical Properties</i>	92
3.2.5	<i>Morphology</i>	96
3.3	Conclusion	98
3.4	Experimental	99
3.4.1	<i>Materials</i>	99
3.4.2	<i>Instrumental methods</i>	100
3.4.3	<i>Sample preparation</i>	102
3.4.4	<i>Synthesis of PCL-MDI copolymer (B3)</i>	103
3.4.5	<i>Synthesis of PCL-MDI-BD copolymer (D1)</i>	104
3.4.6	<i>Synthesis of PCL-MDI-PD copolymer (P1)</i>	105
3.4.7	<i>Synthesis of PCL-MDI-BU (U1)</i>	106
3.5	References.....	107
4	Exploration of reversible Diels-Alder chemistry within linear thermoplastic polyurethanes	110
4.1	Introduction.....	111
4.2	Results and discussion.....	114
4.2.1	<i>Comparison of thermally reversible covalent TPUs to traditional chain extended TPUs</i> 114	
4.2.2	<i>TPUs comprising thermally reversible covalent bonds and highly crystalline backbones</i>	131
4.2.3	<i>Amorphous TPUs comprising thermally reversible covalent bonds</i>	148
4.3	Conclusions.....	164
4.4	Experimental	167
4.4.1	<i>Materials</i>	167
4.4.2	<i>Instrumental methods</i>	168
4.4.3	<i>Sample preparation</i>	170
4.4.4	<i>Synthesis of furfuryl-terminated prepolymers (PPFX)</i>	171
4.4.5	<i>Synthesis of hydroxyethyl maleimide-terminated prepolymers (PPHX)</i>	174

4.4.6	<i>Synthesis of final linear TPU copolymers (DAX)</i>	176
4.5	References.....	179
5	Designing linear TPU copolymers containing semi-crystalline and amorphous polyols covalently bonded <i>via</i> Diels-Alder chemistry	182
5.1	Introduction.....	183
5.2	Results and discussion.....	185
5.2.1	<i>Determination of polyol compatibility</i>	185
5.2.2	<i>Synthesis of linear TPUs containing semi-crystalline and amorphous polyols covalently bonded via Diels-Alder chemistry</i>	191
5.2.3	<i>Structural characterisation of DAX-AX copolymers</i>	195
5.2.4	<i>Melt phase properties</i>	203
5.2.5	<i>Mechanical properties</i>	205
5.2.6	<i>Determination of reversibility via Diels-Alder chemistry</i>	209
5.3	Conclusions.....	216
5.4	Experimental.....	219
5.4.1	<i>Materials</i>	219
5.4.2	<i>Instrumental methods</i>	219
5.4.3	<i>Sample preparation</i>	222
5.4.4	<i>Preparation of blended polyols without covalent attachment (X-AX)</i>	222
5.4.5	<i>Synthesis of furfuryl-terminated prepolymers (PPFX)</i>	223
5.4.6	<i>Synthesis of hydroxyethyl maleimide terminated prepolymers (PPHX)</i>	225
5.4.7	<i>Synthesis of final linear TPU copolymers comprising a blend of semi-crystalline and amorphous polyols (DAX-AX)</i>	226
5.5	References.....	228
6	Conclusions and future work	230
6.1	Conclusions.....	231
6.2	Future work.....	235

List of Figures

Figure 1.1(a) Example of the typical increase in molecular weight during step-growth polymerisation against extent of reaction (p). (b) Representation of the polymer formation from bifunctional monomers in step-growth polymerisation.....	2
Figure 1.2 Isocyanates react with alcohols and amines to reversibly form urethane and urea functionalities, respectively.....	5
Figure 1.3 Representation of PU composition.....	7
Figure 1.4 The repeating units of common polyols used in PU SS. (a) polyesters. (b) polyethers. (c) poly(caprolactone). (d) polycarbonate.....	9
Figure 1.5 A selection of some aromatic and aliphatic diisocyanates commonly used in the synthesis of PUs.....	11
Figure 1.6 Examples of some common and more specialised chain extenders.....	13
Figure 1.7 Typical morphology of a PU, some phase mixing and separation. Blue lines represent the SS polyol, red blocks are the HS (diisocyanate and CE) and the red dashed circles mark a phase change.....	15
Figure 1.8 Simple representation of the change in physical properties of a polymer with temperature.....	15
Figure 1.9 The switchboard model first proposed by Flory with random re-entry.....	17
Figure 1.10 The solidification model. The level of disorder in the melt (left) is largely retained in the semi-crystalline solid state (right). Adapted from the work of Dettenmaier et al. ⁴⁷	19
Figure 1.11 Annealing increases the effective hard block region to improve mechanical properties.....	20

Figure 1.12 The difference in HS stacking between CEs with an odd (left) and even (right) number of methylene units. Based on the work of Blackwell et al. ^{61, 62}	22
Figure 1.13 Chain restriction in a (a) phase mixed morphology and a (b) phase separated morphology with respective examples of CEs found in each system. ^{68, 69}	23
Figure 1.14 The degree of HS order decreases (arrows) with increasing branching from left to right. ³⁵	24
Figure 1.15 H-bonding between (a) urethane groups (monodentate) and urea groups in a (b) monodentate manner and (c) bidentate manner.	25
Figure 1.16 Order of increased phase separation, adapted from the work of Kalajahi et al. ⁷⁸	26
Figure 1.17 [4+2] cycloaddition occurs in a concerted manner across two π systems.....	27
Figure 1.18 (a) The HOMO of the diene interacts with the LUMO of the dienophile. (b) The Diels-Alder is a symmetry allowed process.	29
Figure 1.19 (a) Furan and maleimide react via the Diels-Alder reaction to form either the endo product (left) or the exo product (right). (b) Secondary orbital interactions (purple dashed lines) lower the energy of the endo transition state.	30
Figure 1.20 Model for the cross-section of an adhesive bond. The polymeric adhesive is represented by the coloured regions comprising the bulk (blue), interphase (orange) and interface (green).	33
Figure 1.21 Representations of (a) good surface wetting and (b) poor surface wetting of an adhesive on a substrate surface.	34
Figure 1.22 Common physical hardening mechanisms of an adhesive.....	35

Figure 1.23 Forming an adhesive bond from a solid TPU film. Heat is applied to the entire system to melt the adhesive, followed by pressure and cooling to form the final solid polymer adhesive bond.....	38
Figure 1.24 Individual components of a composite material could be separated via heating to remove the low melt viscosity adhesive. The materials could be reused or recycled and the adhesive could be reused in another composite material.	41
Figure 2.1 ^1H NMR spectrum of B3 as a representative of TPUs copolymers. Arrows denote an increase or decrease in resonance intensity as OH : NCO tends to 1.0 : 1.0. Integrals are relative to PCL initiator, neopentyl glycol (NPG). (400 MHz, 298 K, CDCl_3).....	55
Figure 2.2 FTIR spectra of PCL before copolymerisation and after copolymerisation of PCL with MDI (B3). Dashed red lines indicate the region where NCO absorption would appear.	56
Figure 2.3 ^1H NMR spectra for copolymers prepared by bulk (B3) and solution (S3) processes, respectively. (400 MHz, 298 K, CDCl_3).	57
Figure 2.4 Changes in number average molecular weight (M_n) and weight average molecular weight (M_w) with stoichiometry of OH : NCO.....	58
Figure 2.5 FTIR spectra of N-H regions for copolymers made in bulk (a) and solution (b) and C=O regions for copolymers made in bulk (b) and solution (d). The black dashed lines mark the boundary between free and H-bonded C=O or N-H.	60
Figure 2.6 T_g from first heating cycles as a function of M_n for copolymers prepared via bulk and solution polymerisation.	63
Figure 2.7 DSC thermograms of pure PCL and TPU copolymers of different M_n prepared in (a) bulk and (b) solution. Solid and dashed boxes surround regions of T_g and T_m , respectively. First heating cycles shown. Exo up.	64

Figure 2.8 Enthalpy of melting as a function of M_n . Values are proportional to the degree of crystallinity of PCL.....	65
Figure 2.9 The effect of stoichiometry on molecular weight (M_n and M_w).....	67
Figure 2.10 wt% _{MDI} as a function of NCO/OH for both series of different polyol molecular weight.....	68
Figure 2.11 Spectra (a) and (c) are N-H regions for series B and L, respectively. Spectra (b) and (d) are C=O regions for series B and L, respectively. The black box shows H-bonded urethane carbonyl. The black dashed line marks the boundary between free and H-bonded N-H.....	69
Figure 2.12 The effect of copolymer molecular weight on T_g for the L and B series (first heat run).....	71
Figure 2.13 DSC thermograms of copolymers -90 to 100 °C (10 °C.min ⁻¹). (a) and (b) and the first and second heating ramps, respectively, for series B. (c) and (d) are the first and second heating ramps, respectively, for series L. Exo up.....	72
Figure 2.14 Change in enthalpy of melt as a function of M_n for both heat cycles. The initial data points in each series at the lowest M_n are for unincorporated PCL polyol (PCL and PCLL for B and L series, respectively).....	73
Figure 3.1 The three different CEs used, BD, PD and BU.....	83
Figure 3.2 FTIR spectra of the carbonyl region of the four copolymers. The solid black box highlights absorbance due to H-bonded urethane and the dashed black box indicates urea functionality.....	86
Figure 3.3 The different types of H-bonding present in the copolymers studied: (a) urethane, (b) monodentate urea and (c) bidentate urea.....	87

Figure 3.4 (a) DSC thermograms of the four copolymers studied. Boxes highlight SS transitions and ovals indicate the transitions of the HS. (b) Close up of HS transitions. First heating cycles used at a heating rate of 10 °C.min ⁻¹ . Exo up.	89
Figure 3.5 DMA results showing the effect of temperature on storage modulus (left y-axis) and tan δ (right y-axis) for all copolymer samples. Heating rate of 3 °C.min ⁻¹	90
Figure 3.6 Complex viscosity as a function of temperature from 50 to 150 °C for the different TPU copolymers, using the rheometer in oscillatory mode with a set amplitude of 1 % and angular frequency of 1 rad.s ⁻¹	92
Figure 3.7 Tensile stress-strain data for the three chain extended copolymers.....	93
Figure 3.8 (a) Solid bar samples (10 × 40 mm) were prepared, cut and then healed via heating. (b) tensile stress-strain curves for bar samples of D1 and U1 before cutting (solid lines/boxes) and after cutting/healing (dashed lines/boxes). Values are the σ_{\max} of each material in MPa.	95
Figure 3.9 (a) Bond strengths from adhesion testing of beechwood substrates. (b) Beechwood substrates after testing showing cohesive failure (D1 & P1) and adhesive/ substrate failure (U1).....	95
Figure 3.10 Optical microscopy of TPU copolymer 37 μm films. (a) B3. (b) D1. (c) P1. (d) U1.	97
Figure 3.11 Suggested morphologies for copolymers comprising different chain extenders (a) PD, (b) BD and (c) BU. Grey lines represent the polyol SS and the coloured boxes represent the HS from copolymerised MDI-CE units.	98
Figure 4.1 ¹ H NMR spectrum of DA1 with resonances associated with the DA cycloadduct labelled. All other resonances correspond to the PCL-MDI backbone. (400 MHz, 298 K, CDCl ₃).	116

Figure 4.2 FTIR spectra of the carbonyl region for two copolymers (D1 and DA1) and prepolymers (PPH1 and PPF1). The dashed line at $\nu_{\max} = 1720 \text{ cm}^{-1}$ represents the ester carbonyl which is present in all samples.	118
Figure 4.3 (a) urethane-urethane H-bonding. (b) urethane-imide H-bonding.....	118
Figure 4.4 (a) DSC thermograms of the four materials, thermal transitions are highlighted and labelled. (b) Close up of high temperature ($> T_{m(\text{pol})}$) transitions. First heating cycle used at a heating rate of $10 \text{ }^{\circ}\text{C}\cdot\text{min}^{-1}$. Exo up.....	120
Figure 4.5 DMA of reference copolymer (D1) and DA copolymer (DA1) at a heating rate of $3 \text{ }^{\circ}\text{C}\cdot\text{min}^{-1}$	121
Figure 4.6 Temperature sweeps of D1 and DA1 at fixed 1 % and $1 \text{ rad}\cdot\text{s}^{-1}$ showing complex viscosity (η^*) as a function of temperature. The dashed black line represents the ‘target viscosity’ of $10 \text{ Pa}\cdot\text{s}^{-1}$	123
Figure 4.7 Tensile stress-strain data for D1 and DA1. Extension rate of $10 \text{ mm}\cdot\text{min}^{-1}$	124
Figure 4.8 (a) Bond strengths from adhesion testing of beechwood (BW) and aluminium (AL) substrates. (b) Beechwood substrates after testing (DA1 and D1).....	126
Figure 4.9 The variation of M_n (left y-axis) and M_w (right y-axis) with time at ambient temperature after melt application for DA1. The prepolymer molecular weights are marked with short dashed lines. D1 M_n and M_w are marked with orange dashed lines. Determined by SEC in CHCl_3 against PMMA standards.	128
Figure 4.10 (a) Change in absorbance at 696 cm^{-1} (free maleimide) against time after melt application. (b) Decrease in relative absorbance of band at 696 cm^{-1} . Time = 0 is set as 100 %.....	129
Figure 4.11 (a) The development of DSC thermograms of DA1 over 28 days at ambient temperature after melt application. Important transitions are highlighted and labelled. (b)	

Close up of regions of rDA. First heating cycles used at a heating rate of 10 C.min ⁻¹ . Exo up.	130
Figure 4.12 FTIR spectra showing carbonyl regions of DAX copolymers, PPHX and PPFX prepolymers for (a) DA2, PPH2 and PPF2, (b) DA3, PPH3 and PPF3 and (c) DA4, PPH4 and PPF4.	134
Figure 4.13 Melting endotherms of materials based on (a) Dynacoll 7360, (c) Dynacoll 7380 and (e) Dynacoll 7490. High temperature transitions of materials based on (b) Dynacoll 7360, (d) Dynacoll 7380 and (f) Dynacoll 7490. 7360, 7380 and 7490 refer to the non-copolymerised polyols. First heating cycle used at a heating rate of 10 °C.min ⁻¹ . Exo up.....	137
Figure 4.14 DMA of DA2, DA3 and DA4. Storage modulus (E') (left y-axis) and tan δ (right y- axis) as a function of temperature. Heating rate of 3 °C.min ⁻¹	138
Figure 4.15 Rheological analysis of DA2, DA3 and DA4. Complex viscosity (η*) (left y-axis) and tan δ (right y-axis) as a function of temperature. The short dashed black line represents the target η* of 10 Pa.s ⁻¹	140
Figure 4.16 Stress-strain curves of DA2, DA3 and DA4 measured at a speed of 10 mm.min ⁻¹ . Sample rupture is marked with a cross.	141
Figure 4.17 Bond strengths of DA2-4 with (a) beechwood (b) and aluminium substrates. (c) Substrate failure of beechwood substrates. (d) cohesive failure of aluminium substrates..	142
Figure 4.18 M _n as a function of time at ambient after melt application for DA2, DA3 and DA4. For clarity, the average prepolymer molecular weights (PPX) of respective PPFX and PPHX are marked with dashed lines. Determined by SEC in CHCl ₃ against PMMA standards.....	144
Figure 4.19 Relative intensities of FTIR absorbance at ν _{max} = 696 cm ⁻¹ with time at ambient after melt application for DA2, DA3 and DA4.....	145

Figure 4.20 DSC thermograms of rDA regions against time for (a) DA2 (b) DA3 and (c) DA4. First heating cycle used at a heating rate of 10 °C.min ⁻¹ . Exo up.	147
Figure 4.21 Composition of Capa 8025 (copolymer of ε-caprolactone and lactic acid) and approximate structure of Priplast 1838. R represents undefined diacid copolymerised.	149
Figure 4.22 FTIR spectra showing carbonyl regions of (a) DAA1, PPHA1 and PPFA1 and (b) DAA2, PPHA2 and PPFA2.	151
Figure 4.23 DSC thermograms of the four materials, thermal transitions are highlighted and labelled. (a) DAA1, PPHA1, PPFA1 and Capa 8025. (b) DAA2, PPHA2, PPFA2 and Priplast 1838. First heating cycles used at a heating rate of 10 °C.min ⁻¹ . Exo up.....	154
Figure 4.24 DMA of DAA1 and DAA2 with a heating rate of 3 °C.min ⁻¹ . Storage modulus (E') (left y-axis) and tan δ (right y-axis) as a function of temperature.....	155
Figure 4.25 Rheological analysis of DAA1 and DAA2. Complex viscosity (η*) (left y-axis) and tan δ (right y-axis) as a function of temperature. The horizontal short dashed black line represents the target η* of 10 Pa.s ⁻¹ . The vertical dotted line represents the T _{rDA} for both materials.	157
Figure 4.26 Stress-strain curves of DAA1 and DAA2. DAA1 did not break within the measured strain. Rate of 10 mm.min ⁻¹	158
Figure 4.27 Bond strengths for DAA1 and DAA2 with beechwood substrates.	160
Figure 4.28 M _n (left y-axis) and M _w (right y-axis) as a function of time at ambient temperature after melt application for DAA1. The prepolymer molecular weights are marked with horizontal dashed lines. Determined by SEC in CHCl ₃ against PMMA standards.....	161
Figure 4.29 Relative intensities of FTIR absorbance at ν _{max} = 696 cm ⁻¹ with time at ambient temperature after melt application for DAA1 and DAA2.....	162

Figure 4.30 Increase in ΔH_{rDA} with time for (a) DAA1 and (b) DAA2. First heating run used at a rate of $10\text{ }^{\circ}\text{C}\cdot\text{min}^{-1}$. Exo up. (c) Plot of ΔH_{rDA} as a function of time.....	163
Figure 4.31 DSC thermograms of DAA2 as a function of time. Thermal features are highlighted and labelled. First heating cycles used at a heating rate of $10\text{ }^{\circ}\text{C}\cdot\text{min}^{-1}$. Exo up.....	164
Figure 5.1 Method for basic testing of compatibility of polyols by visual inspection.	187
Figure 5.2 DSC thermograms of (a) pure amorphous polyols. (b) pure semi-crystalline polyols. Amorphous polyols are mixed in turn with (c) Capa 2200, (d) Dynacoll 7360, (e) Dynacoll 7380 and (f) Dynacoll 7490. Red = unblended amorphous polyols, blue = unblended semi-crystalline polyols, black = immiscible mixtures and purple = miscible mixtures. First heat cycle used at a heating rate of $10\text{ }^{\circ}\text{C}\cdot\text{min}^{-1}$. Exo up.....	190
Figure 5.3 Carbonyl regions of FTIR spectra for DAX-AX copolymers. 1 = polyol backbones ester. 2 = H-bonded urethane. 3 = imide carbonyl.....	196
Figure 5.4 DSC heating thermograms of copolymers and physical blends. (a) DA1-A1 and 1-A1, (b) DA1-A2 and 1-A2, (c) DA4-A1 and 4-A1 and (d) DA4-A2 and 4-A2. First heating cycle used at a heating rate of $10\text{ }^{\circ}\text{C}\cdot\text{min}^{-1}$. Exo up.	198
Figure 5.5 DMA results of (a) DA1-A1 and DA1-A2, (b) DA4-A1 and DA4-A2 which are compared to reference copolymers (c) DA1 and DA4 (semi-crystalline) and (d) DAA1 and DAA2 (amorphous). Heating rate of $3\text{ }^{\circ}\text{C}\cdot\text{min}^{-1}$	201
Figure 5.6 Rheological temperature sweeps of (a) DA1-A1 and DA1-A2 and (b) DA4-A1 and DA4-A2. Dashed black horizontal line marks the target viscosity.	204
Figure 5.7 Stress-strain curves from tensile testing on (a) four DAX-AX copolymers comprising both semi-crystalline and amorphous segments and (b) four reference copolymers DAX and DAAX from the previous chapter comprising either semi-crystalline or amorphous segments. X marks sample failure by breaking.	205

Figure 5.8 Adhesion testing on beechwood substrates for DAX-AX comprising both semi-crystalline and amorphous segments with reference to semi-crystalline DAX and amorphous DAAX copolymers.....	208
Figure 5.9 Variation of M_n with time after melt application of DAX-AX. Average prepolymer M_n are labelled as PPX. Determined by SEC in CHCl_3 against PMMA standards.....	210
Figure 5.10 Change in intensity of absorbance at $\nu_{\text{max}} = 696 \text{ cm}^{-1}$ with time after melt application for (a) DA1-A1 and DA1-A2 and (b) DA4-A1 and DA4-A2 copolymers.	212
Figure 5.11 Change in ΔH_{rDA} with time after melt application for DAX-AX measured via DSC at a heating rate of $10 \text{ }^\circ\text{C}\cdot\text{min}^{-1}$	213
Figure 5.12 DSC thermograms showing crystallinity of (a) DA1-A1, (b) DA1-A2, (c) DA4-A1 and (d) DA4-A2 as a function of time after melt application. First heat cycle used at a heating rate of $10 \text{ }^\circ\text{C}\cdot\text{min}^{-1}$. Exo up.....	215

List of Tables

Table 1.1 Chemically hardening adhesive polymers.....	35
Table 2.1. All copolymers synthesised from the copolymerisation of PCL and MDI.....	54
Table 2.2 Wavenumbers of significant functionalities. For clarity, only B3 is shown as a representative material.	56
Table 2.3 Data from SEC experiments showing molecular weights and dispersity for series B and S made in bulk and solution, respectively.	59
Table 2.4 Thermal data of all polymers from initial heat cycle from DSC.	62
Table 2.5 SEC data for TPUs synthesised via bulk polymerisation with 2.0 kDa and 1.0 kDa PCL at varying stoichiometry.	66
Table 2.6 DSC thermal data of all copolymers for two heat cycles. Multiple melting peaks for one endotherm are written as ‘first peak & second peak’ and the enthalpy is total area of both peaks.	70
Table 3.1 TPU copolymers synthesised using different chain extenders compared to the PCL-MDI copolymer without chain extender. PCL ($M_n = 2.0$ kDa).....	84
Table 3.2 Thermal data obtained via DSC. Values taken from initial heating runs (-90 °C to 150 °C at 10 °C.min ⁻¹).....	88
Table 3.3 Summary of Data obtained via DMA for all TPU copolymers.....	90
Table 3.4 Summary of mechanical data obtained from tensile stress-strain measurements for the copolymers comprising chain extenders.....	94
Table 3.5 Mechanical data obtained via tensile testing for pristine TPU materials and healed materials.	94
Table 4.1 Composition of the TPU copolymers synthesised with corresponding SEC data. .	117

Table 4.2 Thermal data of the two copolymers and the two prepolymers, obtained via DSC.	119
Table 4.3 Thermal data for D1 and DA1 obtained via DMA using a heating rate of 3 °C.min ⁻¹	122
Table 4.4 Summary of mechanical data obtained from tensile stress-strain measurements for the two copolymers. 10 mm.min ⁻¹	125
Table 4.5 Time dependent molecular weight values for DA1 and D1 at ambient temperature. PPH1 and PPF1 were only measured once and not as a function of time.	127
Table 4.6 Thermal data of DA1 obtained via DSC over 28 days.	129
Table 4.7 Structures of semi-crystalline polyols used with DSC data.....	131
Table 4.8 Composition of the semi-crystalline TPU copolymers synthesised with corresponding SEC data.	132
Table 4.9 Thermal data of the three copolymers their respective prepolymers and the crystalline polyols, obtained via DSC.	135
Table 4.10 Thermal data of DA2-4 obtained via DMA at a heating rate of 3 °C.min ⁻¹	139
Table 4.11 Summary of mechanical data obtained from tensile stress-strain measurements for the two copolymers at a speed of 10 mm.min ⁻¹	141
Table 4.12 Time dependent molecular weight values for copolymers DA2, DA3 and DA4 with time. Prepolymers PPHX and PPFX were only measured once and not as a function of time and the averages are labelled as PPX.	143
Table 4.13 Thermal data of DA2, DA3 & DA4 obtained via DSC over 28 days.	146
Table 4.14 Composition of amorphous TPU copolymers synthesised with corresponding SEC data.	149

Table 4.15 Thermal analysis data of the two copolymers, two prepolymers and polyols for materials based on Capa 8025 and Priplast 1838, obtained via DSC.	153
Table 4.16 Thermal data of DAA1-2 obtained via DMA at a heating rate of 3 °C.min ⁻¹	156
Table 4.17 Summary of mechanical data obtained from tensile stress-strain measurements for DAA1 and DAA2 at a rate of 10 mm.min ⁻¹	159
Table 5.1 Results from visual inspection of basic mixing of molten polyols to determine compatibility.	188
Table 5.2 Key thermal data obtained via DSC for determining compatibility of semi-crystalline polyols with amorphous polyols. Compatible mixtures are purple. Blends highlighted in yellow fulfil criteria for further investigation.	189
Table 5.3 Composition of the TPU copolymers and prepolymers synthesised with various polyols with correlating SEC data.	194
Table 5.4 Thermal data collected from DSC analysis for copolymers DAX-AX and blends without covalent attachment X-AX. First heating cycle used at a heating rate of 10 °C.min ⁻¹	197
Table 5.5 Thermal data obtained for the four copolymers (DAX-AX) compared to semi-crystalline (DAX) and amorphous (DAAX) reference copolymers via DMA with a heating rate of 3 °C.min ⁻¹	202
Table 5.6 Mechanical properties data of DAX-AX from tensile testing compared to reference DAX and DAAX reported in the previous chapter.....	207
Table 5.7 Time dependent M _n values for DAX-AX at ambient temperature. PPX were only measured once and not as a function of time.....	210
Table 5.8 Thermal data of DA1-A1, DA1-A2, DA4-A1 & DA4-A2 obtained via DSC over 28 days.	213

List of Schemes

Scheme 1.1 Generic reaction scheme of step-growth polymerisation. A and B represent different functional groups.....	2
Scheme 1.2 Summary of the chemistry possible with isocyanates and urethanes.	6
Scheme 2.1 Copolymerisation of PCL and MDI with an imbalanced OH : NCO molar ratio to produce OH-terminated TPUs.....	53
Scheme 3.1 Stepwise synthesis route from PCL and MDI to chain extended prepolymer via an NCO terminated intermediate.....	85
Scheme 4.1 Step 1 bulk synthesis of NCO-terminated prepolymer. Step 2 synthesis of HEMI-terminated prepolymer (a) and FA-terminated prepolymer (b). Step 3 bulk copolymerisation of PPHX and PPFX to produce DAX. X = 1, 2, 3, 4, A1 or A2.....	115
Scheme 5.1 Structures of polyols investigated. Semi-crystalline (left) and amorphous (right and bottom). R' and R'' represent different undefined diacids.	186
Scheme 5.2 (a) Synthesis of furan-terminated prepolymer containing semi-crystalline polyol (PPFX). (b) Synthesis of furan- and maleimide-terminated prepolymers containing amorphous polyol (PPFAX and PPHAX, respectively). (c) Synthesis of DAX-AX from a mixture of semi-crystalline and amorphous based prepolymers. X = 1, 2 or 4).....	193

List of Abbreviations

ΔH_m	Enthalpy change of melting
$\Delta H_{m(HS)}$	Enthalpy change of melting of the hard segment
$\Delta H_{m(pol)}$	Enthalpy change of melting of the polyol
$\Delta H_{m(SS)}$	Enthalpy change of melting of the soft segment
ΔH_{rDA}	Enthalpy change of retro-Diels-Alder
ϵ_{max}	Maximum strain
η^*	Complex viscosity
σ_{max}	Ultimate tensile strength
BD	1,4-butenadiol
BU	Bisureadiol
CE	Chain extender
DA	Diels-Alder
D_M	Dispersity
DMA	Dynamic mechanical analysis
DSC	Differential scanning calorimetry
E	Young's modulus
E'	Storage modulus

E''	Loss modulus
FA	Furfuryl alcohol
FTIR	Fourier-transform infrared
HEMI	Hydroxyethyl maleimide
HS	Hard segment
MDI	4,4'-methylene diphenyl diisocyanate
M_n	Number average molecular weight
M_w	Weight average molecular weight
N	Number of monomers present at given time
N_0	Number of monomers at the start of reaction
NMR	Nuclear magnetic resonance
p	Extent of reaction
PCL	Poly(ϵ -caprolactone)
PD	1,2-propanediol
PU	Polyurethane
PUU	Poly(urethane urea)
r	Stoichiometric ratio of monomers
rDA	retro-Diels-Alder

SEC	Size-exclusion chromatography
SS	Soft segment
T_g	Glass transition temperature
$T_{g(HS)}$	Glass transition temperature of the hard segment
$T_{g(pol)}$	Glass transition temperature of the polyol
$T_{g(SS)}$	Glass transition temperature of the soft segment
T_m	Melting temperature
$T_{m(HS)}$	Melting temperature of the hard segment
$T_{m(pol)}$	Melting temperature of the polyol
$T_{m(SS)}$	Melting temperature of the soft segment
TPU	Thermoplastic polyurethane
T_{rDA}	Temperature of retro-Diels-Alder
U_T	Modulus of toughness
$wt\%_{HS}$	Weight percent hard segment
$wt\%_{MDI}$	Weight percent MDI
$wt\%_{SS}$	Weight percent soft segment
\bar{X}_n	Number average degree of polymerisation

Conferences

Poster Presentation - Bordeaux Polymer Conference 2022, Bordeaux, France

Oral Presentation – Young Researchers Meeting 2022, Nottingham, UK

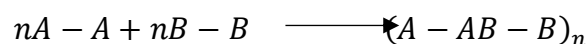
Poster Presentation – American Chemical Society Fall 2022, Chicago, USA

Oral Presentation – American Chemical Society Fall 2022, Chicago, USA

1 Introduction

1.1 Step-growth polymerisation

In step-growth polymerisation a polymer is formed from the polyaddition of multifunctional monomers. Typically, bifunctional monomers are used to give a linear product. The general pathway involves the functional groups of two monomers reacting to form one product containing a new linking group (**Scheme 1.1**).¹



Scheme 1.1 Generic reaction scheme of step-growth polymerisation. *A* and *B* represent different functional groups.

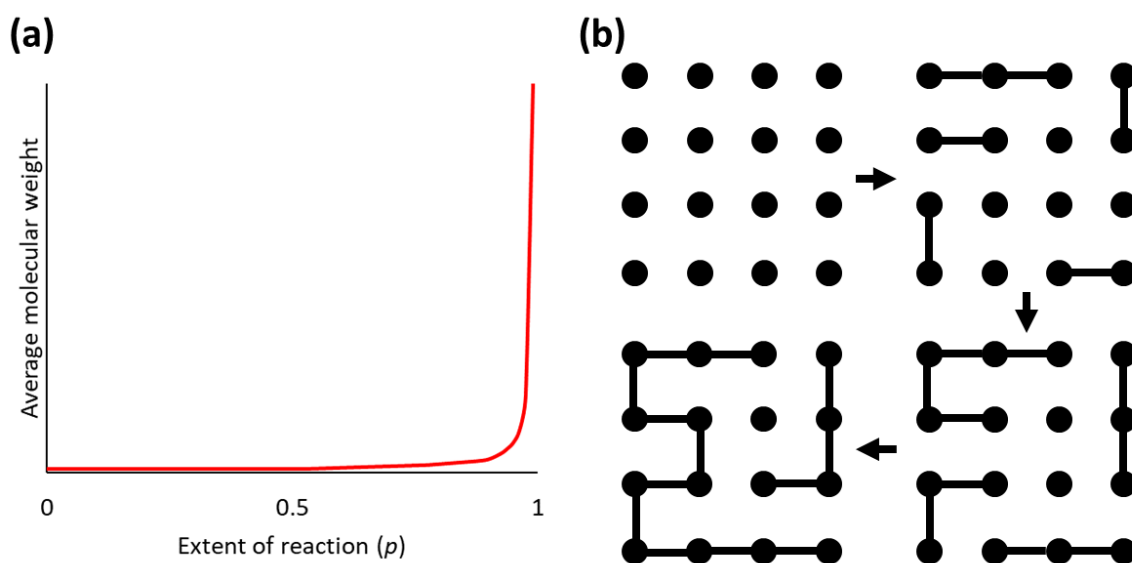


Figure 1.1(a) Example of the typical increase in molecular weight during step-growth polymerisation against extent of reaction (p). **(b)** Representation of the polymer formation from bifunctional monomers in step-growth polymerisation.

In step-growth polymerisation a high conversion of monomers is required to achieve high molecular weights (**Figure 1.1(a)**). Monomers react in the early stages of the reaction to form dimers and trimers (**Figure 1.1(b)**). These relatively small species then react with one another to form oligomers which continue to react with one another to finally form high molecular

weight polymers. Molecular weight determines polymer properties and often low molecular weight polymers display poor mechanical performance as a consequence of a larger number of chain ends, so the reaction must reach its full extent to form useful products.²

This trend can be described mathematically with the Carothers equation **(1)**:³

$$\bar{X}_n = \frac{1}{(1-p)} \quad (1)$$

where \bar{X}_n is the number average degree of polymerisation (the number of polymer units within a chain) and p is the extent of reaction and can be calculated as **(2)**:

$$p = \frac{(N_0 - N)}{N_0} \quad (2)$$

where N_0 is the number of monomers in the sample before the start of polymerisation and N is the number of monomers present at time t . Therefore, a high p is necessary for a significant value of \bar{X}_n , meaning high molecular weight products are only present at the very end of the reaction.

The molecular weight also depends on the relative concentration of monomer units. For step-growth polymerisations where there is a stoichiometric excess of one monomer then the Carothers equation becomes:

$$\bar{X}_n = \frac{(1+r)}{(1+r-2rp)} \quad (3)$$

where r is stoichiometric ratio of monomers and is always less than 1. At the end of the reaction ($p = 1$) the equation is simplified to:

$$\bar{X}_n = \frac{(1+r)}{(1-r)} \quad (4)$$

allowing for determination of the final \bar{X}_n of the polymer product. Therefore, stoichiometric control allows for targeting specific molecular weight products for desired properties.

1.2 Brief history of polyurethanes

Polyurethanes (PUs), discovered by Otto Bayer and co-workers in 1937, are polymers made from step-growth polymerisation, typically comprising of diols and diisocyanates.⁴ Since the 1930s, PUs have been developed extensively so that they now occupy a significant share of the polymer market, at an estimated value of \$72.82 billion in 2021.⁵ Their popularity arises from the diverse properties offered, as the only class of polymer to encompass thermosetting, thermoplastic and elastomeric characteristics.⁶ The range of raw materials is vast, allowing for tailoring products to a desired application, such as footwear, construction and automotive industries in the form of elastomers, foams, coatings, adhesives, *etc.*⁷ PUs are commonly the plastic of choice on account of their well-documented excellent mechanical properties and durability.⁶

1.3 The urethane reaction

Isocyanates are highly reactive functional groups. Primary reactions with NCO involve alcohols and amines to form urethanes and ureas, respectively (**Figure 1.2**). Both urethane and urea bonds are reversible.⁸ The urea product can form stronger hydrogen-bonds (H-bonds) due to the possibility of bidentate H-bonding, whereas urethane groups can only form monodentate H-bonding.⁹ The high reactivity of isocyanates makes them a potential health hazard as a result of the formation of highly toxic and carcinogenic amines upon reaction with atmospheric moisture.

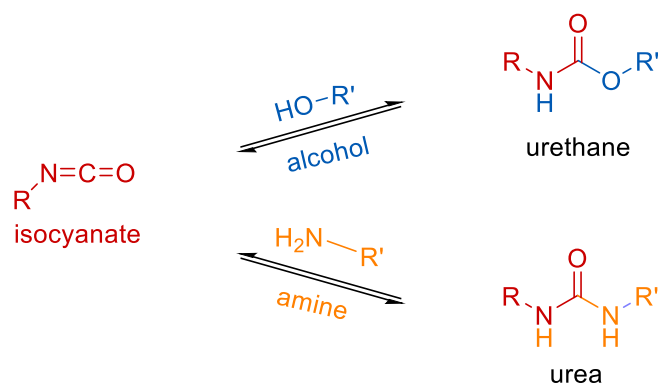
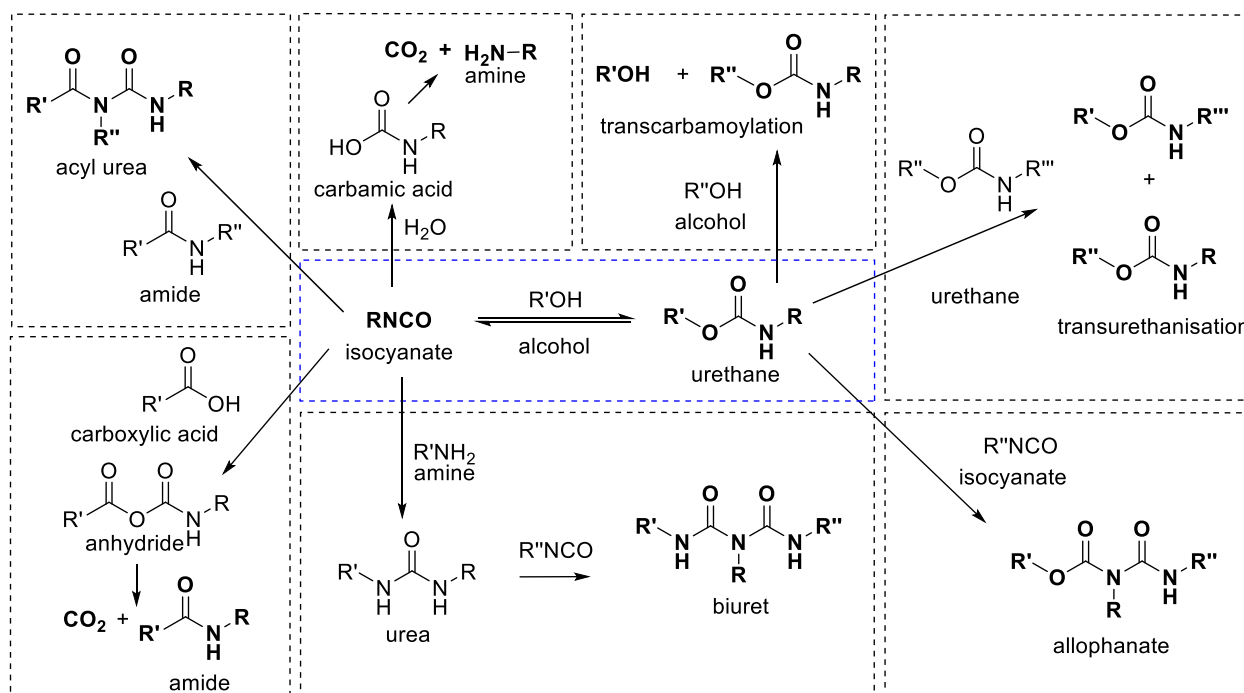


Figure 1.2 Isocyanates react with alcohols and amines to reversibly form urethane and urea functionalities, respectively.

The reactivity of isocyanates is relatively complex (**Scheme 1.2**). Isocyanates react with water to give amine and carbon dioxide *via* a carbamic acid intermediate.¹⁰ This reaction is common in moisture-cure adhesives where a NCO-terminated prepolymer is crosslinked upon reaction with atmospheric moisture.^{11,12} The evolution of CO₂ is useful as a blowing agent in PU foams. However, water often competes with the desired hydroxyl-containing compounds for the isocyanate.¹³ Therefore, moisture must be excluded to prevent either premature crosslinking or the formation of unwanted side products. To achieve dry conditions the polymerisation is conducted under vacuum or an inert atmosphere.

Under the right conditions, urethanes can react further to form other products with various R groups *via* transcarbamylation and transurethanisation.¹⁴ At elevated temperatures, the high reactivity of NCO allows for secondary reactions with urethanes, ureas and amides to form allophanates, biurets and acyl ureas, respectively.¹⁵⁻¹⁷ Depending on the aim, these reactions can be unwanted side products or desired to provide a mechanism of crosslinking

that increases the mechanical properties of the network. Isocyanates can also react with carboxylic acid to afford an amide and carbon dioxide.¹⁶



Scheme 1.2 Summary of the chemistry possible with isocyanates and urethanes.

Polymerisations can be performed in various ways, such as in bulk, organic solvent or water.^{8,18} In bulk there is no further product purification required, but the high melt viscosity in synthesis limits achievable molecular weights. This issue is resolved by diluting the precursors in an organic solvent to reduce the viscosity which makes higher molecular weight products feasible. The choice of solvent is very important, it not only needs to solubilise the reagents (polyol, isocyanate, chain extender *etc.*), which vary significantly in molecular structure, but also the final PU to prevent precipitation before completion of polymerisation. The use of solvent is becoming increasingly unpopular as a consequence of the associated negative environmental and health impacts, therefore solvent-free waterborne PUs seem an attractive alternative. However, the potential competition between water and desired OH-

containing species gives rise to the need for additional components resulting in a more complex system.¹⁹

Sánchez-Adsuar *et al.* demonstrated how the synthesis conditions (time and temperature) affected the properties of a poly(ϵ -caprolactone)-4,4'-methylene diphenyl diisocyanate-1,4-butanediol PU copolymer.²⁰ After a threshold was reached (3 hours above 80 °C) of the prepolymer step, molecular weight and viscosity increases which improves mechanical and adhesive properties. However, both the times of the prepolymer and chain extension steps do not influence the structural organisation, *e.g.* degree of phase separation.

1.4 Polyurethane composition

A typical PU composition is a multiblock copolymer of polyol, diisocyanate and chain extender (CE) which are covalently bonded *via* a polyaddition reaction and are connected by urethane linkages (**Figure 1.3**). The various components make up different segments, described as the soft segment (SS) (from the polyol) and hard segment (HS) (from the diisocyanate and chain extender).

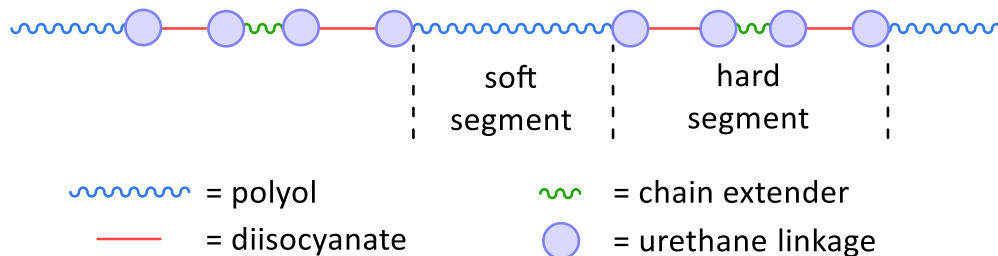


Figure 1.3 Representation of PU composition.

1.4.1 Soft segment

The soft segment of a PU is normally made up of a long chain diol called a polyol. It is classically a flexible linear polymer with a molecular weight between 500 – 10 000 g.mol⁻¹ and a

functionality of 2.0. This component determines the low temperature properties of the final PU.^{7, 21} A common choice for the SS is polyester or polyether and in special cases poly(caprolactone) or polycarbonates if specific enhanced properties are required.

Polyesters are commonly made *via* esterification of adipic acid and short chain glycols, such as ethylene glycol and propylene glycol (**Figure 1.4(a)**). PUs containing polyesters exhibit good oil resistance and mechanical properties but suffer from poor hydrolytic stability and inadequate flexibility at low temperatures. The number of carbon atoms in the chain influences the stability of the polymer, a polyester with a longer carbon chain is less polar due to the low molar concentration of ester groups and therefore is less prone to degradation. Depending on the composition, polyesters can be amorphous (with a low or high glass transition temperature (T_g)) or semi-crystalline.

Polyethers are usually formed by ring-opening epoxides, such as ethylene oxide and propylene oxide (**Figure 1.4(b)**). Compared to other polyols, polyethers are more cost effective, have good hydrolytic stability and flexibility at low temperature, but show inferior mechanical properties.²² Properties are governed by the different functional groups along the polymer backbone. Esters have a significant dipole charge and therefore are susceptible to hydrolysis, whereas ether analogues are less polar on account of having only a single oxygen atom embedded in the hydrocarbon chain. Another factor to consider is introducing branching along the polyol backbone which influences the stiffness and stability of the final PU.²³

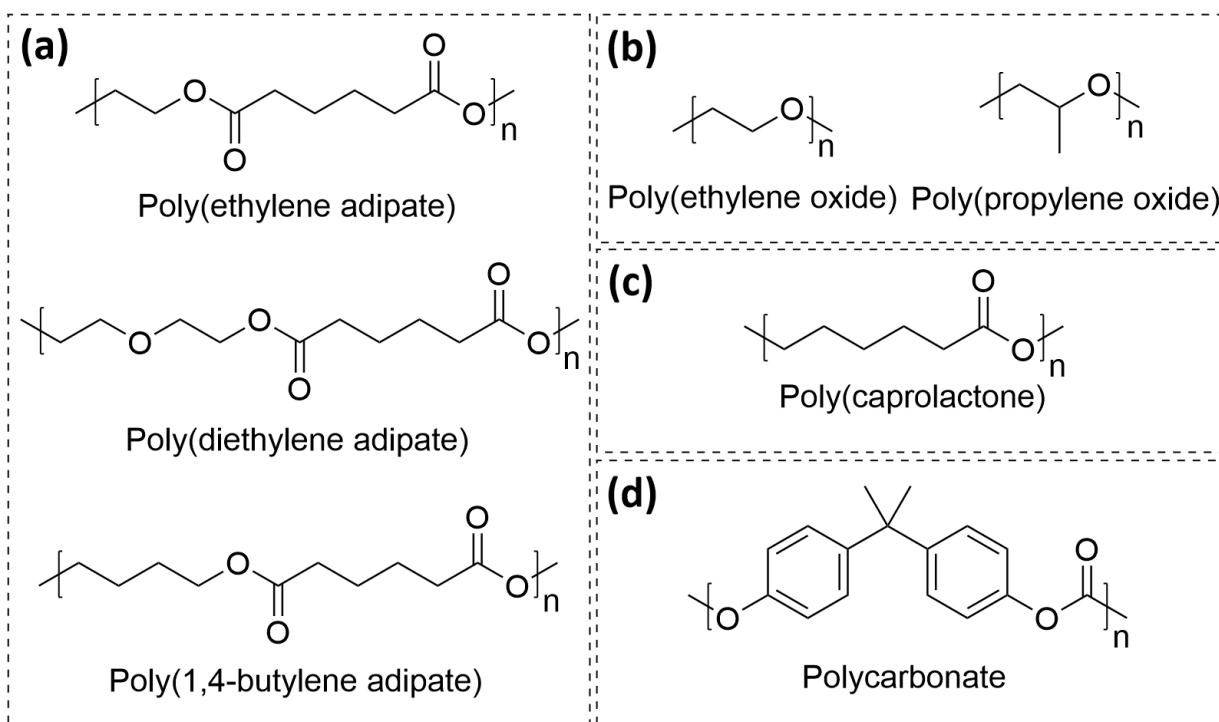


Figure 1.4 The repeating units of common polyols used in PU SS. **(a)** polyesters. **(b)** polyethers. **(c)** poly(caprolactone). **(d)** polycarbonate.

Poly(caprolactone) (PCL) (**Figure 1.4(c)**) affords enhanced polyurethane properties. It is an OH-terminated aliphatic polyester formed by the ring-opening polymerisation (ROP) of ϵ -caprolactone, initiated by a short diol such as diethylene glycol or neopentyl glycol. ROP is advantageous over traditional polyester synthesis as it produces polymers of narrower molecular weight distribution and lower viscosity compared to classically synthesised polyesters, but ROP is air-sensitive and a slower process. PCL is semi-crystalline (~50 %) and biocompatible with a melting temperature (T_m) up to 60 °C depending on molecular weight.²⁴⁻
²⁶ A very low T_g (-60 °C) gives superior low temperature properties.²⁵ However, PCL is more expensive compared to traditional polyesters and therefore is reserved for applications requiring higher performance.⁷

Polycarbonates also show improved properties (**Figure 1.4(d)**).⁶ Increased hydrolytic stability is granted by the unstable carbonic acid derivative formed upon hydrolysis.⁷ They are biodegradable polymers formed *via* transesterification of low molecular weight carbonic acid ester and diol.^{24, 27} Furthermore, they are potentially a green alternative as they can be synthesised from waste carbon dioxide as opposed to fossil fuel feedstock.²⁸

1.4.2 Hard segment - diisocyanates

The hard segment is comprised of isocyanate and chain extender which act as physical crosslinks within the PU network *via* intermolecular interactions. The urethane groups in the HS typically associate *via* favourable H-bonding. The HS dictates the high temperature behaviour of PUs as a result of the thermal stability gained by these associations. Additionally, the mechanical stability is often a reflection of the number and strength of H-bonds formed involving the urethane groups in the HS.

For linear PUs the diisocyanate has a functionality of 2.0. Diisocyanates can be one molecule or polymeric species. The most widely used is methylene diphenyl diisocyanate (MDI), which exists as several isomers (**Figure 1.5**). The 4,4'-MDI isomer has NCO groups of equivalent reactivity whereas the 2,4'-MDI isomer introduces preferential reactivity.²⁹ Another typical diisocyanate is toluene diisocyanate (TDI). Both MDI and TDI have symmetrical and asymmetrical variations which alters the properties of final PUs. Symmetrical isocyanates afford PUs with good elastomeric properties, whereas asymmetrical alternatives are transparent and more flexible.⁷ Aliphatic diisocyanates include hexamethylene diisocyanate (HDI) and saturated MDI (H₁₂MDI) which are both symmetrical. HDI is a flexible and linear monomer with a reactivity around two orders of magnitude less than 4,4'-MDI.⁷ Both HDI and

H₁₂MDI are symmetrical and offer good light stability as they do not contain aromatic rings which are unstable to UV light.

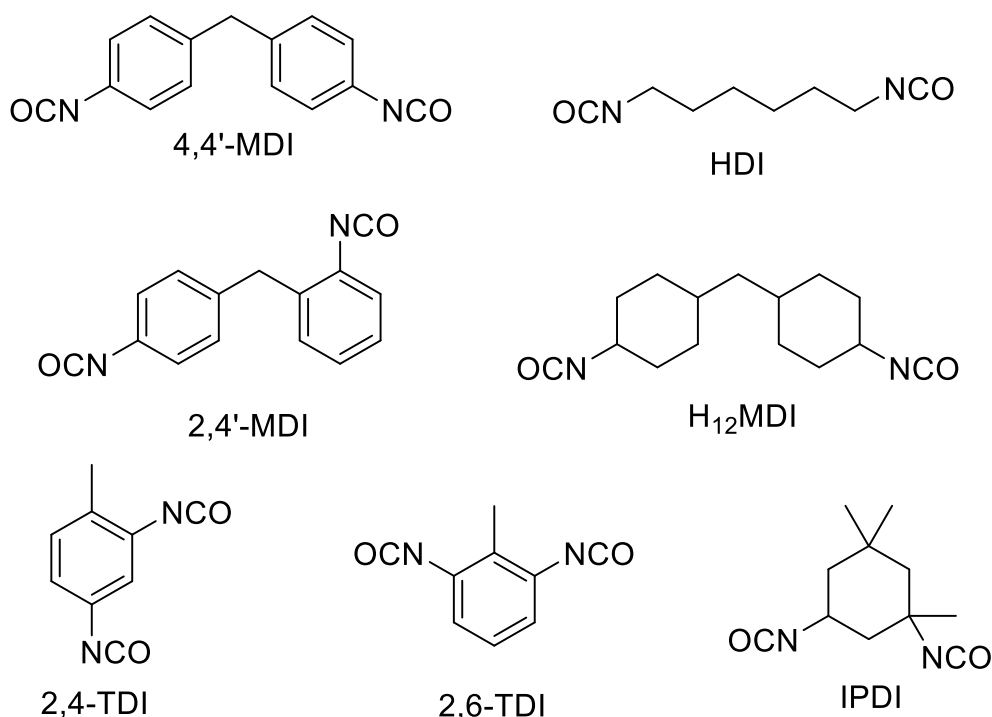


Figure 1.5 A selection of some aromatic and aliphatic diisocyanates commonly used in the synthesis of PUs.

Aromatic isocyanates are more common, but aliphatic alternatives are still used. The aromatic structure introduces an element of rigidity, the addition of conjugation increases the overall polarity of the system and restricts free rotation of the polymer chain, as observed by Liaw.³⁰ NCO groups are more reactive in aromatic isocyanates as a result of the electron withdrawing effect of the aromatic rings on the NCO carbon atom.¹ This carbon has greater electrophilicity and therefore is more susceptible to attack from a nucleophilic source. In general the easier the urethane bond is formed, the less stable it will be.⁸ Therefore, urethanes formed over a longer time by alkyl isocyanates tend to be more stable than those formed from aromatic isocyanates.^{8, 31} Furthermore, the presence of aryl rings causes discolouration of the PU product from white to yellow over time when exposed to UV light.⁷ Aliphatic isocyanates are

therefore the preferred choice for applications where aesthetics is important, such as films and coatings.

1.4.3 *Hard segment – chain extenders*

Chain extenders are short chain length molecules normally with a functionality of 2.0. They are terminated by hydroxyl or amine groups, which react with NCO to form urethane and urea linkages, respectively.¹⁹ The synthesis of PUs is often performed in two steps: firstly, the polyol reacts with an excess of diisocyanate to give an NCO-terminated prepolymer, this intermediate species is then reacted with an excess of diol chain extender in a subsequent step. The stoichiometry in the chain extension step can be used to control the copolymer molecular weight. While a two-step process, the steps are carried out in one reaction vessel consecutively, to exclude moisture and prevent premature reaction of the NCO end groups (one-pot, two-steps).

The purpose of the chain extender is to enhance the mechanical properties by increasing the molecular weight and the number of favourable interactions within the network.²⁷ The first example of a chain extender was water, however outside use in foam applications, water has little advantage.²¹ Therefore other diols are more frequently used as chain extenders, such as neopentyl glycol (NPG) and hexamethylene diamine (HMDA) (**Figure 1.6**). The shape and functionality of the chain extender can dictate the HS order and so have a large influence on the properties of the final copolymer.

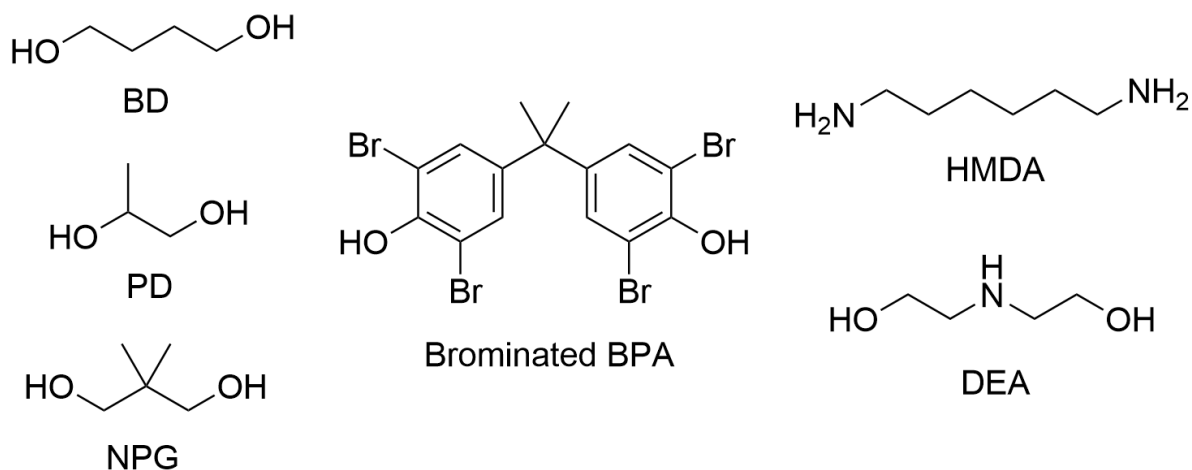


Figure 1.6 Examples of some common and more specialised chain extenders.

Linear aliphatic chains with an even number of carbon atoms are preferred for higher mechanical properties. For example, 1,4-butanediol (BD) produces a highly regular and well-packed HS forming dense physical networks that achieve superior properties.³² For this reason, BD is the industry standard CE of choice for commercial TPU products in structural applications in order to maximise the mechanical performance. However, due to the stability of an extensive physical network, TPUs containing BD exhibit high melt viscosity as interactions persist in the melt state.³³

Additives can be included in PU formulations to enhance the properties of products. They can be small organic or inorganic compounds added in very small quantities. Examples are sterically hindered aromatic carbodiimides to improve hydrolytic resistance,²¹ sterically hindered phenols as UV absorbers³⁴ and oxazolidine derivatives as moisture scavengers.²³

1.5 Morphology of thermoplastic polyurethanes

The composition and architecture of thermoplastic polyurethanes (TPUs) determine its morphology which in turn influences the mechanical properties of the material. Therefore, it is important to fully understand the morphology of a system and the structure-property

relationships to allow for optimisation for a specific application. A typical PU is composed of soft and hard segments which are covalently attached, one single molecule can even span several domains.

Polyurethanes typically have a phase separated morphology (**Figure 1.7**). Phase separation is a thermodynamic process which is largely driven by the incompatibility of the segments and occurs *via* spinodal decomposition as the reaction mixture cools. The difference in polarity between the relatively non-polar SS and polar HS promotes a separate domain morphology. As previously discussed, the SS tends to be relatively long non-polar with a low concentration of functional groups, whereas the HS is short and polar with functional groups like urethanes and phenyl rings.

PU multiblock copolymers are often viewed as HS dispersed in a soft matrix with the hard domains acting as physical crosslinking sites that increase the strength and elasticity of the network, visible through an increase in T_g .³⁵ The SS and HS work in synergy, offering flexibility and strength, respectively.³⁶ The long chain diols reorient upon the application of stress from a largely entangled state to fully extended chains along the direction of force while the stronger HS remains unaffected, to a certain point. After the removal of stress, the SS is able to relax and return to its original conformation.³⁷ However, there is often an optimum HS content for enhanced mechanical properties.⁷ The HS is known to disrupt the crystallinity of the SS, especially when CEs are introduced.³⁸ It is possible for there to be one completely mixed phase or two discrete phases or most probably somewhere between these two extreme cases. The degree of phase mixing is controlled by the compatibility between the segments.

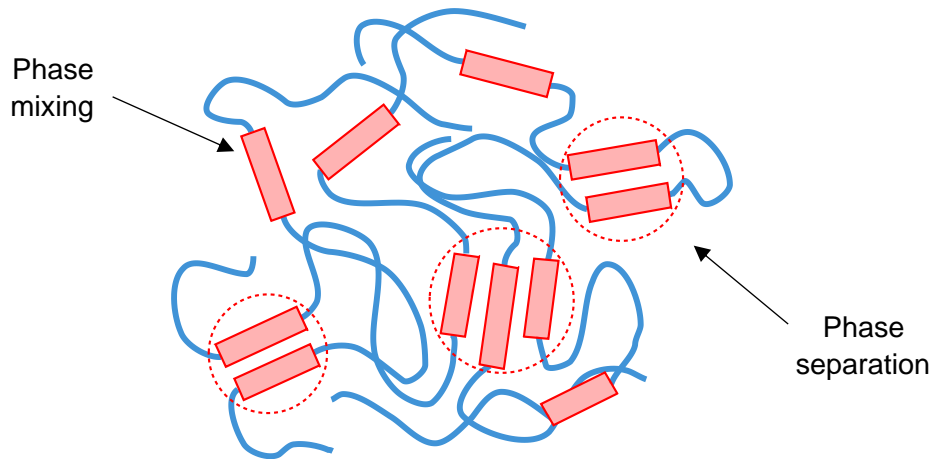


Figure 1.7 Typical morphology of a PU, some phase mixing and separation. Blue lines represent the SS polyol, red blocks are the HS (diisocyanate and CE) and the red dashed circles mark a phase change.

There are three distinct thermal regimes a TPU elastomer can maintain (**Figure 1.8**). Between the T_g and T_m is defined as the 'service temperature range' where the material properties are at an optimum and is the temperature range in which the polymer is used. At temperatures below T_g , the polymer is in a frozen 'glassy' state where it is very brittle as a consequence of minimal chain motion. Above T_m , the polymer is molten and behaves as a viscous fluid.

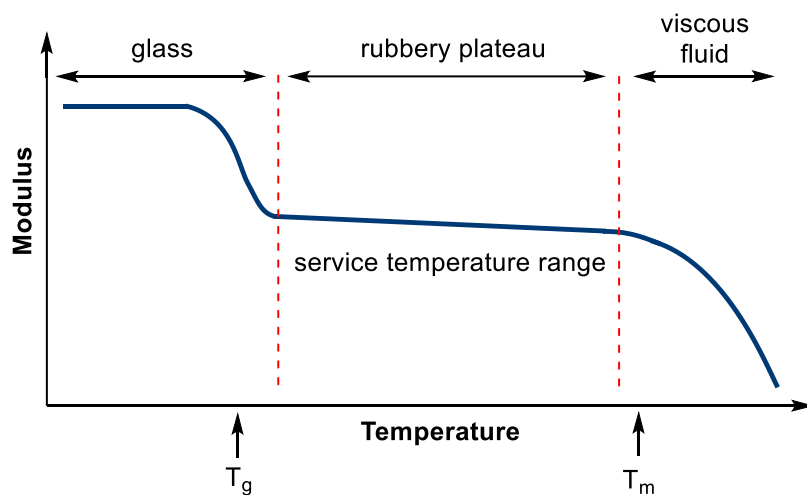


Figure 1.8 Simple representation of the change in physical properties of a polymer with temperature.

1.5.1 Effects of the soft segment

The soft segment is named on account of the length and flexibility of the polyol composition relative to the rigidity of the hard segment. Both amorphous and crystalline states are common in the soft domain, but completely crystalline polymers are not observed. Semi-crystalline polyols comprise of a mix of ordered and disordered regions. The ratio and organisation of these two states influences the properties of the final PU, for example crystallinity can increase polymer strength and adhesion, although this would be at the cost of flexibility.^{37, 39} Korley *et al.* demonstrated how crystallites within the SS were able to increase PU toughness by dissipating energy in a similar manner to the HS.⁴⁰ However, SS crystallinity can be sensitive to structural changes.

The choice of soft segment directly influences the T_g of the PU and therefore the low temperature properties it exhibits. Chain structure, flexibility and molecular weight are factors that can affect the energy barrier for chain rotation and thus, influence the T_g .⁴¹ Highly symmetrical and flexible chains decrease T_g , whereas pendent groups cause steric hindrance or interactions with surrounding chains to prevent chain rotation. Polyols of higher molecular weight are more entangled and therefore require more energy to move, observed through a higher T_g . A low T_g is desired for good low temperature properties as well as to maximise the service temperature range of the PU.²¹

Crystallisation occurs when intermolecular interactions between polymer chains are strong, so the chains align together in low energy conformations. This process is favourable when polymer melts begin to cool and free volume decreases. Typically, two factors influence the ability of a polymer chain to crystallise, chain symmetry and functional group interactions that stabilise the crystals. Interactions can be van der Waals forces in closely packed polymers,

dipole – dipole if polar groups are included (*e.g.* polyesters and polyamides) and H-bonding.⁴² Pendent groups and chain branching usually decrease crystallinity. Short rigid pendent groups prevent packing and restrict chain movement which increases T_m , whereas longer flexible chains decrease T_m on account of increasing free volume.

Crystallisation was described by Flory in 1962 with the random-re-entry switchboard model (**Figure 1.9**).⁴³ This work built on previous studies by Keller who discovered polymer chain folding in both solution and bulk grown crystals.⁴⁴ In the switchboard model, chains align and fold alongside one another in parallel lamellae where they leave and re-enter various crystalline lamellar in a statistical manner. The lamellae stack together with amorphous interlayers to form crystallites.⁴⁵

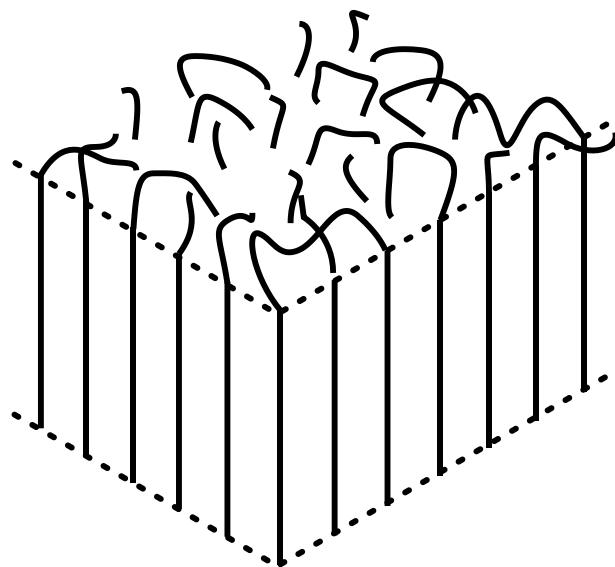


Figure 1.9 The switchboard model first proposed by Flory with random re-entry.

Crystallites are typically 1 – 100 nm which means one single polymer chain can span several crystallites. Therefore, if a polymer chain is involved in multiple regions of crystallisation, it can cause imperfections in one area on account of the strain caused by the crystallisation process in another area.⁴⁵ Moreover, higher molecular weights lead to a greater chance of

entanglement in the amorphous interlayers which hinders crystallisation.⁴⁶ Therefore, polymer molecular weight has a significant influence on crystallinity, especially the T_m . The T_m provides information about the perfection and size of the crystallites, with smaller crystals tending to melt at lower temperatures.⁴²

Polymer morphology is highly dependent on crystallisation conditions. This fact can be explained with the solidification model which states that there is minimal long-range diffusion of polymer chains (**Figure 1.10**).⁴⁷ Therefore, there is no mass reordering of chains travelling far to form 'perfect' crystallinity, but rather they remain relatively stationary from the melt. Straightening of the polymers causes crystallisation where they are already positioned.

The polymer properties between T_g and T_m are largely determined by crystallinity. Wang *et al.* showed that amorphous PCL can crystallise in the direction of applied stress on account of disentanglement.³⁷ This phenomenon is known as strain- or stress-induced crystallisation. However, after the removal of stress, the PCL is unable to reassume its original amorphous state because of the restriction on reorientation by the newly formed crystallinity. The result is a significantly different material after testing to before testing on account of the presence of crystallinity.

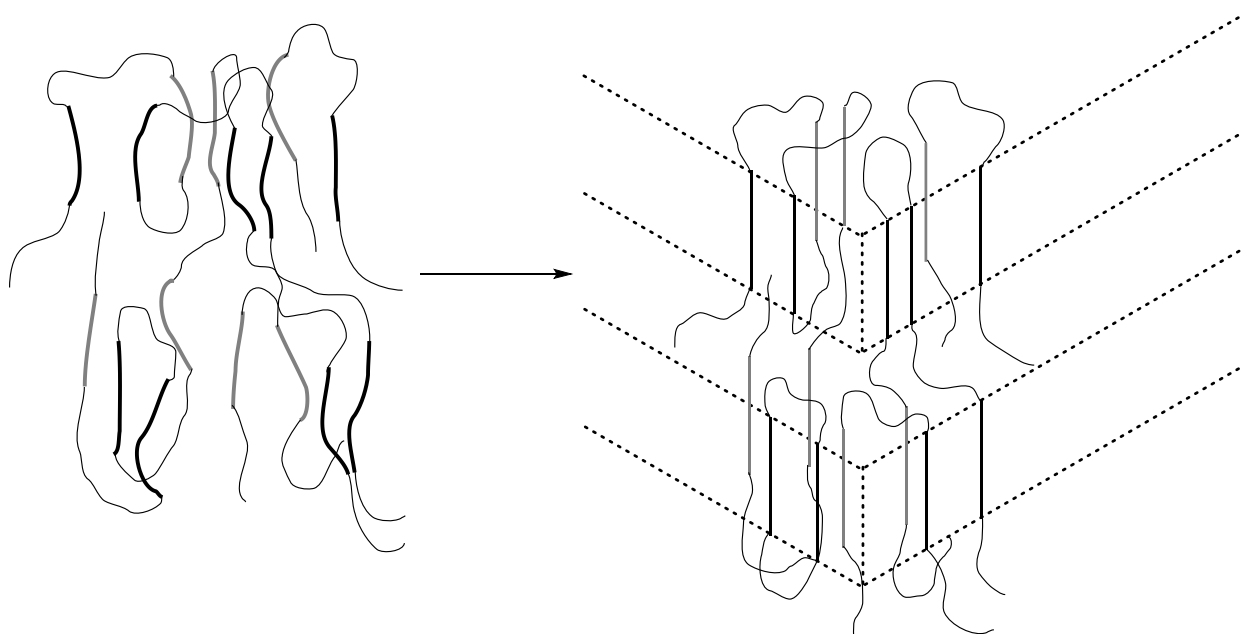


Figure 1.10 The solidification model. The level of disorder in the melt (left) is largely retained in the semi-crystalline solid state (right). Adapted from the work of Dettenmaier *et al.*⁴⁷

Multiple polyols can be blended in one TPU copolymer to improve overall properties, such as mechanical performance. For example, there is extensive research on blending poly(lactic acid) (PLA) with more flexible polyesters in order to overcome the brittleness of pure PLA, while maintaining good biocompatibility and biodegradability.⁴⁸⁻⁵⁵ Often polyols appear immiscible, but covalently linking the two polymers with MDI increases compatibility, as shown in a study by Pan *et al.*⁵¹ However, in this work the properties of the copolymer show a dependence on MDI content.

Additionally, work has been conducted investigating polymer compatibility *via* modelling software using Hansen's Solubility Parameters (HSP) to discern how similar polymers are to one another.^{56,57} This technique is also starting to be used in respect to the segmented nature of TPUs, but is rarely employed in favour of the traditional 'low-effort' trial and error method.⁵⁸

1.5.2 Effects of the hard segment

The HS is more compact than the SS, consisting of shorter components that pack closely together. At room temperature, the HS prevents the permanent deformation of the SS by acting as rigid physical crosslinking regions. When heated above the melting temperature of the HS ($T_{m(HS)}$), the TPU transitions into a viscous melt, losing network stability. However, after cooling below $T_{m(HS)}$ it regains its strength due to the reformation of H-bonds.²² Therefore, the $T_{m(HS)}$ should be relatively high, but lower than the decomposition temperature of the SS, for a balance between performance and processability.

TPU annealing helps to improve the HS stability, through heating the network to just below T_m allowing chains freedom to rearrange into the most favourable conformation.³⁵ Annealing increases the effective hard block region, decreases the interphase region and therefore improves mechanical properties (**Figure 1.11**).⁷ However, relatively high temperatures and long annealing times (12 hours at 190 °C) are often required for substantial HS crystallisation.²¹

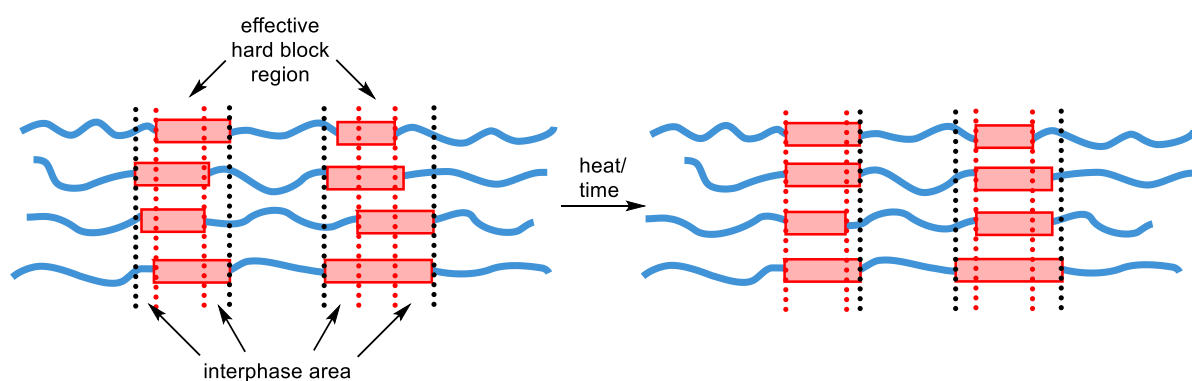


Figure 1.11 Annealing increases the effective hard block region to improve mechanical properties.

The HS can also be either amorphous or crystalline and the morphology is determined by both the diisocyanate and the CE.²¹ Crystallinity in the HS increases polymer modulus in a similar

manner to the SS.³⁵ The symmetry of the diisocyanate is important, higher symmetry tends to improved packing with more regular HS-HS interactions.³⁸

The choice of chain extender also has a significant impact of the TPU morphology as they can either assist or hinder intermolecular interactions within the copolymer. Studies by Rinke and Bonart on polyurethane ureas identified how urea and urethane groups form H-bonding bridges between adjacent chains, the stability of which influences the copolymer microstructure.^{59, 60} The key variables of a chain extender that affect these interactions are the main chain length, the presence of pendent groups, symmetry and additional functionality.

Blackwell *et al.* performed a series of investigations on the influence of CE chain length and determined that even chain lengths adopt lower energy states for improved HS crystallinity (**Figure 1.12**).^{61, 62} Recently in 2021, Akram *et al.* examined the amount of H-bonding as a function of CE length for purely evenly numbered methylene units. The degree of H-bonding decreases with CE length on account of an increase in distance between H-bonding sites.^{32, 63} Moreover, Schuur *et al.* found that the chain extender must be of uniform length for improved mechanical properties, otherwise using multiple CEs of various lengths causes disruption in the chain packing.⁹ Therefore, as the number of methylene units in the CE dramatically affect the HS, it can be deduced that it also influences the degree of phase separation.⁶⁴

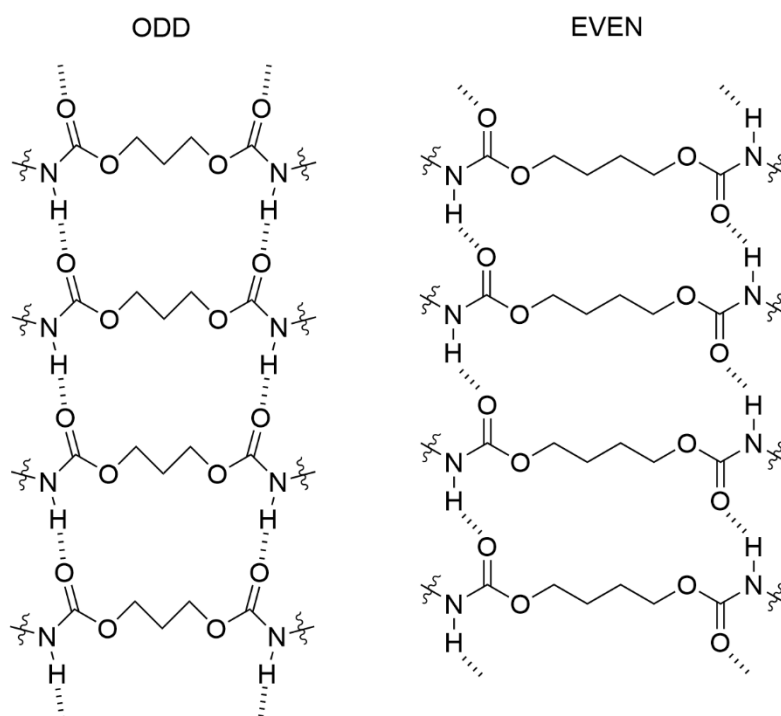


Figure 1.12 The difference in HS stacking between CEs with an odd (left) and even (right) number of methylene units. Based on the work of Blackwell *et al.*.^{61, 62}

The linearity of a CE dramatically affects the degree of phase mixing.³⁵ The introduction of pendent groups increases intermolecular urethane - urethane distance, resulting in longer and weaker H-bonding interactions.⁶⁵ Therefore, a less ordered HS forms which in turn favours phase mixing.^{66, 67} Sheikhy *et al.* reported a decrease in mechanical properties on account of using a branched CE.⁶⁶ Additionally, branched CEs can increase the T_g by either anchoring the HS because of internal steric hinderance which restricts SS mobility (phase separated)³⁵ or by directly mixing in with the SS and therefore hindering chain movement (phase mixed) (**Figure 1.13**).⁶⁸

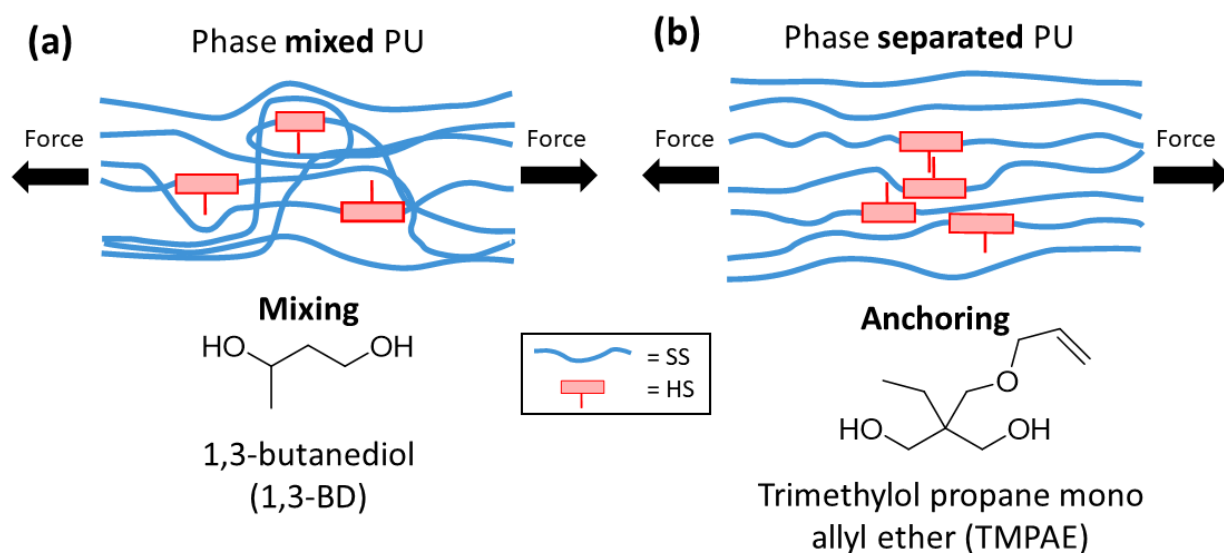


Figure 1.13 Chain restriction in a **(a)** phase mixed morphology and a **(b)** phase separated morphology with respective examples of CEs found in each system.^{68,69}

Furthermore, increasing the number of pendent methyl groups along the CE or on one single carbon atom also increases the T_g and can potentially have a negative impact on copolymer properties. Bae *et al.* showed how non-linear CEs decrease the thermal stability of the physical network as a function of branching (**Figure 1.14**).³⁵ However, in this study little attention was paid to the effect of pendent group length. Generally, increasing branch length increases T_g on account of steric hinderance preventing chain mobility. After a certain length the T_g begins to decrease as the branch becomes long and flexible enough to increase the surrounding free volume.⁴² Moreover, studies by Guo *et al.* showed that generally increasing the volume of CE, while maintaining a constant CE length, decreases HS order thereby increasing phase mixing which decreases SS crystallinity and mechanical performance as a result.⁷⁰

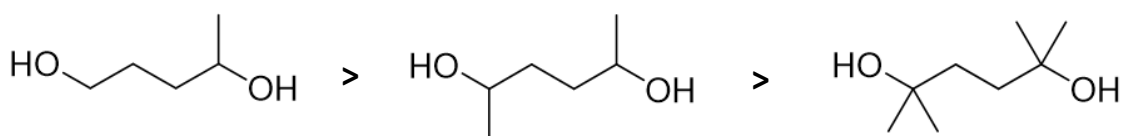


Figure 1.14 The degree of HS order decreases (arrows) with increasing branching from left to right.³⁵

A comparison between the influences of CE carbon chain length, branching and volume shows that all three features have a similar impact on copolymer properties. In separate studies, CEs with either an odd number of methylene units or a ring structure were comparable to a CE with an even carbon length but one pendent methyl group.^{66,68}

So far, none of these studies examine the effect of the pendent methyl group position, *i.e.* the influence of CE symmetry. Guelcher *et al.* displayed how asymmetry has a more pronounced influence on HS order than branching.⁶⁷ Good symmetry is seen to enhance HS packing and crystallinity and subsequently gives greater phase separation.⁷¹

Additional functionality in CEs (*e.g.* heteroatoms) alter the polarity of the unit which in turn determines the HS packing and degree of phase mixing. Polar groups such as ethers, amines and sulfonyls have good compatibility with the HS, thereby increasing phase separation.^{30,71,}

⁷² Conversely, apolar groups, such as $C(CF_3)_2$, increase phase mixing which is often displayed by an increase in T_g .³⁰

Research into sustainable CEs was conducted by Zhang *et al.* by copolymerising poly(tetramethylene ether glycol) (PTMG), isophorone diisocyanate (IPDI), dimethylolpropionic acid, 1,4-butanediol with the naturally sourced curcumin.⁷³ Small additions of

curcumin were shown to improve mechanical properties, however reported properties declined with further addition.

Amine terminated chain extenders are used when high mechanical performance is required. Amines react readily with NCO functionality to form urea groups. Poly(urethane urea)s show a greater degree of intermolecular interactions due to the bidentate and three-dimensional urea H-bonding which allows for a highly ordered HS (**Figure 1.15**).^{74,75} The strong association within the HS of poly(urethane urea)s results in greater phase separation and therefore improved mechanical performance when compared with standard polyurethanes.⁷⁶ Furthermore, the N-C bonds within the urea group show double bond character due to conjugation, which restricts rotation and strengthens the PU.⁷⁷

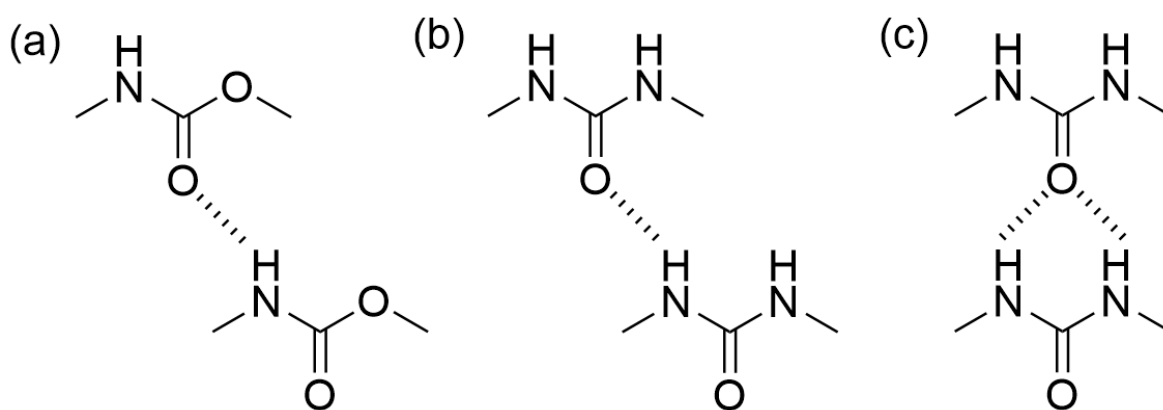


Figure 1.15 H-bonding between (a) urethane groups (monodentate) and urea groups in a (b) monodentate manner and (c) bidentate manner.

The effect of CE length in poly(urethane urea)s closely follows that which was previously discussed. Work by Kalajahi *et al.* demonstrated that longer diamine CEs decrease PU mechanical properties on account of greater compatibility of the two domains.⁷⁸ Interestingly, they showed that using a cycloaliphatic CE structure increased chain stiffness to

produce copolymers with improved phase separation and therefore enhanced mechanical performance (**Figure 1.16**).

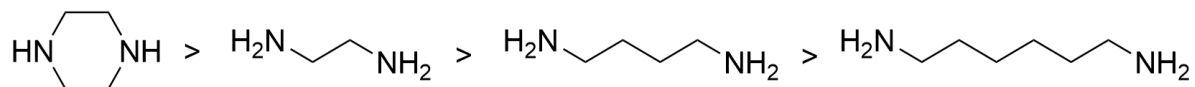


Figure 1.16 Order of increased phase separation, adapted from the work of Kalajahi *et al.*⁷⁸

A highly cohesive HS comes at the cost of self-healing ability as the physical crosslinking density is too high to allow sufficient movement of chains.⁷⁹ Additionally, poly(urethane urea)s are inherently difficult to synthesise and process without the use of solvents on account of the strong HS association that forms during synthesis which prevents sufficient stirring in bulk.⁸⁰ Reactions between isocyanates and amines are also very fast and can be difficult to control. The use of solvent introduces negative environmental and economical factors. Houton *et al.* investigated a faster and cleaner synthetic route *via* ball milling to mitigate both solvent and the issue of gelation in bulk reactions.⁸¹ Another factor when considering polyurethane ureas is that they are less thermally stable relative to polyurethane analogous and therefore cannot be used in applications which require high working temperatures and are often not suitable for TPUs.^{21,82}

In an interesting study by Li *et al.* they exploited the difference in reactivity between OH and NH groups with NCO to afford a urea CE with available pendent OH functionality.⁸³ This system allowed for extensive H-bonding physical network with enhanced mechanical properties. However, the material showed high dependence of modulus on temperature, so that the service temperature range would be very narrow. To overcome this issue, the group incorporated an amount of permanent covalent crosslinking which prevented loss of modulus below 150 °C, but these crosslinks would inhibit the reprocessability of the material.

Recent work by Pugar *et al.* offers an alternative method of mitigating the complexity of choosing PU constituents *via* physiochemical modelling and machine learning.⁸⁴ This method uses monomer chemistry to predict molecular interactions on the polymer scale which produces estimated values of parameters, such as Young's modulus.

1.6 The Diels-Alder reaction

The Diels-Alder (DA) reaction is a [4+2] cycloaddition between a diene (4 π -electrons) and a dienophile (2 π -electrons) first observed by Diels and Alder in 1928.⁸⁵ Cycloadditions involve the formation of two σ -bonds across the ends of two π -systems. This process fits into the class of pericyclic reactions where electrons move in a closed loop in a concerted manner (**Figure 1.17**). It is a reversible reaction so that the two separate starting materials can reform at elevated temperatures in what is termed the retro-Diels-Alder reaction (rDA). The dynamic is possible on account of the gain in entropy from reforming the starting materials, which becomes more significant with an increase in temperature ($\Delta G = \Delta H - T.\Delta S$). Therefore, the forwards DA reaction dominates at lower temperatures while the rDA dominates at higher temperatures (typically > 100 °C). The temperature at which the reverse reaction is possible is denoted the rDA temperature (T_{rDA}).

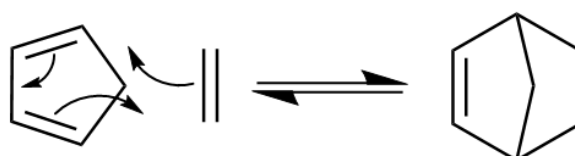


Figure 1.17 [4+2] cycloaddition occurs in a concerted manner across two π systems.

For a successful reaction, the diene must be in the *s-cis* conformation on account of geometrical limitations associated with forming what would be an extremely strained σ -bond

from the *s-trans* conformation. Therefore, structures that have a fixed *s-cis* conformation are favourable for DA reactions, such as cyclopentadiene and furan.

To understand the reaction further, it is necessary to examine the frontier molecular orbitals of the reactants.⁸⁶ Typically, the highest occupied molecular orbital (HOMO) of the diene (Ψ_2) interacts with the lowest unoccupied molecular orbital (LUMO) of the dienophile (π^*) (**Figure 1.18(a)**). It is important to note that this process is orbital symmetry allowed because of the match of phases of frontier orbitals. This orbital symmetry also explains why the diene must adopt the *s-cis* conformation (**Figure 1.18(b)**).

Typically, the dienophile is made electron-poor by incorporating electron-withdrawing groups next to the double bond, while the diene is made electron-rich by including electron-donating groups. The electron-donating group of the diene increases the energy of the HOMO (and LUMO) and the electron-withdrawing group of the dienophile decreases the energy of the LUMO (and HOMO). These effects result in Ψ_2 and π^* being closer in energy which equates to better orbital overlap and therefore a more favourable interaction. Conjugation of both components also aids the forwards DA reaction.

The furan-maleimide pairing is a common choice for the DA reaction on account of mild synthesis conditions, high conversion rates and minimal side reactions (**Figure 1.19(a)**).⁸⁷⁻⁸⁹

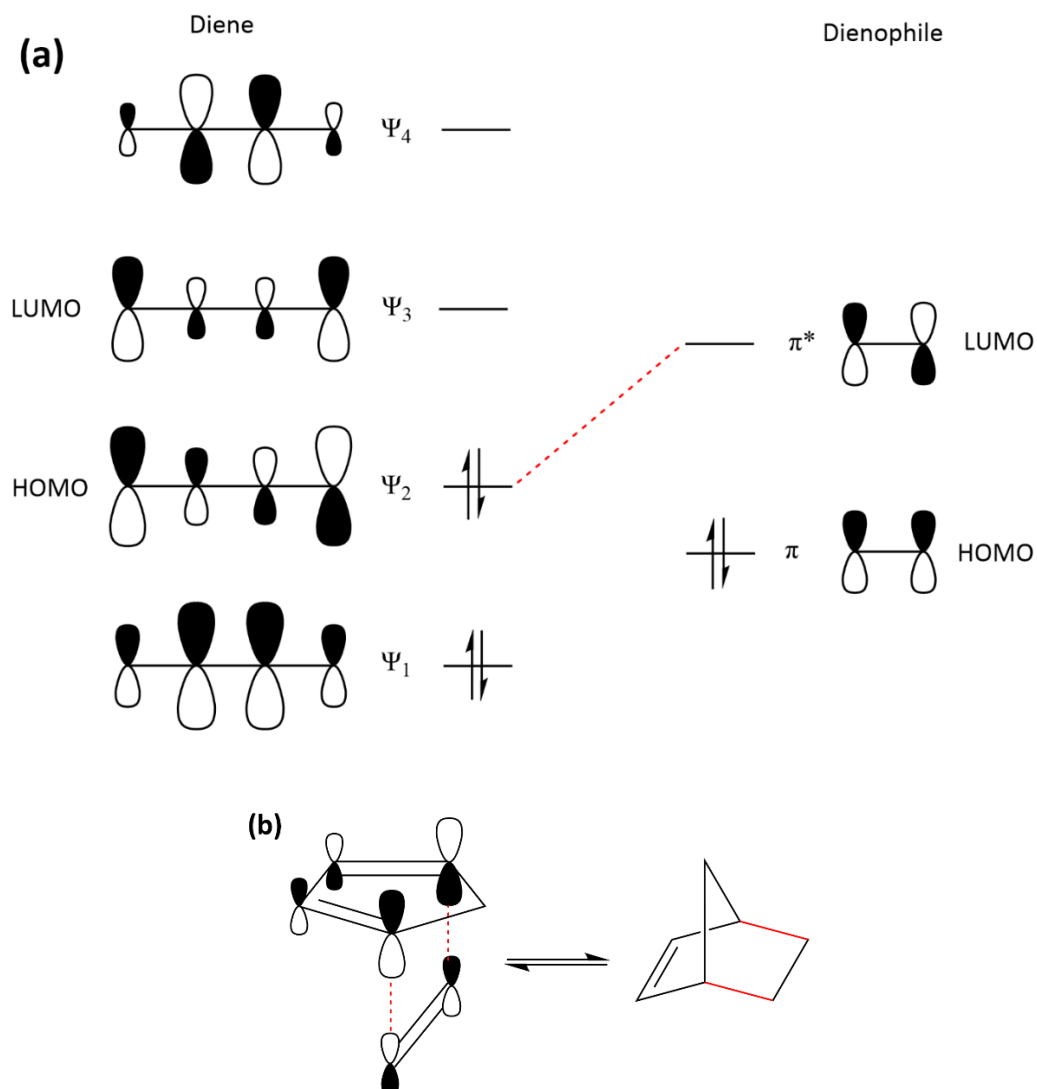


Figure 1.18 (a) The HOMO of the diene interacts with the LUMO of the dienophile. **(b)** The Diels-Alder is a symmetry allowed process.

There are two possible products from the DA reaction, the *endo* (carbonyls point down) or the *exo* (carbonyls point out) (**Figure 1.19(a)**). The *exo* product is the thermodynamic product, favoured on account of minimal steric hinderance relative to the *endo* product. However, under kinetic control, the *endo* product is formed preferentially. This difference can be accounted for by investigating the transition states of both pathways. In the *endo* transition state, there are secondary orbital interactions between the carbonyl carbons and the smaller orbitals of the diene (**Figure 1.19(b)**). While not resulting in bond formation, the interaction

stabilises the transition state and therefore reduce its energetic barrier. However, this stability is not present in the *exo* configuration as the dienophile points in the opposite direction.

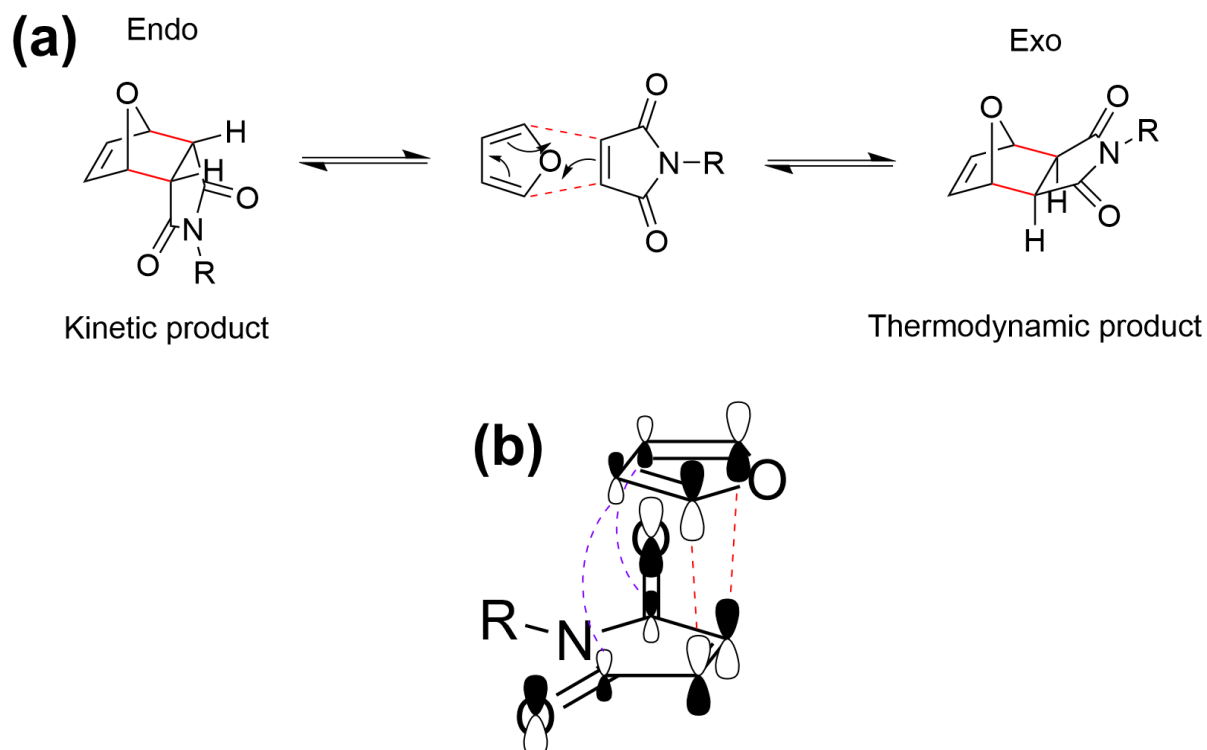


Figure 1.19 (a) Furan and maleimide react via the Diels-Alder reaction to form either the *endo* product (left) or the *exo* product (right). **(b)** Secondary orbital interactions (purple dashed lines) lower the energy of the *endo* transition state.

There is extensive literature describing DA chemistry in polymer systems.⁸⁷ By including the DA adduct in the polymer system, it grants thermal reversibility within the chain and therefore dynamic cleavage of the polymer at specific sites. Breaking up the polymer decreases its molecular weight and can give reversibility between the solid and melt states as a function of temperature, determined by the T_{rDA} . Therefore, it is possible to have a temperature controlled molecular weight, a highly attractive feature as a lower molecular weight decreases melt viscosity and therefore eases polymer processing.

There are many examples in literature of incorporating DA moieties into polyurethane backbones.⁹⁰⁻⁹³ Furan and maleimide functionalities are typically used to crosslink linear polymers to one another. Crosslinking increases mechanical performance to afford tougher materials. However, when crosslinking semi-crystalline prepolymers, the degree of crystallinity is decreased which results in lower values of Young's modulus.^{94,95} Moreover, a competition between crystal formation and DA adduct formation exists in crosslinked semi-crystalline systems but can be controlled with post-synthesis heat treatment.^{96,97} While annealing at both low and high temperatures allows for a range of properties, a trade-off is required between crystal size (strength) and degree of crosslinking (elasticity). Other studies have explored the combination of DA chemistry and H-bonded physical networks.^{94,98} However, there is currently very little work on exploring the dual effect of DA adduct and H-bonding in linear thermoplastic semi-crystalline PU copolymers.⁹⁹⁻¹⁰¹

Wu *et al.* successfully incorporated DA chemistry in linear polyurethanes for hot melt adhesive applications.¹⁰² They found reproducible adhesion measurements accompanied with temperature dependent melt viscosity on account of the activation of the rDA. However, they failed to demonstrate the mechanical properties of the materials and used 4,4'-diphenylmethane bismaleimide (BMI) as a linker, a toxic compound which would be liberated above T_{rDA} , greatly reducing the possible applications of the adhesive. In fact, many studies of incorporating DA chemistry within PU materials in literature use BMI as a linker.

1.7 Adhesives and adhesion

Adhesion is the bonding of two substrates together to prevent separation. Cohesive forces within a polymeric adhesive are governed by the strength of the internal polymer network

within the polymer itself, whereas adhesive forces are determined by interactions between the substrate surface and the adhesive.

A model of an adhesive bond shows the cross-section of a polymeric adhesive bonding multiple substrates together (**Figure 1.20**). At the centre of the joint (blue), the polymeric adhesive behaves as if it were a bulk polymer and the cohesion depends on the internal intermolecular forces within the polymer. At the interface between the polymeric adhesive and the substrate (green), the structure is dominated by intermolecular forces between the polymer and substrate. In the interphase region between the bulk and interface (orange) the composition of the joining polymer gradually changes between the bulk and the interface. Bonds can fail in different ways; cohesive failure is caused by weakness in the adhesive bulk, adhesive failure is due to lack of interactions at the interface between the surface and adhesive and substrate failure is when the substrate breaks because it is weaker than the adhesive. Bonds typically fail with cohesive failure, therefore bond strength is commonly dictated by the cohesion of the adhesive which means the internal order of the polymer is of interest to improve adhesion. Moreover, failure can be caused by mixed modes in a single test if the upper strength limit of multiple factors (*i.e.* adhesive and substrate) are similar.¹⁰³

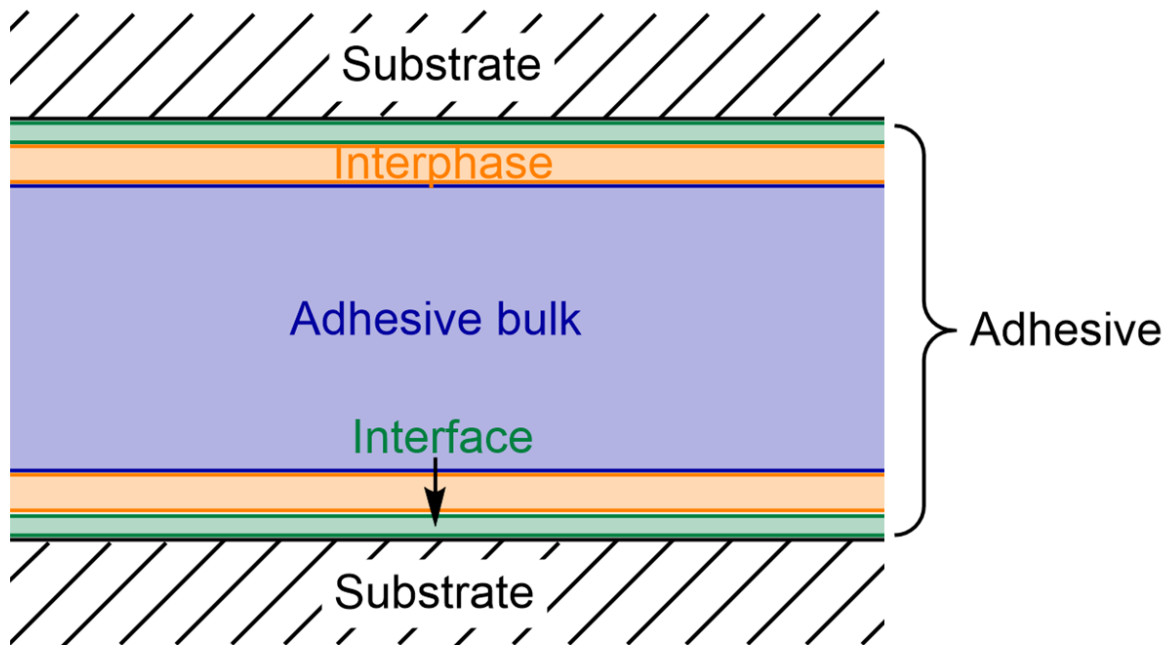


Figure 1.20 Model for the cross-section of an adhesive bond. The polymeric adhesive is represented by the coloured regions comprising the bulk (blue), interphase (orange) and interface (green).

Both adhesion and cohesion depend on intermolecular forces which can be *via* covalent or ionic bonding (primary bond formation); *via* H-bonding and van der Waal forces (secondary bond formation); or other surface reactions such as mechanical interlocking and electrostatic forces. Therefore, substrate surfaces should be clean for optimum adhesion. Sheikhy *et al.* determined the level of interactions by measuring the contact angle of a PU on water.⁶⁶ The contact angle relates to the wettability of an adhesive, which is the ability to spread evenly on a surface and can be influenced by surface tension.⁷ Surface wetting is highly important in adhesion as larger areas of contact promote adhesion, yet good wetting does not guarantee good adhesion and is considered as a prerequisite. Wettability is not only determined by interactions between the adhesive and substrate, but also the viscosity of the adhesive. The viscosity is largely dependent on molecular weight, structure and polarity of the copolymer. Due to surface imperfections, adhesives with low visosity usually have good wettability,

however these may have poorer cohesion (**Figure 1.21(a)**). Additionally, too low a viscosity would cause the adhesive to run and spill. High viscosity can leave voids in the bond line, acting as impurities and decreasing adhesion (**Figure 1.21(b)**). Therefore, a balance between wettability and viscosity is highly important.¹⁰⁴ Typical viscosity values of polymer melts are 1 – 1 000 Pa.s⁻¹.¹⁰⁵ Liquid honey has a viscosity of 10 Pa.s⁻¹ and is a good reference to help imagine suitable viscosity for easy adhesive application.

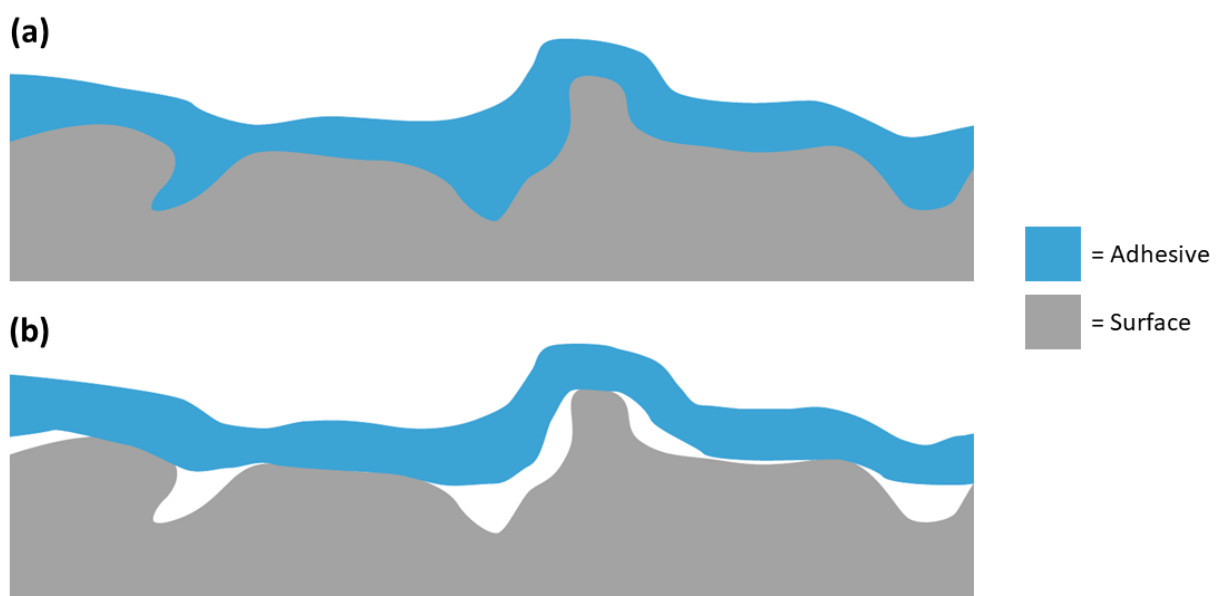


Figure 1.21 Representations of **(a)** good surface wetting and **(b)** poor surface wetting of an adhesive on a substrate surface.

Adhesives can be categorised by mechanism of hardening, either chemical or physical. Chemically hardening adhesives are those that cure from liquid prepolymers *via* chemical reactions *in situ*. These highly and irreversibly crosslinked polymers can be formed by a variety of chemistries (**Table 1.1**).¹⁰⁵

Table 1.1 Chemically hardening adhesive polymers.

Polymerisation	Chemistry
Free-radical	Cyanoacrylates Methyl methacrylate (MMA)
Step-growth addition	Polyurethanes (PUs) Epoxies
Step-growth condensation	Silicones Phenolics

Physically hardening adhesives are applied as fluids, then solidified *in situ*, without undergoing any chemical reactions and the transition from fluid to solid is reversible. Examples of physical hardening include loss of a solvent or water from a polymer or cooling of a hot melt resulting in a strong physical polymer network (**Figure 1.22**). Different adhesives lend themselves to varying situations, depending on important factors such as cure time and mechanism, strength, flexibility, physical appearance and resistance to harsh environments.

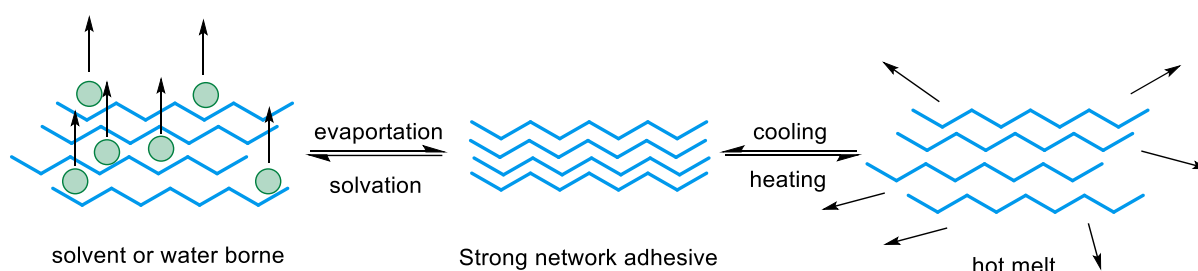


Figure 1.22 Common physical hardening mechanisms of an adhesive.

1.7.1 Traditional polyurethane adhesives

PUs are a popular choice of adhesives on account of their high performance, durability and potential to bind a range of surface types allowing for the manufacture of complex composite materials.⁶ Current polyurethane adhesives are typically crosslinked materials that are either one component (1K) or two components (2K) and final properties of the adhesive are largely dependent on the crosslinking density. 1K systems are classically NCO-terminated

prepolymers, which are liquid or solid at ambient temperature for simple moisture curing systems or reactive hot melts, respectively. While simple moisture curing systems are low viscosity liquid prepolymers, reactive hot melts consist of high molecular weight prepolymers therefore they cure both physically (cooling – fast adhesion to hold joint in place) and chemically (crosslinking – slow adhesion to maximise strength). After application to the substrates, the NCO groups react with moisture from the atmosphere or present in the substrates themselves at ambient temperatures ranging from 5 – 40 °C or at higher temperatures (*e.g.* 50 – 100 °C) for reactive hot melts.¹⁰⁵ The crosslinking processes is largely diffusion controlled, relying on water travelling through the prepolymer matrix to react with chain ends.¹⁰³ 2K systems consist of a prepolymer and an activating agent (crosslinker) which are supplied separately but premixed immediately before application to the substrates. The chemical reaction between the components begins on mixing and can take a couple of hours to several days. As both components comprise prepolymers, they tend to have low viscosity and therefore good surface wetting.

1K systems are simpler to use on account of the single component aspect, since 2K systems require carefully controlled mixing to provide the correct stoichiometry to build a high molecular weight fully crosslinked network. The 1K moisture curing approach tends to be used most due to convenience, but the final properties are inferior to the higher crosslinking density obtained with 2K adhesives. The latter are used in high performing structural applications which have more demanding requirements, where higher mechanical performance and durability are needed.¹⁰³ Both require specialised packaging for storage and application to prevent premature crosslinking. The resulting covalent crosslinks makes both types of adhesives highly durable, although the network is permanent and irreversible.

Permanently crosslinked adhesives are unattractive when considering the environmental impact of a composite material comprising different substrates joined together, as reprocessing of the raw substrates would be impossible. Therefore, there is a drive towards reversible adhesion where recovery of source substrates is possible for reuse and recycling. It is critical to design new adhesive materials which can both provide performance in use and also enable facile separation at the end-of-life.

1.7.2 Thermoplastic polyurethanes as adhesives

TPUs which are 1K unreactive hot melts are a potential alternative as adhesives since they do not require moisture curing. Traditionally used for solid applications, such as plastic elastomers, they show reversibility *via* response to thermal or solvent stimuli (**Figure 1.22**). While these materials are solid at room temperature, they become viscous melts above T_m or with solvation. Previously, the focus for TPUs has largely been on forming the highest molecular weight possible for the best durability and performance as engineering plastics. However, the high molecular weights (typically > 40 kDa) cause highly cohesive melts due to the quantity of entanglement points and interactions occurring, such as H-bonding between urethane groups. Interestingly, incorporation of amorphous polyols has been described as increasing melt viscosity, whereas semi-crystalline polyols have the inverse effect.¹⁰³ High melt viscosity demands the need for high shear equipment like hot melt screw extruders for application which are expensive but suitable for producing high volumes of engineering plastics.¹⁰⁶ Alternatively, hot melt adhesives can be applied as a solid film between two substrates before heat and pressure are applied to form the bond upon cooling (**Figure 1.23**). However, conventional reactive hot melt adhesives are typically applied at low volumes using facile, inexpensive low shear application equipment, where a typical melt viscosity is 10 Pa.s⁻¹

^{1,107} Such a material is fluid enough to provide good wetting when hot but the should provide adequate bond strength on cooling to ambient temperature, either by the formation of strong non-covalent interactions or covalent bonds. A desirable TPU hot melt adhesive would require a large difference in the physical properties of the molten material (low viscosity for wetting) and the solid material at ambient temperature (high mechanical properties). So far, there are no TPUs available which can be applied with low melt viscosity using conventional bulk adhesive processing equipment. Currently all materials are either prepared *via* solvent casting or high-pressure compression moulding.^{108,109}

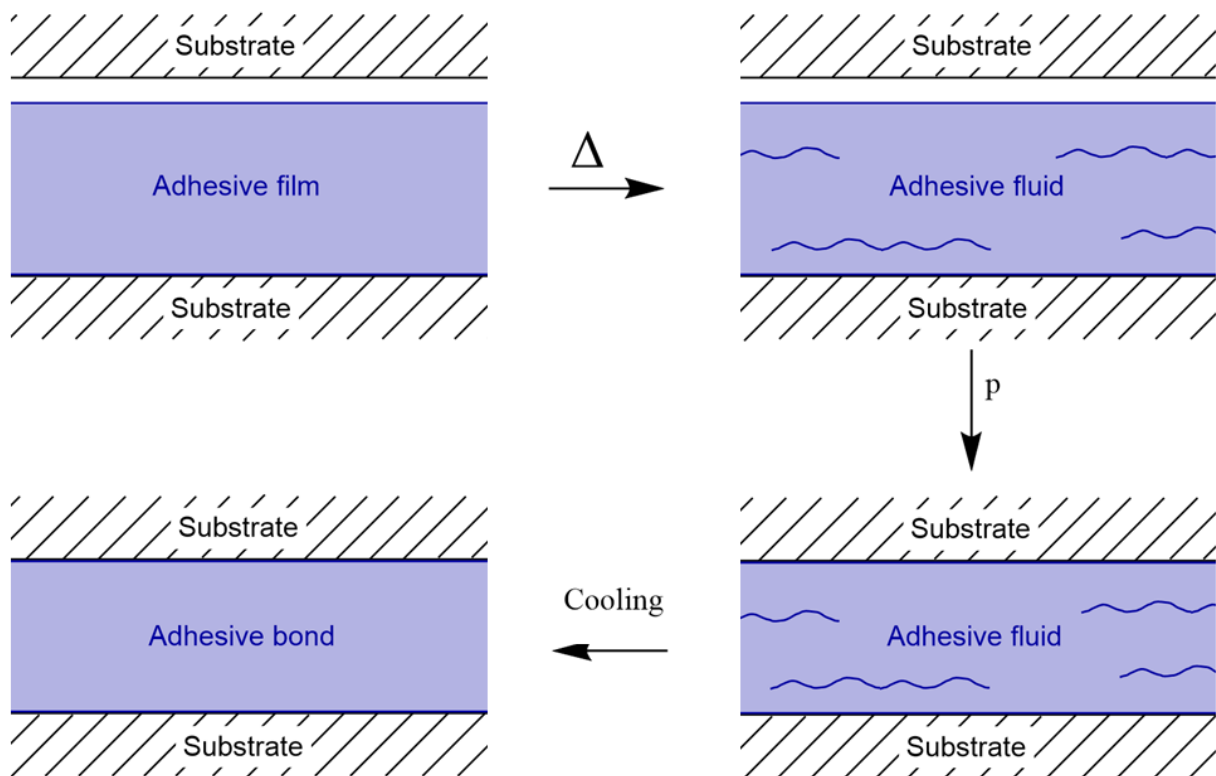


Figure 1.23 Forming an adhesive bond from a solid TPU film. Heat is applied to the entire system to melt the adhesive, followed by pressure and cooling to form the final solid polymer adhesive bond.

1.7.3 Recycling and life cycle analysis

The use of plastics has grown exponentially over the past several decades on account of their variety of impressive properties (*e.g.* durability, chemical resistance and light weight) coupled with their ease and low cost production.¹¹⁰ Plastics are so useful and commonplace, it is nearly impossible to imagine modern life without them. However, issues regarding waste management are becoming clearer, only 9 % of the 6.3 billion metric ton of plastic waste has been recycled as of 2017 and last year microplastics were found in human blood for the first time.^{111, 112} Therefore, the need to reuse, recycle and remanufacture materials is growing increasingly important. Traditionally, the life cycle of plastic was linear, *i.e.* production, use and then disposal, thereby giving the plastic only one lifetime (single-use plastics).¹¹⁰ Inappropriate disposal of plastic waste not only has detrimental impacts on the environment and eco-systems due to the extremely long decomposition time of plastics, but is also a huge waste of resources. Therefore, a circular economy is desired to avoid these issues which requires a life cycle analysis (LCA) of all materials to determine their environmental impact throughout their entire lifetime, *i.e.* from cradle to grave.¹¹³ A circular economy is a more sustainable approach to using resources and is based on reusing materials to minimise loss to the environment. Circularity not only involves, designing new materials to be reused or recycled easily at end-of-life, but also encompasses using sustainable feedstocks and reverting the damage already caused by previous mismanagement of waste.¹¹⁰ It is beneficial to minimise the frequency of particularly demanding processes such as sourcing raw materials and disposing waste. Reusing materials in various ways is a viable option as it increases the lifetime of an article which overall decreases its mark on the environment. The ability of a material to maintain properties of high enough standard for use in a desired application over

multiple reuses must be assessed to enable circularity. Examination of the polymer morphology after several reuses would highlight any likely changes to material properties.

Mechanical recycling involves the separation of waste plastics, followed by reprocessing to either reform the original material or more likely 'down-cycle' to a less economically valuable material. This method of recycling is a popular option to minimise use of virgin plastics and has been proven to have a relatively low environmental impact from several LCAs.¹¹⁴ However, mechanically recycling more complex materials consisting of multiple types of materials is not possible as the individual materials cannot be separated before reprocessing. These 'useless' rejects are then incinerated for energy recovery.¹¹² Therefore, the adhesion of these complex waste materials is of environmental importance.

Adhesives play an extremely important role in larger systems across different sectors, such as packaging, automotive and construction industries. They bond different substrates together to afford composites to achieve improved properties. For example, crisp packets consist of several laminated materials that, when in unison, provide favourable properties to ensure crisps do not perish and in fact live up to their name.¹¹⁰ The ability to reverse the adhesion process and recover the separate raw materials for reuse is highly appealing. Such a material should provide robust performance in service conditions and then be triggered by a stimulus to facilitate easy separation when the material comes to its end-of-life and needs to be reused or recycled (**Figure 1.24**).

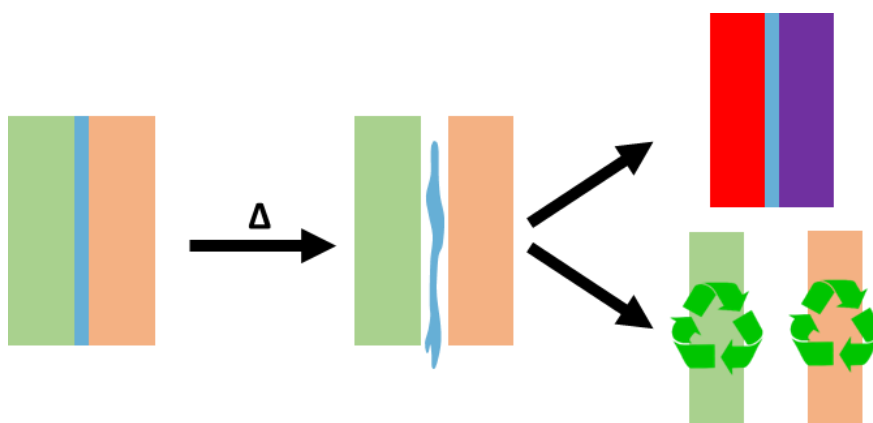


Figure 1.24 Individual components of a composite material could be separated via heating to remove the low melt viscosity adhesive. The materials could be reused or recycled and the adhesive could be reused in another composite material.

In the context of the information above, this work aims to firstly explore basic TPU structure-property relationships on simple model copolymers. These investigations are to form the basis of further work on the possibility of exploiting reversible physical networks present in TPUs to allow for a dynamic change of material properties. The effects of chain extender structure (symmetry, branching and functionality) on TPU microstructure and properties will also be studied. It is important to understand the microstructure of the TPU copolymer as it will determine the mechanical and adhesive properties of the material, allowing for optimised performance for designing materials in the future.

Other work will discuss the use of dynamic covalent bonds in copolymer backbones for temperature controlled molecular weight. As mechanical properties and melt viscosity are largely determined by molecular weight, this approach should allow for a strong and cohesive solid at ambient temperature, but a low viscosity fluid at elevated temperatures. These switchable physical states would enable simple application and removal of material in adhesive applications and therefore facilitate recycling of composite materials in the drive towards a circular economy. Different constituent polyols will be explored, with particular

interest on semi-crystalline materials which should offer enhanced strength for structural adhesives. Finally, dynamic covalent bonds will be incorporated into copolymers containing both semi-crystalline and amorphous segments. This work will explore the potential of synthesising copolymers with targeted properties from simple bulk polymerisation of benign prepolymers chosen from a wide library of semi-crystalline and amorphous prepolymers.

1.8 References

1. G. Odian, *Principles of Polymerization*, Wiley-Interscience, New York, 1991 edn., 1991.
2. R. W. Nunes, J. R. Martin and J. F. Johnson, *Polym. Eng. Sci.*, 1982, **22**, 205-228.
3. W. H. Carothers, *T. Faraday Soc.*, 1936, **32**, 39-49.
4. J. Brandrup, E. H. Immergut, E. A. Grulke, A. Abe and D. R. Bloch, *Polymer handbook*, Wiley New York, 1999.
5. G. V. Research, *Polyurethane Market Size, Share & Trends Analysis Report By Product (Rigid Foam, Flexible Foam), By Application (Construction, Furniture & Interiors), By Region, And Segment Forecasts, 2022 - 2030*, Report 978-1-68038-262-4, San Francisco, 2022.
6. H. W. Engels, H. G. Pirkl, R. Albers, R. W. Albach, J. Krause, A. Hoffmann, H. Casselmann and J. Dormish, *Angew. Chem. Int. Ed.*, 2013, **52**, 9422-9441.
7. D. Randall and S. Lee, *The Polyurethanes Book*, Wiley, New York, 3rd edn., 2003.
8. J.-P. P. E. Delebecq, B. Boutevin and F. Ganachaud, *Chem. Rev.*, 2013, **113**, 80-113.
9. M. van der Schuur, B. Noordover and R. J. Gaymans, *Polymer*, 2006, **47**, 1091-1100.
10. M. Modesti, N. Baldoin and F. Simioni, *Eur. Polym. J.*, 1998, **34**, 1233-1241.
11. D. Chattopadhyay, P. Prasad, B. Sreedhar and K. Raju, *Prog. Org. Coat.*, 2005, **54**, 296-304.

12. H. Jiang, Z. Zheng, W. Song and X. Wang, *J. Appl. Polym. Sci.*, 2008, **108**, 3644-3651.
13. I. Yilgör, E. Yilgör and G. L. Wilkes, *Polymer*, 2015, **58**, A1-A36.
14. T. Prenveille, C. Garreau, M. Matner, D. Dijkstra, W. Oppermann and D. Johannsmann, *J. Polym. Sci. A1*, 2019, **57**, 621-629.
15. F. B. A. Lapprand, F. Delolme, F. Méchin and J.-P. Pascault, *Polym. Degrad. Stabil.*, 2005, **90**, 363-373.
16. A. L. Silva and J. C. Bordado, *Rev. Catal.*, 2004, **46**, 31-51.
17. T. Micich, *J. Am. Oil Chem. Soc.*, 1982, **59**, 92-94.
18. N. Pérez-Moral and A. Mayes, *Anal. Chim. Acta*, 2004, **504**, 15-21.
19. Y.-K. Jhon, I.-W. Cheong and J.-H. Kim, *Colloid Surface. A*, 2001, **179**, 71-78.
20. M. Sánchez-Adsuar, E. Papon and J. J. Villenave, *J. Appl. Polym. Sci.*, 2000, **76**, 1590-1595.
21. G. Holden, H. R. Kricheldorf and R. P. Quirk, *Thermoplastic Elastomers*, Hanser, Germany, 3rd edn., 2004.
22. G. Holden, *Understanding thermoplastic elastomers*, Hanser Verlag, 2000.
23. E. S. a. F. Zafar, in *Polyurethane*, ed. F. Z. a. E. Sharmin, IntechOpen, 2012, ch. 1, pp. 3-16.
24. Y. Ikada and H. Tsuji, *Macromol. Rapid Comm.*, 2000, **21**, 117-132.
25. P. D. O. Coulembiera, J. L. Hedrickb and P. Dubois, *Prog. Polym. Sci.*, 2006, **31**, 723-747.
26. H. Yan, Z. Zhou, Y. Pan, T. Huang, H. Zhou, Q. Liu, H. Huang, Q. Zhang and W. Wang, *J. Macromol. Sci. B*, 2016, **55**, 839-848.
27. C.-H. Tsou, H.-T. Lee, H.-A. Tsai, H.-J. Cheng and M.-C. Suen, *Polym. Degrad. Stabil.*, 2013, **98**, 643-650.

28. S. J. Poland and D. J. Darensbourg, *Green Chem.*, 2017, **19**, 4990-5011.
29. L. Nagy, T. Nagy, Á. Kuki, M. Purgel, M. Zsuga and S. Kéki, *Int. J. Chem. Kinet.*, 2017, **49**, 643-655.
30. D. J. Liaw, *J. Appl. Polym. Sci.*, 1997, **66**, 1251-1265.
31. D. K. C. a. D. C. Webster, *Prog. Polym. Sci.*, 2009, **34**, 1068-1133.
32. N. Akram, S. Saleem, K. M. Zia, M. Saeed, M. Usman, S. Maqsood, N. Mumtaz and W. G. Khan, *J. Polym. Res.*, 2021, **28**, 1-15.
33. W. Lei, C. Fang, X. Zhou, Y. Cheng, R. Yang and D. Liu, *Thermochim. Acta*, 2017, **653**, 116-125.
34. C. Schollenberger and F. Stewart, *J. Elastoplast.*, 1972, **4**, 294-331.
35. J. Bae, D. Chung, J. An and D. Shin, *J. Mater. Sci.*, 1999, **34**, 2523-2527.
36. A. Lopez, E. Degrandi, E. Canetta, J. L. Keddie, C. Creton and J. M. Asua, *Polymer*, 2011, **52**, 3021-3030.
37. S. C. F. Wanga, Q. Wua, R. Zhang and P. Sun, *Polymer*, 2019, **163**, 154-161.
38. S. McCreath, P. Boinard, E. Boinard, P. Gritter and J. Liggat, *International Journal of Adhesion Adhesives*, 2018, **86**, 84-97.
39. M. Sánchez-Adsuar, *International journal of adhesion adhesives*, 2000, **20**, 291-298.
40. L. T. J. Korley, B. D. Pate, E. L. Thomas and P. T. Hammond, *Polymer*, 2006, **47**, 3073-3082.
41. G. W. H. Höhne, W. Hemminger and H.-J. Flammersheim, *Differential Scanning Calorimetry An Introduction for Practitioners*, Springer, New York, 1996.

42. J. M. G. Cowie, *Polymers: chemistry and physics of modern materials*, Stanley Thornes Ltd, Cheltenham, 1991.
43. P. J. Flory, *J. Am. Chem. Soc.*, 1962, **84**, 2857-2867.
44. A. Keller, *Philos. Mag.*, 1957, **2**, 1171-1175.
45. U. W. Gedde, *Polymer Physics*, Springer Netherlands, 2013.
46. M. Jenkins and K. Harrison, *Polym. Adv. Technol.*, 2006, **17**, 474-478.
47. M. Dettenmaier, E. Fischer and M. Stamm, *Colloid Polym. Sci.*, 1980, **258**, 343-349.
48. H.-M. Dou, J.-H. Ding, H. Chen, Z. Wang, A.-F. Zhang and H.-B. Yu, *RSC Adv.*, 2019, **9**, 13104-13111.
49. B. Cui, Q.-Y. Wu, L. Gu, L. Shen and H.-b. Yu, *Chinese J. Polym. Sci.*, 2016, **34**, 901-909.
50. T. Gurunathan, S. Mohanty and S. K. Nayak, *J. Mater. Sci.*, 2014, **49**, 8016-8030.
51. H. Pan, Z. Li, J. Yang, X. Li, X. Ai, Y. Hao, H. Zhang and L. Dong, *RSC Adv.*, 2018, **8**, 4610-4623.
52. S. Aslan, L. Calandrelli, P. Laurienzo, M. Malinconico and C. Migliaresi, *J. Mater. Sci.*, 2000, **35**, 1615-1622.
53. L. Jiang, M. P. Wolcott and J. Zhang, *Biomacromolecules*, 2006, **7**, 199-207.
54. A. Nijenhuis, E. Colstee, D. Grijpma and A. Pennings, *Polymer*, 1996, **37**, 5849-5857.
55. H. Chen, M. Pyda and P. Cebe, *Thermochim. Acta*, 2009, **492**, 61-66.
56. S. Abbott and C. M. Hansen, *Hansen solubility parameters in practice*, Hansen-Solubility, 2008.
57. S. Abbott, *Curr. Opin. Colloid In.*, 2020, **48**, 65-76.
58. R. Gallu, F. Méchin, F. Dalmas, J.-F. Gérard, R. Perrin and F. Loup, *Polymer*, 2020, **207**, 122882.
59. H. Rinke, *Angew. Chem. Int. Ed. Engl.*, 1962, **1**, 419-424.

60. R. Bonart, *J. Macromol. Sci. B*, 1968, **2**, 115-138.
61. J. Blackwell and M. Nagarajan, *Polymer*, 1981, **22**, 202-208.
62. J. Blackwell, M. Nagarajan and T. Hoitink, *Polymer*, 1981, **22**, 1534-1539.
63. D. Favero, V. Marcon, C. A. Figueroa, C. M. Gómez, A. Cros, N. Garro, M. J. Sanchis, M. Carsí and O. Bianchi, *J. Appl. Polym. Sci.*, 2021, **138**, 50709.
64. A. Takahara, J.-i. Tashita, T. Kajiyama, M. Takayanagi and W. J. MacKnight, *Polymer*, 1985, **26**, 978-986.
65. O. W. J. Zhai, W. Zhao, X. Tao, S. L. Hsu and A. Slark, *J. Polym. Sci. Pol. Phys.*, 2018, **56**, 1265-1270.
66. H. Sheikhy, M. Shahidzadeh, B. Ramezanzadeh and F. Noroozi, *Journal of Industrial Engineering Chemistry*, 2013, **19**, 1949-1955.
67. S. A. Guelcher, K. M. Gallagher, J. E. Didier, D. B. Klinedinst, J. S. Doctor, A. S. Goldstein, G. L. Wilkes, E. J. Beckman and J. O. Hollinger, *Acta Biomater.*, 2005, **1**, 471-484.
68. K. Gisselält and B. Helgee, *Macromol. Mater. Eng.*, 2003, **288**, 265-271.
69. W.-K. Liu, Y. Zhao, R. Wang, F. Luo, J.-S. Li, J.-H. Li and H. Tan, *Chinese J. Polym. Sci.*, 2018, **36**, 514-520.
70. Y. Guo, R. Zhang, Q. Xiao, H. Guo, Z. Wang, X. Li, J. Chen and J. Zhu, *Polymer*, 2018, **138**, 242-254.
71. P. H. Chen, Y. F. Yang, D. K. Lee, Y. F. Lin, H. H. Wang, H. B. Tsai and R. S. Tsai, *Adv. Polym. Technol.*, 2007, **26**, 33-40.
72. W. Li, A. J. Ryan and I. K. Meier, *Macromolecules*, 2002, **35**, 6306-6312.
73. T. Zhang, Y. Deng, W. Zhang, G. Wang, Y. Zhong, C. Su and H. Li, *Polymer*, 2022, **239**, 124465.

74. C. B. Wang and S. L. Cooper, *Macromolecules*, 1983, **16**, 775-786.
75. J. P. Sheth, A. Aneja, G. L. Wilkes, E. Yilgor, G. E. Atilla, I. Yilgor and F. L. Beyer, *Polymer*, 2004, **45**, 6919-6932.
76. R. L. O. a. M. I. Y. E. Ayres, *Eur. Polym. J.*, 2007, **43**, 3510-3521.
77. B. C. Chun, T. K. Cho and Y.-C. Chung, *Eur. Polym. J.*, 2006, **42**, 3367-3373.
78. A. Eyvazzadeh Kalajahi, M. Rezaei, F. Abbasi and G. Mir Mohamad Sadeghi, *Polym.-Plast. Technol.*, 2017, **56**, 1977-1985.
79. Y. Wang, Y. Li, M. He, J. Bai, B. Liu and Z. Li, *J. Appl. Polym. Sci.*, 2021, **138**, 51371.
80. C. Spaans, J. De Groot, F. Dekens and A. Pennings, *Polym. Bull.*, 1998, **41**, 131-138.
81. K. A. Houton, G. M. Burslem and A. J. Wilson, *Chem. Sci.*, 2015, **6**, 2382-2388.
82. M. Shoaib and A. Bahadur, *e-Polymers*, 2016, **16**, 411-418.
83. X. Li, J. Ke, J. Wang, C. Liang, M. Kang, Y. Zhao and Q. Li, *J. CO2 Util.*, 2018, **26**, 52-59.
84. J. A. Pugar, C. Gang, C. Huang, K. W. Haider and N. R. Washburn, *ACS Appl. Mater. Inter.*, 2022, **14**, 16568-16581.
85. O. Diels and K. Alder, *Liebigs Ann. Chem.*, 1928, **460**, 98-122.
86. R. Hoffmann and R. B. Woodward, *Accounts Chem. Res.*, 1968, **1**, 17-22.
87. A. Gandini, *Prog. Polym. Sci.*, 2013, **38**, 1-29.
88. B. Briou, B. Ameduri and B. Boutevin, *Chem. Soc. Rev.*, 2021, **50**, 11055-11097.
89. X. Liu, P. Du, L. Liu, Z. Zheng, X. Wang, T. Joncheray and Y. Zhang, *Polym. Bull.*, 2013, **70**, 2319-2335.
90. S. Chen, F. Wang, Y. Peng, T. Chen, Q. Wu and P. Sun, *Macromol. Rapid Comm.*, 2015, **36**, 1687-1692.
91. P. Du, M. Wu, X. Liu, Z. Zheng, X. Wang, T. Joncheray and Y. Zhang, *J. Appl. Polym. Sci.*, 2014, **131**.

92. K.-K. Tremblay-Parrado, C. Bordin, S. Nicholls, B. Heinrich, B. Donnio and L. Avérous, *Macromolecules*, 2020, **53**, 5869-5880.
93. M. Thys, J. Brancart, G. Van Assche, R. Vendamme and N. Van den Brande, *Macromolecules*, 2021, **54**, 9750-9760.
94. P. Wu, H. Cheng, X. Wang, R. Shi, C. Zhang, M. Arai and F. Zhao, *Green Chem.*, 2021, **23**, 552-560.
95. K. Ishida, Y. Nishiyama, Y. Michimura, N. Oya and N. Yoshie, *Macromolecules*, 2010, **43**, 1011-1015.
96. X. Kuang, G. Liu, L. Zheng, C. Li and D. Wang, *Polymer*, 2015, **65**, 202-209.
97. Y. Zhang, Z. Dai, J. Han, T. Li, J. Xu and B. Guo, *Polym. Chem.*, 2017, **8**, 4280-4289.
98. M. Li, R. Zhang, X. Li, Q. Wu, T. Chen and P. Sun, *Polymer*, 2018, **148**, 127-137.
99. J. D. Mayo and A. Adronov, *J. Polym. Sci. A1*, 2013, **51**, 5056-5066.
100. C. Lakatos, K. Czifrák, R. Papp, J. Karger-Kocsis, M. Zsuga and S. Kéki, *Express Polym. Lett.*, 2016, **10**, 324-336.
101. K. Ishida and N. Yoshie, *Macromol. Biosci.*, 2008, **8**, 916-922.
102. M. Wu, Y. Liu, P. Du, X. Wang and B. Yang, *Int. J. Adhes. Adhes.*, 2020, **100**, 102597.
103. L. Thiele, *Polyurethane Adhesives for Industrial Applications - A Progress Report*, Buchbinderei Terbeck, Germany, 2008.
104. H. Choi, J. Ko, J. Song and S. Woo, *Polyurethane Reactive (PUR) Adhesive to Improve Heat Resistance for Car Seat Attachment Techniques*, Report 0148-7191, SAE Technical Paper, 2017.
105. B. B. Norbert Banduhn, Gerhard Gierenz, Andreas Gross, Axel Hessland, Irene Janssen, Heinz Wambach and Wolfgang Weber, *Bonding/Adhesives*, Barm Water, Dusseldorf, 2004.

106. B. Claeys, A. Vervaeck, X. K. Hillewaere, S. Possemiers, L. Hansen, T. De Beer, J. P. Remon and C. Vervaet, *Eur. J. Pharm. Biopharm.*, 2015, **90**, 44-52.
107. Q. Tang, J. He, R. Yang and Q. Ai, *J. Appl. Polym. Sci.*, 2013, **128**, 2152-2161.
108. J. R. Gouveia, R. R. de Sousa Júnior, A. O. Ribeiro, S. A. Saraiva and D. J. dos Santos, *Eur. Polym. J.*, 2020, **131**, 109690.
109. C. Wongsamut, R. Suwanpreedee and H. Manuspiya, *Int. J. Adhes. Adhes.*, 2020, **102**, 102677.
110. D. G. Bucknall, *Philosophical Transactions of the Royal Society A*, 2020, **378**, 20190268.
111. R. Geyer, J. R. Jambeck and K. L. Law, *Science advances*, 2017, **3**, e1700782.
112. H. A. Leslie, M. J. Van Velzen, S. H. Brandsma, A. D. Vethaak, J. J. Garcia-Vallejo and M. H. Lamoree, *Environment international*, 2022, **163**, 107199.
113. C. Bernardo, C. L. Simões and L. M. C. Pinto, 2016.
114. L. F. J.-C. Michaud, O. Jan, B. Kjaer, I. Bakas, *Environmental benefits of recycling—2010 update.* , Waste & Resources Action Programme (WRAP), Banbury, UK, 2010.

2 Thermoplastic polyurethanes from copolymerisation without chain extenders

2.1 Introduction

Thermoplastic polyurethanes (TPUs) are well known and have a wide variety of possible copolymer compositions which can be made *via* different synthetic techniques. However, little work directly compares how synthetic techniques affect the final TPU. Previous work has examined the influence of altering some parameters on polyurethane (PU) products. Fiorio *et al.* showed how reaction temperature can introduce branching and side reactions which in turn affects copolymer crystallinity, morphology and decomposition temperature.¹ Work by Sánchez-Adsuar *et al.* demonstrated how reaction time only affects the prepolymer step and not the chain extension step in TPU synthesis.² However, keeping parameters constant across different synthesis types is not well studied in literature.

Bulk polymerisations are typically performed on a large scale (>100 g) to ensure sufficient stirring of raw materials. In this process the largest mass contributor (polyol) is the reaction medium in which the other components (diisocyanate and chain extender) dissolve and react. Heating increases mobility of the polyol by disrupting interactions, such as causing crystals to melt. Bulk polymerisation is advantageous as it is solvent-free and does not require additional steps to isolate the polymer. However, as viscosity is largely determined by molecular weight, there is a potential of high melt viscosity as molecular weight increases with copolymerisation.

Solution polymerisation uses a common solvent to solubilise the raw materials. The choice of solvent is imperative as the copolymer should not precipitate out before the end of reaction. Solvent facilitates the mobility of the reaction matrix, so when combined with heat, much higher molecular weight products are possible. In contrast to bulk reactions, solution polymerisation products need to be isolated, either by evaporating the solvent or

precipitating the polymer in a non-solvent. Additional time, resources and waste disposal are required and there are negative environmental impacts, such as toxicity, associated with using organic solvents.

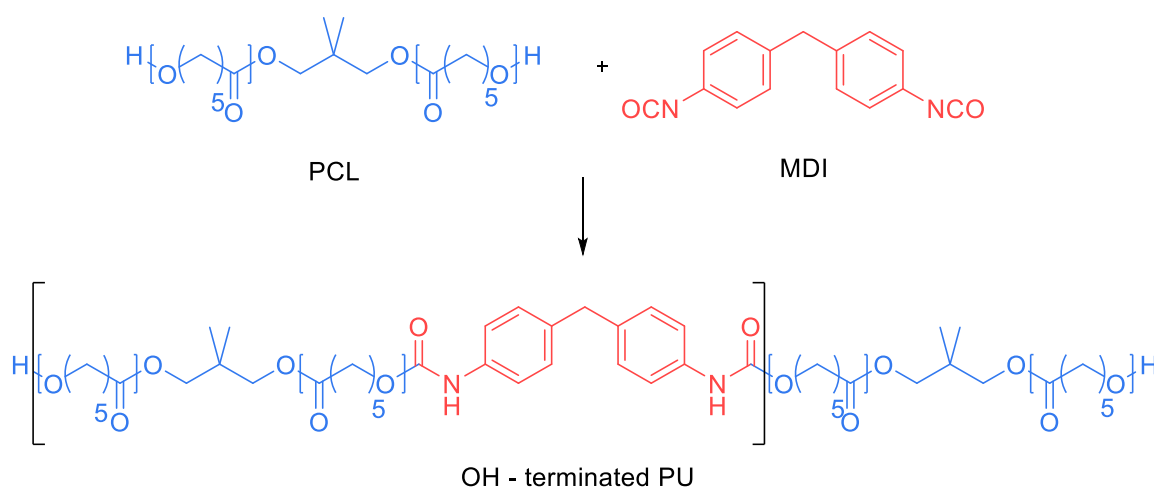
Polyol composition greatly affects final TPU behaviour, especially flexibility and low temperature properties. Polyol features that impact TPU properties include chemical composition, molecular weight and degree of crystallinity.³ This study uses poly(ϵ -caprolactone) (PCL) which is a linear aliphatic polyester with a narrower dispersity (D_M) and higher thermal and hydrolytic stability relative to traditional polyesters. A short-chain diol initiates the ring-opening polymerisation of ϵ -caprolactone to form an OH – terminated polymer. Depending on molecular weight, PCL is semi-crystalline with a melting point of approximately 60 °C.⁴⁻⁶ Enhanced low temperature properties are possible because of a low glass transition temperature (T_g) of -60 °C. While PCL is commonly used in TPU copolymerisation, to the best of our knowledge there is no research into the effect of polyol in non-chain extended TPUs.

In this chapter, bulk and solution polymerisation methods are critically compared by synthesising TPU copolymers using the same reagents in different techniques. The effect of polyol molecular weight on TPU morphology is also explored. Simple copolymerisations are performed of PCL polyol and 4,4'-methylene diphenyl diisocyanate (MDI) without chain extenders for providing model, simplified copolymers to establish polymerisation and characterisation protocols.

2.2 Results and Discussion

2.2.1 Synthesis of Thermoplastic Polyurethanes

TPUs were synthesised as a copolymer of PCL and MDI (**Scheme 2.1**). The Carothers equation was employed for a stoichiometric imbalance of OH : NCO moieties in order to limit the molecular weight of the TPU copolymers produced.⁷ Polyol was always used in excess to afford OH-terminated TPUs and prevent any further chain growth caused by reaction of free isocyanate groups. A range of copolymer molecular weights were synthesised by altering the stoichiometry of functional groups. All copolymers were characterised *via* NMR spectroscopy, FTIR spectroscopic analysis, size-exclusion chromatography (SEC) analysis and differential scanning calorimetry (DSC) (**Table 2.1**). PCL (2.0 kDa) was used to make series **B** in bulk and **S** in solution. PCL (1.0 kDa) was used to make series **L** in bulk.



Scheme 2.1 Copolymerisation of PCL and MDI with an imbalanced OH : NCO molar ratio to produce OH-terminated TPUs.

¹H NMR spectroscopic analysis shows successful copolymerisation in all cases. Resonances associated with the formation of urethane functionality were detected at $\delta = 6.75$ and 4.16 ppm corresponding to the urethane NH proton and the methylene of the PCL chain adjacent to the urethane oxygen, respectively (**Figure 2.1**). Neither of these resonances were present

in either spectra of pure PCL or pure MDI. As the OH : NCO molar ratio tends to 1, there is an increase in the integration of resonances at $\delta = 4.16, 6.75, 7.13$ and 7.32 ppm associated with MDI relative to those of PCL, which is evidence of a higher incorporation of MDI in the copolymer. As expected, integrals of resonances representing the end groups ($\delta = 3.32$ and 3.68 ppm) decrease, as the MDI content increases.

Table 2.1. All copolymers synthesised from the copolymerisation of PCL and MDI.

Series	Copolymer	Method	PCL (kDa)	Molar ratio	
				OH	NCO
B	PCL^a	-	2.0	1.00	0.00
B	B1	Bulk	2.0	2.00	1.00
B	B2	Bulk	2.0	1.50	1.00
B	B3	Bulk	2.0	1.30	1.00
B	B4	Bulk	2.0	1.20	1.00
B	B5	Bulk	2.0	1.10	1.00
S	S1	Solution	2.0	2.00	1.00
S	S2	Solution	2.0	1.50	1.00
S	S3	Solution	2.0	1.30	1.00
S	S4	Solution	2.0	1.20	1.00
S	S5	Solution	2.0	1.10	1.00
S	S6	Solution	2.0	1.05	1.00
S	S7	Solution	2.0	1.01	1.00
L	PCLL^b	-	1.0	1.00	0.00
L	L1	Bulk	1.0	2.00	1.00
L	L2	Bulk	1.0	1.50	1.00
L	L3	Bulk	1.0	1.30	1.00
L	L4	Bulk	1.0	1.20	1.00
L	L5	Bulk	1.0	1.10	1.00

^a PCL without MDI, **PCL** (2.0 kDa)

^b PCL without MDI, **PCLL** (1.0 kDa)

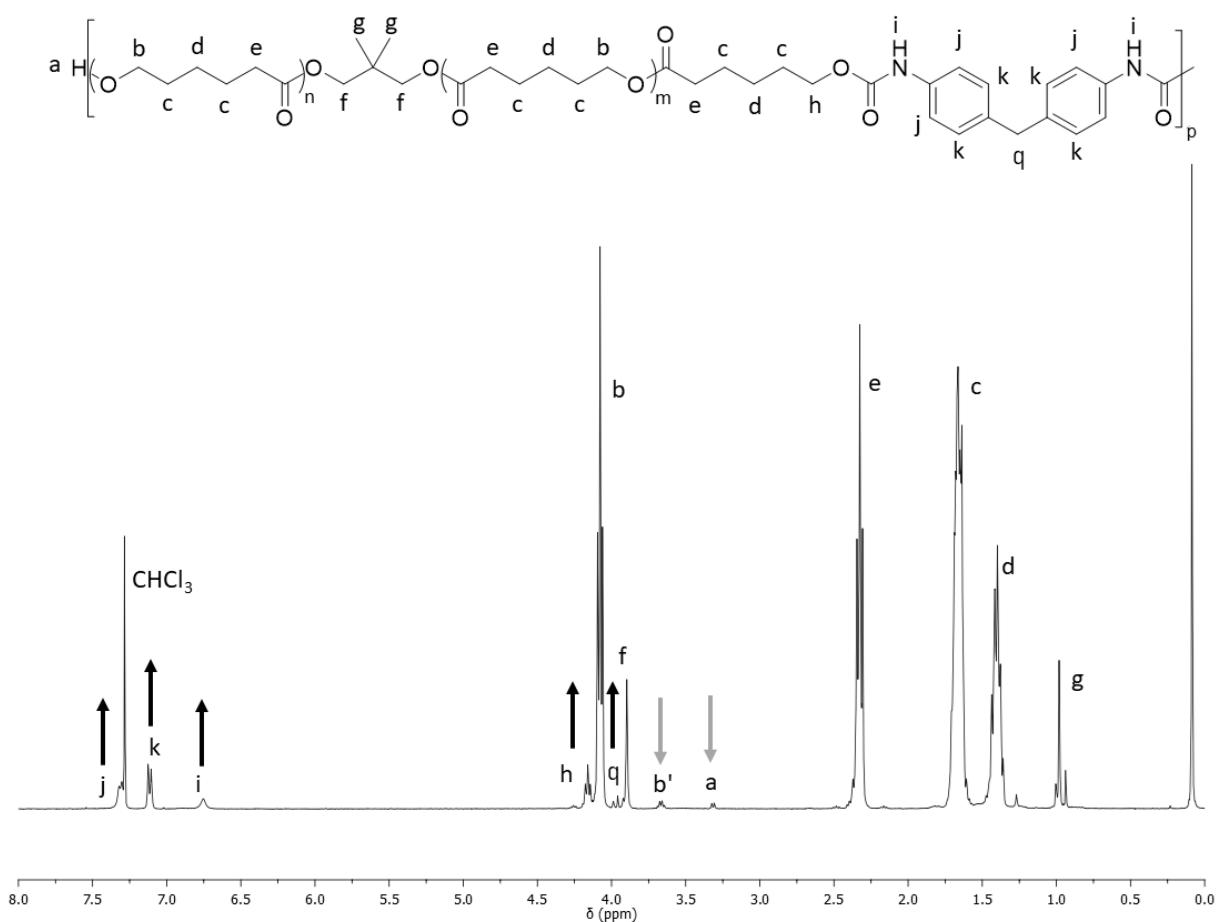


Figure 2.1 ¹H NMR spectrum of **B3** as a representative of TPUs copolymers. Arrows denote an increase or decrease in resonance intensity as OH : NCO tends to 1.0 : 1.0. Integrals are relative to PCL initiator, neopentyl glycol (NPG). (400 MHz, 298 K, CDCl₃).

Formation of the copolymers is also confirmed *via* FTIR spectroscopy. Comparison of the absorptions between copolymer product and pure PCL shows the presence of urethane linkages (**Table 2.2**). The stretch at $\nu_{\max} = 3442 \text{ cm}^{-1}$ corresponding to the O-H of PCL is reduced while a new resonance develops at $\nu_{\max} = 3347 \text{ cm}^{-1}$ showing the emergence of N-H in the newly formed urethane group (**Figure 2.2**). After addition of MDI, the absorption of the C=O broadens to reflect the increase in complexity of the carbonyl region, as both ester and urethane C=O are present in this region. The aliphatic CH₂ of the PCL backbone is present in all spectra at $\nu_{\max} = 2941$ and 2865 cm^{-1} . The aromatic C=C at $\nu_{\max} = 1598 \text{ cm}^{-1}$ appears in the

copolymer which matches the phenyl rings of MDI. A band at $\nu_{\max} = 1532 \text{ cm}^{-1}$ representing C-N further proves incorporation of MDI. There is no absorbance around $\nu_{\max} = 2260 \text{ cm}^{-1}$ showing all the NCO has reacted.⁸ There is also no urea detected between $\nu_{\max} = 1680 - 1625 \text{ cm}^{-1}$, meaning moisture was successfully excluded from the reaction.⁹ Overall the analysis agrees with data from NMR spectroscopy and shows the formation of urethane functionality.

Table 2.2 Wavenumbers of significant functionalities. For clarity, only **B3** is shown as a representative material.

Sample	Wavenumber (cm^{-1})					
	O-H	N-H	NCO	C=O	Ar. C=C	C-N
PCL	3442	-	-	1722 (ester)	-	-
MDI	-	-	2260	-	1578	1521
B3	-	3347	-	1721 (multi)	1598	1532

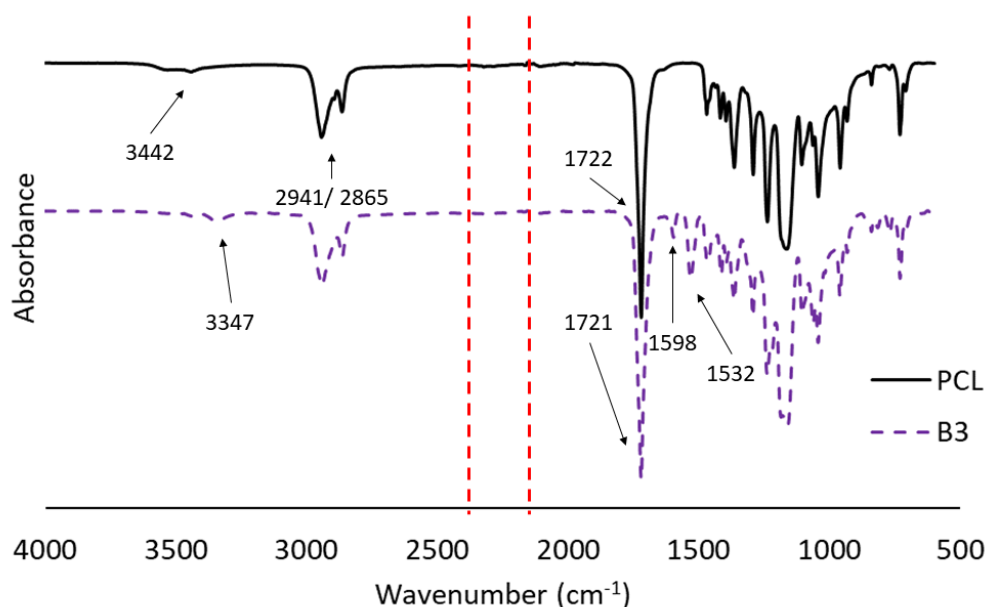


Figure 2.2 FTIR spectra of **PCL** before copolymerisation and after copolymerisation of **PCL** with **MDI (B3)**. Dashed red lines indicate the region where **NCO** absorption would appear.

2.2.2 Effect of polymerisation process on polymer properties

It is worth noting that the same polyol (**PCL**) and diisocyanate (**MDI**) is used in all comparisons. Only the stoichiometry of OH : NCO is changed to achieve a series of TPUs of different molecular weights to deduce what effect the synthesis method has on the copolymer properties across a range of molecular weights. The ^1H NMR spectra of both bulk and solution polymerisations display proton resonances at almost identical chemical shifts and with very similar integrations (**Figure 2.3**). This similarity represents protons in the same environment and therefore TPU copolymers that are structurally the same, independent of the polymerisation process used.

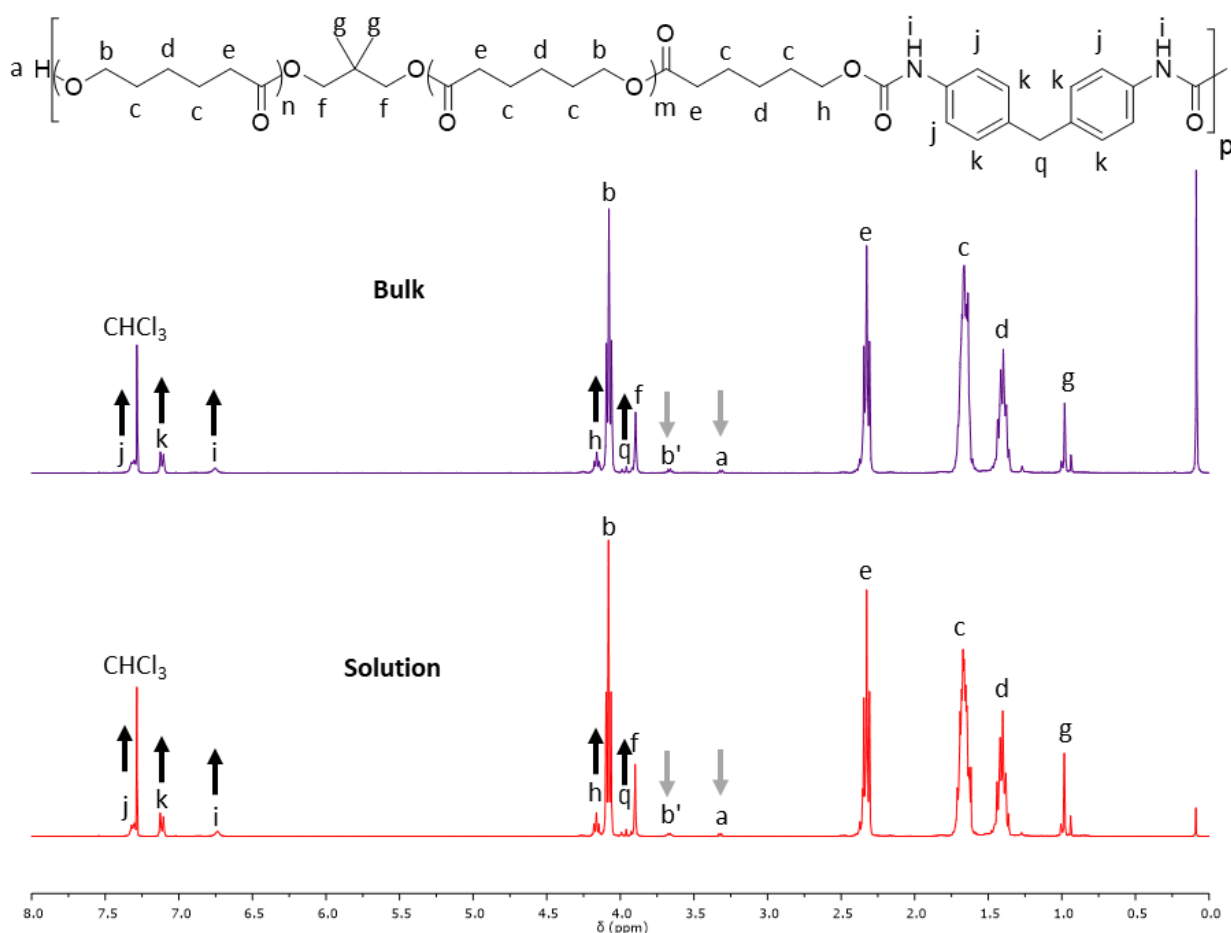


Figure 2.3 ^1H NMR spectra for copolymers prepared by bulk (**B3**) and solution (**S3**) processes, respectively. (400 MHz, 298 K, CDCl_3).

Molecular weight results *via* SEC follow the same trend typically observed in step-growth polymerisations, with an exponential increase as stoichiometry tends to 1.0 : 1.0 (**Figure 2.4**). Molecular weights are almost identical and independent of synthesis method at a given stoichiometry (**Table 2.3**).

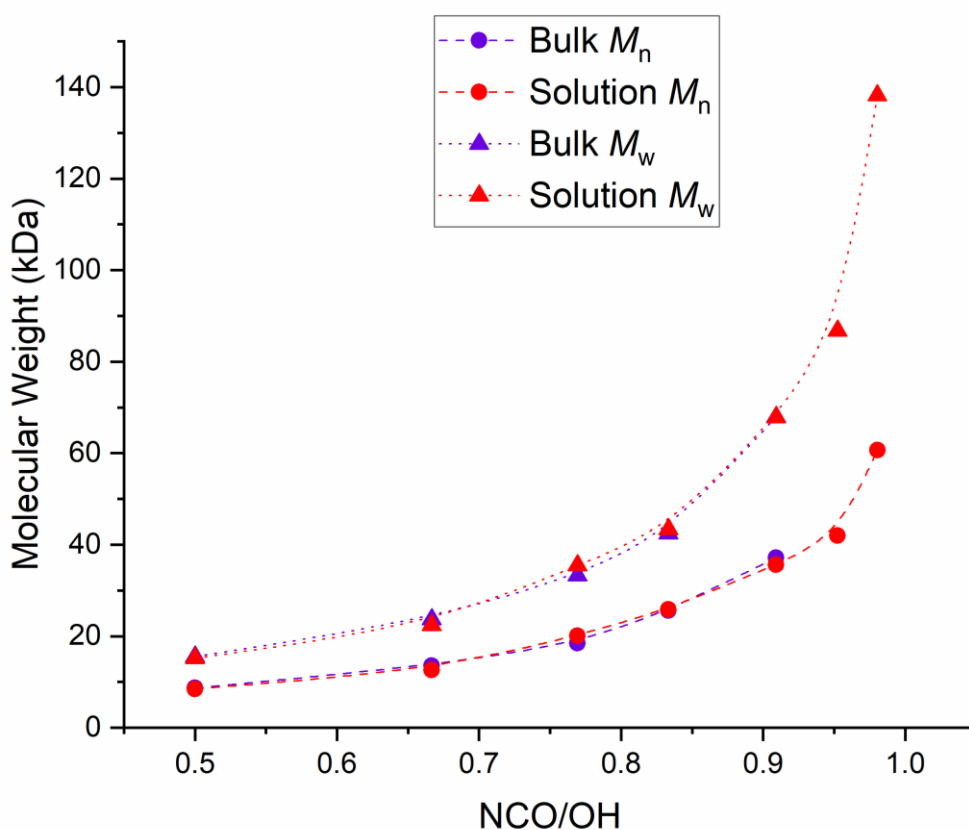


Figure 2.4 Changes in number average molecular weight (M_n) and weight average molecular weight (M_w) with stoichiometry of OH : NCO.

Significantly higher molecular weights are achievable *via* solution polymerisation (**Figure 2.4**). At a stoichiometry of 1.01 : 1.00 (OH : NCO), a TPU was formed with a number average molecular weight (M_n) of 60.7 kDa and a weight average molecular weight (M_w) of 138.2 kDa. The practical upper limit of the bulk process is approximately 1.10 : 1.00 (OH : NCO) (M_n = 37.2 and M_w = 68.0 kDa). Above this point mechanical stirring becomes too difficult due to high melt viscosity and there is the risk of equipment breaking. The product wraps around the

shaft of the anchor stirrer and climbs upwards. This movement can cause the whole reaction flask to twist free of its clamps and the glassware to shear open.

Table 2.3 Data from SEC experiments showing molecular weights and dispersity for series **B** and **S** made in bulk and solution, respectively.

Sample	NCO/OH	M_n^a (kDa)	M_w^a (kDa)	D_M^a
PCL	N/A	4.2	7.5	1.81
B1	0.50	8.7	15.6	1.79
B2	0.67	13.6	23.7	1.75
B3	0.77	18.5	33.3	1.80
B4	0.83	25.6	42.5	1.66
B5	0.91	37.2	68.0	1.83
S1	0.50	8.5	15.2	1.79
S2	0.67	12.6	22.5	1.79
S3	0.77	20.1	35.5	1.77
S4	0.83	22.0	41.1	1.87
S5	0.91	35.6	67.8	1.91
S6	0.95	42.0	86.8	2.07
S7	0.98	60.7	138.2	2.28

^a Determined by SEC in $CHCl_3$ against PMMA standards.

Qualitative analysis of the carbonyl region within the FTIR spectra of each copolymer indicates the extent of hydrogen bonding in each system and can improve understanding of PU morphology.¹⁰ The relative strength of the H-bond can be determined by the wavenumber at which the absorbance appears. Carbonyls involved in stronger H-bonds shift to lower wavenumbers, whereas weak and free carbonyls appear at higher wavenumbers. The carbonyls of urethane groups are typically present around $\nu_{max} = 1700 \text{ cm}^{-1}$, with free

urethane ranging $\nu_{\max} = 1730 - 1760 \text{ cm}^{-1}$ and H-bonded C=O urethane between $\nu_{\max} = 1680 - 1730 \text{ cm}^{-1}$.⁹

All materials show a peak absorption at $\nu_{\max} = 1720 \text{ cm}^{-1}$ corresponding to the ester carbonyl in PCL segments. Copolymerisation of PCL with MDI broadens the C=O absorbance as a consequence of the formation of urethane groups (**Figure 2.5(b) & (d)**).

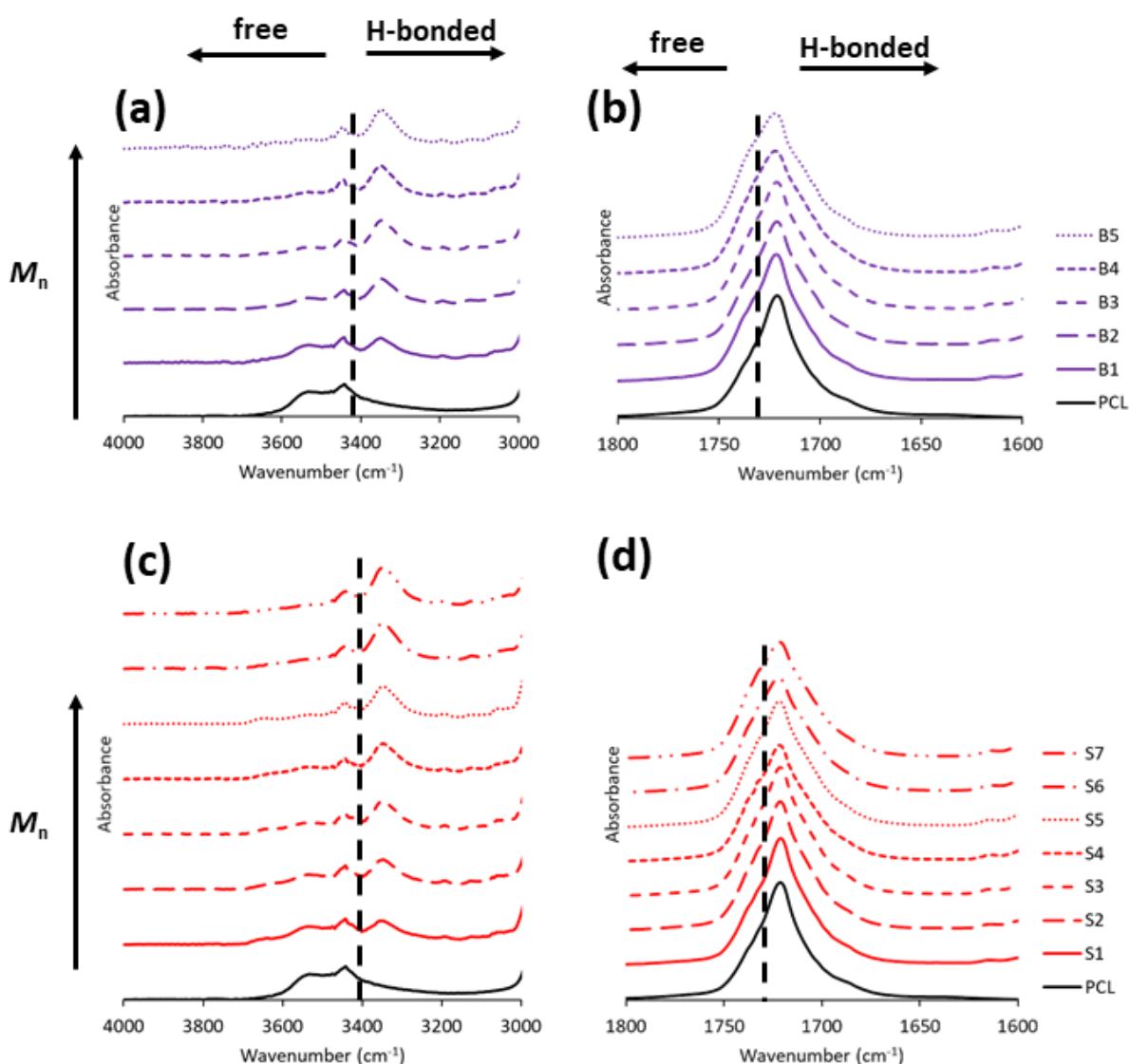


Figure 2.5 FTIR spectra of N-H regions for copolymers made in bulk **(a)** and solution **(b)** and C=O regions for copolymers made in bulk **(b)** and solution **(d)**. The black dashed lines mark the boundary between free and H-bonded C=O or N-H.

Noticeably, resonance shoulders begin to grow at $\nu_{\max} = 1730$ and 1710 cm^{-1} with an increase in molecular weight, resulting from free and H-bonded urethane, respectively. Increasing molecular weight increases the amount of urethane and therefore the amount of H-bonding as a consequence of the higher concentration of copolymerised MDI.

This effect is mirrored in the N-H region between $\nu_{\max} = 3400 - 3300 \text{ cm}^{-1}$, where copolymerisation and subsequent increasing molecular weight broadens the absorbance (**Figure 2.5(a) & (c)**). The band at $\nu_{\max} = 3442 \text{ cm}^{-1}$ caused by the OH end groups of the PCL diminishes and is replaced with an absorption at $\nu_{\max} = 3347 \text{ cm}^{-1}$ corresponding to urethane N-H. The intensities at $\nu_{\max} = 3347$ and 3442 cm^{-1} increase and decrease, respectively, with rising molecular weight as the OH end group concentration falls and the amount of urethane copolymerised increases.

These effects are identical for copolymers formed from both bulk and solution polymerisation, suggesting the amount of H-bonding is independent of the synthesis method (**Figure 2.5(b) vs (d) and (a) vs (c)**). Upon close inspection of the spectra, **S7** has the broadest C=O region as it is the copolymer with the highest molecular weight and so contains the largest quantities of urethane carbonyl groups.

Thermal properties of the TPU copolymers were determined *via* DSC (**Table 2.4**). Prior to analysis, all materials were heated to $70 \text{ }^{\circ}\text{C}$ for 4 hours to remove thermal history from the different methods of polymerisation and isolation. All copolymers were subjected to two heating cycles (-90 to $100 \text{ }^{\circ}\text{C}$), with a cooling cycle in between, at a rate of $10 \text{ }^{\circ}\text{C}\cdot\text{min}^{-1}$. Pure PCL exhibits a glass transition temperature (T_g) at $-67 \text{ }^{\circ}\text{C}$ which shifts to a higher temperature when copolymerised with MDI. Copolymerised MDI associates through physical interactions, such as H-bonding between urethanes and π - π stacking of the phenyl rings, to suppress chain

motion. Restriction of chain mobility requires more energy to overcome and subsequently a higher T_g . Values of T_g increase with molecular weight of TPU copolymer (**Figure 2.6**). This observation follows typical trends for polymers where a higher concentration of end groups, which is present in lower molecular weight copolymers, provides additional free volume for chain rotation and therefore lowers T_g . However, above approximately $M_n = 20.0$ kDa, T_g plateaus which is likely on account of negligible concentration of chain ends. This trend can be described by the Flory Fox equation:¹¹

$$T_g = T_{g,\infty} - \frac{K}{M_n}$$

Where $T_{g,\infty}$ is the maximum T_g obtainable from a theoretical infinite molecular weight and K is a parameter relating to free volume present.

Table 2.4 Thermal data of all polymers from initial heat cycle from DSC.

TPU	M_n^a (kDa)	T_g (°C)	T_m (°C)	ΔH_m (J.g ⁻¹)
PCL	4.2	-67	53	83
B1	8.7	-51	45	56
B2	13.6	-47	45	50
B3	18.5	-46	44	42
B4	25.6	-46	44	44
B5	37.2	-45	40	33
S1	8.5	-49	46	58
S2	12.6	-47	45	50
S3	20.1	-45	44	43
S4	22.0	-46	44	41
S5	35.6	-45	38	33
S6	42.0	-45	38 & 43	37
S7	60.7	-44	36 & 43	26

^a Determined by SEC in CHCl₃ against PMMA standards.

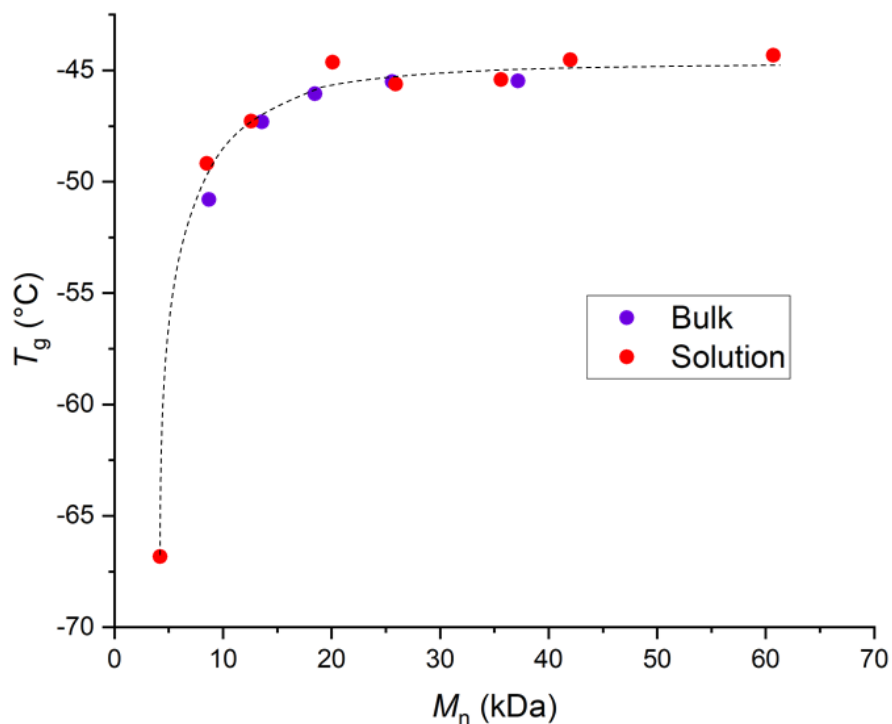


Figure 2.6 T_g from first heating cycles as a function of M_n for copolymers prepared via bulk and solution polymerisation.

A melting endotherm which appears at higher temperatures (36 – 53 °C) corresponds to PCL segment crystallinity (**Figure 2.7**). The melting temperature (T_m) decreases slightly after copolymerisation with MDI, which is a typical consequence of copolymerising units of different T_m in block copolymers.¹² Increasing molecular weight gradually decreases T_m implying that there is greater disruption of the crystalline phase, likely caused by greater entanglements within the amorphous interlayers which strains and hinders crystallisation.¹³ At the highest molecular weight (**S6 & S7**) there are two T_m recorded suggesting that the crystalline phase is polymorphic.¹⁴

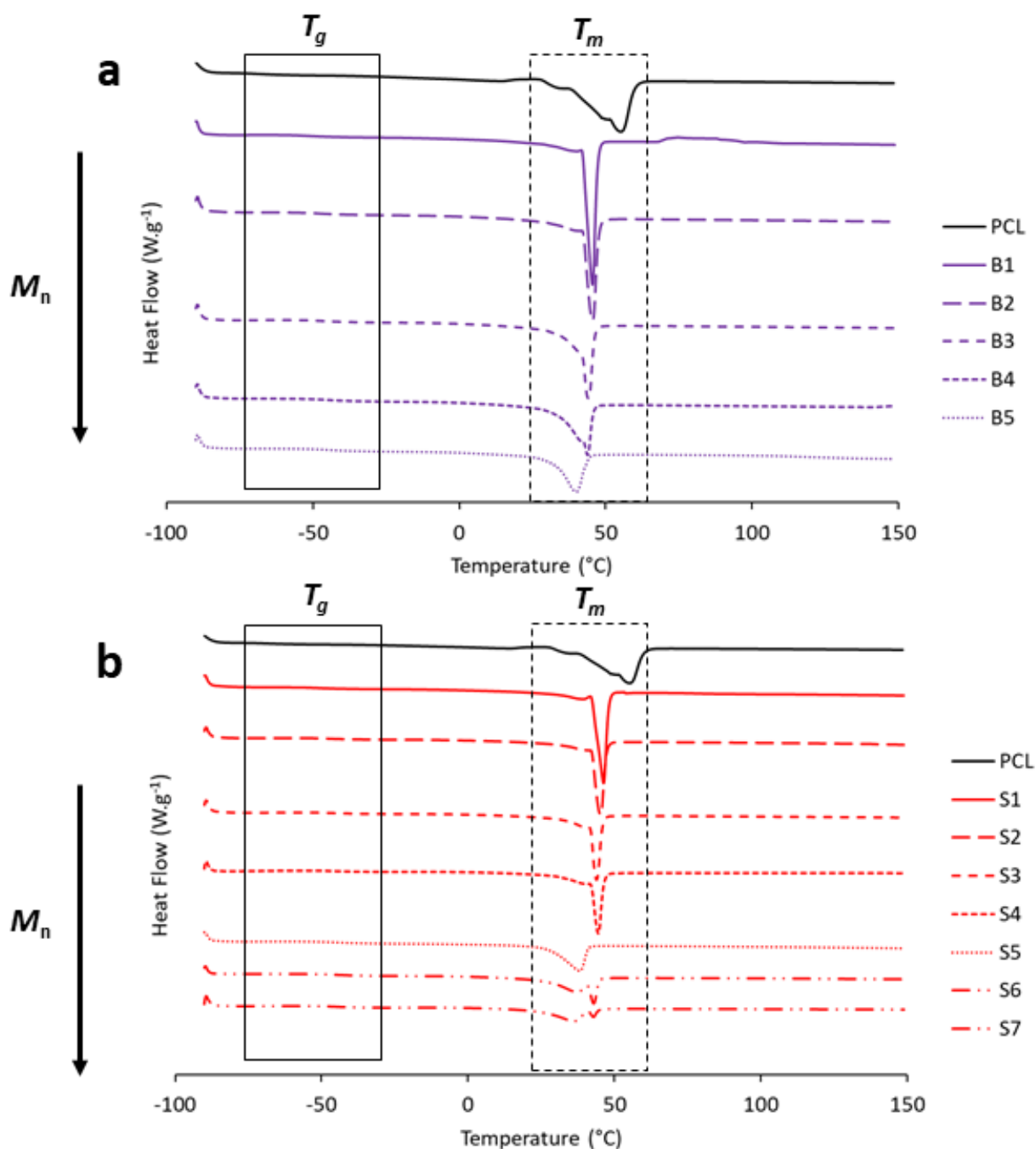


Figure 2.7 DSC thermograms of pure PCL and TPU copolymers of different M_n prepared in **(a)** bulk and **(b)** solution. Solid and dashed boxes surround regions of T_g and T_m , respectively. First heating cycles shown. Exo up.

The enthalpy of melting (ΔH_m) reduces substantially after incorporation of MDI (**Figure 2.8**).

This decrease is amplified by molecular weight, so at $M_n = 60.7$ kDa, ΔH_m is less than 31 % of pure PCL. Evidently, the MDI is disrupting order of PCL chains which decreases crystallinity.

This effect is not surprising as the crystallinity of PCL has previously been reported to be very sensitive to molecular weight of the accompanying block.¹⁵

The effects described above were seen in products of both bulk and solution polymerisations. DSC thermograms and values of T_g , T_m and ΔH_m appeared very similar for copolymers of similar molecular weight, regardless of polymerisation method (**Figure 2.7(a) vs (b)**).

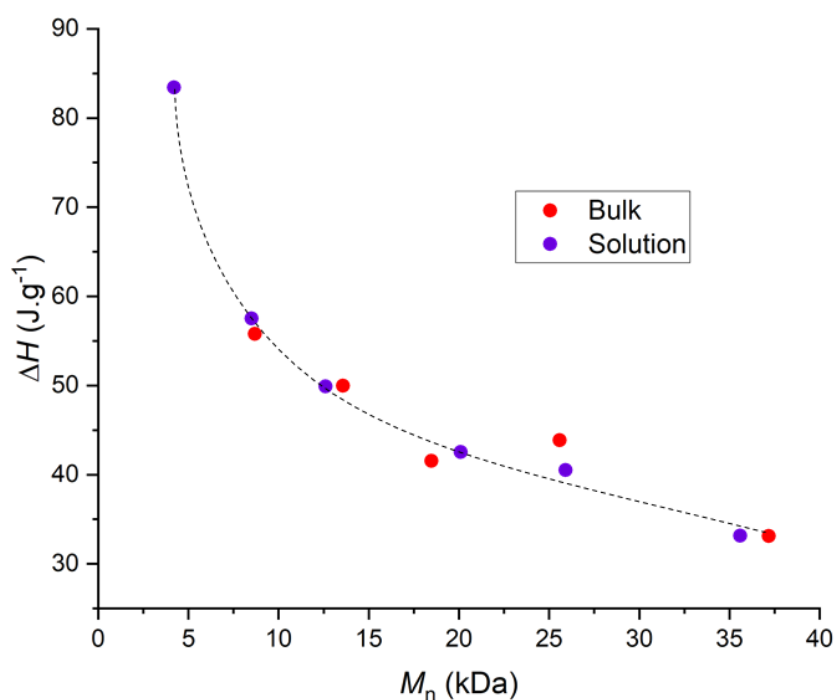


Figure 2.8 Enthalpy of melting as a function of M_n . Values are proportional to the degree of crystallinity of PCL.

2.2.3 Effect of PCL molecular weight on TPU copolymer properties

PCL was copolymerised with MDI *via* bulk polymerisation using both approximately 2.0 and 1.0 kDa polyols to create two series of copolymers with a range of molecular weights, comprising different PCL segment lengths (**Table 2.5**).

Table 2.5 SEC data for TPUs synthesised via bulk polymerisation with 2.0 kDa and 1.0 kDa PCL at varying stoichiometry.

Sample	PCL (kDa)	Molar Ratio		M_n^a (kDa)	M_w^a (kDa)	\mathcal{D}_M^a
		OH	NCO			
PCL	2.0	1.0	0.0	4.2	7.5	1.81
B1	2.0	2.0	1.0	8.7	15.6	1.79
B2	2.0	1.5	1.0	13.6	23.7	1.75
B3	2.0	1.3	1.0	18.5	33.3	1.80
B4	2.0	1.2	1.0	25.6	42.5	1.66
B5	2.0	1.1	1.0	37.2	68.0	1.83
PCLL	1.0	1.0	0.0	2.2	3.5	1.64
L1	1.0	2.0	1.0	4.9	8.9	1.81
L2	1.0	1.5	1.0	6.5	12.5	1.91
L3	1.0	1.3	1.0	8.0	15.6	1.94
L4	1.0	1.2	1.0	11.2	23.5	2.10
L5	1.0	1.1	1.0	15.6	33.4	2.10

^a Determined by SEC in CHCl_3 against PMMA standards.

Values of M_n and M_w for the pure polyols (**PCL** and **PCLL**) are approximately twice as high from SEC as expected, as a consequence of being close to the calibration limit of the SEC column and the difference between the standards used (polymethyl methacrylate (PMMA)) and the TPU copolymers.¹⁶ Upon copolymerisation with MDI, an increase in M_n and M_w is observed as OH : NCO molar equivalents tends to 1.0 : 1.0 for both series of TPUs. M_n varied from 4.9 to 15.6 kDa and 8.7 to 37.2 kDa for the copolymers comprising 1.0 and 2.0 kDa PCL, respectively. As expected, at a fixed value of OH : NCO, TPUs containing higher molecular weight PCL afford higher molecular weight products (**Figure 2.9**). An exponential increase in molecular weight is observed for both **L** and **B** series as the molar ratio of OH : NCO approaches 1.0 : 1.0, consistent with the expected step-growth mechanism. Higher molecular weight samples tend to show higher dispersity (\mathcal{D}_M), increasing from 1.8 to 2.1 (**Table 2.5**).

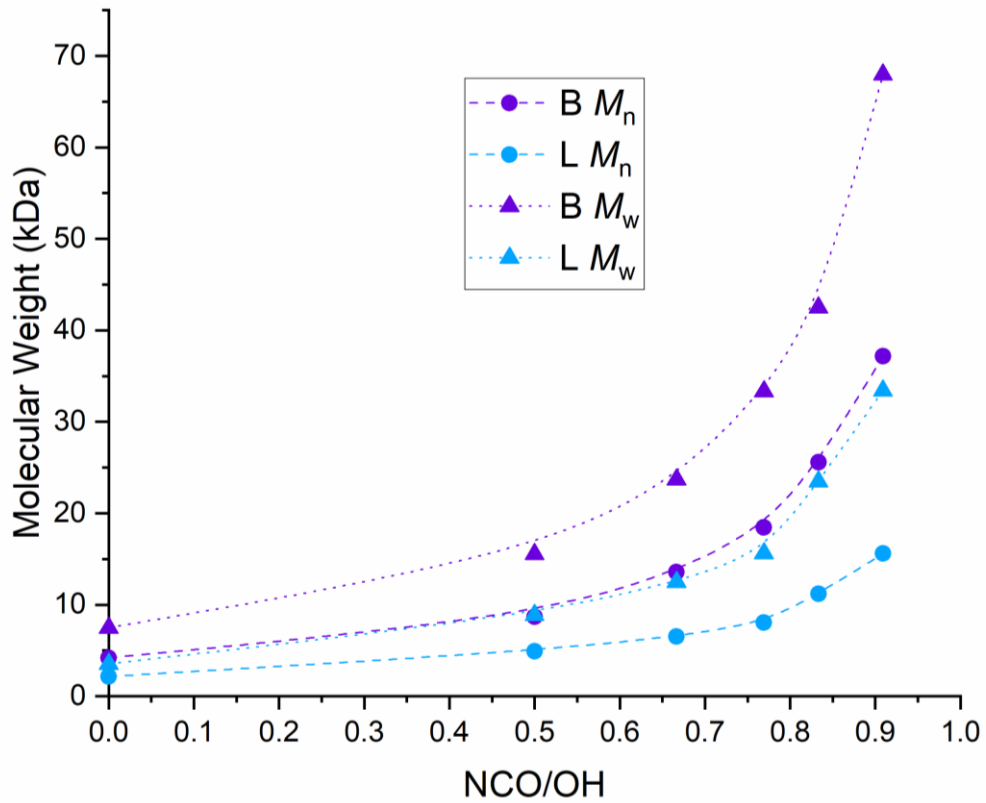


Figure 2.9 The effect of stoichiometry on molecular weight (M_n and M_w).

Before interpretation of analysis of the two series, it is important to note that the weight percent of MDI copolymerised ($wt\%_{MDI}$) in series **L** is higher than series **B** and both series increase in $wt\%_{MDI}$ as OH : NCO tends to 1.0 : 1.0. (**Figure 2.10**). The MDI content is known to have a marked influence on the properties of TPUs.¹⁷

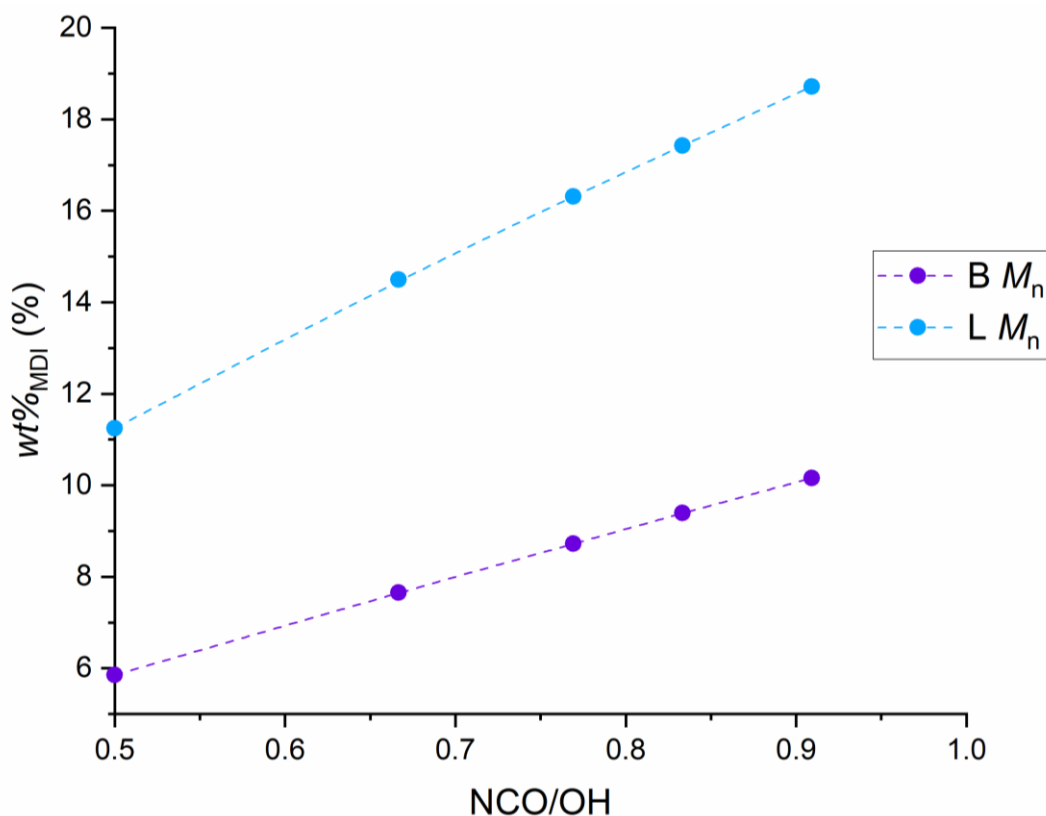


Figure 2.10 $wt\%_{MDI}$ as a function of NCO/OH for both series of different polyol molecular weight.

Inspection of the C=O and the N-H stretches in FTIR spectroscopy for all samples revealed differences in amount of H-bonding between copolymers with different PCL segment lengths (**Figure 2.11**). Both **PCLL** and **PCL** only show one absorption at $\nu_{max} = 1722 \text{ cm}^{-1}$ which is characteristic of free ester C=O (**Figure 2.11(b) & (d)**). The **L** series displays variation of the carbonyl stretch as OH : NCO tends to 1.0 : 1.0, notably the emergence of increasing urethane absorption at approximately $\nu_{max} = 1710 \text{ cm}^{-1}$. This shoulder grows in intensity as the molecular weight and therefore $wt\%_{MDI}$ increases. However, with the **B** series, there is only a slight and gradual broadening, implying a lower degree of H-bonding as fewer urethane groups are present (lower $wt\%_{MDI}$). Within the H-bonded N-H range, the N-H stretch for series **L** is larger than series **B** and at lower wavenumbers, between $\nu_{max} = 3345 - 3342 \text{ cm}^{-1}$ and ν_{max}

= 3347 – 3350 cm^{-1} , respectively. This data confirms observations of the C=O region that series L contains more H-bonding. (**Figure 2.11(a) & (c)**).

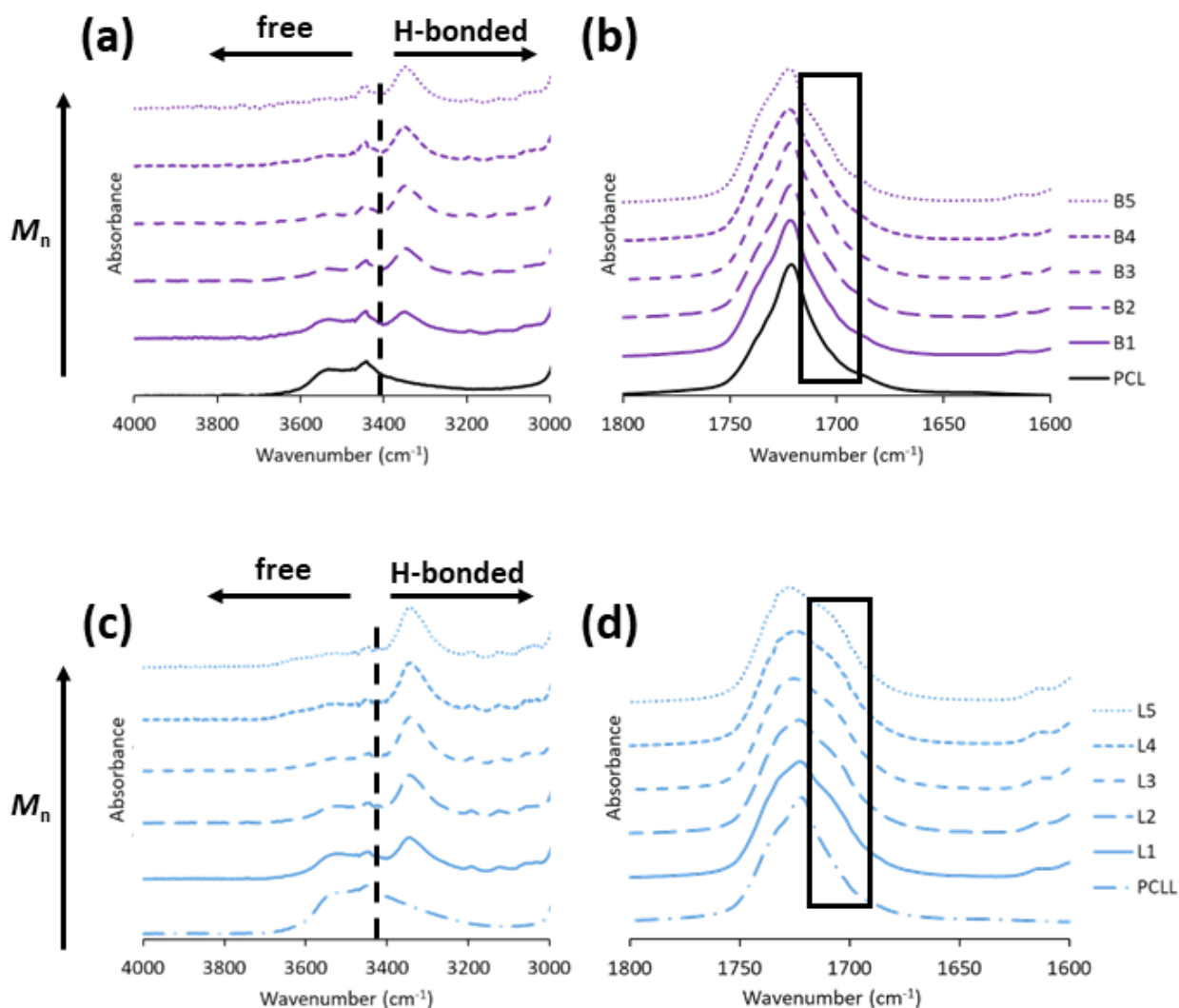


Figure 2.11 Spectra (a) and (c) are N-H regions for series B and L, respectively. Spectra (b) and (d) are C=O regions for series B and L, respectively. The black box shows H-bonded urethane carbonyl. The black dashed line marks the boundary between free and H-bonded N-H.

Analysis of the thermal properties of the TPU materials *via* DSC, determined that only one T_g is observed for all copolymers (**Table 2.6**). In the first heating cycle, the T_g of pure polyol PCL is $-76\text{ }^\circ\text{C}$ and $-67\text{ }^\circ\text{C}$ for molecular weights 1.0 and 2.0 kDa, respectively. PCL is higher than PCLL as a consequence of the lower number of end groups.¹¹ T_g increases after copolymerisation with MDI up to a molecular weight of 15.0 kDa (**Figure 2.12**). T_g increases

more as a function of molecular weight for series **L**, as it comprises a higher urethane concentration which hinders chain mobility.

Table 2.6 DSC thermal data of all copolymers for two heat cycles. Multiple melting peaks for one endotherm are written as 'first peak & second peak' and the enthalpy is total area of both peaks.

Sample	T_g		1st heating cycle		1st cooling cycle	2nd heating cycle	
	1 st heat	2 nd heat	T_m (°C)	ΔH_m (J.g ⁻¹)	ΔH_c (J.g ⁻¹)	T_m (°C)	ΔH_m (J.g ⁻¹)
PCL	-67	-67	53	83	71	44 & 48	72
B1	-52	-52	50	69	55	37 & 45	56
B2	-48	-49	49	61	36	34 & 44	52
B3	-47	-56	47	56	30	43	50
B4	-43	-54	46	52	34	41	43
B5	-44	-52	45	40	32	40	34
PCLL	-76	-72	36 & 41	49	54	26 & 36	53
L1	-48	-55	40	43	30	32	32
L2	-40	-46	33	33	-	34	0.44
L3	-35	-42	37	28	-	-	-
L4	-39	-39	-	-	-	-	-
L5	-34	-34	-	-	-	-	-

For most materials, endotherms are observed in the range of 33 to 53 °C, corresponding to the melting of crystalline PCL segments (**Figure 2.13(a) & (c)**).¹⁸ T_m and ΔH_m are higher for copolymers in series **B** made from the higher molecular weight PCL. All copolymers in the **B** series are crystalline but higher molecular weight copolymers in the **L** series are amorphous (**Figure 2.14**). For both **L** and **B** series, T_m decreases with an increase in molecular weight during the first heating run. Additionally, both series **L** and **B** show a decrease in ΔH_m with increasing molecular weight, indicating a decline in the degree of PCL crystallinity, resulting from increasing urethane content disrupting the organisation of PCL crystalline regions.¹⁸ Exotherms correlating to the recrystallisation of PCL chains are observed upon cooling to -

90 °C for many of the copolymers (**Table 2.6**). However, the recrystallisation of **L2-5** is beyond the limit of the experiments which indicates recrystallisation is a slow process for these materials. In all cases the enthalpy of crystallisation (ΔH_c) is less than ΔH_m during the first run, suggesting the PCL chains require more time than given in the experiment to fully recrystallise.

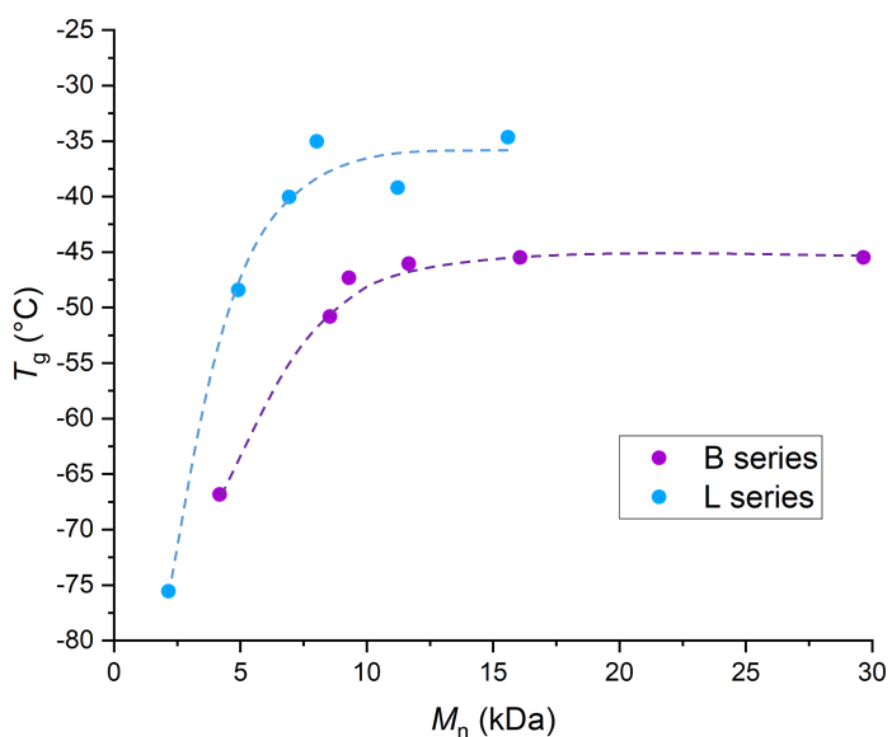


Figure 2.12 The effect of copolymer molecular weight on T_g for the **L** and **B** series (first heat run).

Melt endotherms in the second heat runs are significantly different to those of the first runs, especially for TPUs comprising PCL of 1.0 kDa (**Figure 2.14**). This change is likely a result of slow crystallisation and insufficient time for recrystallisation to occur during the timescale of the experiment.¹⁹ **PCL**, **B1** and **B2** show two T_m , implying there are two degrees of PCL order: a highly crystalline ($T_m > 44$ °C) and less ordered PCL chains ($T_m < 44$ °C).¹⁴ **B3**, **B4** & **B5** crystallise during the second heat run between T_g and T_m , likely as a result of higher molecular weight polymers slowing the kinetics of recrystallisation.¹³ The data shows that copolymers in the **L** series are much less crystalline during the second run due to the lower PCL segment length (**Figure 2.14**).

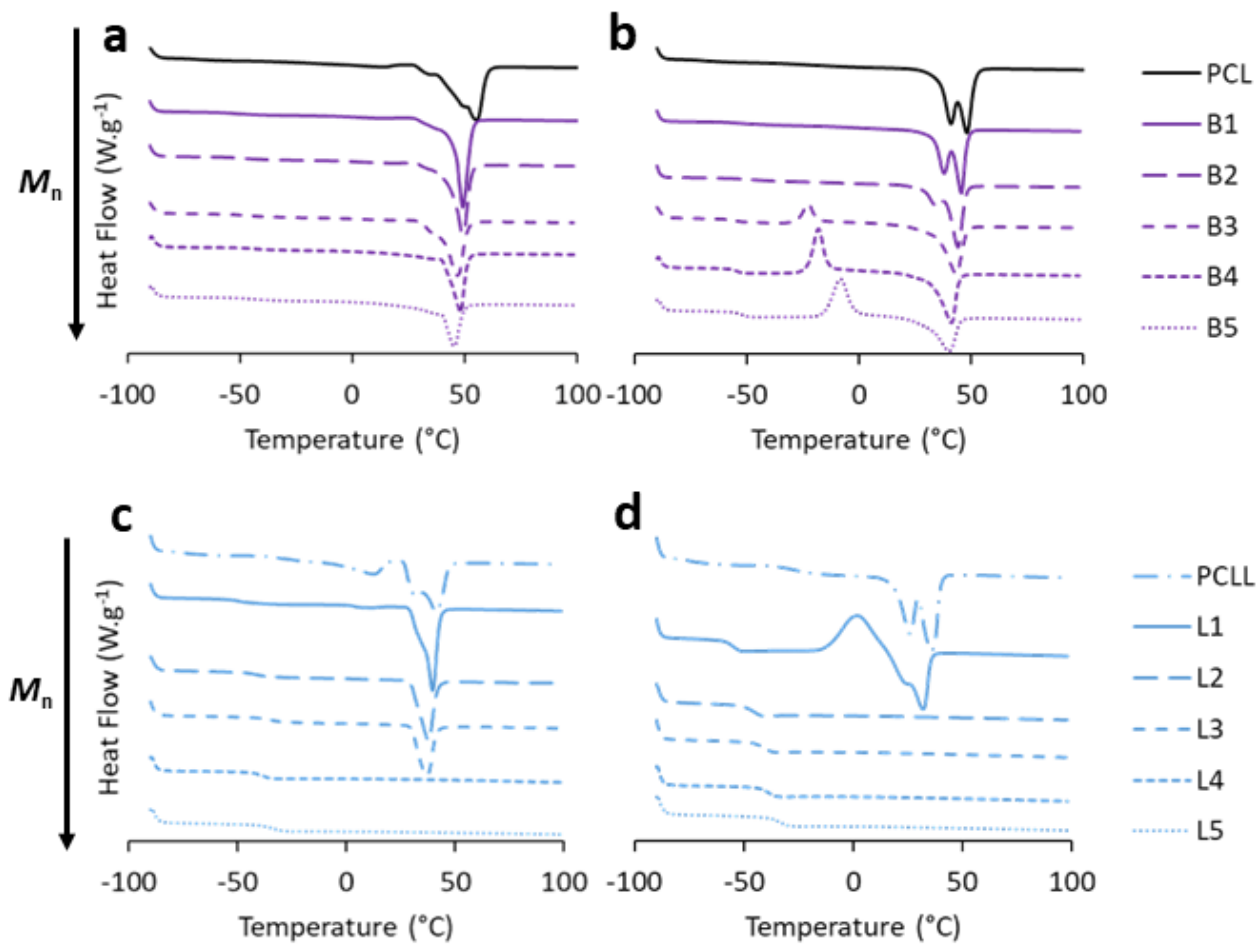


Figure 2.13 DSC thermograms of copolymers -90 to 100 °C (10 °C.min⁻¹). (a) and (b) and the first and second heating ramps, respectively, for series B. (c) and (d) are the first and second heating ramps, respectively, for series L. Exo up.

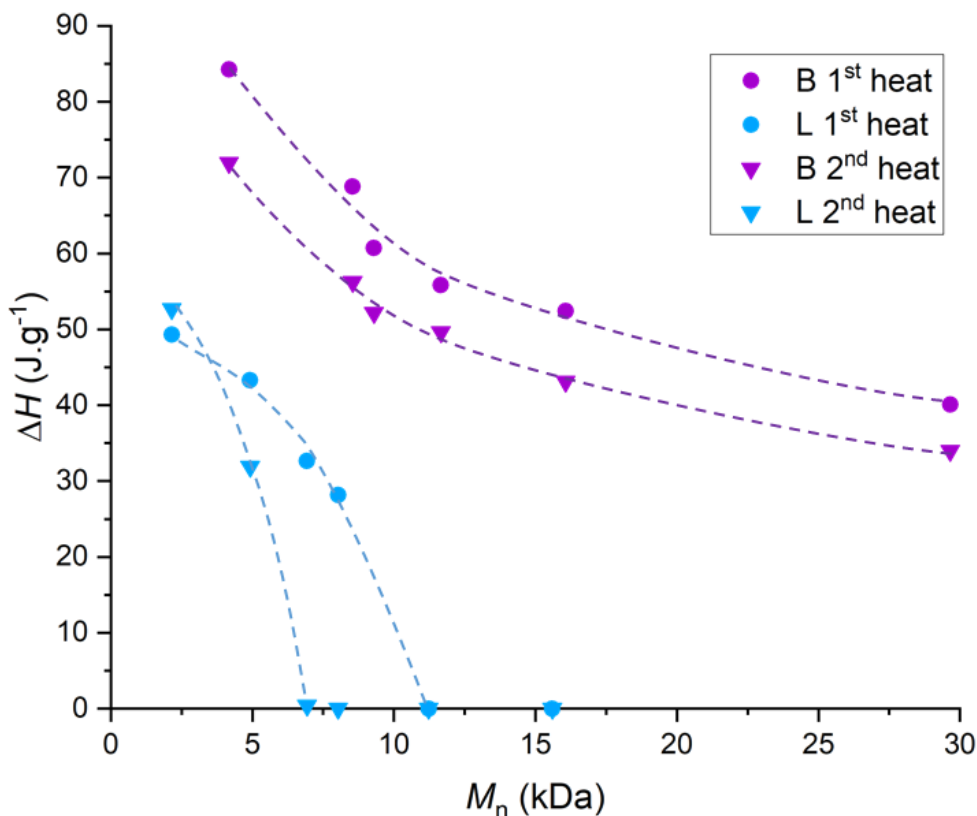


Figure 2.14 Change in enthalpy of melt as a function of M_n for both heat cycles. The initial data points in each series at the lowest M_n are for unincorporated PCL polyol (PCL and PCLL for **B** and **L** series, respectively).

2.3 Conclusion

TPU copolymers were synthesised using 2.0 kDa PCL diol and MDI without chain extender with varying OH : NCO stoichiometry. Successful copolymerisation was proven *via* ^1H NMR and FTIR spectroscopies and SEC analysis. Copolymerisation of PCL with MDI increased H-bonding and values of T_g , but decreased T_m and ΔH_m . This effect was enhanced by increasing copolymer molecular weight, up to approximately $M_n = 20.0$ kDa.

The effect of synthetic methodology employed was examined by comparing analogous copolymer products from bulk and solution polymerisations. Bulk copolymers were easier and safer to synthesise on a larger scale, however there is limit to obtainable molecular weights (1.00 : 1.10 for bulk vs 1.00 : 1.01 for solution). The solution route offered higher molecular weight copolymer products but required significantly more resources, time and precautions

due to safety concerns. Good consistency was observed between data obtained from bulk and solution copolymers, including NMR and FITR spectroscopies, SEC and DSC. Molecular weight, H-bonding and thermal properties were all determined to be independent of synthesis method, across a range of OH : NCO stoichiometries.

Another series of TPU was synthesised *via* bulk polymerisation using PCL of 1.0 kDa and MDI. Comparison with analogous copolymers made with 2.0 kDa PCL determined the influence of polyol molecular weight on TPU properties without chain extension. Copolymers made from 1.0 kDa PCL have a higher urethane content which increased H-bonding and influenced material thermal properties. The T_g of 1.0 kDa PCL increased significantly after copolymerisation with MDI. The ΔH_m was higher for 2.0 kDa PCL and resulting copolymers, with the crystallinity of 1.0 kDa PCL segments completely suppressed by incorporation of MDI above a M_n of 8.0 kDa.

2.4 Experimental

2.4.1 Materials

Capa™ 2100J and Capa™ 2200J were provided by Perstorp. 4,4'-methylenebis (phenyl isocyanate) (98 %), n-hexane (HPLC grade %) and chloroform-d (99.8 atom % D) were purchased from Sigma-Aldrich. Anhydrous toluene was obtained from a Grubbs purification system. All reagents were used as received.

2.4.2 Instrumental methods

Grubbs dry solvent service was used to obtain anhydrous toluene. This system involves the storage of solvents in a pressurised environment under an inert gas. The solvent is then passed through two filters which absorb any moisture from the solvent. **Proton (^1H) nuclear magnetic resonance (NMR)** spectra were recorded using a Bruker Avance 400 spectrometer

(400 MHz). Spectra were analysed on MestReNova v6.0.2. Samples were prepared in CDCl_3 as the solvent. All chemical shifts were recorded in parts per million (ppm) relative to a reference peak of chloroform solvent at $\delta = 7.26$ ppm. **Molecular weights and dispersities** were determined *via* size-exclusion chromatography (SEC) using an Agilent 1260 Infinity GPC system equipped with a refractive index detector. Two Agilent PL gel 5 μm Mixed-C columns and a guard column were connected in series and maintained at 35 °C. HPLC grade chloroform containing 0.25 % w/w TEA was used as the eluent and the flow rate was set at 1.0 mL.min⁻¹. The refractive index detector was used for calculation of molecular weights and dispersities by calibration using a series of near-monodisperse poly methyl methacrylate standards. Analysis was performed on Agilent GPC/ SEC software. **Attenuated Total Reflectance Fourier Transform Infrared (ATR-FTIR)** All FTIR spectra was collected on a PerkinElmer Spectrum Two instrument with a UATR Two accessory. Spectra were collected with 16 scans at a resolution of 1 cm⁻¹. Analysis was performed on PerkinElmer Spectrum software. **Differential scanning calorimetry (DSC)** was performed on a Discovery DSC 25 TA instrument. All runs were carried out under a nitrogen atmosphere with a rate of 10 °C.min⁻¹. Pre-weighed samples of 2 ± 1 mg in standard aluminium pans were loaded at 25 °C, cooled to -90 °C and heated to 150 °C, cooled again to -90 °C and finally reheated to 150 °C. T_g was taken as the midpoint of inflexion and T_m was measured as the temperature at the minimum heat flow of a melt endotherm. Analysis was performed on TRIOS v5.1.1 software.

2.4.3 General synthesis of PCL-MDI copolymers via bulk polymerisation

All bulk copolymers were synthesised in a similar method, a typical procedure was as follows: PCL (250 g, 0.25 mol for Capa™ 2100J/ 250 g, 0.12 mol for Capa™ 2200J) was loaded in to a 1 L flange flask equipped with a mechanical stirrer, thermometer and vacuum inlet at 80 °C and

once all molten, stirred under vacuum. After 1 hour, the vacuum was removed and a predetermined mass of flake MDI (based on stoichiometry) was added to the reaction at 110 °C with increased stirring speed for 15 minutes without vacuum and then 1 hour with vacuum. Reaction completion was determined by monitoring the disappearance of the isocyanate absorbance *via* FTIR spectroscopy. After reaction completion, the molten product was decanted and stored.

2.4.4 General synthesis of PCL-MDI copolymers via solution polymerisation.

All solution copolymers were synthesised in a similar method, a typical procedure was as follows: PCL (20 g, 0.01 mol) was loaded in to a 250 mL three-neck round-bottom flask equipped with a magnetic stirrer, thermometer and vacuum inlet, at 80 °C and once all molten, stirred under vacuum. After 1 hour, the vacuum was removed and replaced with a gentle nitrogen flow and the stopped was replaced with a reflux condenser. Anhydrous toluene (20 mL) was added followed by a predetermined mass of flake MDI (based on stoichiometry) at 110 °C with increased stirring speed. The reaction was left for one hour and the endpoint was determined by monitoring the disappearance of the isocyanate absorbance *via* FTIR spectroscopy. After reaction completion, the mixture was cooled to room temperature then precipitated dropwise in n-hexane (300 mL) cooled by liquid nitrogen and left for 12 hours. Residual solvent was removed with heat and vacuum (4 hours at 80 °C).

¹H NMR and ATR-FTIR spectra were similar for all copolymers.

¹H NMR (400 MHz, 298 K, CDCl₃): δ = 7.31 (d, J = 7.8 Hz, Ar), 7.12 (d, J = 8.3 Hz), 6.75 (s, NH), 4.16 (t, $^3J_{\text{H-H}}$ = 6.6 Hz, CH₂OC=ONH), 4.80 (t, $^3J_{\text{H-H}}$ = 6.7 Hz, CH₂OC=O), 3.99 (s, MDI CH₂Ar), 3.95 (s, NPG CH₂O), 3.92 (s, MDI CH₂Ar), 3.89 (s, NPG CH₂O), 3.66 (m, CH₂OH), 3.32 (d, J = 6.5 Hz,

OH), 2.33 (t, $^3J_{\text{H-H}} = 7.5$ Hz, $\text{CH}_2\text{C}=\text{OO}$), 0.97 (dd, $J = 18.9, 7.4$ Hz, NPG CH_3), 1.66 and 1.40 (all remaining hydrogens) ppm.

ATR-FTIR: $\nu_{\text{MAX}} = 3347$ (N-H), 2944 – 2864 (C-H), 1721 (C=O), 1598 (C-N), 1532 (Ar C=C), 1293, 1238 and 1161 (C-O) cm^{-1} .

SEC (CHCl_3): **B1** $M_n = 8.7$ kDa, $M_w = 15.6$ kDa, $\mathcal{D}_M = 1.79$; **B2** $M_n = 13.6$ kDa, $M_w = 23.7$ kDa, $\mathcal{D}_M = 1.75$; **B3** $M_n = 18.5$ kDa, $M_w = 33.3$ kDa, $\mathcal{D}_M = 1.80$; **B4** $M_n = 25.6$ kDa, $M_w = 42.5$ kDa, $\mathcal{D}_M = 1.66$; **B5** $M_n = 37.2$ kDa, $M_w = 68.0$ kDa, $\mathcal{D}_M = 1.83$; **S1** $M_n = 8.5$ kDa, $M_w = 15.2$ kDa, $\mathcal{D}_M = 1.79$; **S2** $M_n = 12.6$ kDa, $M_w = 22.5$ kDa, $\mathcal{D}_M = 1.79$; **S3** $M_n = 20.1$ kDa, $M_w = 35.5$ kDa, $\mathcal{D}_M = 1.77$; **S4** $M_n = 22.0$ kDa, $M_w = 41.1$ kDa, $\mathcal{D}_M = 1.87$, **S5** $M_n = 35.6$ kDa, $M_w = 67.8$ kDa, $\mathcal{D}_M = 1.91$; **S6** $M_n = 42.0$ kDa, $M_w = 86.8$ kDa, $\mathcal{D}_M = 2.07$, **S7** $M_n = 60.7$ kDa, $M_w = 138.2$ kDa, $\mathcal{D}_M = 2.28$; **L1** $M_n = 4.9$ kDa, $M_w = 8.9$ kDa, $\mathcal{D}_M = 1.81$; **L2** $M_n = 6.5$ kDa, $M_w = 12.5$ kDa, $\mathcal{D}_M = 1.91$; **L3** $M_n = 8.0$ kDa, $M_w = 15.6$ kDa, $\mathcal{D}_M = 1.94$; **L4** $M_n = 11.2$ kDa, $M_w = 23.5$ kDa, $\mathcal{D}_M = 2.10$; **L5** $M_n = 15.6$ kDa, $M_w = 33.4$ kDa, $\mathcal{D}_M = 2.10$.

2.5 References

1. R. Fiorio, V. Pistor, A. Zattera and C. Petzhold, *Polym. Eng. Sci.*, 2012, **52**, 1678-1684.
2. M. Sánchez-Adsuar, E. Papon and J. J. Villenave, *J. Appl. Polym. Sci.*, 2000, **76**, 1590-1595.
3. G. W. H. Höhne, W. Hemminger and H.-J. Flammersheim, *Differential Scanning Calorimetry An Introduction for Practitioners*, Springer, New York, 1996.
4. Y. Ikada and H. Tsuji, *Macromol. Rapid Comm.*, 2000, **21**, 117-132.
5. P. D. O. Coulembiera, J. L. Hedrickb and P. Dubois, *Prog. Polym. Sci.*, 2006, **31**, 723-747.

6. H. Yan, Z. Zhou, Y. Pan, T. Huang, H. Zhou, Q. Liu, H. Huang, Q. Zhang and W. Wang, *J. Macromol. Sci. B*, 2016, **55**, 839-848.
7. W. H. Carothers, *T. Faraday Soc.*, 1936, **32**, 39-49.
8. W.-K. Liu, Y. Zhao, R. Wang, F. Luo, J.-S. Li, J.-H. Li and H. Tan, *Chinese J. Polym. Sci.*, 2018, **36**, 514-520.
9. C. Tan, T. Tirri and C.-E. Wilen, *Polymers*, 2017, **9**, 184.
10. W. Li, A. J. Ryan and I. K. Meier, *Macromolecules*, 2002, **35**, 6306-6312.
11. T. G. Fox Jr and P. J. Flory, *J. Appl. Phys.*, 1950, **21**, 581-591.
12. J. M. G. Cowie, *Polymers: chemistry and physics of modern materials*, Stanley Thornes Ltd, Cheltenham, 1991.
13. M. Jenkins and K. Harrison, *Polym. Adv. Technol.*, 2006, **17**, 474-478.
14. M. A. Gorbunova, E. V. Komov, L. Y. Grunin, M. S. Ivanova, A. F. Abukaev, A. M. Imamutdinova, D. A. Ivanov and D. V. Anokhin, *Phys. Chem. Chem. Phys.*, 2022, **24**, 902-913.
15. L. Peponi, I. Navarro-Baena, J. E. Báez, J. M. Kenny and A. Marcos-Fernández, *Polymer*, 2012, **53**, 4561-4568.
16. S. Cakir, R. Kierkels and C. Koning, *J. Polym. Sci. A1*, 2011, **49**, 2823-2833.
17. K. Nakamae, T. Nishino and S. Asaoka, *Int. J. Adhes. Adhes.*, 1996, **16**, 233-239.
18. S. Mondal, *Polym. Int.*, 2006, **55**, 1013-1020.
19. W. Lei, C. Fang, X. Zhou, Y. Cheng, R. Yang and D. Liu, *Thermochim. Acta*, 2017, **653**, 116-125.

3 Synthesis and characterisation of thermoplastic polyurethanes with different chain extenders

3.1 Introduction

Thermoplastic polyurethanes (TPUs) are copolymers which are typically phase separated, containing soft and hard segments. The soft segment (SS) is typically an OH-terminated polyol of moderate molecular weight (500 – 5000 g.mol⁻¹).¹ The hard segment (HS) is made of low molecular weight diisocyanates and chain extenders. The diisocyanate and chain extender promote intermolecular interactions by forming H-bonds between adjacent polymer chains to give discrete hard domains, dispersed in the soft matrix.² These interactions can be reversed with a stimulus, such as heat or solvent, and then reformed with subsequent removal of the stimulus which allows for material recycling and reprocessing. The association of the HS provides rigidity and strength to the TPU by acting as physical crosslinks within the SS matrix. The chain extender can have a marked influence on the type and degree of interactions within the HS which in turn affects the relationship between the soft and hard phases.³ The interplay between the soft and hard phases determines the thermal and mechanical properties of the TPU copolymer. Therefore, the chain extender can greatly affect the final properties of the material.

Chain extenders are most commonly OH- or primary NH-terminated short chain molecules that react with isocyanates to form urethane and urea functionalities, respectively. The chain extender used mostly for industrial applications is 1,4-butanediol (BD), which has been shown to assist the formation of strong hydrogen bonds in hard segments comprising MDI as a result of geometrically favourable interactions.⁴ H-bonding promotes hard segment association and phase separation resulting in improved mechanical properties for TPUs in performance-based applications. However, when reprocessing above the service temperature of the material, the strong hard segment interactions often persist in the melt phase. Therefore, TPU copolymers

made with BD require high temperatures and shear rates to flow adequately.⁵ Typically, extrusion processes are necessary which increases cost and limits the practical use of these materials as conventional adhesives, where low melt viscosity is typically required for adequate substrate wetting. Therefore, an alternative TPU design is required which allows low melt viscosity at high temperature but where high cohesion is obtained at low temperature.

Chain extenders can vary in chain length, number of branches, length of branches and functionality.^{2, 4, 6-10} Previous work demonstrated that even carbon chain lengths provide more H-bonding and therefore increased microphase separation and mechanical properties.⁴ Non-linear (*i.e.* branched) chain extenders have also been explored, showing a significant influence on the glass transition temperature (T_g) of the SS. Branching on an even carbon backbone was reported to have a comparable influence to odd carbon chain numbers in the backbone.¹¹ Higher symmetry of the chain extender has also been reported as improving HS packing.⁹ Amine groups have been shown to improve compatibility of the chain extender with the HS on account of similar polarities.¹⁰

Amine functionalised CEs are used to form poly(urethane urea)s (PUUs) which are typically used for high performance applications. The enhanced mechanical performance is granted by increased phase separation driven by the association of urea groups *via* stable bidentate H-bonding.¹²⁻¹⁴ A study by Kalajahi *et al.* showed how using an amine-terminated CE based on a cycloaliphatic ring increased chain stiffness which proved greater phase separation and therefore improved mechanical performance for poly(caprolactone) (PCL) based TPU copolymers.¹⁵ However, the strong association of the urea groups restricts chain mobility which leads to very high melt viscosity and poor self-healing properties.^{16, 17} Therefore, it is

almost practically impossible to synthesis PUUs *via* bulk polymerisation. Moreover, the urea groups are less thermally stable relative to urethane analogues which limits their use for high temperature applications.^{18,19}

Previous work has investigated bisurea functionality for enhanced H-bonding interactions. Proximity of urea groups to phenyl rings affords strong H-bonding, but at the cost of a very high melting temperature (T_m) and viscosity which is a result of the formation of long rigid fibrillar species.²⁰⁻²² To overcome these issues, Melia *et al.* studied asymmetrical bisureas used in PUs which were seen to arrange into highly ordered structures.²³ However, the T_m of these materials were still higher than the typical processing temperatures of TPUs.

While previous work gives a good basis for understanding the effect chain extenders have on copolymer properties, few studies directly compare a range of structural changes in the chain extender for one type of TPU copolymer, where the polyol and diisocyanate are fixed. Additionally, exploring the effects chain extenders have on thermal reversibility would provide a new perspective.

This work aims to investigate the effect of different chain extender compositions on the thermal, rheological and mechanical properties of TPU copolymers. We seek to explore if controlling the intermolecular forces can differentiate between low melt viscosity at high temperature and high cohesion at lower temperature. Three different chain extenders are studied in order to explore the effects of symmetry, branching and intermolecular forces.

3.2 Results and discussion

3.2.1 Synthesis of copolymers and molecular architecture

A series of TPU copolymers were polymerised using PCL and MDI and one of three different chain extenders. PCL and MDI are both commonly used monomers in TPU polymerisations, as a consequence of MDI forming strong hydrogen bonds in the HS and the semi-crystallinity of PCL offering good flexibility in the typical working temperature range for TPUs.²⁴ The chain extenders evaluated were 1,4-butanediol (BD), 1,2-propanediol (PD) and a novel bisureadiol (BU) (**Figure 3.1**). BD is highly symmetrical and a solid below 16 °C, whereas PD is a branched diol which is a liquid at room temperature ($T_m = -59$ °C) comprising primary and secondary alcohol groups. BU is a symmetrical diol containing two urea groups, previously reported as a crystalline solid with a T_m of 121 °C.²⁵ Bisureas tend to be highly crystalline materials with high melting points, this material was deliberately chosen due to its relatively low crystallinity and low melting point.²³ A series of three copolymers of PCL and MDI with these different chain extenders were synthesised and compared to a copolymer of PCL (2.0 kDa) and MDI without chain extender (**B3**), in order to directly evaluate the effect of the chain extender (**Table 3.1**).

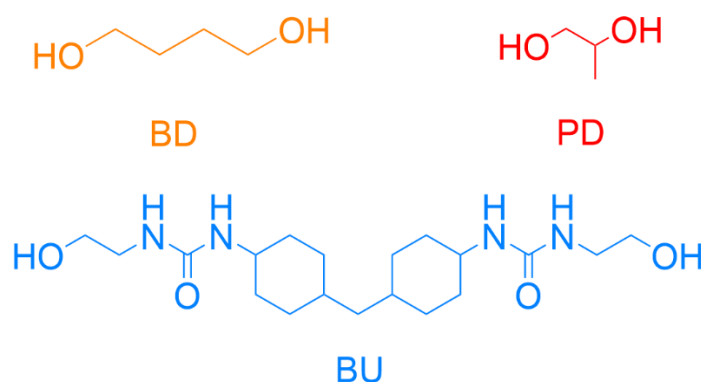


Figure 3.1 The three different CEs used, BD, PD and BU.

Table 3.1 TPU copolymers synthesised using different chain extenders compared to the PCL-MDI copolymer without chain extender. PCL ($M_n = 2.0$ kDa).

Copolymer	Molar Ratio ^b			CE	wt% _{HS}	M_n^d (kDa)	M_w^d (kDa)	\mathcal{D}_M^d
	PCL	MDI	CE					
B3	1.3	1.0	-	-	9 ^c	18.5	33.3	1.78
D1	1.0	2.0	1.3	BD	23	18.8	36.0	1.92
P1	1.0	2.0	1.3	PD	23	18.1	36.2	2.00
U1^a	1.0	2.0	1.3	BU	33	17.3	39.1	2.26

^a Made via solution polymerisation, all other copolymers were prepared in bulk

^b Molar ratio of functional groups

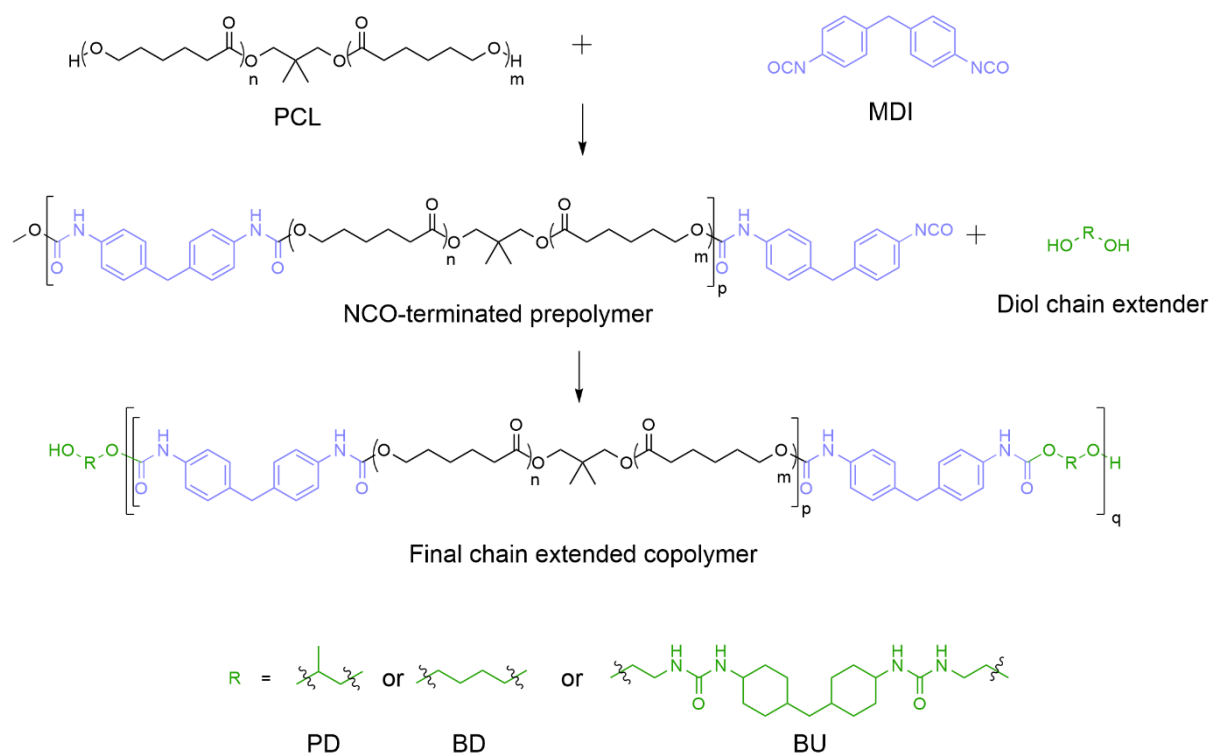
^c No HS is present in **B3**, therefore wt%_{HS} is taken as wt%_{MDI}

^d Determined by SEC in CHCl₃ against PMMA standards, except **U1** which was in DMF against PMMA standards

Copolymers incorporating BD and PD (**D1** and **P1**, respectively) were synthesised *via* bulk polymerisation, whereas the BU copolymer (**U1**) was synthesised in DMF on account of relatively high melt viscosity at the reaction temperature. Firstly, MDI was copolymerised with PCL at 2.0 : 1.0 molar equivalence to form an NCO-terminated prepolymer. The diol chain extender was then added to the prepolymer in excess to form an OH-terminated copolymer to prevent permanent crosslinking from further reactions of free NCO groups (**Scheme 3.1**).

¹H NMR spectroscopy proved successful incorporation of all chain extenders into the PCL-MDI prepolymer. Proton resonances corresponding to the chain extender methylene adjacent to the urethane oxygen atoms appear at $\delta = 4.20$, 4.23 and 3.39 ppm for **D1**, **P1** and **U1**, respectively.

Size exclusion chromatography (SEC) results show that copolymers were synthesised within the same molecular weight range (both in terms of M_n and M_w), independent of chain extender. All samples were evaluated in a CHCl₃ eluent, except for **U1** which is only soluble in DMF.



Scheme 3.1 Stepwise synthesis route from PCL and MDI to chain extended prepolymer via an NCO terminated intermediate.

The weight percent of hard segment ($wt\%_{\text{HS}}$) was calculated for the four copolymers analysed, which is determined by the mass of reagents added into the polymerisation and has a dramatic effect on final TPU properties.²⁶ $wt\%_{\text{HS}}$ was calculated for all samples based on the work of Tsou *et al.*:²⁷

$$wt\%_{\text{HS}} = \frac{(wt_{\text{MDI}} + wt_{\text{CE}})}{(wt_{\text{MDI}} + wt_{\text{CE}} + wt_{\text{PCL}})} \times 100 \quad (3.1)$$

$$wt\%_{\text{SS}} = 100 - wt\%_{\text{HS}} \quad (3.2)$$

The mass of reagents added to the reaction flask is defined as wt_{MDI} , wt_{CE} and wt_{PCL} for mass of MDI, chain extender and PCL, respectively. The HS consists of MDI and chain extender

which can potentially form intermolecular interactions to increase physical properties. PCL is the sole contributor to the SS and its weight contribution is labelled as $wt\%_{SS}$ (**3.2**).

To obtain materials with the same M_n , different hard segment contents were unavoidable due to the differences in chain extender molecular weights. The value of $wt\%_{HS}$ increases in the order **B3** < **P1** = **D1** < **U1** (**Table 3.1**). **U1** is therefore expected to have higher mechanical properties as a consequence of having the highest $wt\%_{HS}$.

FTIR spectroscopy was used to gain understanding on how the chain extender influences the physical interactions within the copolymers as the carbonyl region provides qualitative information on the type and strength of H-bonding. FTIR spectroscopy was performed on bulk materials at ambient temperature and the carbonyl region analysed in detail (**Figure 3.2**).

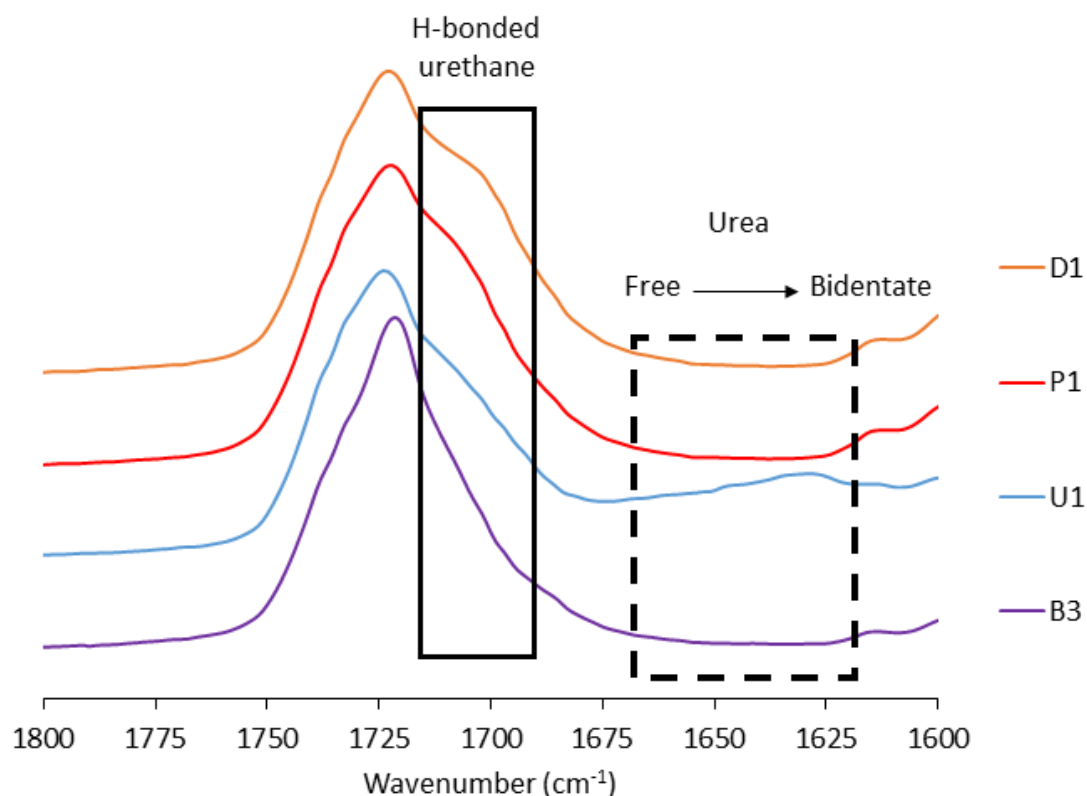


Figure 3.2 FTIR spectra of the carbonyl region of the four copolymers. The solid black box highlights absorbance due to H-bonded urethane and the dashed black box indicates urea functionality.

The most dominant absorbance at $\nu_{\max} = 1720 \text{ cm}^{-1}$ relates to the ester carbonyl in the backbone of the PCL SS. The shoulder at approximately $\nu_{\max} = 1710 \text{ cm}^{-1}$ corresponds to H-bonded urethane (**Figure 3.3(a)**), with the relative intensities increasing in the order **B3** < **U1** < **P1** < **D1**. This order shows that **D1** has the most H-bonded urethane on account of the favourable packing abilities of BD. The shoulder is less intense with **P1** because of the steric hindrance of the pendent methyl group in PD which hinders urethane-urethane interactions. While the intensity of absorption at $\nu_{\max} = 1710 \text{ cm}^{-1}$ is low in **U1**, there is significant absorption between $\nu_{\max} = 1650$ and 1620 cm^{-1} , associated with the urea functionality.²⁸ Therefore, **U1** has apparently few urethane interactions, but significantly more urea H-bonding which can either be mono- or bi-dentate (**Figure 3.3(b) & (c)**). The lower wavenumber is indicative of stronger interactions.

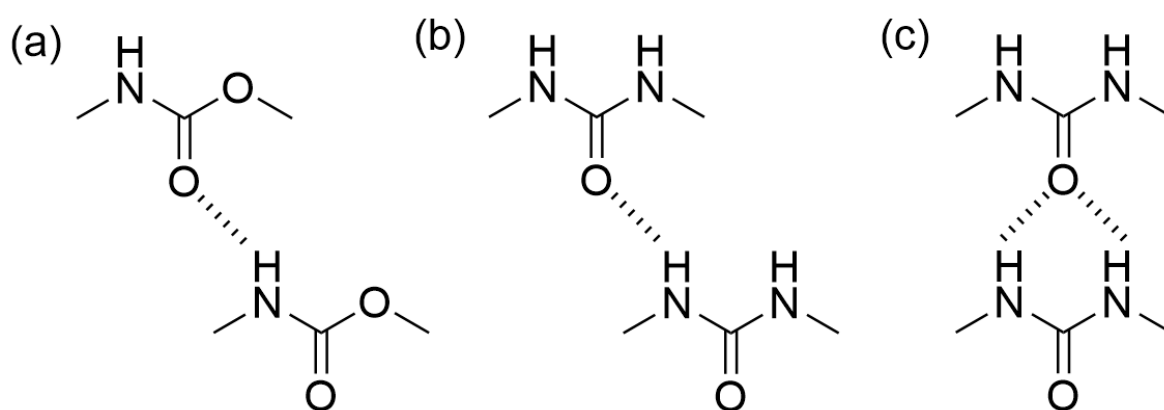


Figure 3.3 The different types of H-bonding present in the copolymers studied: **(a)** urethane, **(b)** monodentate urea and **(c)** bidentate urea.

3.2.2 Thermal Properties

The thermal properties of the copolymers were investigated *via* differential scanning calorimetry (DSC) between -90 and $150 \text{ }^\circ\text{C}$ (**Table 3.2**). The glass transition temperature of the soft segment ($T_{g(SS)}$) increases in the order **B3** < **U1** < **D1** << **P1**. **D1** and **U1** display very similar values of $T_{g(SS)}$ to **B3** without chain extender (-47 , -44 and $-46 \text{ }^\circ\text{C}$, respectively). Since **B3** does

not contain a hard segment, these results indicate that the copolymerised BU and BD chain extenders have minimal interaction with the SS which implies **D1** and **U1** are phase separated copolymers. **P1** has the highest $T_{g(SS)}$ at $-30\text{ }^{\circ}\text{C}$ as a consequence of the pendent methyl group hindering mobility and therefore requiring more energy to induce chain motion.

Table 3.2 Thermal data obtained via DSC. Values taken from initial heating runs ($-90\text{ }^{\circ}\text{C}$ to $150\text{ }^{\circ}\text{C}$ at $10\text{ }^{\circ}\text{C}\cdot\text{min}^{-1}$).

Copolymer	$T_{g(SS)}$ ($^{\circ}\text{C}$)	$T_{m(SS)}$ ($^{\circ}\text{C}$)	$\Delta H_{(SS)}$ ($\text{J}\cdot\text{g}^{-1}$)	$T_{m(HS)}$ ($^{\circ}\text{C}$)	$\Delta H_{(HS)}$ ($\text{J}\cdot\text{g}^{-1}$)	$T_{g(HS)}$ ($^{\circ}\text{C}$)
B3	-47	47	56	- ^a	- ^a	- ^b
D1	-44	35 & 45	19	107	3	- ^b
P1	-30	35 & 43	21	- ^a	- ^a	- ^b
U1	-46	48	24	- ^a	- ^a	129

^a No HS melt detected

^b No HS glass transition detected

All samples exhibit a melting endotherm between 30 and $50\text{ }^{\circ}\text{C}$, corresponding to crystallinity in the PCL SS. Compared to **B3**, the enthalpy of melting of the soft segment ($\Delta H_{(SS)}$) ($56\text{ J}\cdot\text{g}^{-1}$) decreases when copolymerised with the three chain extenders. The $\Delta H_{(SS)}$ for **U1** is the highest amongst TPUs copolymerised with CE at $24\text{ J}\cdot\text{g}^{-1}$. Amine-terminated CEs have previously been reported as showing higher PCL crystallinity relative to urethane analogues on account of greater phase separation.¹⁷ $T_{m(SS)}$ of **U1** ($48\text{ }^{\circ}\text{C}$) is very similar to **B3** ($47\text{ }^{\circ}\text{C}$), reaffirming the theory that BU has little interaction with the SS. The thermograms for **P1** and **D1** are more complex, with two distinct $T_{m(SS)}$ visible, especially in the **P1** thermogram at 35 and $43\text{ }^{\circ}\text{C}$ (**Figure 3.4(a)**). This duality suggests polymorphic PCL with regions of lower and higher PCL regularity. Disruption of PCL packing by PD is the likely cause of the double-melting point behaviour.

There are no other transitions observed for **B3** and **P1**. However, **D1** and **U1** differ by displaying a third feature which appears above $100\text{ }^{\circ}\text{C}$ (**Figure 3.4(b)**). **D1** shows a melting point ($T_{m(HS)}$) at $107\text{ }^{\circ}\text{C}$ and **U1** shows a second glass transition temperature ($T_{g(HS)}$) at $129\text{ }^{\circ}\text{C}$.

Since these features appear well above $T_{m(SS)}$, they imply a phase separated morphology of discrete HS and SS domains. The melting point in **D1** likely corresponds to a crystalline hard segment made of well-ordered BD and MDI units.⁷ Such a transition occurs in high molecular weight commercially available TPUs with the same hard segment. The $T_{g(HS)}$ in **U1** is very close to the T_m of molecular BU (121 °C) and therefore suggestive of partial order of polar urea moieties associating together, separated from the relatively non-polar PCL SS.²⁵

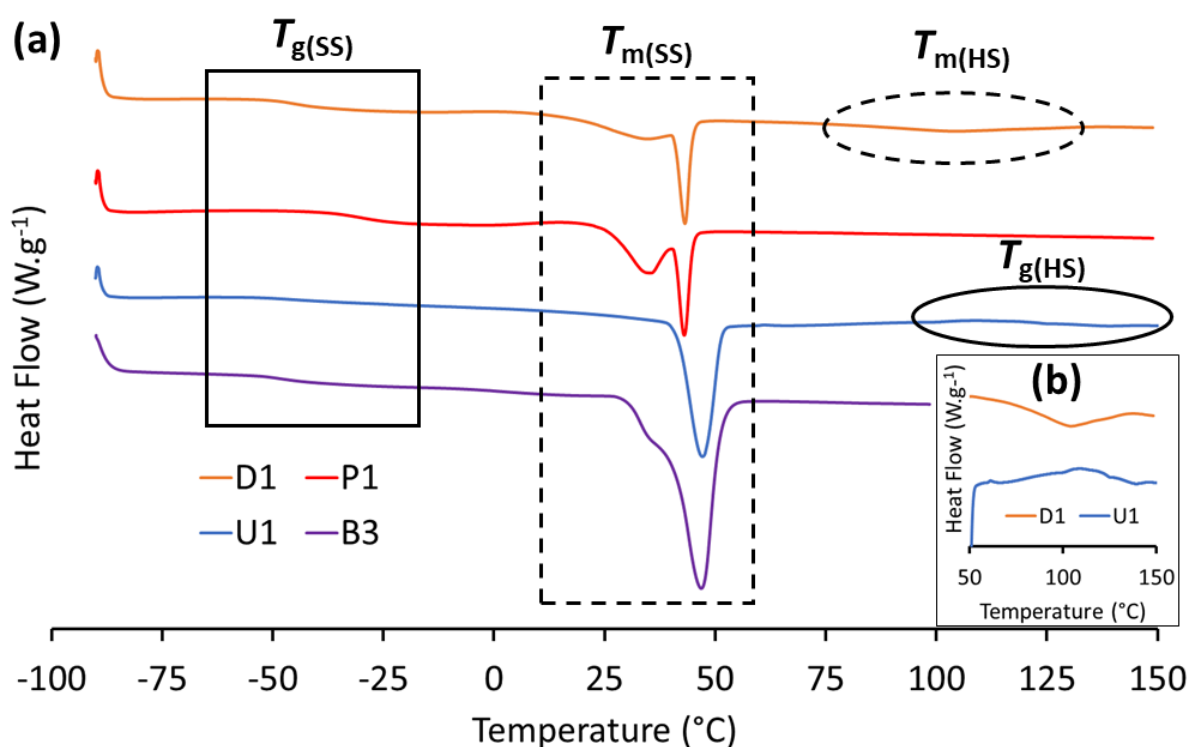


Figure 3.4 (a) DSC thermograms of the four copolymers studied. Boxes highlight SS transitions and ovals indicate the transitions of the HS. **(b)** Close up of HS transitions. First heating cycles used at a heating rate of 10 °C.min⁻¹. Exo up.

Dynamic mechanical analysis (DMA) was performed on all copolymers, consisting of heating a solid bar sample from -80 to 150 °C at 3 °C.min⁻¹ (**Figure 3.5**). In each case, storage modulus (E') decreases as a function of temperature, which is typical for a thermoplastic material. **B3** and **U1** show the highest value of E' below T_g on account of higher quantity of crystalline PCL segments and substantial H-bonding, respectively (**Table 3.3**).

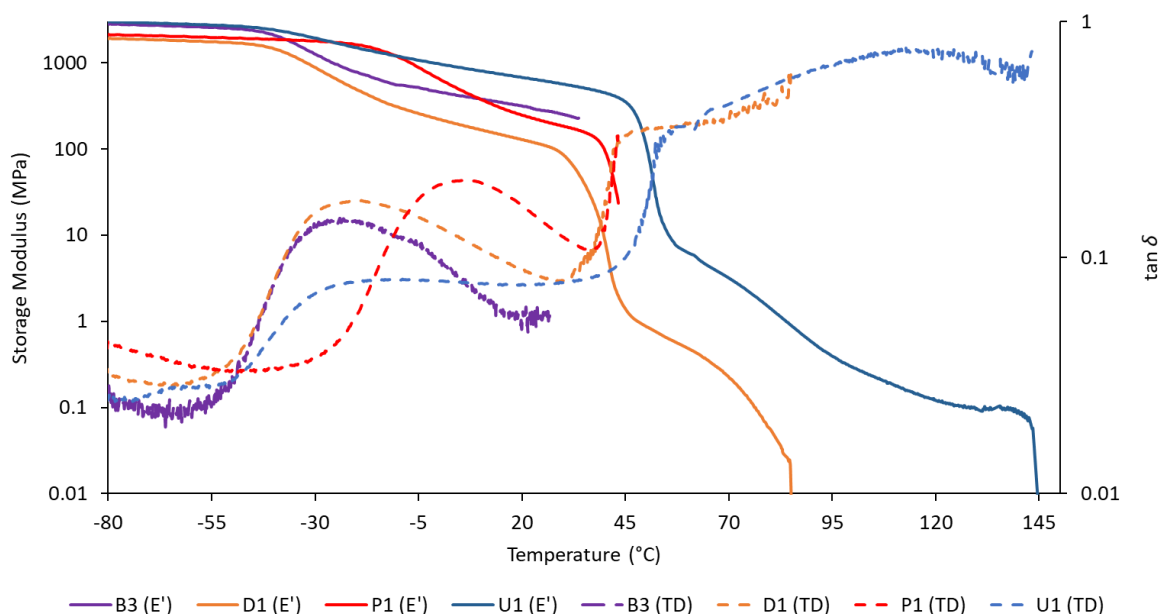


Figure 3.5 DMA results showing the effect of temperature on storage modulus (left y-axis) and $\tan \delta$ (right y-axis) for all copolymer samples. Heating rate of $3\text{ }^{\circ}\text{C}\cdot\text{min}^{-1}$.

E' decreases by an order of magnitude above T_g for all copolymers, corresponding to main chain relaxation. The peak in $\tan \delta$ corresponding to T_g of **P1** is significantly higher than that of the other materials, confirming the observations *via* DSC. All copolymers show a rubbery plateau at temperatures above T_g , which is common of elastomeric materials. **U1** has the highest storage modulus at $20\text{ }^{\circ}\text{C}$ of 570 MPa, likely a consequence of the H-bonding of urea functional groups, not present in the other materials. The E' of **B3**, **P1** and **D1** are all significantly lower ($< 300\text{ MPa}$), which suggests they have a weaker physical network.

Table 3.3 Summary of Data obtained *via* DMA for all TPU copolymers.

Copoly.	E' @ $-50\text{ }^{\circ}\text{C}$ (MPa)	$T_{g(\text{SS})}$ ($^{\circ}\text{C}$)	E' @ $20\text{ }^{\circ}\text{C}$ (MPa)	$T_{m(\text{SS})}$ ($^{\circ}\text{C}$)	E' @ $70\text{ }^{\circ}\text{C}$ (MPa)	$T_{m(\text{HS})}$ ($^{\circ}\text{C}$)	$T_{g(\text{HS})}$ ($^{\circ}\text{C}$)
B3	2560	-26	290	32	- ^a	-	-
D1	2020	-21	130	33	0.3	80	-
P1	1980	7	250	39	- ^a	-	-
U1	2320	-22	570	47	2.7	-	119

^a Sample fractured at a lower temperature

A sudden reduction in E' is observed between 30 and 50 °C for all samples, corresponding to the melting of the crystalline PCL SS. At this point, both **B3** and **P1** completely lose integrity and break in the experiment, indicating they are not reinforced by phase separation. On the contrary, both **D1** and **U1** remain cohesive above $T_{m(SS)}$ where E' decreases as a function of temperature. Values of E' are reported as 0.3 and 2.7 MPa at 70 °C for **D1** and **U1**, respectively. This additional stability is granted by separate and well-ordered hard domains, unperturbed above $T_{m(SS)}$. At higher temperatures, there is a further drop in E' with a corresponding peak in $\tan \delta$ at 80 and 119 °C for **D1** and **U1** respectively, indicating another phase transition.

3.2.3 Rheology

Rheology of the copolymers in the melt was performed through temperature sweeps from 50 to 150 °C. The aim of these rheological experiments is to determine how easy it would be to induce flow within the materials to estimate surface wetting abilities and ease of application and removal in reversible adhesive applications. A temperature above $T_{m(SS)}$ was chosen as the starting point to prevent solid samples from slipping during experimentation. As expected, all materials display a decrease in complex viscosity (η^*) with temperature caused by an increase in chain mobility from heat energy transfer (**Figure 3.6**).²⁹ **B3** exhibited the lowest η^* across all temperatures because it does not contain a chain extender and has a relatively low urethane content which means it contains the least amount of H-bonding interactions. This data suggests **B3** is likely to be reasonably simple to apply to and remove from substrates. **P1** follows the same trend as **B3** with increasing temperature, but with a higher η^* as a consequence of being a singular phase network but having a higher urethane content. **D1** shows a high η^* at lower temperatures with a sudden decrease of two orders of magnitude from 1.14×10^4 to 1.20×10^2 Pa.s⁻¹ at approximately 100 °C, corresponding to

melting of the HS. For **U1**, η^* remains constantly high throughout the temperature range studied ($2.09 \times 10^4 - 8.07 \times 10^3 \text{ Pa}\cdot\text{s}^{-1}$). This relatively high viscosity suggests a stable physical network formed of urea H-bonding present up to 150 °C and that urea H-bonds are less sensitive to thermal changes than urethane H-bonds. This material is likely difficult to reprocess or apply to a substrate without specialist equipment. The temperature sweep was capped at 150 °C on account of the thermal instability of urea groups.¹⁸

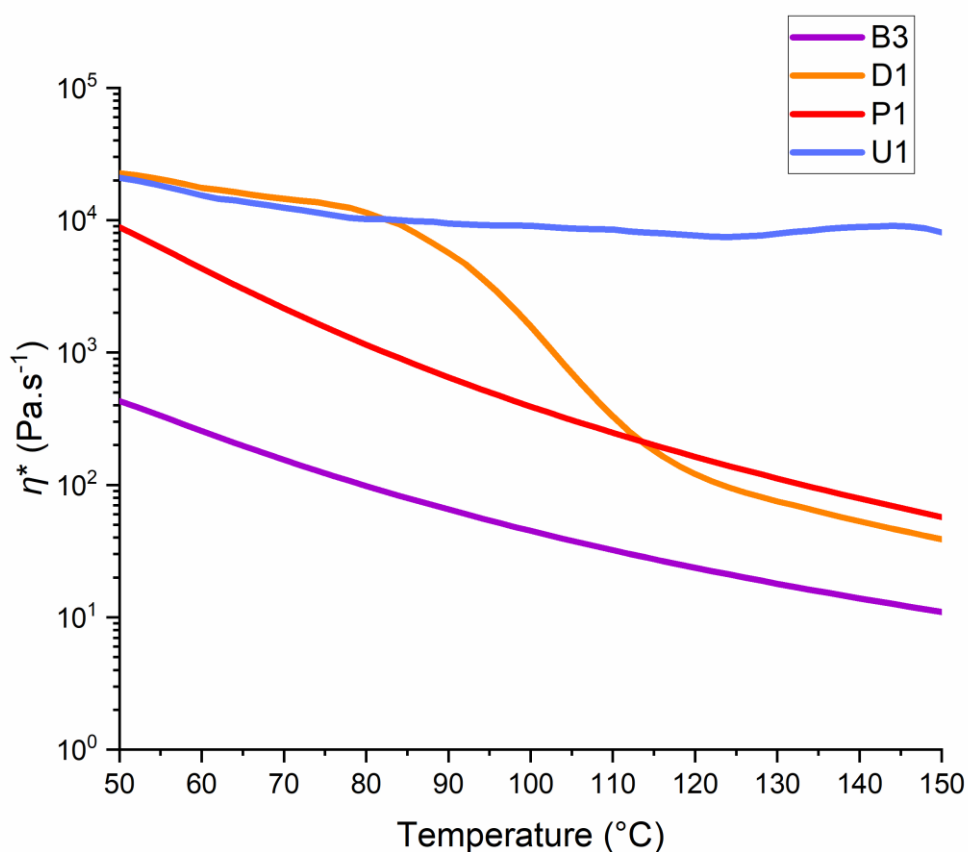


Figure 3.6 Complex viscosity as a function of temperature from 50 to 150 °C for the different TPU copolymers, using the rheometer in oscillatory mode with a set amplitude of 1 % and angular frequency of $1 \text{ rad}\cdot\text{s}^{-1}$.

3.2.4 Mechanical Properties

To gain understanding of the mechanical properties of the copolymers, tensile testing was performed on 500 μm film dog bone samples to produce stress-strain curves (**Figure 3.7**).

Data could not be obtained for **B3** because it was too brittle to be held in the clamps without shattering, probably caused by the low urethane content.

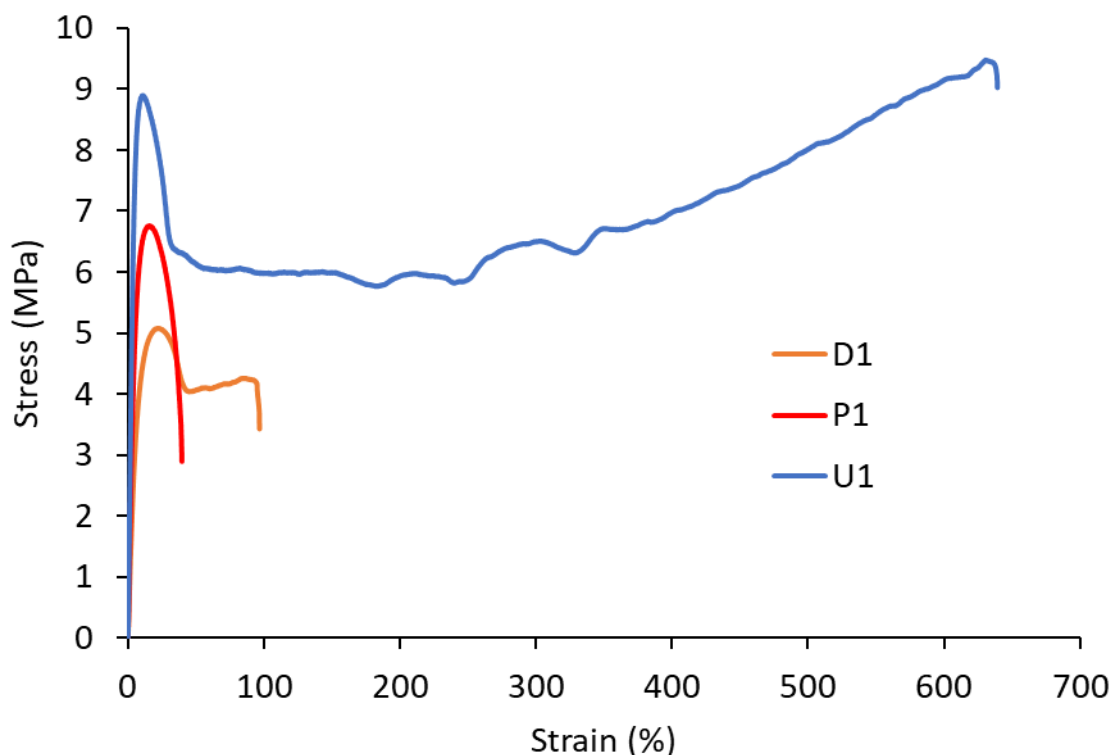


Figure 3.7 Tensile stress-strain data for the three chain extended copolymers.

P1 is relatively stiff and brittle, breaking immediately after its initial yield point, as a consequence of the lack of strength offered by a single-phase system. However, both **D1** and **U1** show further extension after their initial yield points, likely as a result of their multiphase arrangement. Both **D1** and **U1** show strain-hardening with elongation of the polymer materials.³⁰ The effect is much larger for **U1**, suggesting a strong influence from the additional interactions provided by the urea functional groups. **U1** records the highest values of Young's modulus (E) (210 ± 16 MPa), ultimate tensile strength (σ_{\max}) (9.6 ± 0.6 MPa), modulus of toughness (U_T) (4140 ± 1140 MPa) and strain at break (ϵ_{\max}) (640 ± 25 %) (**Table 3.4**). These values are remarkable for a TPU of such low molecular weight ($M_n = 17.3$ kDa for **U1**), previous studies of TPUs ($M_n = 6.1$ kDa) recorded much weaker mechanical properties.³¹ Such a result

is typically obtained from conventional TPUs with $M_n > 50.0$ kDa.³² These improved mechanical properties are possible on account of the superior H-bond strength accessible via urea functionality.

Table 3.4 Summary of mechanical data obtained from tensile stress-strain measurements for the copolymers comprising chain extenders.

Copolymer	E^a (MPa)	σ_{\max}^b (MPa)	U_T^c (MPa)	ϵ_{\max}^d (%)
D1	72 ± 8	5.0 ± 0.3	520 ± 285	125 ± 75
P1	121 ± 11	6.3 ± 0.5	140 ± 40	35 ± 10
U1	210 ± 16	9.6 ± 0.6	4140 ± 1140	640 ± 25

^a Young's modulus is calculated from the initial gradient before the Yield point.

^b Ultimate tensile strength is the maximum recorded stress the sample can withstand before failure.

^c Modulus of toughness is measured as the area under the curve and represents the total energy a material can withstand without breaking.

^d Elongation at break is the strain (%) at which the sample breaks.

Preliminary self-healing studies were carried out on **D1** and **U1**. Solid bar samples of each copolymer were cut in half and then reheated to reform one specimen (**Figure 3.8(a)**). Tensile testing was then performed on the healed samples and compared to pristine uncut bar samples. The healed samples recorded similar stress-strain curves to the uncut samples with only a small decrease in E and ϵ_{\max} (**Figure 3.8(b)**). E , σ_{\max} , U_T , and ϵ_{\max} were all similar, which suggests both copolymers have a dynamic physical network (**Table 3.5**). However, only one sample was run so further analysis is required for a full conclusion.

Table 3.5 Mechanical data obtained via tensile testing for pristine TPU materials and healed materials.

Sample	E^a (MPa)	σ_{\max}^b (MPa)	U_T^c (MPa)	ϵ_{\max}^d (%)
D1 before	23	6.0	290	65
D1 healed	21	5.8	310	72
U1 before	26	8.9	3570	567
U1 healed	21	8.5	3490	513

^a Young's modulus is calculated from the initial gradient before the Yield point.

^b Ultimate tensile strength is the maximum recorded stress the sample can withstand before failure.

^c Modulus of toughness is measured as the area under the curve and represents the total energy a material can withstand without breaking.

^d Elongation at break is the strain (%) at which the sample breaks.

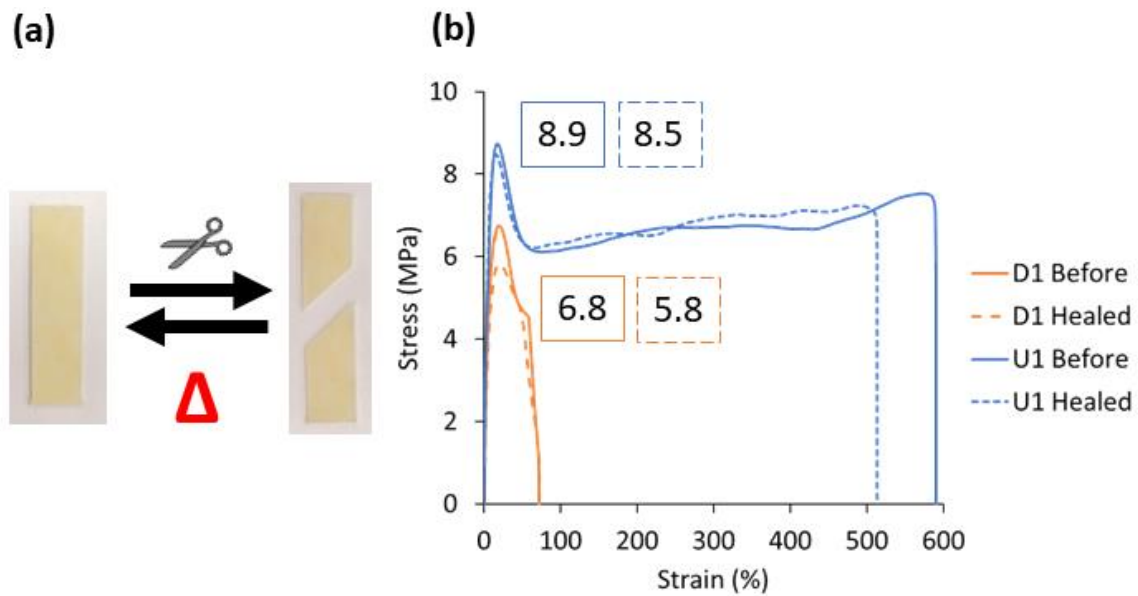


Figure 3.8 (a) Solid bar samples (10 × 40 mm) were prepared, cut and then healed via heating. **(b)** tensile stress-strain curves for bar samples of **D1** and **U1** before cutting (solid lines/boxes) and after cutting/healing (dashed lines/boxes). Values are the σ_{max} of each material in MPa.

The adhesive properties of the three materials including CE were determined *via* lap shear tests. **B3** was not measured as it was too brittle. Square film samples with a thickness of 250 μm were first prepared and then used to bond two overlapping beechwood substrates together by applying slight pressure and heating for 20 minutes at 140 °C. Lap shear samples were given at least one week to equilibrate under ambient conditions before analysis.

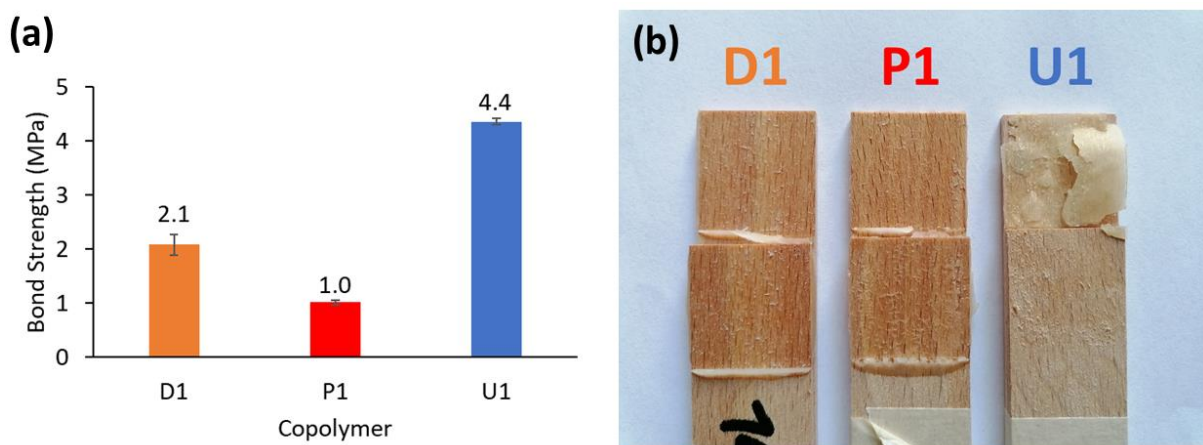


Figure 3.9 (a) Bond strengths from adhesion testing of beechwood substrates. **(b)** Beechwood substrates after testing showing cohesive failure (**D1** & **P1**) and adhesive/ substrate failure (**U1**).

The reference TPU copolymer **D1** displays a bond strength of 2.1 ± 0.4 MPa, but when the branched CE is used, the bond strength is decreased by over 50 % to 1.0 ± 0.1 MPa in **P1** (**Figure 3.9(a)**). This decrease in performance is a likely consequence of the single-phase morphology in **P1**. However, the TPU copolymerised with BU CE (**U1**) shows more than double the adhesive strength of **D1** at 4.4 ± 0.1 MPa, which is granted by the extensive urea H-bonding present. The bond strength of the thermoplastic **U1** is only slightly less than that of a typical irreversible moisture-cured PU, previously reported.³³ While both **D1** and **P1** show cohesive failure, **U1** displays adhesive failure and partially tears the beechwood substrate (**Figure 3.9(b)**).

3.2.5 Morphology

Initial optical microscopy studies were used to improve understanding of the morphology of PCL crystallinity (**Figure 3.10**). It is important to note that in order to prepare a film of **U1**, the material was taken above 150 °C so there may be a question concerning potential decomposition. **B3** showed the largest and most heterogenous PCL crystals, as expected from the large and broad $T_{m(SS)}$ observed in DSC analysis (**Figure 3.4(a)**). Introduction of CE decreases the amount of PCL visible which corresponds with the drop in $\Delta H_{m(SS)}$ for CE copolymers. Both **D1** and **U1** show finer PCL crystals, especially **U1** which seems to contain more regular and much smaller features (**Figure 3.10(b) & (d)**). This observation infers that the copolymerised bisurea diol has more influence on the crystallisation behaviour of the PCL segments. Such a finer morphology could explain the outstanding mechanical properties obtained with **U1** where more stress can be dissipated from the larger interfacial surface area.

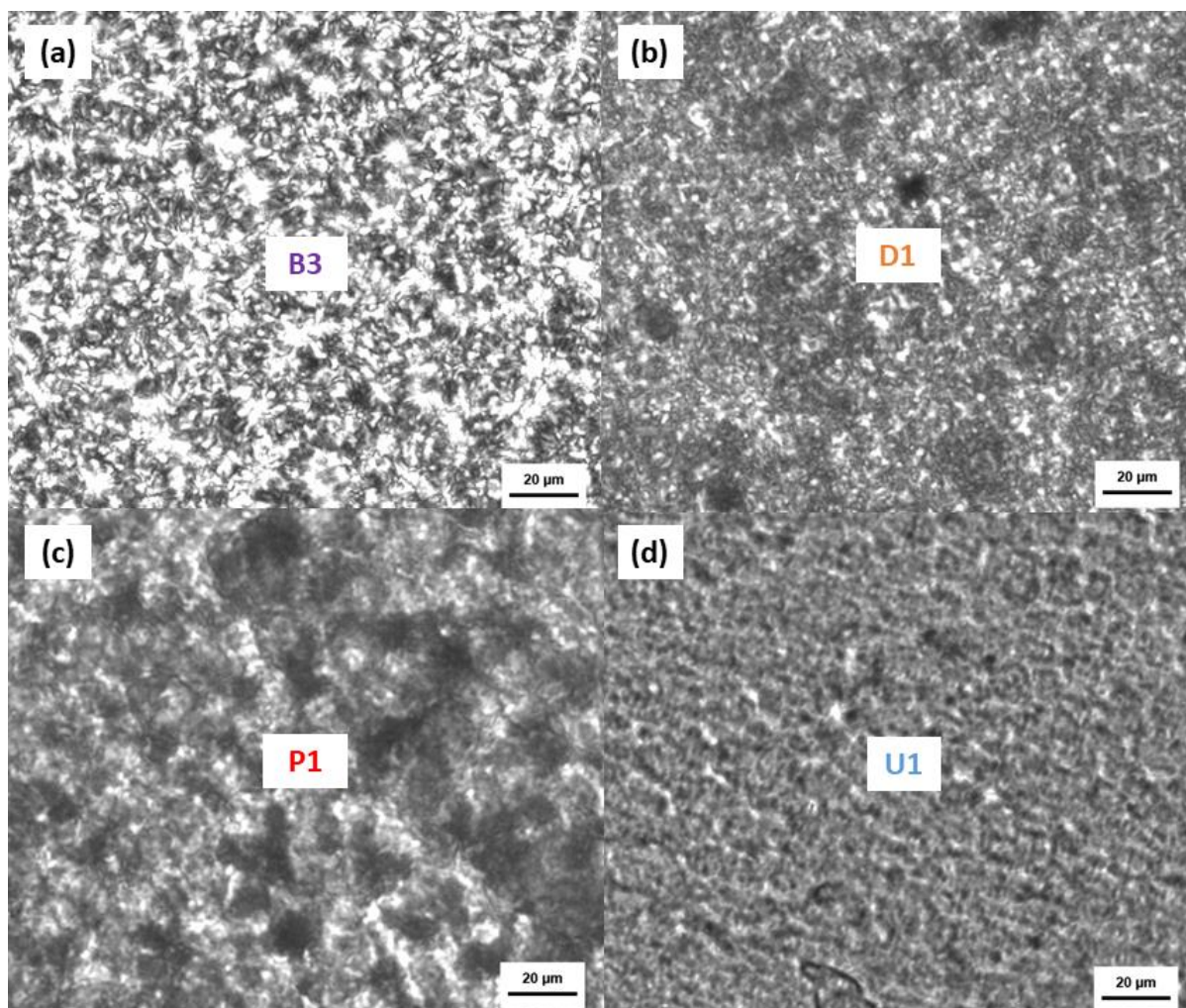


Figure 3.10 Optical microscopy of TPU copolymer 37 μm films. (a) B3. (b) D1. (c) P1. (d) U1.

Analysis of the data collected above gives an idea of the type of morphologies present in each chain extended copolymer. BD gives a well phase separated morphology with discrete crystalline hard and soft domains, BD associating in an efficient manner (**Figure 3.11(a)**). PD hinders urethane interaction to give a highly phase mixed system (**Figure 3.11(b)**). Finally, BU allows for significant intermolecular interactions, notably urea H-bonding, to produce a highly phase separated morphology with crystalline SS and a partially ordered glassy HS (**Figure 3.11(c)**).

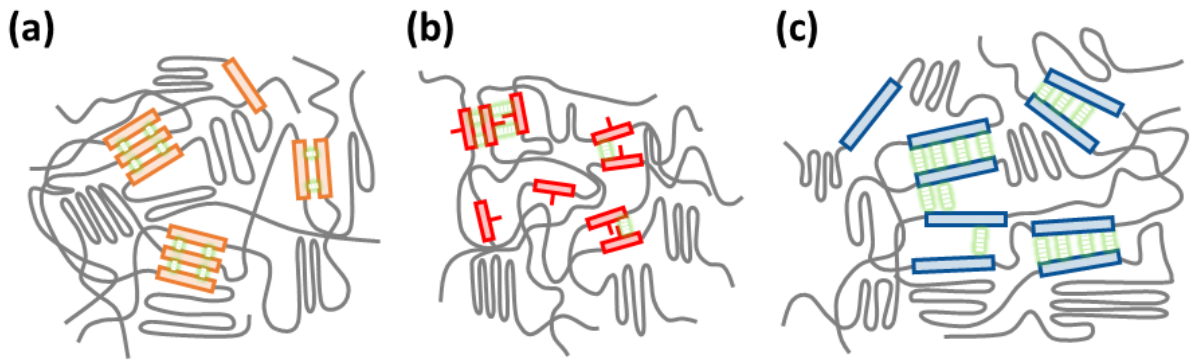


Figure 3.11 Suggested morphologies for copolymers comprising different chain extenders **(a)** PD, **(b)** BD and **(c)** BU. Grey lines represent the polyol SS and the coloured boxes represent the HS from copolymerised MDI-CE units.

3.3 Conclusion

Three different chain extended TPU copolymers were synthesised and compared to a non-chain extended PCL-MDI copolymer as a reference. The influence of CE symmetry, branching and urea functionality were examined. All copolymers were made at similar M_n to discount the influence of molecular weight. Successful synthesis was proven *via* NMR and FTIR spectroscopies and SEC.

While copolymerisation with symmetrical BD promotes more H-bonded urethane than other CEs studied, incorporation of BU shows urea H-bonding, known to be stronger than urethane H-bonding. In fact, use of the bisurea CE increased copolymer modulus at ambient temperature, which is likely on account of this urea H-bonding. Copolymerisation with all CE decreases PCL crystallinity due to disruption of chain arrangement. Copolymers including either BD or BU display greater PCL homogeneity as a consequence of phase separated morphologies where CE-MDI units associate separately from the PCL SS. On the other hand, using a branched CE, which displayed little urethane H-bonding, increases phase mixing and therefore disrupts PCL crystallinity more than the other CE. Distinct HS act as reinforces and allow for cohesion above $T_{m(SS)}$ until $T_{m(HS)}$ or $T_{g(HS)}$ as in the case of copolymers containing BD

or BU respectively. However, while an increase in temperature has a marked influence of urethane-urethane interactions in **D1** (manifested as a reduction in melt viscosity), urea interactions display minimal sensitivity in the temperature range studied, limiting potential in reversible adhesion.

Tensile testing revealed that copolymers comprising PD and BD chain extenders are mechanically poor materials, to be expected for materials with a relatively low molecular weight. However, the copolymer comprising the BU chain extender displayed outstanding mechanical properties, usually observed from TPU materials with much higher molecular weight. Optical microscopy revealed that copolymerisation with CE decreases the amount and size of PCL crystals. The copolymer comprising BU appeared to contain especially fine and more regular PCL crystals, correlating with the high mechanical properties obtained. Adhesion testing highlighted that the TPU comprising BU also provided the highest bond strength. Preliminary self-healing studies showed that copolymers comprising both the BD and BU chain extenders have potential for efficient self-healing.

3.4 Experimental

3.4.1 Materials

Capa™ 2200J was supplied by Perstorp. 4,4'-methylene bis(phenyl isocyanate) (98 %), 1,4-butanediol *ReagentPlus*® (99 %), 1,2-propanediol ACS reagent (≥99.5 %), n-hexane ACS reagent (≥99 %) and chloroform-d (99.8 atom % D) were purchased from Sigma-Aldrich. Bisurea diol was provided by the Hayes Research Group of the University of Reading. Anhydrous dimethylformamide (DMF) was obtained from a Grubbs purification system. All reagents were used as received.

3.4.2 Instrumental methods

Grubbs dry solvent service was used to obtain anhydrous toluene. This system involves the storage of solvents in a pressurised environment under an inert gas. The solvent is then passed through two filters which absorb any moisture from the solvent. **Proton (^1H) nuclear magnetic resonance (NMR)** spectra were recorded using a Bruker Avance 400 spectrometer (400 MHz). Spectra were analysed on MestReNova v6.0.2. Samples were prepared in CDCl_3 as the solvent. All chemical shifts were recorded in parts per million (ppm) relative to a reference peak of chloroform solvent at $\delta = 7.26$ ppm. **Molecular weights and dispersities** were determined *via* size-exclusion chromatography (SEC) using an Agilent 1260 Infinity GPC system equipped with a refractive index detector. Two Agilent PL-gel 5 μm Mixed-C columns and a guard column were connected in series and maintained at 35 $^\circ\text{C}$. HPLC grade chloroform containing 0.25 % v/v NEt_3 was used as the eluent and the flow rate was set at 1.0 $\text{mL}\cdot\text{min}^{-1}$. The refractive index detector was used for calculation of molecular weights and dispersities by calibration using a series of near-monodisperse poly(methyl methacrylate) standards. Analysis was performed on Agilent SEC software. **U1** copolymer molecular weight distributions were assessed using a SEC set-up comprising two Agilent PL gel 5 μm Mixed-C columns and a guard column connected in series to an Agilent 1260 Infinity GPC system operating at 60 $^\circ\text{C}$ and equipped with a refractive index detector and a UV-visible detector ($\lambda = 309$ nm). The SEC eluent was HPLC-grade DMF containing 10 mM LiBr at a flow rate of 1.0 $\text{mL}\cdot\text{min}^{-1}$. DMSO was used as a flow-rate marker. Calibration was achieved using a series of ten near-monodisperse poly(methyl methacrylate) standards (ranging in M_p from 625 to 618 000 $\text{g}\cdot\text{mol}^{-1}$). Chromatograms were analysed using Agilent GPC/SEC software. **Attenuated Total Reflectance Fourier Transform Infrared (ATR-FTIR)** spectra were collected on PerkinElmer Spectrum Two instrument with a UATR Two accessory. Analysis was performed

on PerkinElmer Spectrum software. **Differential scanning calorimetry (DSC)** was performed on a Discovery DSC 25 TA instrument. All experiments were carried out under a nitrogen atmosphere with a heating rate of $10\text{ }^{\circ}\text{C}\cdot\text{min}^{-1}$. Pre-weighed samples of $2 \pm 1\text{ mg}$ were loaded at $25\text{ }^{\circ}\text{C}$, cooled to $-90\text{ }^{\circ}\text{C}$ and heated to $150\text{ }^{\circ}\text{C}$, cooled again to $-90\text{ }^{\circ}\text{C}$ and finally reheated to $150\text{ }^{\circ}\text{C}$. T_g was taken as the midpoint of inflexion and T_m was measured as the temperature at the minimum heat flow of a melt endotherm. Analysis was performed on TRIOS v5.1.1 software. **Dynamic Mechanical Analysis (DMA)** was performed on TA Instruments Q800 Dynamic Mechanical Analyser with an ACS-3 (Refrigerated Chiller System). Samples of approximately $40 \times 5 \times 1\text{ mm}$ were loaded at room temperature and clamped lightly (finger tight). A sample length of 10 mm was used for all measurements. For each measurement, the sample was first cooled to $-80\text{ }^{\circ}\text{C}$ and held at this temperature for a minimum of 5 minutes to fully equilibrate. The furnace was then opened and the sample clamped to a pressure of 4.5 psi using a small torque wrench. After clamping the furnace was then immediately closed and temperature re-equilibration established at $-80\text{ }^{\circ}\text{C}$. The method was then started. The thermal method used is: Motor Drive Off, Data Storage Off, equilibrate at $-80\text{ }^{\circ}\text{C}$, isotherm 5 minutes, Motor Drive ON, Data Storage ON, ramp $3\text{ }^{\circ}\text{C}\cdot\text{min}^{-1}$ to $100\text{ }^{\circ}\text{C}$. The measurement parameters used were as follows: strain applied (0.05 %), force track (110 %), initial sample length (10 mm), with deformation frequency (1 Hz) fixed. Sample dimensions were calculated as follows: width was measured using digital callipers at three positions along the sample (End 1, Middle, End 2). Thickness was measured using digital callipers at three positions along the sample (End 1, Middle, End 2). Average values calculated and used. The software used was TA Instruments Advantage Control Software and data analysis was performed on TA Instruments Universal Analysis Data Analysis Program. **Rheological temperature sweeps** were performed on an Anton Paar MCR502 with 25 mm disposable geometry and a disposable bottom plate

fixture. Tests were run in oscillatory mode at a fixed amplitude (1 %) and angular frequency (1 rad.s⁻¹) from 50 – 150 °C. Sample sizes were approximately 25.0 mm diameter discs of 0.8 mm height. **Tensile tests** were performed on approximately films approximately 300 µm thick, according to ISO 527-2 type 5B on a Zwickiline tensometer. The general procedure is as follows: dimensions of dog bone measured with digital calliper and noted on the system. The zero gap is set within Zwick software so the gauge length is known. The sample is then securely clamped in and the absolute cross head length is reset. The force is then zeroed. The test is performed at 10 mm.min⁻¹ until sample failure and the results analysed on TestXpert II software. **Self-healing tensile tests** were carried out on an AML instrument™ single column tensiometer rectangular samples of approximately 40.0 × 10.0 × 0.8 mm at a rate of 10 mm.min⁻¹. Only one sample of each material was run. **Adhesion lap shear tests** were performed on films 250 µm thick that were cut to 25 × 25 mm. Lap shear joints were assembled by carefully applying the film between beechwood test pieces using an overlap of 25 mm and a width of 25 mm, applying light pressure. The materials were placed in an oven for 20 minutes at 140 °C to melt the copolymers. Bonded samples were then allowed to equilibrate for 14 days at ambient conditions before measurement. The lap shear strength was determined from an average of four bonded samples using an Instron tensiometer with a load cell of 30 kN and a displacement speed of 1.27 mm.min⁻¹.

3.4.3 Sample preparation

Rheology discs of 25.0 × 0.8 mm were prepared with a MeltPrep vacuum compression mould. **B3**, **P1** and **D1** (approx. 0.40 g) were separately melted in the chamber at 70, 120 and 150 °C, respectively. Melting was followed by 10 seconds (**B3**) or 30 seconds (**P1** and **D1**) of pressure (0.1 mbar). Vacuum was removed and materials were then cooled with compressed air and

allowed to solidify before being removed from the chamber. **U1** was prepared by adding the sample (0.40 g) into the chamber at 140 °C with immediate addition of pressure (0.1 mbar). After 10 minutes, vacuum was removed and the chamber was cooled with compressed air and the sample allowed to solidify in the chamber. **DMA bars** were prepared in a similar way as the rheology discs. However, a 10 x 40 mm insert and chamber were used instead of cylindrical versions. Once solidified, samples were cut down the middle lengthwise to give two bars of 0.5 x 40 mm. **Self-healing tensile bars** were prepared in the same way as described for the rheology discs, but instead the 10 x 40 mm bar vacuum chamber was used. Pristine samples were measured as made. Healed samples were cut in half then healed in the MeltPrep vacuum chamber following the procedure above. **Tensile testing dog bones** were prepared from film samples (300 µm) which were made by coating out molten material (1 hour at 140 °C) with a 500 µm coating block on release paper. After films were allowed to solidify, dog bone shapes were cut out using a ZwickRoell knee manual cutting press ZCP 020 with cutting device for ISO 527-2 type 5B die attachment. **Adhesion films** of **B3**, **P1** and **D1** were prepared by heating some material in an oven at 150 °C for approximately 20 minutes, after which a film was drawn with a coating block with an approximate thickness of 250 µm. Squares of 25 x 25 mm were then cut out of the film for use in the lap shear sample preparation. For **U1**, material was processed with a Cryomill and then approximately 0.4 g was heated at 140 °C in a compression mould under pressure (20 bar) for 10 minutes, then allowed to cool. Square samples were then cut as with the previous materials.

3.4.4 Synthesis of PCL-MDI copolymer (B3)

PCL (250 g, 0.12 mol) was loaded in to a 1 L flange flask equipped with a mechanical stirrer, thermometer and vacuum inlet at 80 °C and once all molten, stirred under vacuum. After 1

hour, the vacuum was removed and a predetermined mass of flake MDI (23.93 g, 0.10 mol) was added to the reaction at 110 °C with increased stirring speed for 15 minutes without vacuum and then 1 hour with vacuum. Reaction completion was determined by monitoring the disappearance of the isocyanate absorbance *via* FTIR spectroscopy at $\nu_{\text{max}} = 2260 \text{ cm}^{-1}$. After reaction completion, the molten product was decanted and stored. SEC (CHCl_3): $M_n = 18.5 \text{ kDa}$, $M_w = 33.3 \text{ kDa}$, $D_M = 1.80$.

^1H NMR (400 MHz, 298 K, CDCl_3): $\delta = 7.31$ (d, $J = 7.8 \text{ Hz}$, Ar), 7.12 (d, $J = 8.3 \text{ Hz}$), 6.75 (s, NH), 4.16 (t, $^3J_{\text{H-H}} = 6.6 \text{ Hz}$, $\text{CH}_2\text{O}(\text{C}=\text{O})\text{NH}$), 4.08 (t, $^3J_{\text{H-H}} = 6.7 \text{ Hz}$, $\text{CH}_2\text{OC}=\text{O}$), 3.99 (s, MDI CH_2Ar), 3.95 (s, NPG CH_2O), 3.92 (s, MDI CH_2Ar), 3.89 (s, NPG CH_2O), 3.66 (m, CH_2OH), 3.32 (d, $J = 6.5 \text{ Hz}$, OH), 2.33 (t, $^3J_{\text{H-H}} = 7.5 \text{ Hz}$, $\text{CH}_2(\text{C}=\text{O})\text{O}$), 0.97 (dd, $J = 18.9, 7.4 \text{ Hz}$, NPG CH_3), 1.66 and 1.40 (all remaining hydrogens) ppm.

ATR-FTIR: $\nu_{\text{MAX}} = 3347$ (N-H), 2944 – 2864 (C-H), 1721 (C=O), 1598 (C-N), 1532 (Ar C=C), 1293, 1238 and 1161 (C-O) cm^{-1} .

3.4.5 Synthesis of PCL-MDI-BD copolymer (**D1**)

PCL (250 g, 0.12 mol) was loaded in to a 1 L flange flask equipped with a mechanical stirrer, thermometer and vacuum inlet at 80 °C and once all molten, stirred under vacuum. After 1 hour, the vacuum was removed and a predetermined mass of flake MDI (49.73 g, 0.20 mol) was added to the reaction at 110 °C with increased stirring speed for 15 minutes without vacuum and 1 hour with vacuum. BD (11.46 g, 0.13 mol) was added at temporary reduced stirring speed and left without vacuum for 15 minutes and at least 30 minutes with vacuum. Reaction completion was determined by monitoring the disappearance of the isocyanate absorbance *via* FTIR spectroscopy. After reaction, the molten product was decanted and stored. SEC (CHCl_3): $M_n = 18.8 \text{ kDa}$, $M_w = 36.0 \text{ kDa}$, $D_M = 1.92$.

^1H NMR (400 MHz, 298 K, CDCl_3): δ = 7.30 (m, Ar), 7.11 (m, Ar), 6.79 (s, NH), 4.19 (m, BD $\text{CH}_2\text{O}(\text{C}=\text{O})\text{NH}$), 4.15 (t, $^3J_{\text{H-H}} = 6.6$ Hz, $\text{CH}_2\text{OC}=\text{ONH}$), 4.07 (t, $^3J_{\text{H-H}} = 6.7$ Hz, $\text{CH}_2\text{O}(\text{C}=\text{O})$), 3.98 (s, MDI CH_2Ar), 3.92 (s, MDI CH_2Ar), 3.89 (s, NPG CH_2O), 3.68 (m, BD CH_2O), 2.32 (t, $^3J_{\text{H-H}} = 7.5$ Hz, $\text{CH}_2\text{C}=\text{OO}$), 1.78 (s, BD $\text{CH}_2\text{CH}_2\text{O}$), 1.72 (s, BD $\text{CH}_2\text{CH}_2\text{O}$), 0.99 (d, $J = 8.4$ Hz, NPG), 1.66 and 1.41 (all remaining hydrogens) ppm.

ATR-FTIR: $\nu_{\text{MAX}} = 3337$ (N-H), 2944 – 2866 (C-H), 1723 (C=O), 1597 (C-N), 1531 (Ar C=C), 1294, 1220 and 1162 (C-O) cm^{-1} .

3.4.6 Synthesis of PCL-MDI-PD copolymer (**P1**)

PCL (250 g, 0.12 mol) was loaded in to a 1 L flange flask equipped with a mechanical stirrer, thermometer and vacuum inlet at 80 °C and once all molten, stirred under vacuum. After 1 hour, the vacuum was removed and a predetermined mass of flake MDI (49.73 g, 0.20 mol) was added to the reaction at 110 °C with increased stirring speed for 15 minutes without vacuum and 1 hour with vacuum. PD (9.94 g, 0.13 mol) was added at temporary reduced stirring speed and left without vacuum for 15 minutes and at least 30 minutes with vacuum. Reaction completion was determined by monitoring the disappearance of the isocyanate absorbance *via* FTIR spectroscopy. After reaction, the molten product was decanted and stored. SEC (CHCl_3): $M_n = 18.1$ kDa, $M_w = 36.2$ kDa, $\mathcal{D}_M = 2.00$.

^1H NMR (400 MHz, 298 K, CDCl_3): δ = 7.30 (m, Ar), 7.11 (d, $J = 8.1$ Hz, Ar), 6.77 (s, NH), 4.25 (m, PD $\text{CH}_2\text{O}(\text{C}=\text{O})\text{NH}$), 4.19 (m, $\text{CH}(\text{CH}_3)\text{CH}_2$), 4.08 (t, $^3J_{\text{H-H}} = 6.7$ Hz, $\text{CH}_2\text{O}(\text{C}=\text{O})$), 3.99 (s, MDI CH_2Ar), 3.92 (s, MDI CH_2Ar), 3.90 (s, NPG CH_2O), 3.68 (m, BD CH_2O), 2.32 (t, $^3J_{\text{H-H}} = 7.5$ Hz, $\text{CH}_2(\text{C}=\text{O})\text{O}$), 1.24 (d, $J = 6.2$ Hz, PD CH_3), 0.99 (d, $J = 8.6$ Hz, NPG), 1.66 and 1.40 (all remaining hydrogens) ppm.

ATR-FTIR: $\nu_{\text{MAX}} = 3342$ (N-H), 2943 – 2866 (C-H), 1722 (C=O), 1598 (C-N), 1531 (Ar C=C), 1294, 1236, 1219 and 1162 (C-O) cm^{-1} .

3.4.7 Synthesis of PCL-MDI-BU (**U1**)

PCL (25.01 g, 0.01 mol) was loaded in to a 250 mL three-neck round-bottom flask equipped with a magnetic stirrer, thermometer and vacuum inlet, at 80 °C and once all molten, stirred under vacuum. After 1 hour, the vacuum was removed and replaced with a gentle nitrogen flow and the stopped was replaced with a reflux condenser. Anhydrous DMF (20 mL) was added followed by a predetermined mass of flake MDI (6.22 g, 0.03 mol) at 110 °C with increased stirring speed. The reaction was left for one hour before more anhydrous DMF (20 mL) was added. BU (6.21 g, 0.02 mol) was added and further aliquots of anhydrous DMF (20 mL) were added if needed. The endpoint was determined by monitoring the disappearance of the isocyanate absorbance *via* FTIR spectroscopy. After reaction completion, the mixture was cooled to room temperature then precipitated dropwise in n-hexane (300 mL) cooled by liquid nitrogen and left for 12 hours. Residual solvent was removed with heat and vacuum (48 hours at 80 °C without vacuum, 24 hours at 80 °C with vacuum). SEC (DMF): $M_n = 17.3$ kDa, $M_w = 39.1$ kDa, $D_M = 2.26$.

^1H NMR (400 MHz, 298 K, CDCl_3): $\delta = 7.69$ (d, $J = 8.3$ Hz, Ar), 7.36 (d, $J = 6.5$ Hz, Ar), 6.21 (m, urea NH), 4.96 (d, $J = 3.5$ Hz, OH), 4.29 (m, $\text{CH}_2\text{O}(\text{C}=\text{O})\text{NH}$), 4.25 (t, $^3J_{\text{H-H}} = 6.6$ Hz, $\text{CH}_2\text{O}(\text{C}=\text{O})$), 3.38 (m, $\text{OCH}_2\text{CH}_2\text{Urea}$), 2.76 (m, $\text{OCH}_2\text{CH}_2\text{Urea}$), 2.53 (t, $^3J_{\text{H-H}} = 7.3$ Hz, $\text{CH}_2(\text{C}=\text{O})\text{O}$), 1.80, 1.59 and 1.16 (remaining PCL hydrogens) and 2.00 – 1.00 (BU cyclohexane hydrogens) ppm.

ATR-FTIR: $\nu_{\text{MAX}} = 3334$ (N-H), 2929 – 2864 (C-H), 1724 (C=O), 1629 (C=O (urea)), 1598 (C-N), 1534 (Ar C=C), 1221 and 1162 (C-O) cm^{-1} .

3.5 References

1. D. Randall and S. Lee, *The Polyurethanes Book*, Wiley, New York, 3rd edn., 2003.
2. J. Bae, D. Chung, J. An and D. Shin, *J. Mater. Sci.*, 1999, **34**, 2523-2527.
3. A. Takahara, J.-i. Tashita, T. Kajiyama, M. Takayanagi and W. J. MacKnight, *Polymer*, 1985, **26**, 978-986.
4. N. Akram, S. Saleem, K. M. Zia, M. Saeed, M. Usman, S. Maqsood, N. Mumtaz and W. G. Khan, *J. Polym. Res.*, 2021, **28**, 1-15.
5. W. Lei, C. Fang, X. Zhou, Y. Cheng, R. Yang and D. Liu, *Thermochim. Acta*, 2017, **653**, 116-125.
6. J. Blackwell and M. Nagarajan, *Polymer*, 1981, **22**, 202-208.
7. O. W. J. Zhai, W. Zhao, X. Tao, S. L. Hsu and A. Slark, *J. Polym. Sci. Pol. Phys.*, 2018, **56**, 1265-1270.
8. H. Sheikhy, M. Shahidzadeh, B. Ramezanzadeh and F. Noroozi, *Journal of Industrial Engineering Chemistry*, 2013, **19**, 1949-1955.
9. P. H. Chen, Y. F. Yang, D. K. Lee, Y. F. Lin, H. H. Wang, H. B. Tsai and R. S. Tsai, *Adv. Polym. Technol.*, 2007, **26**, 33-40.
10. W. Li, A. J. Ryan and I. K. Meier, *Macromolecules*, 2002, **35**, 6306-6312.
11. K. Gisselält and B. Helgee, *Macromol. Mater. Eng.*, 2003, **288**, 265-271.
12. R. L. O. a. M. I. Y. E. Ayres, *Eur. Polym. J.*, 2007, **43**, 3510-3521.
13. C. B. Wang and S. L. Cooper, *Macromolecules*, 1983, **16**, 775-786.
14. J. P. Sheth, A. Aneja, G. L. Wilkes, E. Yilgor, G. E. Atilla, I. Yilgor and F. L. Beyer, *Polymer*, 2004, **45**, 6919-6932.

15. A. Eyvazzadeh Kalajahi, M. Rezaei, F. Abbasi and G. Mir Mohamad Sadeghi, *Polym.-Plast. Technol.*, 2017, **56**, 1977-1985.
16. C. Spaans, J. De Groot, F. Dekens and A. Pennings, *Polym. Bull.*, 1998, **41**, 131-138.
17. Y. Wang, Y. Li, M. He, J. Bai, B. Liu and Z. Li, *J. Appl. Polym. Sci.*, 2021, **138**, 51371.
18. G. Holden, H. R. Kricheldorf and R. P. Quirk, *Thermoplastic Elastomers*, Hanser, Germany, 3rd edn., 2004.
19. M. Shoaib and A. Bahadur, *e-Polymers*, 2016, **16**, 411-418.
20. B. Isare, G. Pembouong, F. Boué and L. Bouteiller, *Langmuir*, 2012, **28**, 7535-7541.
21. S. Boileau, L. Bouteiller, F. Lauprêtre and F. Lortie, *New J. Chem.*, 2000, **24**, 845-848.
22. F. Lortie, S. Boileau, L. Bouteiller, C. Chassenieux, B. Demé, G. Ducouret, M. Jalabert, F. Lauprêtre and P. Terech, *Langmuir*, 2002, **18**, 7218-7222.
23. K. Melia, B. W. Greenland, D. Hermida-Merino, L. R. Hart, I. W. Hamley, H. M. Colquhoun, A. T. Slark and W. Hayes, *React. Funct. Polym.*, 2018, **124**, 156-161.
24. L. S. N. a. C. T. Laurencina, *Prog. Polym. Sci.*, 2007, **32**, 762-798.
25. K. Melia, PhD Thesis, University of Reading, 2014.
26. K. Nakamae, T. Nishino and S. Asaoka, *Int. J. Adhes. Adhes.*, 1996, **16**, 233-239.
27. C.-H. Tsou, H.-T. Lee, H.-A. Tsai, H.-J. Cheng and M.-C. Suen, *Polym. Degrad. Stabil.*, 2013, **98**, 643-650.
28. S. Das, I. Yilgor, E. Yilgor and G. L. Wilkes, *Polymer*, 2008, **49**, 174-179.
29. T. G. Fox Jr and P. J. Flory, *J. Appl. Phys.*, 1950, **21**, 581-591.
30. C. B. Cooper, S. Nikzad, H. Yan, Y. Ochiai, J.-C. Lai, Z. Yu, G. Chen, J. Kang and Z. Bao, *ACS Cent. Sci.*, 2021, **7**, 1657-1667.
31. S. Salimi, Y. Wu, M. E. Barreiros, A. Natfji, S. Khaled, R. Wildman, L. Hart, F. Greco, E. Clark and C. Roberts, *Polym. Chem.*, 2020, **11**, 3453-3464.

32. L. Ren, P. N. Shah and R. Faust, *J. Polym. Sci. Pol. Phys.*, 2016, **54**, 2485-2493.
33. L. M. Sridhar, M. O. Oster, D. E. Herr, J. B. Gregg, J. A. Wilson and A. T. Slark, *Green Chem.*, 2020, **22**, 8669-8679.

4 Exploration of reversible Diels-Alder chemistry within linear thermoplastic polyurethanes

4.1 Introduction

Thermoplastic polyurethanes (TPUs) are commonly used materials on account of their diversity and good mechanical performance.¹ The beneficial properties of TPUs result from their dual phase morphology. Typically, the two phases separate from one another as a consequence of thermodynamic incompatibility. The polar units tend to associate together *via* intermolecular interactions, such as H-bonding between urethane groups, to form discrete well-ordered hard segments (HS) which are dispersed within the nonpolar soft segment (SS). Therefore, TPU copolymers contain an extended physical network that offers strength to the material and can also be disrupted by stimuli like heat or solvent.

While the high mechanical properties of TPUs are very attractive, the association of the HS can persist in the melt phase which causes the materials to have very high melt viscosity. With respect to adhesive applications, high viscosity results in poor surface wetting and therefore bond fracture at a lower force. High viscosity also causes difficulty in removing the adhesive from substrates at end of life which prevents the reuse or recycling of composite materials. Moreover, high viscosity materials require expensive, high shear hot melt extruders for processing, which limits potential applications.²

To overcome this issue, good disparity is required between a mechanically robust solid with high mechanical properties and a low viscosity melt for easy processing or recycling. As melt viscosity is largely dependent on molecular weight, one potential route is to synthesise a TPU that has molecular weight which is temperature controlled *via* reversible Diels-Alder (DA) chemistry. The DA reaction is a clean and efficient thermally reversible [4+2] cycloaddition between a diene and a dienophile.³ The forward reaction dominates at ambient temperature,

whereas the reverse reaction- the retro-Diels-Alder (rDA)- occurs upon heating typically above 100 °C. A common diene – dienophile pairing studied is furan and maleimide.⁴

Employing DA chemistry within polymers has been well researched and reported in the literature.^{5,6} Typically, furan and maleimide groups are used to crosslink amorphous linear prepolymers with pendent groups of complimentary functionalities to afford recyclable materials, often with improved mechanical performance.⁷ This method is versatile and has been studied across a variety of polymer backbones.⁸⁻¹¹ A typical example is work by Yu *et al.* who synthesised a recyclable DA crosslinked PU network between pendent maleimide groups and a bifunctional furan crosslinker with improved mechanical properties.¹² DA chemistry is not limited to amorphous materials and several studies have shown that DA cycloadducts are still able to form in semi-crystalline polymer systems, as the reaction takes place at chain ends which are found in the amorphous regions.¹³ While crystalline regions and DA cycloadducts can form and coexist, Kuang *et al.* describes how a competition occurs between crystal formation and DA cycloadduct formation.¹⁴ It has been found that crosslinking a semi-crystalline polymer decreases the amount of crystallinity which has a negative impact on the Young's modulus.^{15,16} Zhang *et al.* also demonstrated that polyester crystallinity with shorter or more random sequence lengths hinders DA cycloadduct formation more than regular block copolymer structures.¹⁷ Interestingly, the relationship between crystallinity and DA cycloadduct is dynamic and can be controlled with post-synthesis annealing. Low temperature annealing (*e.g.* 30 °C) favours large crystals with a lower degree of DA cycloadduct formation, but temperatures higher than T_m of the polymer (*e.g.* 60 °C) produces smaller crystals with higher DA cycloadduct formation.¹⁶

While most examples of using DA chemistry in polymers focuses on reversibly crosslinked systems, either through multifunctional ($f \geq 3$) crosslinkers or pendent functional groups linked with bifunctional crosslinkers, DA chemistry has also been used in linear polymer systems for a significant amount of time.¹⁸ Watanbe *et al.* coupled amorphous furan terminated prepolymers with *N,N'*-(4,4'-methylene diphenyl) bismaleimide (BMI) and successfully showed it was possible to polymerise and depolymerise their material *via* DA chemistry.¹⁹ However, their work did not investigate the influence of the DA cycloadduct on the thermal and mechanical properties of the copolymer. Several studies have explored using DA chemistry to control bulk polymer viscosity.²⁰ Work by Wu *et al.* exploited this dynamic viscosity for use in hot melt adhesives, but their study did not include TPUs based on semi-crystalline polyols.²¹ A further study by Mayo and Adronov presented thermally reversible films with impressive hardness and adhesion.²² Mechanical and thermal properties were determined to be influenced by the bisfuran and bismaleimide spacer units and using a combination of polymers with different spacers granted advantages of both materials. However, as a consequence of short spacers, all materials studied were very brittle which limits potential applications. Additionally, it is important to highlight that most studies mentioned above are solely amorphous based TPUs and use BMI which is toxic compound and liberated upon rDA.

Overall, while using DA chemistry within polymer systems has been studied in length, there has been little research specifically on linear semi-crystalline TPUs.^{23,24} This work aims to gain understanding on how the presence of the DA cycloadducts influences the mechanical and thermal properties of TPUs with different compositions. In particular, this study considers a

potential use for TPUs with DA cycloadducts along the backbone in reversible adhesion applications to enable recycling.

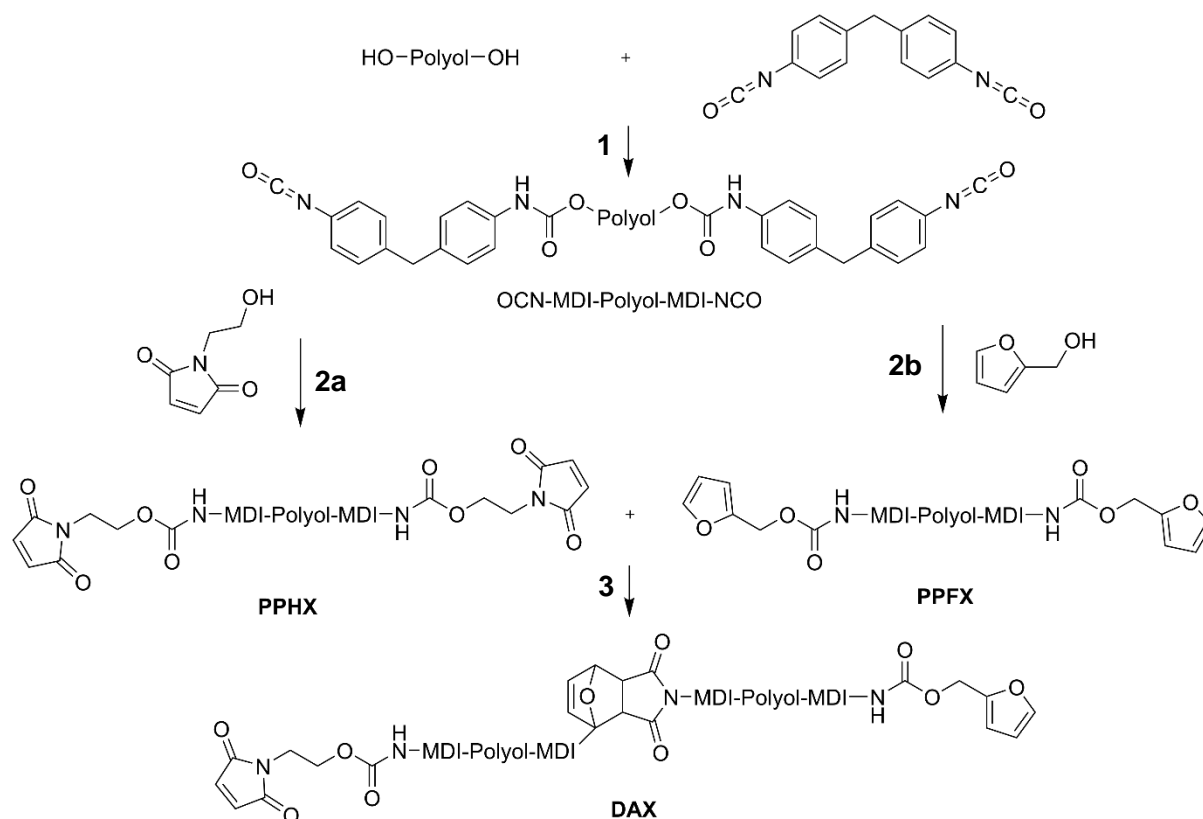
4.2 Results and discussion

4.2.1 Comparison of thermally reversible covalent TPUs to traditional chain extended TPUs

A linear TPU containing DA chemistry was synthesised *via* a solvent-free stepwise process. Firstly, poly(ϵ -caprolactone)diol (PCL) of 2.0 kDa was copolymerised with an excess of 4,4'-methylene diphenyl diisocyanate (MDI) at a stoichiometry of 1.0 : 2.0 (**Scheme 4.1(1)**). NCO-terminated prepolymers were then reacted separately with slight excess of monofunctional 2-hydroxyethylmaleimide (HEMI) or furfuryl alcohol (FA) to afford HEMI- and FA-terminated prepolymers (**PPH1** and **PPF1**, respectively) (**Scheme 4.1(2a & b)**). These prepolymers were then blended together by melting at a functional group stoichiometry of furan : maleimide 1.0 : 1.0 and then copolymerised at ambient temperature for at least 7 days to finally produce the linear TPU copolymer containing DA chemistry (**DA1**) (**Scheme 4.1(3)**). This material was also compared to a traditionally chain extended linear TPU copolymers of PCL, MDI and 1,4-butanediol (BD) (**D1**).

Synthesis of the reference material (**D1**) was described previously (Chapter 3). The successful synthesis of **DA1** was proven *via* NMR and FTIR spectroscopies and size exclusion chromatography (SEC). ^1H NMR spectroscopy of **PPH1** contains resonances at $\delta = 4.32$ and 4.16 ppm which correspond to $\text{CH}_2\text{O}(\text{C}=\text{O})\text{NH}$ adjacent to a urethane group showing covalent linkage of HEMI and PCL to MDI, respectively. **PPF1** shows resonances at $\delta = 5.16$ and 4.17 ppm which correlate to $\text{CH}_2\text{O}(\text{C}=\text{O})\text{NH}$ adjacent to a urethane group showing covalent linkage of FA and PCL to MDI, respectively. **DA1** shows a resonance at $\delta = 5.32$ ppm which corresponds to $\text{CH}(\text{O})(\text{CH})(\text{CH})$ on the DA cycloadduct (**Figure 4.1**). There are also two

resonances at $\delta = 3.03$ and 2.90 ppm which relate to two protons $CH(CH)C=O$ either side of the N atom in the DA cycloadduct.



Scheme 4.1 Step 1 bulk synthesis of NCO-terminated prepolymer. Step 2 synthesis of HEMI-terminated prepolymer (a) and FA-terminated prepolymer (b). Step 3 bulk copolymerisation of PPHX and PPFX to produce DAX. X = 1, 2, 3, 4, A1 or A2.

In FTIR spectroscopy, the absorbance at $\nu_{\max} = 2260 \text{ cm}^{-1}$, corresponding to the $-NCO$ terminus of isocyanate-terminated PCL, diminishes after addition of HEMI and FA in the formation of PPH1 and PPF1, respectively. After blending of the two prepolymers in molten form followed by cooling to ambient temperature, the absorbance at $\nu_{\max} = 696 \text{ cm}^{-1}$ decreases in intensity, marking the reduction in free maleimide and simultaneous formation of the DA cycloadduct.⁷ There is also a resonance at $\nu_{\max} = 1775 \text{ cm}^{-1}$ in the spectrum of DA1 which has been reported to signify DA cycloadduct formation.^{25,26}

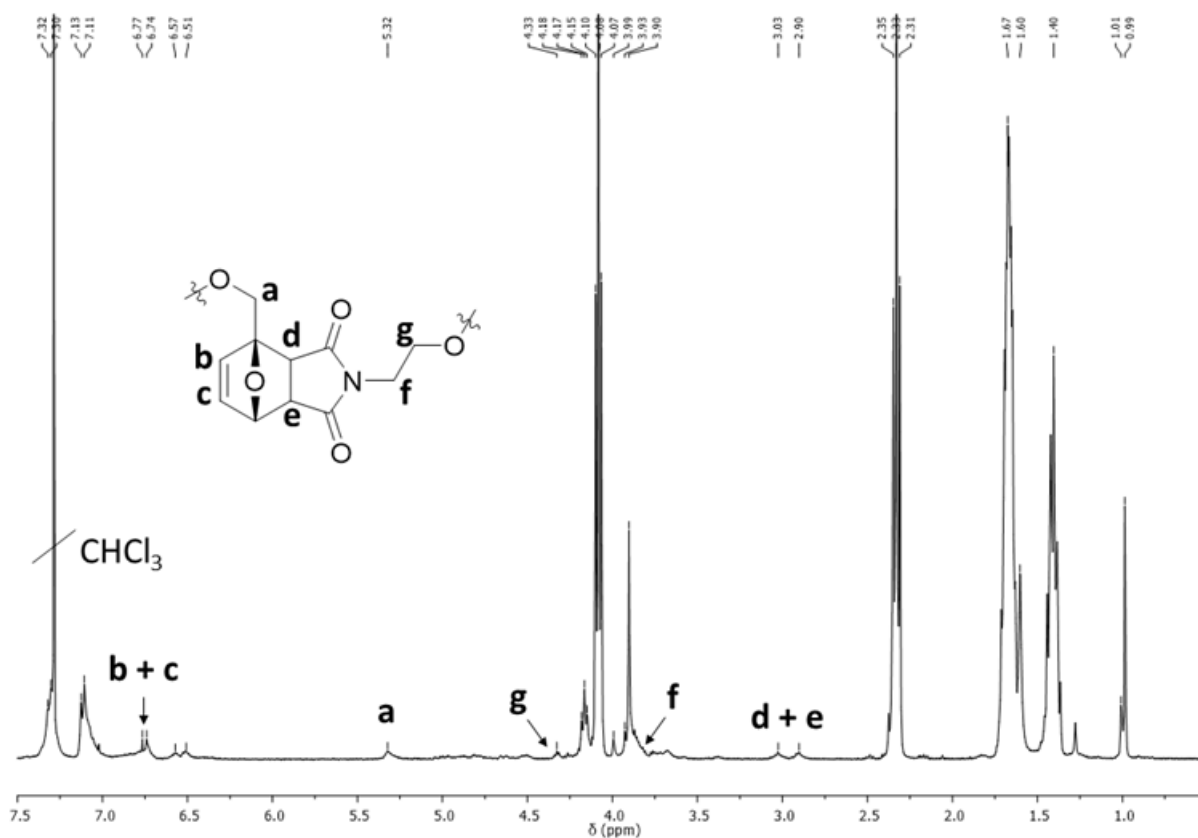


Figure 4.1 ¹H NMR spectrum of **DA1** with resonances associated with the DA cycloadduct labelled. All other resonances correspond to the PCL-MDI backbone. (400 MHz, 298 K, CDCl₃).

SEC results display an increase in molecular weight for the prepolymers **PPH1** ($M_n = 6.5$ kDa) and **PPF1** ($M_n = 6.3$ kDa) relative to non-copolymerised PCL polyol ($M_n = 2.0$ kDa) (**Table 4.1**). A further substantial increase in molecular weight accompanies the copolymerisation of **PPH1** and **PPF1** together at ambient temperature to form **DA1** ($M_n = 20.9$ kDa). This increase in molecular weight indicates successful coupling *via* DA maleimide-furan cycloadducts to produce a linear copolymer.²³ This M_n is similar to that of the reference TPU **D1** ($M_n = 18.8$ kDa).

Table 4.1 Composition of the TPU copolymers synthesised with corresponding SEC data.

Copolymer	Molar Ratio ^a			Comonomer	M_n^c (kDa)	M_w^c (kDa)	D_M^c
	PCL	MDI	CE				
PPF1	1.0	2.0	1.1	FA	6.3	12.6	1.94
PPH1	1.0	2.0	1.1	HEMI	6.5	12.6	2.02
DA1	_ ^b	_ ^b	_ ^b	DA	20.9	54.6	2.63
D1	1.0	2.0	1.3	BD	18.8	36.0	1.92

^a Molar ratio of functional groups

^b Not measured, made from copolymerisation of prepolymers

^c Determined by SEC in CHCl₃ against PMMA standards

Inspection of the carbonyl region within the FTIR spectra of the materials provides qualitative information about the intermolecular interactions that are present in each copolymer. All copolymers display a large absorbance at approximately $\nu_{\max} = 1720 \text{ cm}^{-1}$ which corresponds to ester groups in the PCL backbone (**Figure 4.2**). Copolymerisation incorporating BD gives rise to an absorbance at $\nu_{\max} = 1710 \text{ cm}^{-1}$ in **D1** which relates to H-bonded urethane.²⁷ This resonance is also present in the other materials which shows successful H-bonding between urethane groups occurs in all cases. However, for the furan prepolymer **PPF1** the intensity at $\nu_{\max} = 1710 \text{ cm}^{-1}$ is less than the other materials, which suggests it contains less H-bonding urethane. In the spectrum of **PPH1** there is a significant absorbance at $\nu_{\max} = 1700 \text{ cm}^{-1}$ which is caused by the maleimide carbonyl groups.²⁸ This band is also present in the spectrum of **DA1**, as this material also contains copolymerised maleimide functionality, found within the DA cycloadduct. Interestingly, imide-urethane H-bonding has previously been reported as a stronger interaction, indicated by the lower wavenumber, and therefore thermodynamically favoured over urethane-urethane H-bonding (**Figure 4.3**).²⁹ Additionally, incorporation of imide functionality has been shown to increase mechanical properties of the final PU material.²⁹ Comparison between the carbonyl shoulder ($\nu_{\max} < 1720 \text{ cm}^{-1}$) in the spectra of **D1** and **DA1** shows that **DA1** has greater intensity at lower wavenumbers. This difference implies that **DA1** contains stronger H-bonding, likely on account of the imide-urethane interactions

which are not present in the **D1** copolymer, and indicates potentially greater cohesion within the **DA1** material.

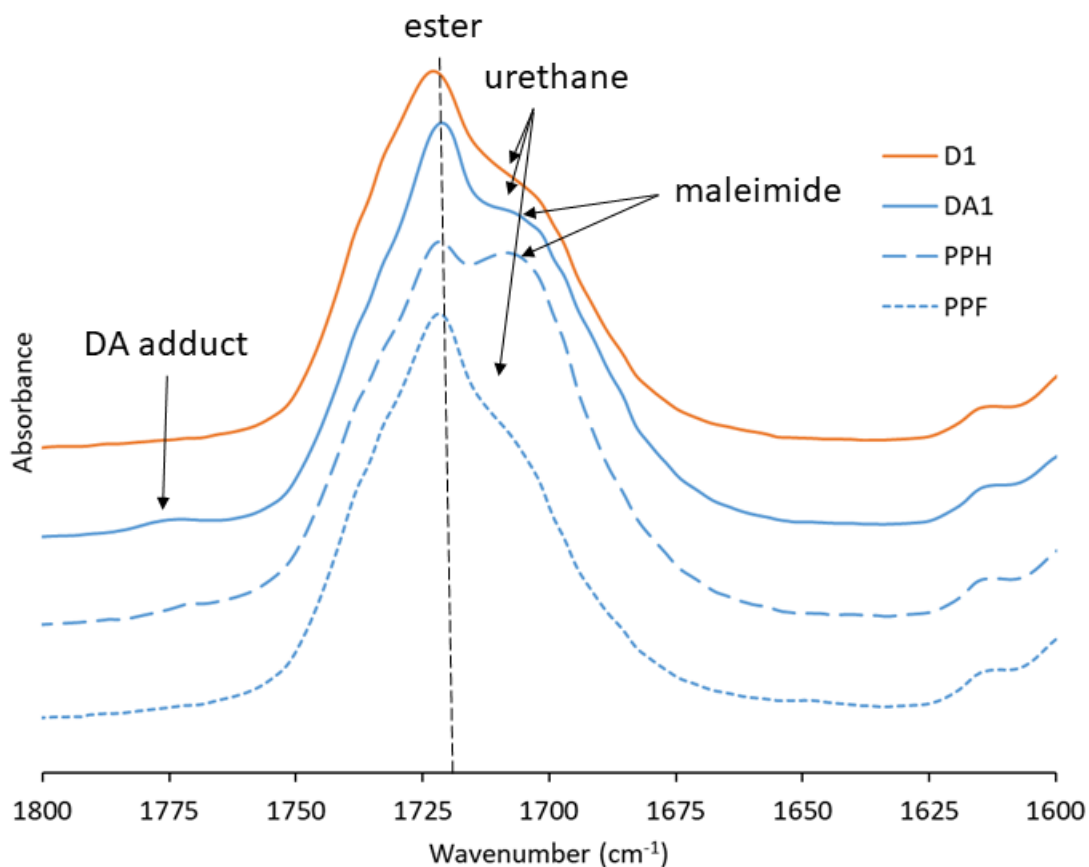


Figure 4.2 FTIR spectra of the carbonyl region for two copolymers (**D1** and **DA1**) and prepolymers (**PPH1** and **PPF1**). The dashed line at $\nu_{max} = 1720 \text{ cm}^{-1}$ represents the ester carbonyl which is present in all samples.

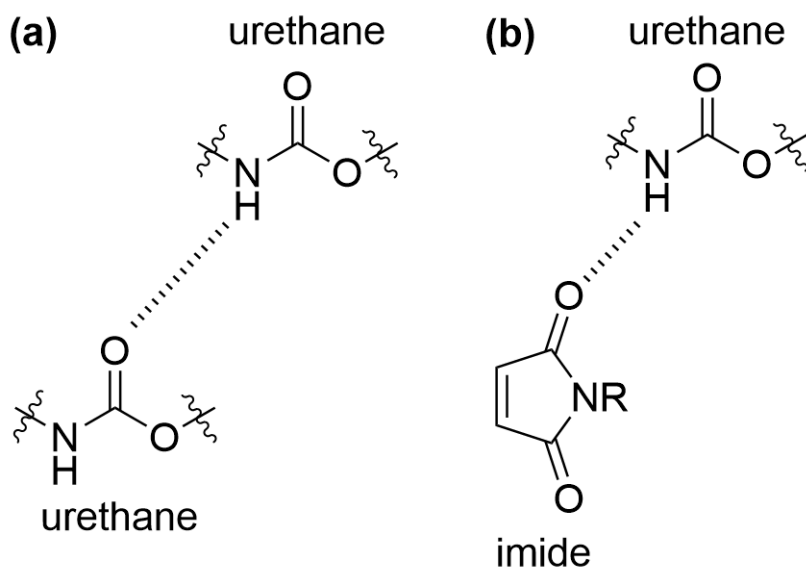


Figure 4.3 (a) urethane-urethane H-bonding. **(b)** urethane-imide H-bonding.

Differential scanning calorimetry (DSC) was used to determine the thermal properties of the four materials (**Table 4.2**). In all cases, the first heating cycle is discussed as a consequence of delayed recrystallisation of the copolymers and the slow formation of DA cycloadducts within the timescales of the DSC experiments. **D1** displays the lowest glass transition temperature (T_g) which implies the PCL chains of the other three materials are less mobile. **DA1** records the highest T_g , potentially because of restriction to rotation about main chain bonds imposed by the formation of the DA cycloadduct. Previous works have reported increased T_g with DA coupling, however in both cases it was thought a consequence of increased rigidity from short and aromatic BMI units.^{30, 31} Additionally, **DA1** shows the lowest change in heat flow below and above T_g which is indicative of greater PCL order.¹³

Table 4.2 Thermal data of the two copolymers and the two prepolymers, obtained via DSC.

Copolymer	T_g (°C)	$T_{m(pol)}$ (°C)	$\Delta H_{m(pol)}$ (J.g ⁻¹)	$T_{m(HS)}$ (°C)	$\Delta H_{m(HS)}$ (J.g ⁻¹)	T_{rDA} (°C)	ΔH_{rDA} (J.g ⁻¹)
PPF1	-31	35 & 42	31	- ^a	- ^a	- ^b	- ^b
PPH1	-32	37 & 42	33	83 & 104	2.1	- ^b	- ^b
DA1	-29	43	27	- ^a	- ^a	117 & 145	8.9
D1	-44	35 & 45	19	107	2.8	- ^b	- ^b

^a No HS detected

^b No rDA detected

Above T_g , all materials display a melting endotherm between 35 and 45 °C which correlates to crystalline PCL (**Figure 4.4(a)**).³² The **D1** reference displays one sharp melting temperature of the copolymerised polyol ($T_{m(pol)}$) at 45 °C and another shallow broad $T_{m(pol)}$ at 35 °C. The two melting temperatures suggest different degrees of PCL crystal order, the higher $T_{m(pol)}$ implies homogenous greater order, whereas the lower $T_{m(pol)}$ indicates irregular crystals of PCL.³³ This feature is exaggerated in both **PPH1** and **PPF1**, with larger enthalpy of melting endotherms ($\Delta H_{m(pol)}$) measured at the broader and lower $T_{m(polyol)}$, especially for **PPF1**. This

distribution of $\Delta H_{m(\text{pol})}$ suggests that there is greater heterogeneity of PCL crystals in these materials. The difference could possibly be an effect of molecular weight. Remarkably, **DA1** records one single sharp $T_{m(\text{pol})}$ which implies good homogeneity of the crystalline PCL suggesting that the cycloadducts facilitate the crystallisation process possibly as a consequence of phase separation.

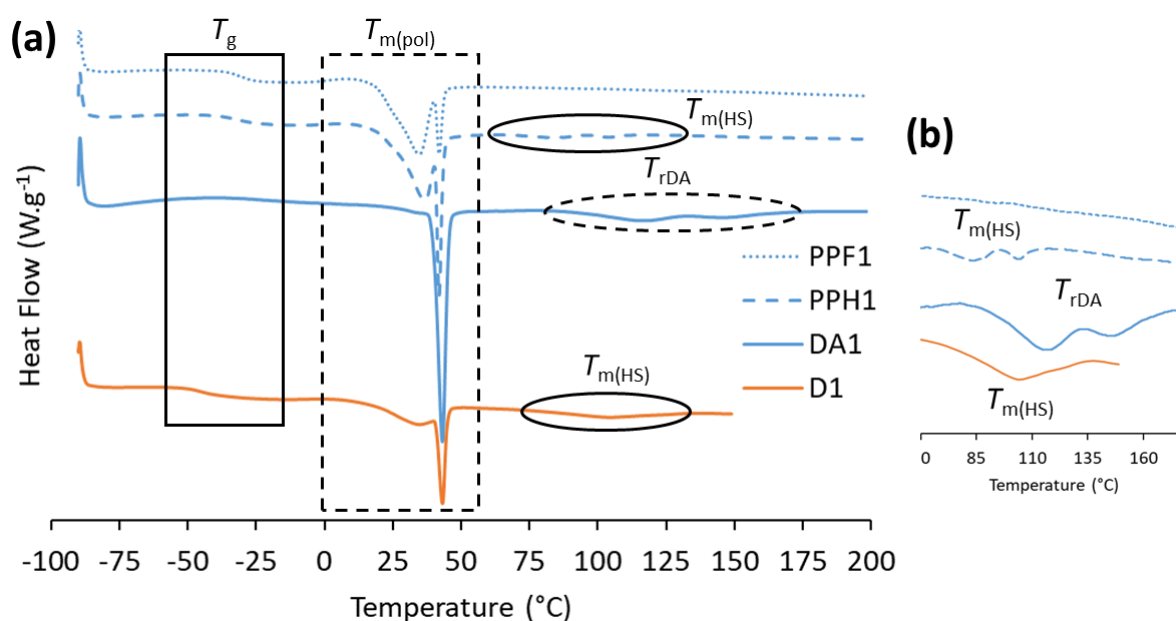


Figure 4.4 (a) DSC thermograms of the four materials, thermal transitions are highlighted and labelled. **(b)** Close up of high temperature ($> T_{m(\text{pol})}$) transitions. First heating cycle used at a heating rate of $10 \text{ }^\circ\text{C}\cdot\text{min}^{-1}$. Exo up.

At temperatures above $T_{m(\text{pol})}$, all materials display further transitions, other than **PPF1** (**Figure 4.4(b)**). **D1** shows a melting endotherm at $107 \text{ }^\circ\text{C}$ which is representative of crystalline BD-MDI HS.²⁷ This melting point shows that the HS is well-ordered and in a separate phase to the SS, typical of TPU copolymers and discussed in the previous chapter. **PPH1** displays two endotherms at 83 and $104 \text{ }^\circ\text{C}$, suggesting phase separation and perhaps ordering of the polar MDI-HEMI end groups. Finally, **DA1** shows two overlapping endotherms at 117 and $145 \text{ }^\circ\text{C}$. These transitions are evidence of the rDA reaction and the two peaks correspond to the *endo* and *exo* isomers, respectively.³¹ Therefore, these endotherms help prove that

copolymerisation of the maleimide prepolymer **PPH1** with the furan prepolymer **PPF1** make a TPU comprising DA cycloadducts in the backbone with thermally reversible covalent bonds.

Dynamic mechanical analysis (DMA) was used to confirm thermal data obtained *via* DSC. As a consequence of the brittleness of **PPH1** and softness of **PPF1**, samples of the prepolymers were not measured, so only **D1** and **DA1** are discussed (**Figure 4.5**). **D1** displays a lower T_g than **DA1**, which matches with the DSC data and reinforces good homogeneity within **DA1**. Above T_g , both materials exhibit a rubbery plateau, but **DA1** shows a higher storage modulus (E') of 390 MPa compared to 135 MPa for **D1** (**Table 4.3**). The higher strength of **DA1** is likely a result of higher PCL crystallinity and the presence of imide-urethane H-bonding.

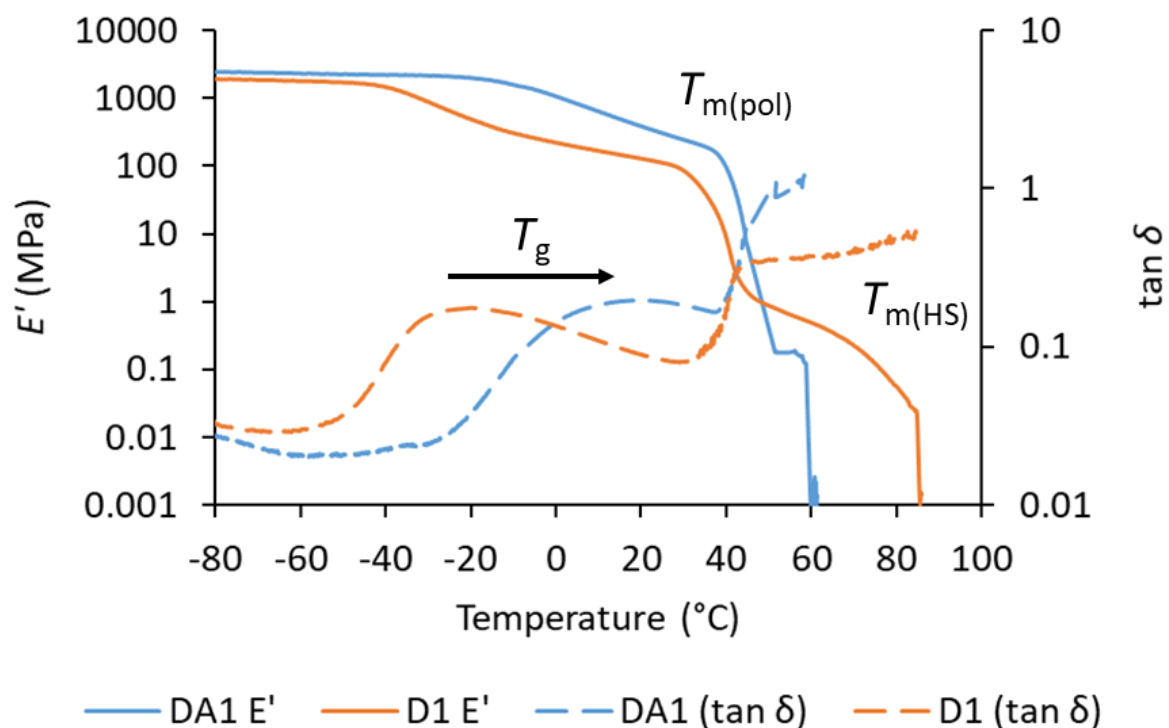


Figure 4.5 DMA of reference copolymer (**D1**) and DA copolymer (**DA1**) at a heating rate of 3 °C.min⁻¹.

There is a steep reduction in E' that begins at 33 and 40 °C for **D1** and **DA1**, respectively, which relates to the $T_{m(pol)}$. Above this temperature, **DA1** appears to lose all its strength, coinciding

with the melting of semi-crystalline regions. However, the sample did not break during the experiment, although E' was too low to measure. This loss suggests that the DA cycloadduct is not present in a sufficient concentration or perhaps there is not enough internal order in the newly amorphous copolymer above $T_{m(\text{pol})}$ to maintain a cohesive material. On the other hand, **D1** displays cohesion above $T_{m(\text{pol})}$, albeit with a strong temperature dependence, on account of the discrete HS which holds the material together. A final drop in E' is recorded for **D1** at 80 °C which relates to the $T_{m(\text{HS})}$.

Table 4.3 Thermal data for **D1** and **DA1** obtained via DMA using a heating rate of 3 °C.min⁻¹.

Copolymer	$E' (T > T_g)^a$ (MPa)	T_g^b (°C)	$E' (T > T_g)^c$ (MPa)	$T_{m(\text{pol})}^d$ (°C)	$E' (T > T_{m(\text{pol})})^e$ (MPa)	$T_{m(\text{HS})}^f$ (°C)
DA1	2280	18	390	40	-	-
D1	2015	-21	135	33	0.30	80

^a Modulus at -50 °C

^b Measured from the peak in $\tan \delta$

^c Modulus at 20 °C

^d Measured as the onset of modulus slope

^e Modulus at 70 °C

^f Estimated from the drop in modulus

The flow properties of **D1** and **DA1** were investigated *via* rheological temperature sweeps. Materials were subjected to oscillatory rheology from 50 to 150 °C at a fixed amplitude (1 %) and angular frequency (1 rad.s⁻¹). A complex viscosity (η^*) of 10 Pa.s⁻¹ is a suitable target, to enable simple application and good surface wetting as an adhesive. Both copolymers show a temperature dependent η^* with a steeper decrease in η^* at similar temperatures, corresponding to the $T_{m(\text{HS})}$ (**D1**) and the $T_{r\text{DA}}$ (**DA1**) (**Figure 4.6**). However, **DA1** reaches a lower η^* than **D1**, which indicates **DA1** can achieve better surface wetting. This suggests that the reversible covalent bonds from the cycloadduct in **DA1** are more temperature sensitive than the reversible hydrogen bonds arising from the classical chain extender. Moreover, **DA1** reaches the target η^* at 127 °C, whereas **D1** does not reach this value within the measured

temperature range. At 140°C, the viscosity of **DA1** is approximately 14 times lower than **D1**. This highly dynamic η^* is granted by the rDA reaction which cleaves the copolymer backbone at specific sites, reducing its molecular weight and η^* as a result.²¹ Therefore, these results suggest **DA1** would be suitable in reversible adhesive applications from the perspective of application and removal at end-of-life.

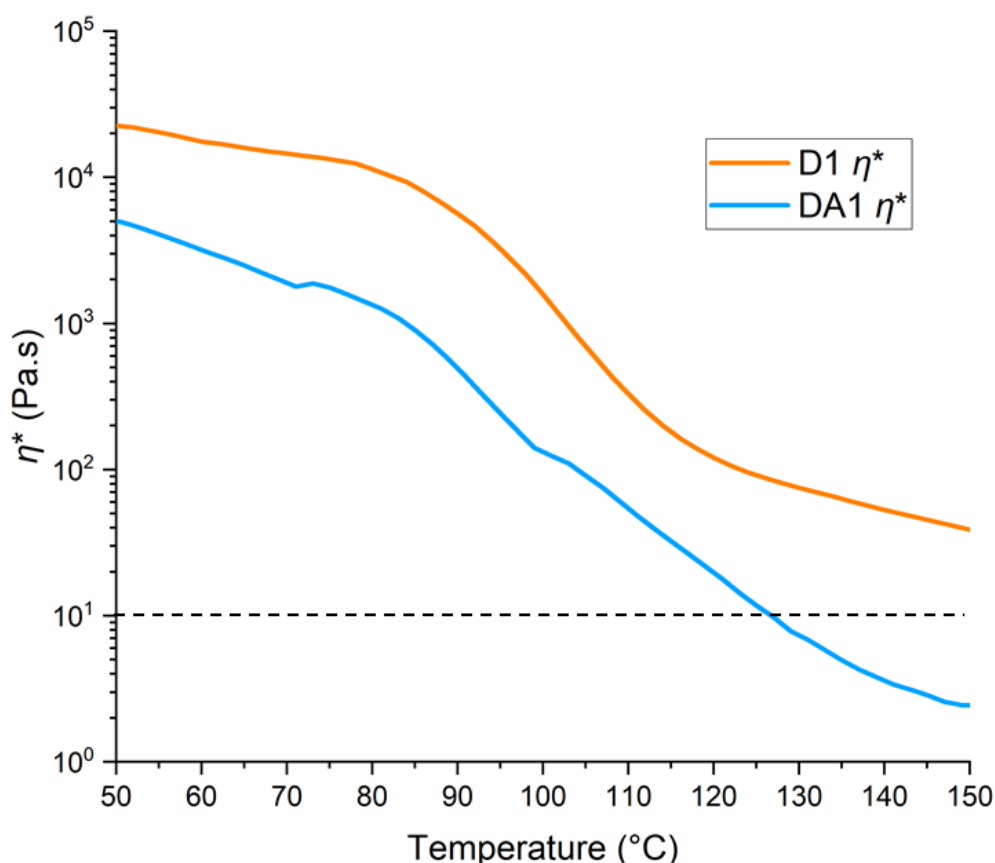


Figure 4.6 Temperature sweeps of **D1** and **DA1** at fixed 1 % and 1 rad.s⁻¹ showing complex viscosity (η^*) as a function of temperature. The dashed black line represents the ‘target viscosity’ of 10 Pa.s⁻¹.

The mechanical performance of **D1** and **DA1** were determined by performing tensile tests on film samples (**Figure 4.7**). Both materials display typical stress-strain curves of semi-crystalline TPUs. Initially, the copolymers experience elastic deformation where stress is proportional to strain. The materials then reach a yield point which marks the ultimate tensile strength (σ_{max})

and the start of plastic deformation. Finally, the samples begin to ‘neck’ in the middle of the dog bone and stress is constant as a function of strain, up until the maximum elongation (ϵ_{\max}) at which point the sample breaks.

The values of Young’s modulus (E) are extremely similar for both materials, but σ_{\max} is slightly higher for **DA1** (**Table 4.4**). This additional strength is likely a consequence of higher crystalline PCL content. The most noticeable difference between the two materials is the elongation, **DA1** records a significantly higher ϵ_{\max} of $165 \pm 5 \%$ compared to $125 \pm 75 \%$ for **D1**. As both materials produce necking at similar values of stress, the greater elongation of **DA1** results in a greater modulus of toughness (U_T). A higher U_T shows that **DA1** is tougher and can withstand more force before fracture than **D1**, making it a more promising material. Encouragingly, both copolymers have similar molecular weights, thereby discounting improved mechanical performance of **DA1** as a result of higher molecular weight.

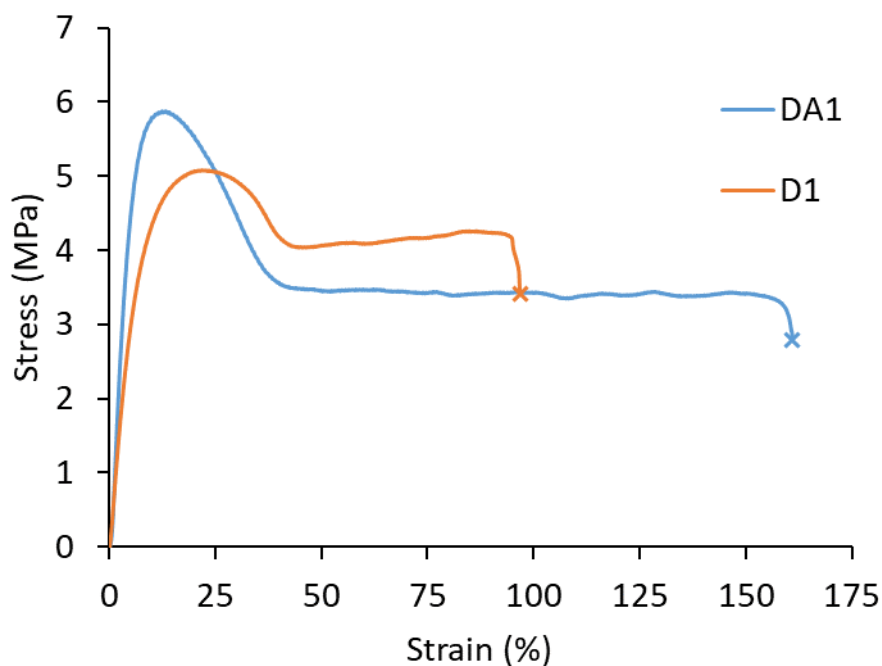


Figure 4.7 Tensile stress-strain data for **D1** and **DA1**. Extension rate of $10 \text{ mm} \cdot \text{min}^{-1}$.

Table 4.4 Summary of mechanical data obtained from tensile stress-strain measurements for the two copolymers. 10 mm.min⁻¹.

Copolymer	E^a (MPa)	σ_{\max}^b (MPa)	U_T^c (MPa)	ϵ_{\max}^d (%)
DA1	121 ± 12	5.9 ± < 0.1	635 ± 55	165 ± 5
D1	72 ± 8	5.0 ± 0.3	520 ± 285	125 ± 75

^a Young's modulus is calculated from the initial gradient before the Yield point.

^b Ultimate tensile strength is the maximum recorded stress the sample can withstand before failure.

^c Modulus of toughness is measured as the area under the curve and represents the total energy a material can withstand without breaking.

^d Elongation at break is the strain (%) at which the sample breaks.

The adhesive properties of **DA1** were determined *via* lap shear testing. Square film samples of **DA1** and the reference **D1** were placed between two overlapping beechwood substrates, heated with a little pressure then allowed to equilibrate for at least 14 days. Encouragingly, **DA1** displayed much improved bond strength (5.6 ± 0.3 MPa) compared to the traditional TPU copolymer **D1** (2.1 ± 0.4 MPa) on beechwood substrates (**Figure 4.8(a)**). While **D1** only showed cohesive failure, several of the **DA1** samples displayed substrate failure (**Figure 4.8(b)**). Therefore, further adhesion measurements were performed on **DA1** using aluminium substrates, which revealed a more realistic bond strength of 11.0 ± 0.5 MPa. It is clear that covalent linking *via* DA chemistry substantially improves the adhesive properties of the TPU copolymer and is more beneficial than the strength offered by a conventional linear TPU made *via* classic chain extenders. The bond strength reported here for **DA1** is higher than previous linear DA PUs using stainless steel substrates (approx. 7.5 MPa), amorphous crosslinked DA networks and a permanently crosslinked moisture cured PU using aluminium substrates (approx. 10 and 5 MPa, respectively).^{21,34}

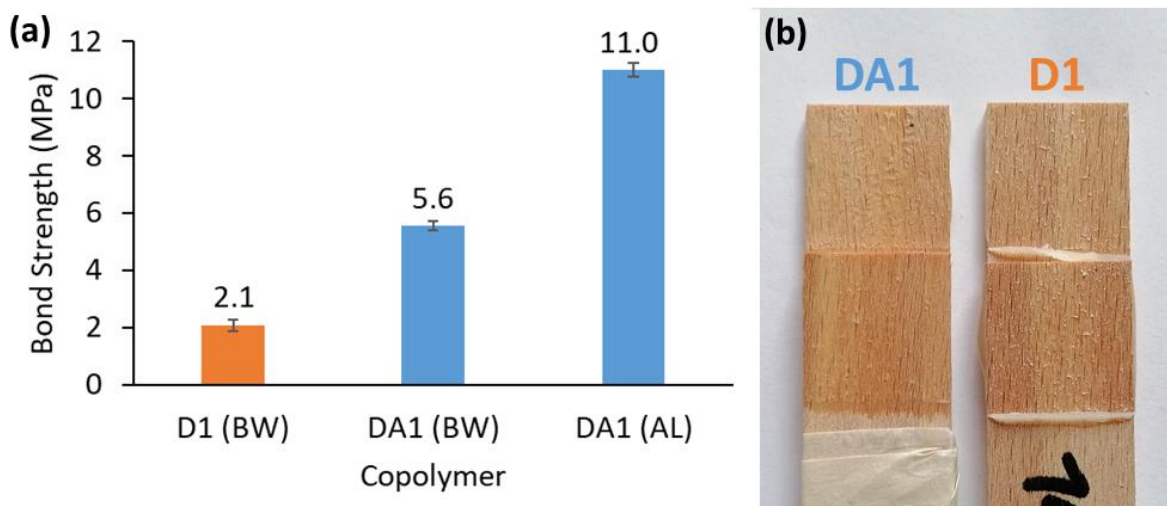


Figure 4.8 (a) Bond strengths from adhesion testing of beechwood (BW) and aluminium (AL) substrates. **(b)** Beechwood substrates after testing (DA1 and D1).

It has been demonstrated that the DA cycloadduct can form at ambient temperature and then be broken with heat *via* rDA. The retro reaction indicates the dissociation of the cycloadduct and the liberation of the two prepolymers (**PPH1** and **PPF1**). The repolymerisation of the prepolymers (to reform **DA1**) *via* DA cycloadduct reformation at ambient temperature after heating was investigated, in order to prove the copolymer is fully reversible and has dynamic properties. A film of **DA1** was coated after preheating for 1 hour at 150 °C and left under ambient conditions throughout testing.³⁵ Measurements were recorded periodically over the course of 28 days and labelled as ‘time after melt application’.

One method of evaluating reformation of the DA cycloadduct is through change in molecular weight which can be easily monitored by SEC.³⁶ Values of M_n and M_w for **DA1** were recorded over time, with reference to the M_n and M_w of the prepolymers **PPH1** and **PPF1**, which are the theoretical molecular weights after the rDA reaction - if all cycloadducts are broken. Comparison was made to the reference TPU (**D1**) (**Table 4.5**). After heating for one hour, the molecular weight of **DA1** (7.7 kDa) is comparable to that of **PPH1** (6.5 kDa) and **PPF1** (6.3 kDa)

which is remarkable and suggests almost complete reversal of **DA1** back to the original prepolymer state.

Table 4.5 Time dependent molecular weight values for **DA1** and **D1** at ambient temperature. **PPH1** and **PPF1** were only measured once and not as a function of time.

Material	Days after melt application ^{a, b}								Equilibrated ^c
	0	1	2	3	4	7	14	28	
PPF1 M_n	6.3								
PPH1 M_n	6.5								
DA1 M_n	7.7	14.4	15.3	18.7	18.8	22.2	18.9	21.6	20.9
PPF1 M_w	12.6								
PPH1 M_w	12.6								
DA1 M_w	16.7	34.0	41.4	48.5	51.4	52.7	54.4	56.7	54.6
D1 M_n	16.3	17.1	16.3	16.4	15.0	16.9	14.0	15.2	15.4
D1 M_w	31.7	36.1	34.6	35.2	34.5	35.4	33.4	32.9	33.9

^a Determined by SEC in $CHCl_3$ against PMMA standards

^b Values reported in kDa

^c Taken as the average of 7, 14 and 28 days

Monitoring the M_n and M_w of **DA1** against time at ambient temperature after melt application shows an initial rapid increase within the first 4 days (**Figure 4.9**). A slower gradual increase follows, before the values appear to plateau after 7 days. Increasing molecular weight signifies the reformation of the DA cycloadduct. These observations match previous reports of DA cycloadducts which required one week to equilibrate in amorphous polyurethane networks at ambient temperature.³⁴ Once an equilibrium has been reached, there is no change in molecular weight. On the other hand, the reference copolymer (**D1**) displays constant molecular weight throughout the 28 days, with no variation due to heating or time, as expected. This dynamic relationship between high and low molecular weights present in **DA1** is key in controlling the η^* .

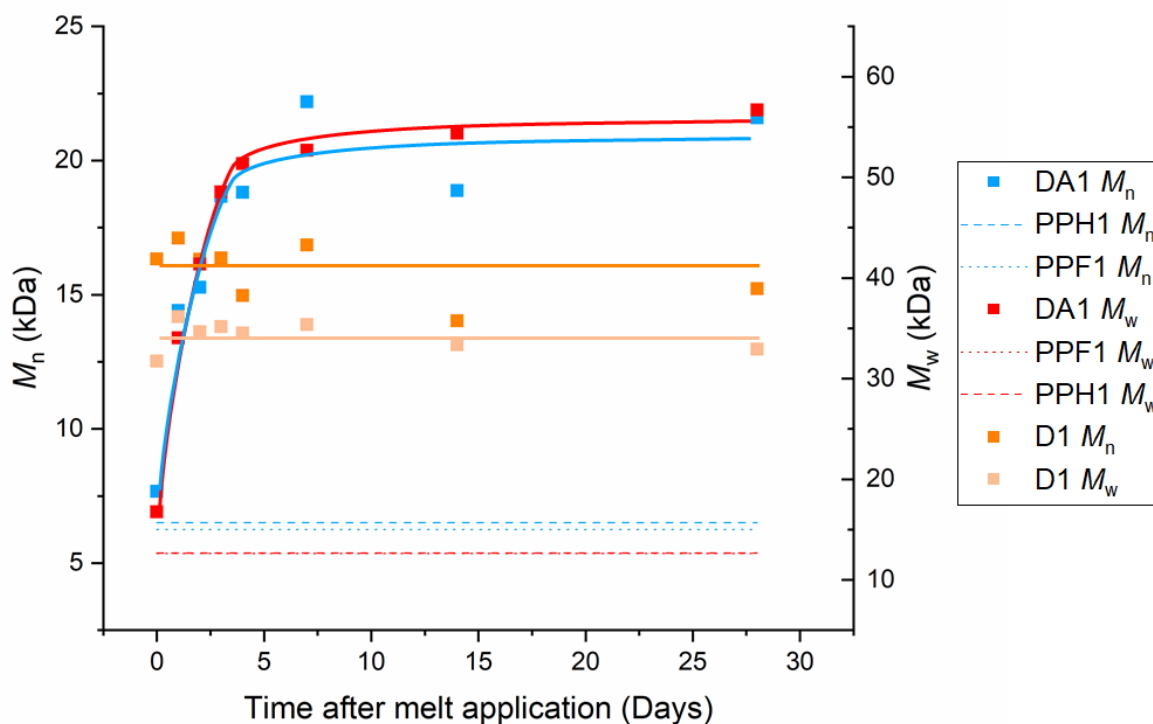


Figure 4.9 The variation of M_n (left y -axis) and M_w (right y -axis) with time at ambient temperature after melt application for **DA1**. The prepolymer molecular weights are marked with short dashed lines. **D1** M_n and M_w are marked with orange dashed lines. Determined by SEC in CHCl_3 against PMMA standards.

FTIR spectroscopy was also used to detect the reformation of DA cycloadducts by monitoring the consumption of **PPH1**. The absorbance at $\nu_{\text{max}} = 696 \text{ cm}^{-1}$ corresponds to the C=C-H of free maleimide which is present in **PPH1** and therefore diminishes in intensity as the maleimide reacts to form the DA cycloadduct (**Figure 4.10(a)**).³⁴ Measuring the area of the absorbance against time shows a similar, but inverted, trend to the change in molecular weight with time (**Figure 4.10(b)**). There is an initial rapid decrease in free maleimide over the first 3 days, however the decrease slows before a plateau is established after 4 days. This plateau indicates that an equilibrium has established between the associative DA reaction and the dissociative rDA reaction.

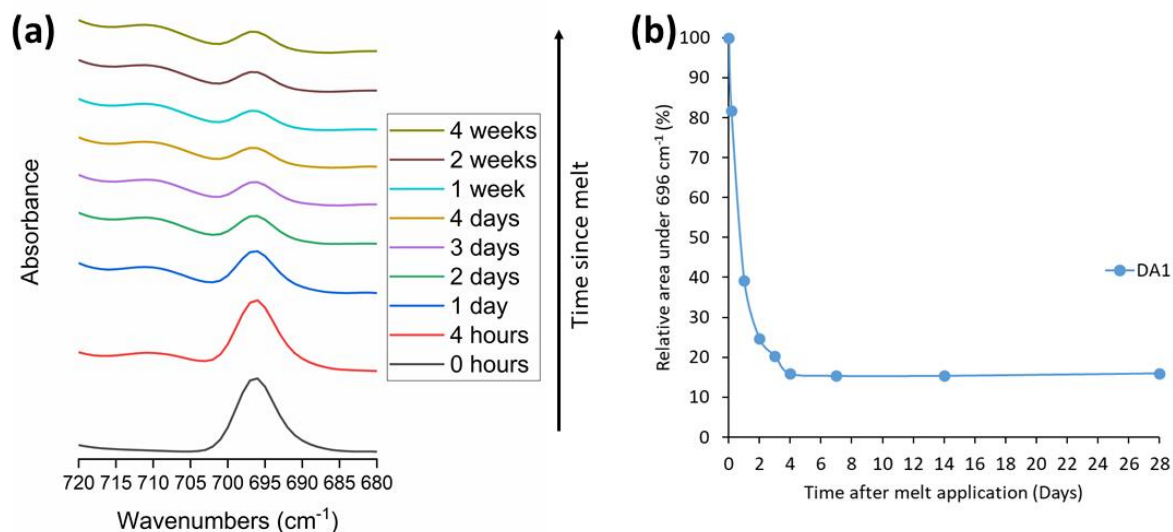


Figure 4.10 (a) Change in absorbance at 696 cm⁻¹ (free maleimide) against time after melt application. **(b)** Decrease in relative absorbance of band at 696 cm⁻¹. Time = 0 is set as 100 %.

Finally, DSC analysis revealed the change in thermal properties of **DA1** over time (**Table 4.6**).

The melting endotherm at 43 °C, corresponding to the crystalline PCL, is not present until the measurement after 7 days (**Figure 4.11(a)**). It is likely that the presence of the DA cycloadduct suppresses the rate of crystallisation of PCL. However, further data would need to be accumulated during the first 7 days to draw full conclusions on the kinetics of crystallisation.

After 14 days, $\Delta H_{m(pol)}$ increases, but remains constant after 28 days indicating that it takes up to 14 days to reach equilibrium for the crystalline phase.

Table 4.6 Thermal data of **DA1** obtained via DSC over 28 days.

Time after melt application (Days)	T_g (°C)	$T_{m(pol)}$ (°C)	$\Delta H_{m(pol)}$ (J.g ⁻¹)	T_{rDA} (°C)	ΔH_{rDA} (J.g ⁻¹)
0	-32	- ^a	- ^a	146	4.9
0.5	-34	38	- ^b	119 & 149	5.8
7	-30	43	17	115 & 148	8.7
14	-23	43	28	116 & 147	9.3
28	-29	43	27	117 & 145	8.7

^a No melting endotherm detected

^b Melting endotherm too small to measure accurately

In contrast, observation of the rDA endotherms shows some cycloadduct is present at $T_m = 146\text{ }^\circ\text{C}$ immediately after cooling the melt to ambient temperature. Recorded values of ΔH_{rDA} increase within the first 7 days and then plateau for the remaining time, as observed in other techniques (**Figure 4.11(b)**).

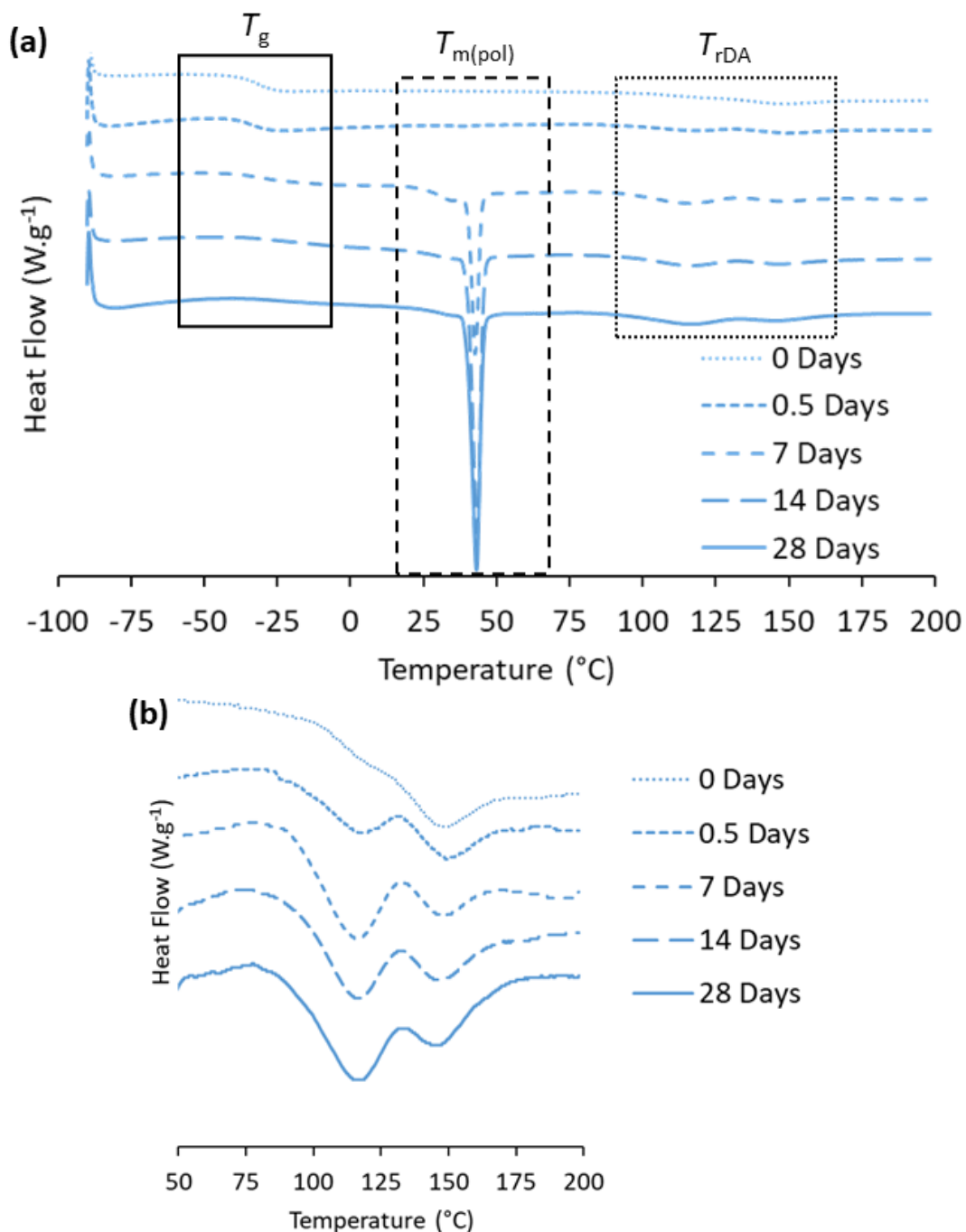
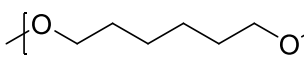
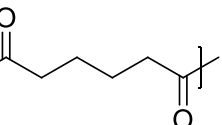
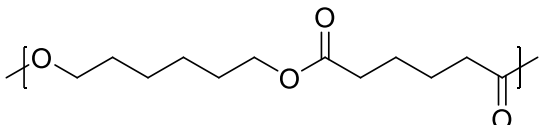
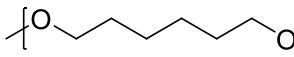
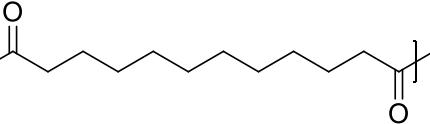
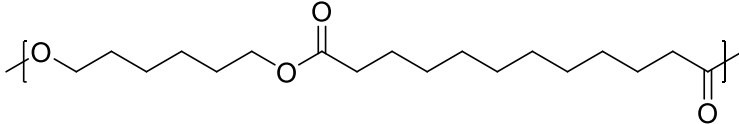
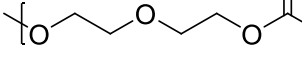
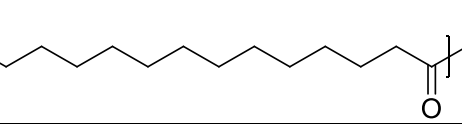
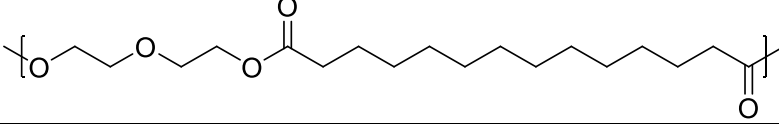


Figure 4.11 (a) The development of DSC thermograms of **DA1** over 28 days at ambient temperature after melt application. Important transitions are highlighted and labelled. **(b)** Close up of regions of rDA. First heating cycles used at a heating rate of $10\text{ }^\circ\text{C}\cdot\text{min}^{-1}$. Exo up.

4.2.2 TPUs comprising thermally reversible covalent bonds and highly crystalline backbones

Following proof of successful incorporation of the DA cycloadducts into a semi-crystalline polymer, the possibility of including reversible covalent chemistry within highly crystalline TPUs was then explored. Three highly crystalline polyols based on copolymers of aliphatic diacids and diols (**Dynacoll 7360**, **Dynacoll 7380** and **Dynacoll 7490**) were used. **Dynacoll 7360** is a copolymer of hexane diol and adipic acid ($T_m = 58\text{ }^\circ\text{C}$), **Dynacoll 7380** is a copolymer of hexanediol and dodecanedioic acid ($T_m = 74\text{ }^\circ\text{C}$) and **Dynacoll 7490** is a copolymer of diethylene glycol and tetradecanoic acid ($T_m = 91\text{ }^\circ\text{C}$) (**Table 4.7**). It is important to note that these commercially available polyols have a higher molecular weight relative to PCL (3.5 kDa vs 2.0 kDa, respectively). Therefore, the resulting DA copolymers based on these polyols will contain a lower concentration of DA cycloadduct compared to the previous **DA1**.

Table 4.7 Structures of semi-crystalline polyols used with DSC data.

Polyol	Structure	$T_{m(\text{pol})}$ ($^\circ\text{C}$)	$\Delta H_{m(\text{pol})}$ ($\text{J}\cdot\text{g}^{-1}$)
Dynacoll 7360	<div style="display: flex; justify-content: space-around;"> <div style="text-align: center;">Hexanediol </div> <div style="text-align: center;">Adipic acid </div> </div> 	58	108
Dynacoll 7380	<div style="display: flex; justify-content: space-around;"> <div style="text-align: center;">Hexanediol </div> <div style="text-align: center;">Dodecanedioic acid </div> </div> 	74	151
Dynacoll 7490	<div style="display: flex; justify-content: space-around;"> <div style="text-align: center;">Diethylene glycol </div> <div style="text-align: center;">Tetradecanoic acid </div> </div> 	91	127

Dynacoll 7360, **7380** and **7490** were copolymerised *via* the same route as **DA1** to form TPUs **DA2**, **DA3** and **DA4**, respectively (**Table 4.8**). Briefly, each Dynacoll polyol was in turn

copolymerised with MDI, followed by reaction with monofunctional HEMI and FA to afford separate HEMI- and FA-terminated prepolymers (**PPHX** and **PPFX**, respectively) (**Scheme 4.1**). **PPHX** and **PPFX** based on the same Dynacoll polyester backbone were then blended in the melt phase followed by subsequent copolymerisation at ambient temperatures to form **DAX**. For simplification during evaluation of the results, **DAX** will be used to represent the three copolymers together with **PPHX** and **PPFX** used to generally represent the HEMI- and FA-terminated prepolymers, respectively. ^1H NMR spectroscopy of **PPH2-4** showed resonances at $\delta = 4.32$ and 4.16 ppm, which relates to $\text{CH}_2\text{O}(\text{C}=\text{O})\text{NH}$ adjacent to a urethane group showing covalent linkage of HEMI and PCL to MDI, respectively. **PPF2-4** shows resonances at $\delta = 5.16$ and 4.17 ppm which correlate to $\text{CH}_2\text{O}(\text{C}=\text{O})\text{NH}$ adjacent to a urethane group showing covalent linkage of FA and PCL to MDI, respectively. **DA2-4** have a weak resonance at $\delta = 5.32$ ppm which corresponds to $\text{CH}(\text{O})(\text{CH})(\text{CH})$ on the DA cycloadduct. There are also two weak resonances at $\delta = 3.03$ and 2.92 ppm which relate to two protons $\text{CH}(\text{CH})\text{C}=\text{O}$ either side of the N atom from the DA cycloadduct as observed with **DA1** (**Figure 4.1**).

Table 4.8 Composition of the semi-crystalline TPU copolymers synthesised with corresponding SEC data.

Copolymer	Molar Ratio ^a			Comonomer	M_n^c (kDa)	M_w^c (kDa)	D_M^c
	PCL	MDI	CE				
PPF2	1.0	2.0	1.1	FA	12.8	24.3	2.18
PPH2	1.0	2.0	1.1	HEMI	9.4	20.3	2.15
DA2	_{-b}	_{-b}	_{-b}	DA	23.7	47.3	2.00
PPF3	1.0	2.0	1.1	FA	12.5	26.2	1.90
PPH3	1.0	2.0	1.1	HEMI	9.6	20.9	2.10
DA3	_{-b}	_{-b}	_{-b}	DA	29.2	74.0	2.55
PPF4	1.0	2.0	1.1	FA	15.2	29.4	1.93
PPH4	1.0	2.0	1.1	HEMI	11.4	25.3	2.22
DA4	_{-b}	_{-b}	_{-b}	DA	31.5	84.3	2.68

^a Molar ratio of functional groups

^b Not measured, made from copolymerisation of prepolymers

^c Determined by SEC in CHCl_3 against PMMA standards

To determine whether DA cycloadducts were present in **DA2**, **DA3** and **DA4**, the materials were analysed by FTIR spectroscopy. After combining prepolymers during melt application, followed by reaction at ambient temperature, all three spectra displayed a disappearance of the absorbance at $\nu_{\max} = 696 \text{ cm}^{-1}$ relating to free maleimide which implies reaction and successful formation of the DA cycloadduct. Additionally, all three **DAX** copolymers exhibit an absorbance at $\nu_{\max} = 1775 \text{ cm}^{-1}$ which is associated with the DA cycloadduct. SEC results show an increase in M_n of all **DAX** copolymers, relative to their respective **PPHX** and **PPFX** prepolymer. An increase in M_n indicates successful cycloaddition of the HEMI and FA prepolymer end groups to form the DA cycloadduct in the backbone.

The carbonyl region within the FTIR spectra of the three **DAX** copolymers and accompanying **PPHX** and **PPFX** prepolymers were then investigated. Results of the carbonyl regions are similar to those of the PCL materials shown previously, **DA1**, **PPH1** and **PPF1** (*Figure 4.2*). The **PPFX** prepolymers all show a relatively narrow absorbance at $\nu_{\max} = 1724 \text{ cm}^{-1}$ which is caused by the polyester backbones with a small shoulder at lower wavenumbers relating to the small amount of urethane present. **PPH3** and **PPH4** show two overlapping absorbances with separate peaks (*Figure 4.12(b) & (c)*), whereas **PPH2** appears more as one major absorbance with a significant shoulder at lower wavenumbers (*Figure 4.12(a)*). The lower absorbance at $\nu_{\max} = 1700 \text{ cm}^{-1}$ indicates maleimide carbonyls which are present in HEMI end groups. In the spectra of **DAX**, a band at $\nu_{\max} = 1724 \text{ cm}^{-1}$ is the major absorbance with a prominent shoulder at approximately $\nu_{\max} = 1700 \text{ cm}^{-1}$ for the imide carbonyl, as discussed previously. These results indicate that despite the high crystallinity of the Dynacoll polyols, the three **DAX** still contain a significant number of intermolecular interactions and likely have good material cohesion.

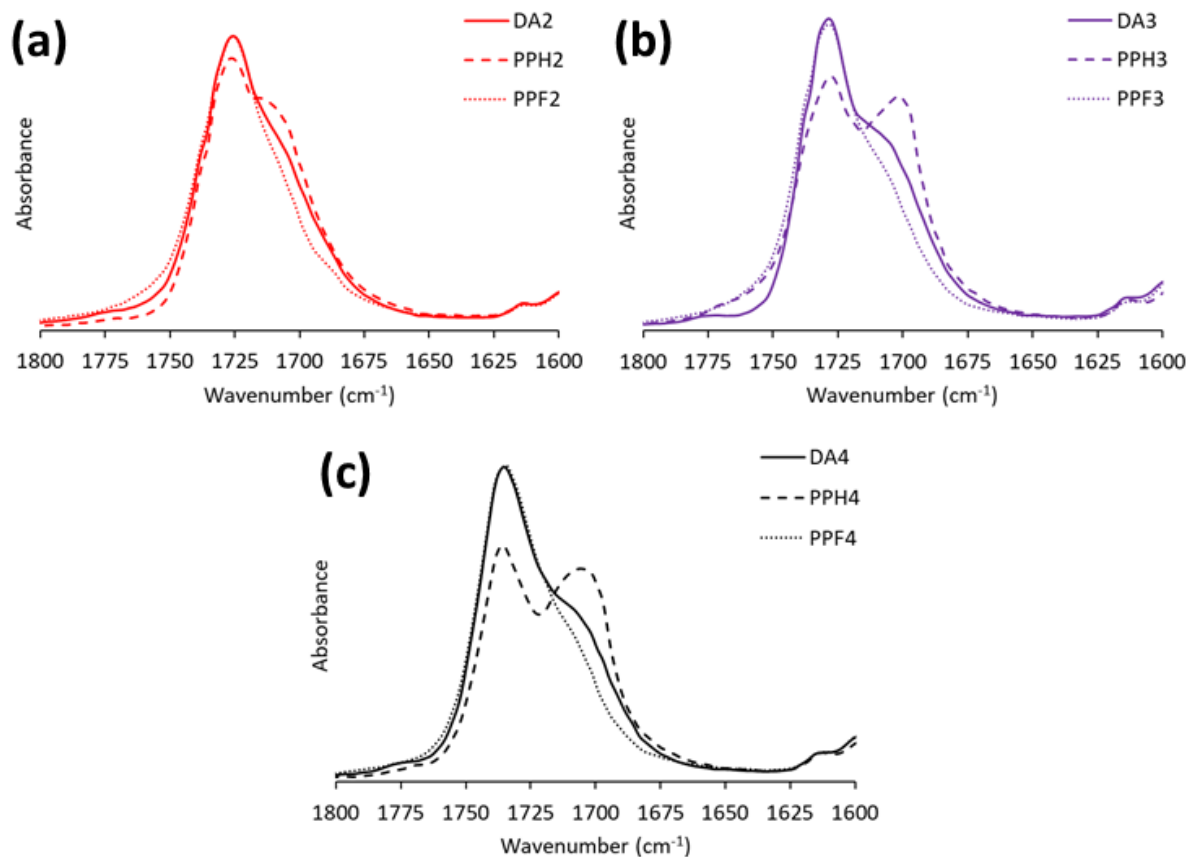


Figure 4.12 FTIR spectra showing carbonyl regions of **DAX** copolymers, **PPHX** and **PPFX** prepolymers for (a) **DA2**, **PPH2** and **PPF2**, (b) **DA3**, **PPH3** and **PPF3** and (c) **DA4**, **PPH4** and **PPF4**.

DSC was used to determine the thermal properties of the materials (**Table 4.9**). Again, the first heating cycle is analysed as a consequence of the slow reformation of the DA cycloadducts. The T_g were too small to be measured accurately, as a consequence of high crystallinity, and are therefore not presented.¹³ Copolymerisation of each polyester polyol with MDI and subsequent reaction with HEMI and FA to form **PPHX** and **PPFX** prepolymers, respectively, decreases the crystalline melting point $T_{m(pol)}$ and $\Delta H_{m(pol)}$ (**Figure 4.13(a)**, **(c)** & **(d)**). This effect is expected as a consequence of the introduction of additional components which disrupt the order of the copolymerised polyester crystallinity. Copolymerisation of **PPHX** and **PPFX** prepolymers to form **DAX** copolymers results in a further decrease in $T_{m(pol)}$ and $\Delta H_{m(pol)}$, a likely a result of the formation of the DA cycloadducts in **DAX** copolymers which

hinders crystallisation. While there is a substantial decrease in the enthalpy of melting $\Delta H_{m(\text{pol})}$, the values recorded are still significantly greater than **DA1** which proves it is possible to maintain a substantial amount of crystallinity upon copolymerisation. The melting points of the resulting copolymers **DA2**, **DA3** and **DA4** (50, 65 and 78 °C, respectively) are higher than **DA1** (43 °C).

Table 4.9 Thermal data of the three copolymers their respective prepolymers and the crystalline polyols, obtained via DSC.

Material	$T_{m(\text{pol})}$ (°C)	$\Delta H_{m(\text{pol})}$ (J.g ⁻¹)	$T_{m(\text{HS})}$ (°C)	$\Delta H_{m(\text{HS})}$ (J.g ⁻¹)	$T_{r\text{DA}}$ (°C)	$\Delta H_{r\text{DA}}$ (J.g ⁻¹)
7360	58	108	- ^a	- ^a	- ^b	- ^b
PPF2	44 & 55	64	- ^a	- ^a	- ^b	- ^b
PPH2	52	69	- ^a	- ^a	- ^b	- ^b
DA2	50	68	- ^a	- ^a	116 & 148	5.2
7380	74	119	- ^a	- ^a	- ^b	- ^b
PPF3	55 & 67	98	- ^a	- ^a	- ^b	- ^b
PPH3	67	81	133	2.3	- ^b	- ^b
DA3	65	74	- ^a	- ^a	117 & 146	5.4
7490	91	127	- ^a	- ^a	- ^b	- ^b
PPF4	82	78	- ^a	- ^a	- ^b	- ^b
PPH4	82	83	111	1.6	- ^b	- ^b
DA4	78	68	- ^a	- ^a	117 & 146	4.5

^a No HS detected

^b No rDA detected

At higher temperatures, **Dynacoll 7360**, **7380** and **7490** and **PPFX** prepolymers do not display any other thermal features. The absence of an additional transition at higher temperatures indicates that **PPFX** prepolymers are single phase. However, **PPH3** and **PPH4** show endotherms at 133 and 111 °C, respectively (**Figure 4.13(d)** & **(f)**). Considering the presence of imide groups, as determined *via* FTIR spectroscopy, this endotherm is possibly caused by

phase separation of the polar end groups in a distinct HS. However, unlike **PPH3** and **PPH4**, **PPH2** does not display an endotherm at higher temperatures which could be a consequence of shorter repeat units (hexanediol and adipic acid) within the backbone, which increases the frequency of polar ester groups along the backbone (**Figure 4.13(b)**). A higher concentration of ester groups could account for greater miscibility with the polar HEMI groups. On the other hand, the backbones in **PPH3** and **PPH4** contain longer aliphatic repeating units which decreases polarity and could promote phase separation of the end groups.

All three **DAX** copolymers exhibit a dual endotherm at approximately 117 and 146 °C which is associated with the rDA reaction, as previously discussed. Therefore, DSC analysis confirms the presence of DA cycloadduct within these highly crystalline TPU copolymers. Values for **DA2-4** ($\Delta H_{rDA} = 4.5 - 5.4 \text{ J.g}^{-1}$) are significantly smaller than for **DA1** ($\Delta H_{rDA} = 8.9 \text{ J.g}^{-1}$). This difference is a consequence of the higher molecular weight of the Dynacoll polyols used to make **DA2-4** which decreases the concentration of DA cycloadducts.

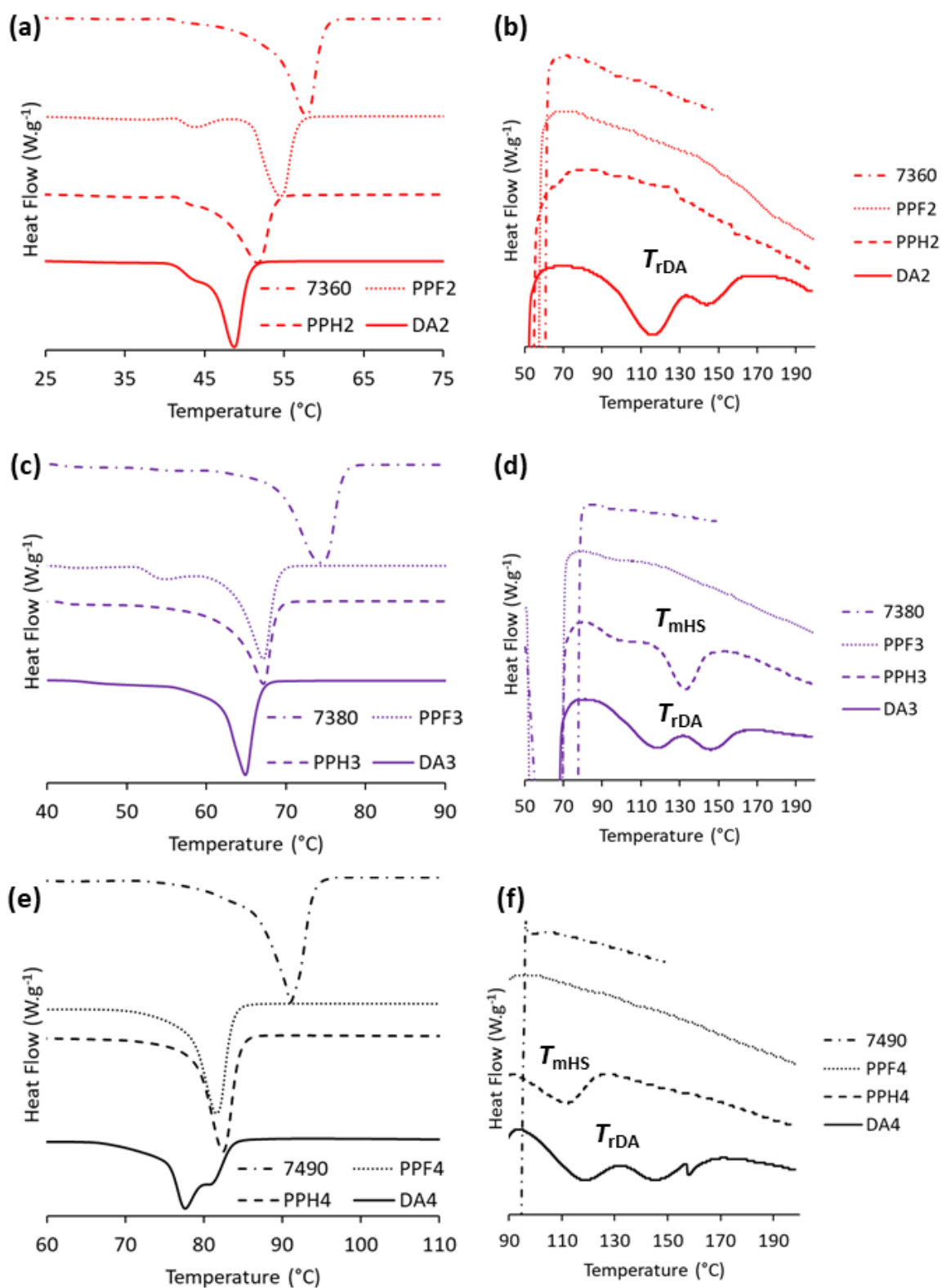


Figure 4.13 Melting endotherms of materials based on (a) Dynacoll 7360, (c) Dynacoll 7380 and (e) Dynacoll 7490. High temperature transitions of materials based on (b) Dynacoll 7360, (d) Dynacoll 7380 and (f) Dynacoll 7490. 7360, 7380 and 7490 refer to the non-copolymerised polyols. First heating cycle used at a heating rate of $10\text{ }^{\circ}\text{C}\cdot\text{min}^{-1}$. Exo up.

The materials were then subjected to DMA as solid bar samples where storage modulus (E') and $\tan \delta$ were measured as a function of temperature (**Figure 4.14**). As with the PCL-based systems, only the **DAX** copolymers were analysed on account of the practical difficulties in preparing samples of the **PPHX** and **PPFX** prepolymers.

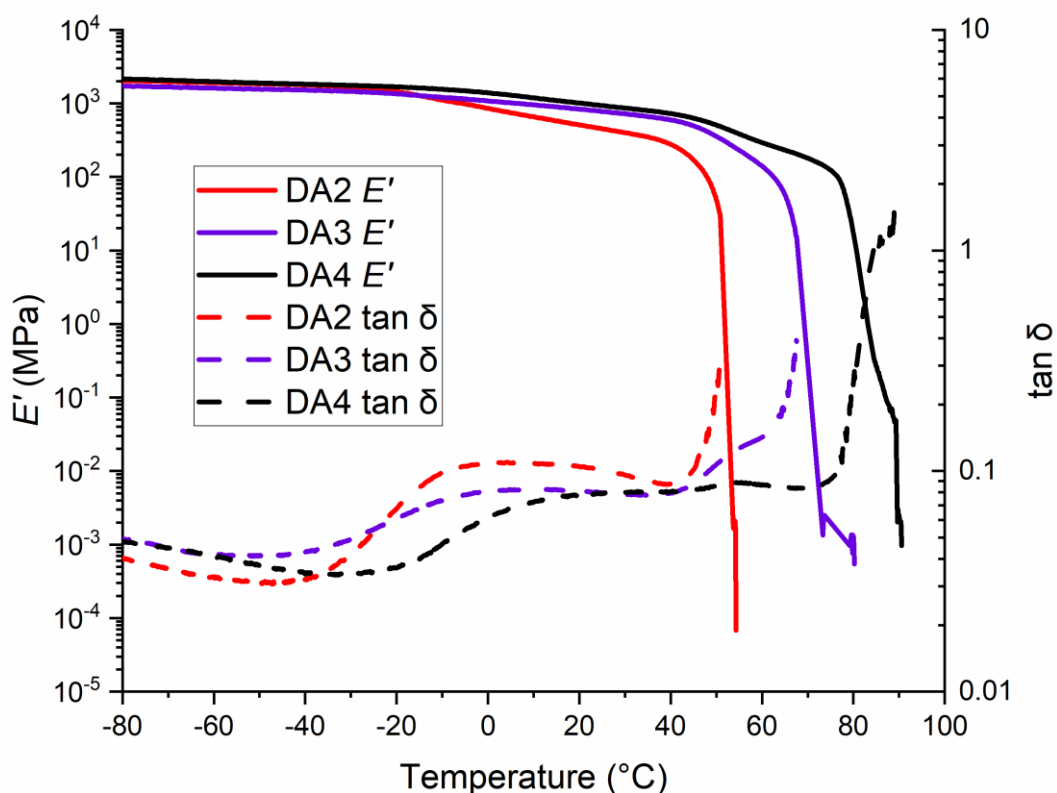


Figure 4.14 DMA of **DA2**, **DA3** and **DA4**. Storage modulus (E') (left y-axis) and $\tan \delta$ (right y-axis) as a function of temperature. Heating rate of $3\text{ }^{\circ}\text{C}\cdot\text{min}^{-1}$.

As temperature increases, all three **DAX** copolymers display a very shallow decrease in E' with an accompanying small change in $\tan \delta$ which indicates a weak T_g . Above T_g , the moduli remain high with a resemblance to a plateau region. All three materials reported higher E' above T_g than **DA1** (**Table 4.10** vs **Table 4.3**). The increase is likely on account of the higher crystallinity of the copolymers containing Dynacoll, with E' increasing in order of $T_{m(\text{pol})}$ (**DA2**

< **DA3** < **DA4**). Finally, each material dramatically decreases in E' over several orders of magnitude at their respective $T_{m(pol)}$. Above this temperature, the values of E' were too low to measure accurately, however the samples themselves did not break during the experiments. As hypothesised with **DA1**, this lack of strength is either a consequence of insufficient DA cycloadduct concentration or internal order of the copolymers above $T_{m(pol)}$.

Table 4.10 Thermal data of **DA2-4** obtained via DMA at a heating rate of $3\text{ }^{\circ}\text{C}\cdot\text{min}^{-1}$.

Copolymer	$E' (T > T_g)^a$ (MPa)	T_g^b ($^{\circ}\text{C}$)	$E' (T > T_g)^c$ (MPa)	$T_{m(pol)}^d$ ($^{\circ}\text{C}$)
DA2	1845	4	505	46
DA3	1555	12	835	64
DA4	1890	17	1015	78

^a Modulus measured at $-50\text{ }^{\circ}\text{C}$

^b Measured as peak in $\tan \delta$

^c Modulus measured at $20\text{ }^{\circ}\text{C}$

^d Measured as the onset of modulus reduction

The flow properties of the **DAX** copolymers were determined with temperature sweeps *via* oscillatory rheology measurements. Both η^* and $\tan \delta$ were monitored as a function of temperature (**Figure 4.15**). At lower temperature below their melting points, all samples initially show high signal-to-noise ratio likely because of slippage of the solid samples. However, once each material passes its respective $T_{m(pol)}$, the data obtained is much smoother due to better sample-to-plate contact in the molten state. As expected, the η^* decreases significantly above $T_{m(pol)}$, as the sample is able to flow. As the temperature continues to increase, there is a substantial decrease in η^* at approximately $100\text{ }^{\circ}\text{C}$ which is accompanied by a peak in $\tan \delta$. These features coincide with the rDA reaction, as the cycloadducts within the backbones break causing molecular weight to decrease and resulting in rapid reduction of η^* . Notably, the complex viscosity of all three materials is well below the target of $10\text{ Pa}\cdot\text{s}^{-1}$ within the temperature range recorded which presents them as potentially suitable materials for reversible adhesive from the perspective of application and removal.

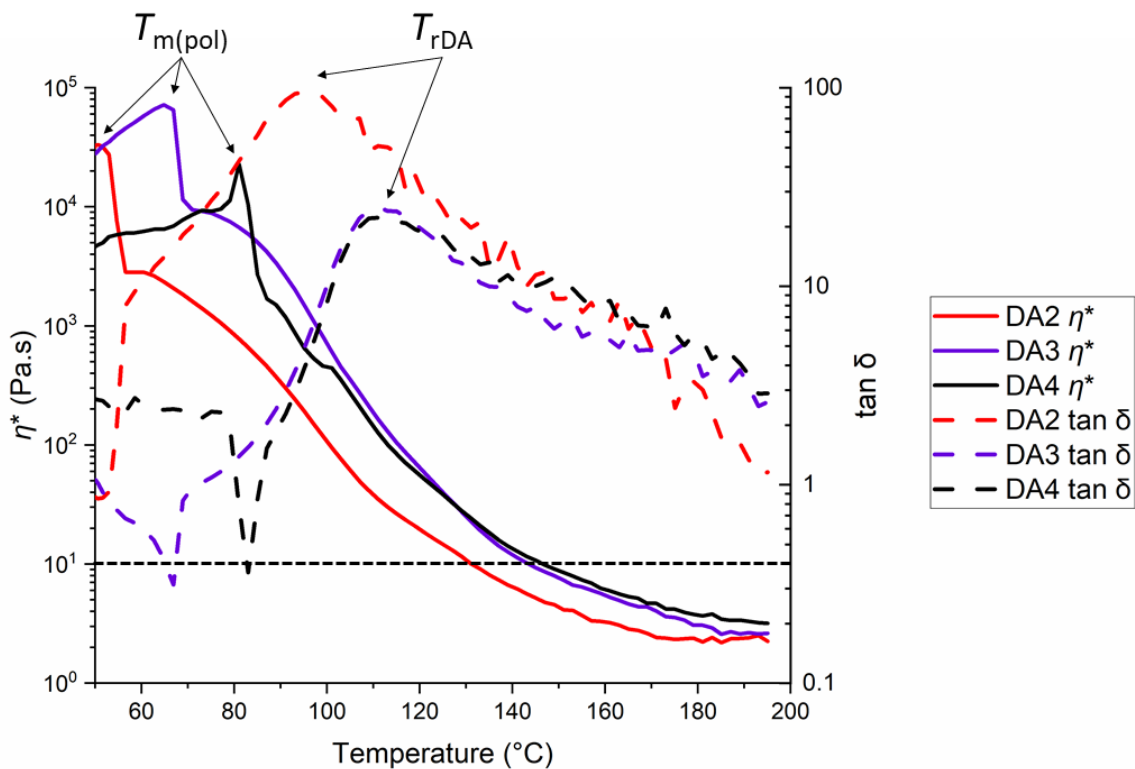


Figure 4.15 Rheological analysis of **DA2**, **DA3** and **DA4**. Complex viscosity (η^*) (left y-axis) and $\tan \delta$ (right y-axis) as a function of temperature. The short dashed black line represents the target η^* of $10 \text{ Pa}\cdot\text{s}^{-1}$.

The three **DAX** copolymers were then evaluated by tensile testing to determine their mechanical properties. The resulting stress-strain curves were analysed (**Figure 4.16**). Each material initially shows elastic deformation at low strain. Despite containing less DA cycloadduct, the modulus values for the Dynacoll based **DAX** copolymers are significantly higher than for **DA1**, which suggests mechanical performance is more dependent on the constituent polyester than DA cycloadduct concentration (**Table 4.11**). The values of E again increase in the order of $T_{m(\text{pol})}$: **DA2** < **DA3** < **DA4**, which matches the order of E' and confirms **DA4** is the strongest material. **DA4** fractures with an impressively high tensile strength ($18 \pm 1 \text{ MPa}$) at $5 \pm < 1 \%$ elongation, which shows it is a strong, brittle material with relatively low toughness ($50 \pm 5 \text{ MPa}$). **DA2** stretches beyond its yield point before fracturing at $40 \pm 1 \%$ elongation. Remarkably, **DA3** displays a stress-strain curve with both elastic and plastic

deformation, with high strength ($E = 489 \pm 22$ MPa and $\sigma_{\max} = 17 \pm < 1$ MPa) and toughness (2465 \pm 65 MPa).

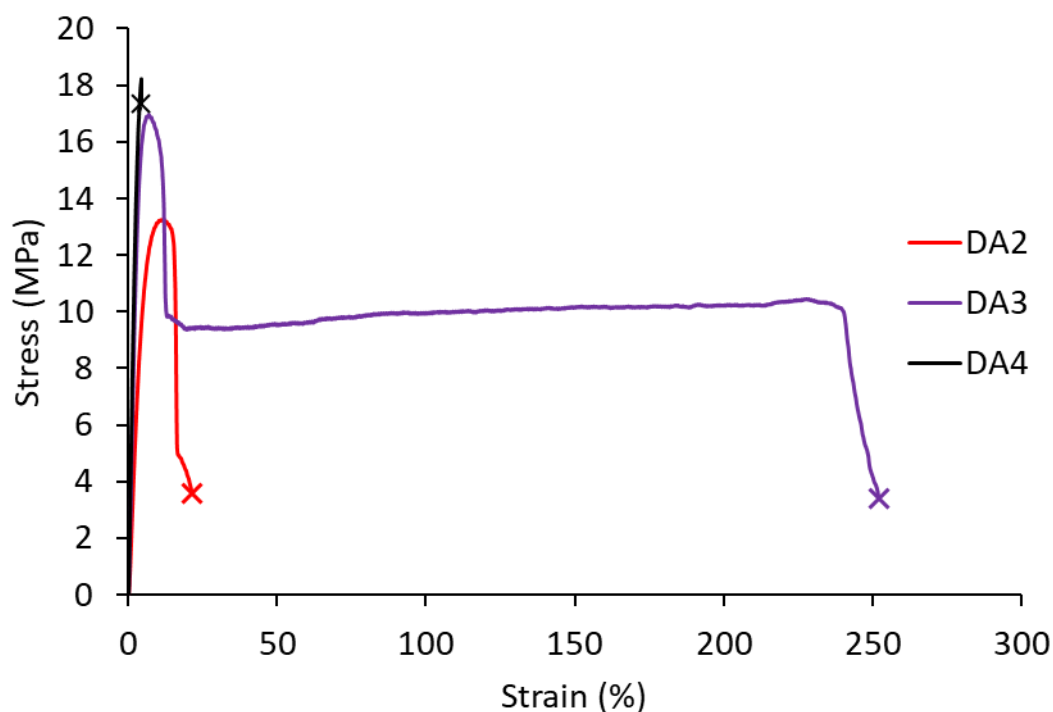


Figure 4.16 Stress-strain curves of **DA2**, **DA3** and **DA4** measured at a speed of 10 mm.min⁻¹. Sample rupture is marked with a cross.

Table 4.11 Summary of mechanical data obtained from tensile stress-strain measurements for the two copolymers at a speed of 10 mm.min⁻¹.

Copolymer	E^a (MPa)	σ_{\max}^b (MPa)	U_T^c (MPa)	ϵ_{\max}^d (%)
DA2	264 \pm 14	12 \pm < 1	300 \pm 35	40 \pm 1
DA3	489 \pm 22	17 \pm < 1	2465 \pm 65	250 \pm 3
DA4	588 \pm 35	18 \pm 1	50 \pm 5	5 \pm < 1

^a Young's modulus is calculated from the initial gradient before the Yield point.

^b Ultimate tensile strength is the maximum recorded stress the sample can withstand before failure.

^c Modulus of toughness is measured as the area under the curve and represents the total energy a material can withstand without breaking.

^d Elongation at break is the strain (%) at which the sample breaks.

The adhesive properties of **DAX** were determined *via* lap shear testing with beechwood substrates. The bond strengths of all three **DAX** are similar, with **DA3** (8.5 \pm 0.9 MPa) and **DA4**

(8.3 ± 1.2 MPa) showing slightly higher values than **DA2** (7.1 ± 0.4 MPa) (**Figure 4.17(a)**). Each copolymer caused extreme substrate failure, with the beechwood tearing or breaking, which shows that the upper limit of the substrate strength was reached (**Figure 4.17(c)**). Therefore, the lap shear tests were repeated with aluminium substrates which provided higher bond strengths for each copolymer. The bond strength for **DA2** increases slightly to 10.9 ± 0.3 MPa, **DA3** displays a large increase to 14.1 ± 0.8 MPa and **DA4** records a substantial increase to 20.3 ± 0.9 MPa which is remarkable for a thermoplastic polymer adhesive (**Figure 4.17(b)**). Each material displays cohesive failure (**Figure 4.17(d)**). These results are extremely promising for adhesive applications, achieving double the strength reported for reversible amorphous crosslinked systems (approx. 10 MPa) and quadruple that of an irreversibly crosslinked PU adhesive (approx. 5 MPa).^{21, 34} As cycloadduct concentration appears to be relatively equal (*via* DSC), it emphasises that the different properties arise from the different constituent polyester backbones which indicates potential for targeted properties.

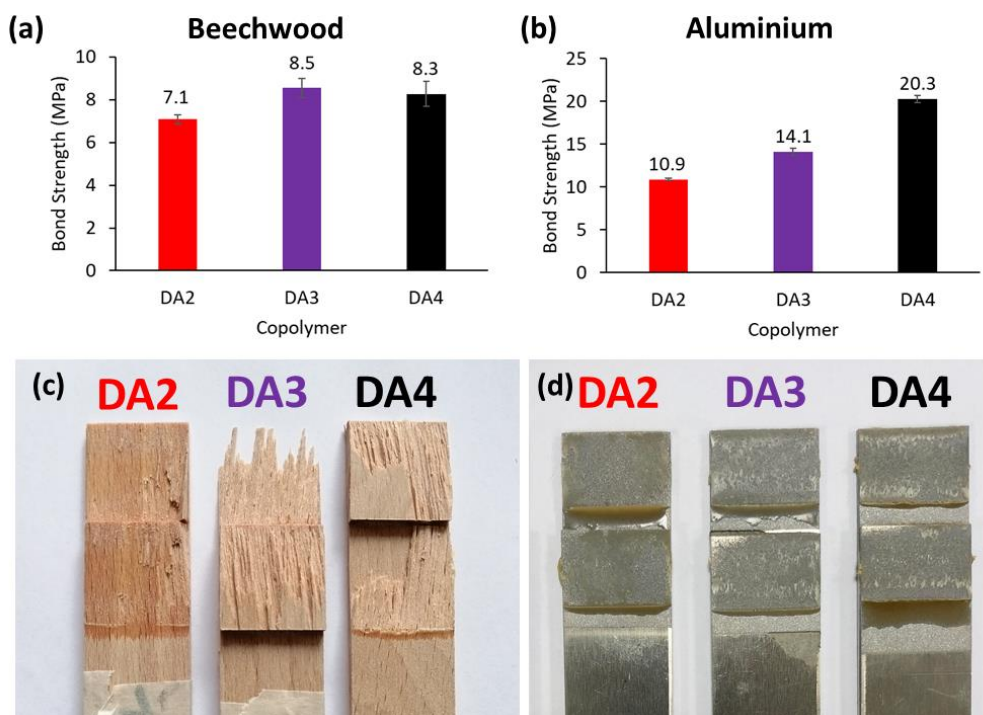


Figure 4.17 Bond strengths of **DA2-4** with **(a)** beechwood **(b)** and aluminium substrates. **(c)** Substrate failure of beechwood substrates. **(d)** cohesive failure of aluminium substrates.

The reversibility of the Dynacoll-based **DAX** copolymers was investigated in the same manner as **DA1** described earlier. Samples of each material were heated to 150 °C for 1 hour then left to equilibrate at room temperature for 28 days, with samples analysed throughout *via* SEC, FTIR analysis and DSC.

SEC results of **DAX** copolymers analysed immediately after heating showed M_n similar to those of the respective prepolymers (**Table 4.12**). These results show successful rDA reaction and good reversibility to return to the prepolymer state. All three **DAX** copolymers increase rapidly in molecular weight at ambient temperature followed by a plateau after 7 days when an equilibrium between the associative and dissociative DA reaction has been achieved. (**Figure 4.18**). This behaviour is similar to **DA1** previously described.

Table 4.12 Time dependent molecular weight values for copolymers **DA2**, **DA3** and **DA4** with time. Prepolymers **PPHX** and **PPFX** were only measured once and not as a function of time and the averages are labelled as **PPX**.

Material	Days after melt application ^{b, c}								Equilibrated ^d
	0	1	2	3	4	7	14	28	
DA2 M_n	8.2	13.7	15.7	17.0	13.2	15.4	18.9	20.5	18.3
PP1 M_n^a	11.1								
DA3 M_n	10.4	21.8	19.9	25.5	29.4	28.4	25.0	34.3	29.2
PP3 M_n^a	11.0								
DA4 M_n	10.5	24.0	23.4	33.1	31.0	31.6	29.3	33.6	31.5
PP4 M_n^a	13.3								

^a **PPX** is the average M_n of both **PPHX** and **PPFX** prepolymers (for clarity)

^b Determined by SEC in $CHCl_3$ against PMMA standards

^c Values reported in kDa

^d Measured as the average of 7, 14 and 28 days

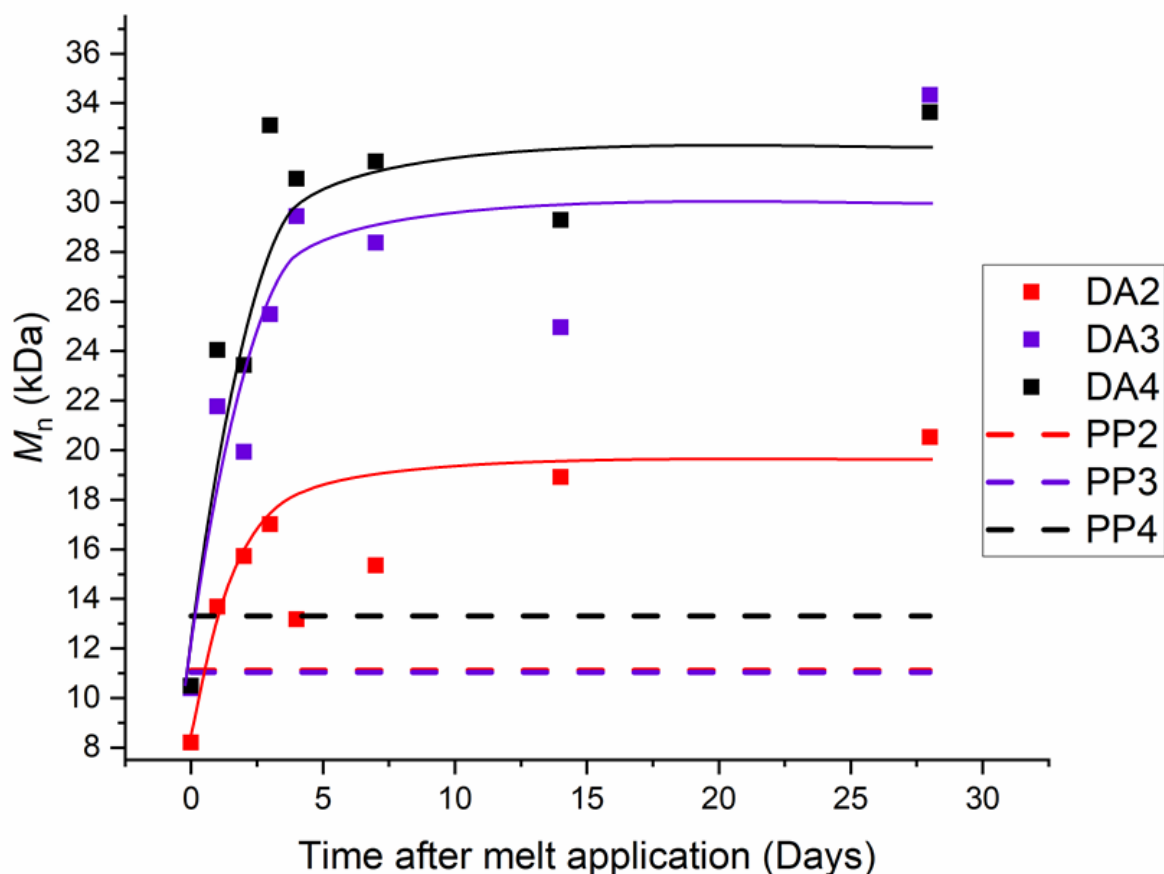


Figure 4.18 M_n as a function of time at ambient after melt application for **DA2**, **DA3** and **DA4**. For clarity, the average prepolymer molecular weights (**PPX**) of respective **PPFX** and **PPHX** are marked with dashed lines. Determined by SEC in CHCl_3 against PMMA standards.

FTIR analysis of **DAX** samples immediately after melt application revealed the appearance of the absorbance at $\nu_{\text{max}} = 696 \text{ cm}^{-1}$ corresponding to free maleimide. This absorbance suggests a reversal of each **DAX** copolymer back into its respective **PPHX** and **PPFX** prepolymers. Each copolymer was monitored over time and the relative intensity of the absorbances at $\nu_{\text{max}} = 696 \text{ cm}^{-1}$ were measured (**Figure 4.19**). After the initial rapid decrease in intensity over the first 7 days, all three **DAX** plateau as expected indicating an equilibrium of the reversible DA reaction is reached. **DA2** and **DA3** show < 30% free maleimide remains after 28 days, whereas **DA4** shows approximately 45%, likely a consequence of the high melting point of **DA4** which is well above ambient temperature at which the material is copolymerised. With comparison

to **DA1** (approximately 15%), the results suggest that more unreacted maleimide is present for materials with higher melting points due to potential issues with chain mobility (**Figure 4.10(b)** vs **Figure 4.19**).

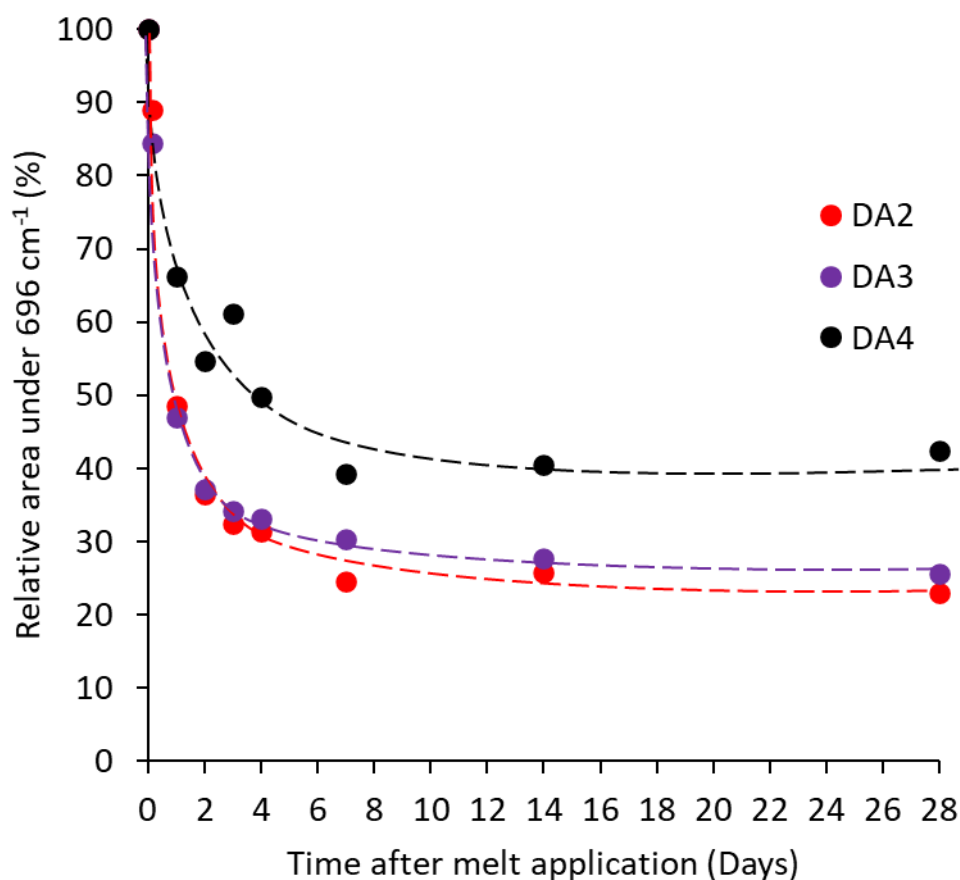


Figure 4.19 Relative intensities of FTIR absorbance at $\nu_{max} = 696 \text{ cm}^{-1}$ with time at ambient after melt application for **DA2**, **DA3** and **DA4**.

Finally, the materials were monitored *via* DSC as a function of time at ambient after melt application. The crystalline melting endotherms were present immediately for all **DAX** materials which show they have much faster crystallisation kinetics relative to **DA1** (**Table 4.13**). **DA4** shows that crystallisation equilibrates within 0.5 days whereas **DA3** and **DA2** equilibrate within 7 days. Fast crystallisation could permit reasonable initial strength to hold substrates in place as the DA cycloadduct forms over time.

Immediately after cooling the miscible molten blend of prepolymers (0 days), all three **DAX** copolymers exhibit a small endothermic peak at 146 – 149 °C, which corresponds to T_{rDA} (**Figure 4.20**). As with **DA1**, the copolymers **DA2-4** require approximately 7 days for ΔH_{rDA} to increase and plateau. This trend in ΔH_{rDA} shows that the DA cycloadduct is present in low concentration initially but increases with time. After 7 days, the material reaches an equilibrium. Therefore, DSC analysis also proves the reversibility of the **DAX** copolymers. It is interesting to note in these studies the kinetics of polyester segment crystallisation do not appear to influence the rate of DA association.

Table 4.13 Thermal data of **DA2**, **DA3** & **DA4** obtained via DSC over 28 days.

Copolymer	Time after melt application (Days)	$T_{m(pol)}$ (°C)	$\Delta H_{m(pol)}$ (J.g ⁻¹)	T_{rDA} (°C)	ΔH_{rDA} (J.g ⁻¹)
DA2	0	49	53	149	0.5
	0.5	48	56	116 & 149	1.9
	7	50	67	116 & 147	5.6
	14	50	67	117 & 147	5.9
	28	49	65	116 & 144	5.6
DA3	0	65	67	147	2.2
	0.5	64	69	118 & 147	3.7
	7	65	74	117 & 146	5.1
	14	65	72	117 & 146	6.0
	28	65	76	119 & 146	5.2
DA4	0	77 & 82	56	146	1.3
	0.5	76 & 83	67	118 & 147	2.5
	7	77 & 81	70	117 & 146	4.4
	14	77 & 81	67	116 & 146	4.4
	28	77	68	118 & 146	4.7

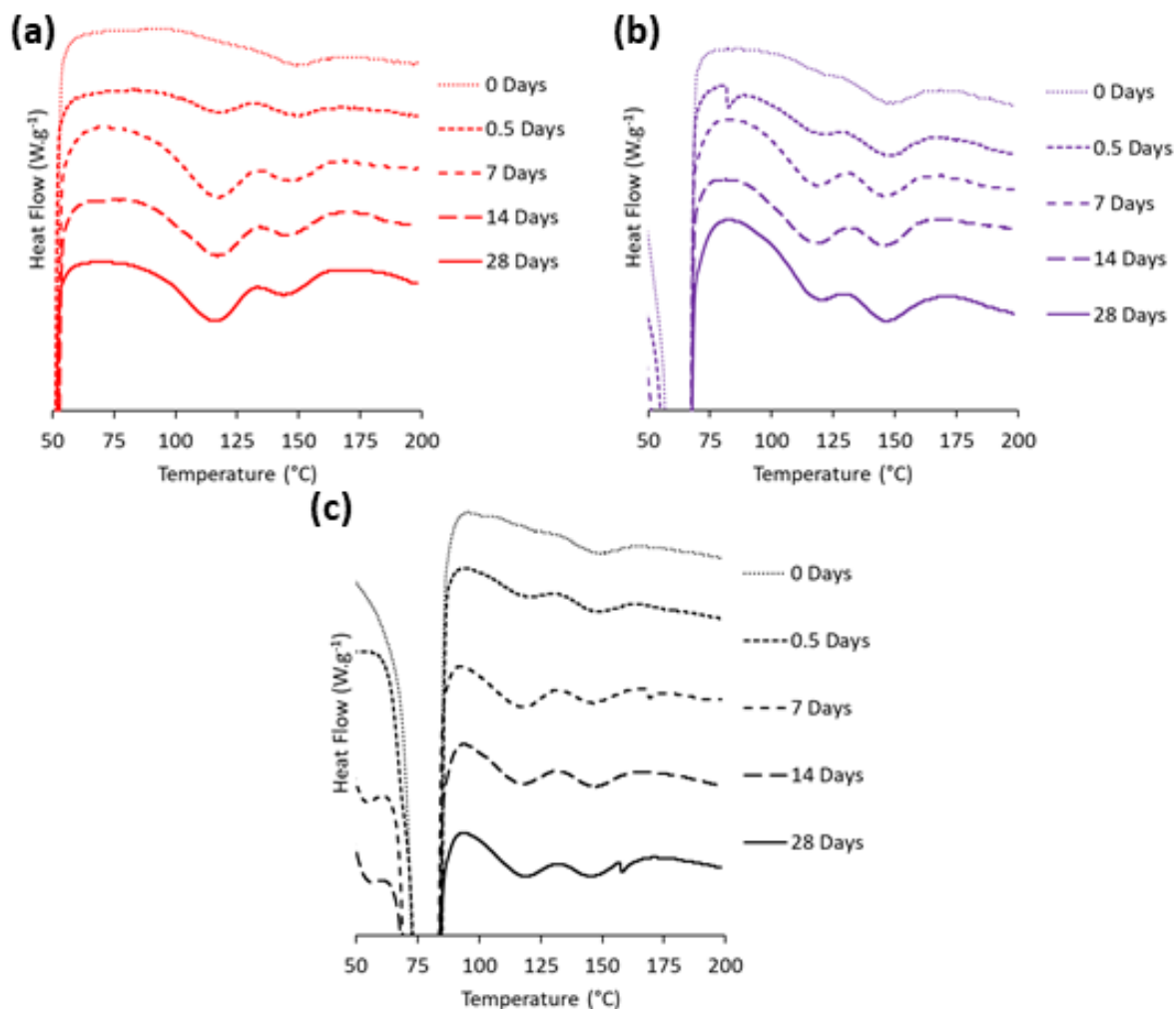


Figure 4.20 DSC thermograms of rDA regions against time for (a) DA2 (b) DA3 and (c) DA4. First heating cycle used at a heating rate of $10\text{ }^{\circ}\text{C}\cdot\text{min}^{-1}$. Exo up.

Overall, the results for the highly crystalline **DAX** copolymers demonstrate that it is still possible to form DA cycloadduct despite large concentrations of crystalline segments with high melting points and extremely fast crystallisation. Importantly, **DAX** copolymers produce very impressive bond strengths, especially **DA4**. However, FTIR spectroscopic data revealed that there is a higher percentage of free maleimide present in **DA2-4** after 28 days relative to **DA1** which is partially reflected in lower values of ΔH_{rDA} . This difference is likely caused by the higher T_m of the Dynacoll based copolymers which promotes crystal formation over DA adduct formation when copolymerising at ambient temperature. Further work could investigate the

potential of increasing the amount of DA cycloadduct formation *via* post synthesis heat treatment with determination of any effects on mechanical performance. Studies have demonstrated the possibility of exploiting the interplay between crystal and DA cycloadduct formation by thermal conditioning to favour formation of one or the other.¹⁶ Therefore, heating to approximately 60 °C could enhance DA cycloadduct conversion, further increasing the molecular weight of the copolymers and their resulting mechanical properties.¹⁷

4.2.3 Amorphous TPUs comprising thermally reversible covalent bonds

As a reference point, the effect of DA cycloadducts within amorphous TPUs was investigated. These experiments were performed to help determine the interplay between polyol crystallinity and DA cycloadduct formation by analysing reference 'zero crystallinity' materials. The polyols on which the amorphous DA TPUs are based are **Capa 8025**, a 75 : 25 random copolymer of ϵ -caprolactone and lactic acid, and **Priplast 1838**, a hydrophobic copolymer of C₃₆ dimer diol containing long aliphatic branches copolymerised with an undefined diacid (trade secret) (**Figure 4.21**). Both polyols are 2.0 kDa, OH-terminated and amorphous at room temperature. These materials were selected as **Capa 8025** is a good reference to the semi-crystalline poly(caprolactone) polyols used previously and **Priplast 1838** is very non-polar with some similarity to the more highly crystalline materials based on long chain linear diacids.

The same reaction pathway as previously described was used to make the amorphous DA copolymers (**Scheme 4.1**). Maleimide- and furan-terminated prepolymers were made separately *via* reaction of NCO-terminated prepolymers with HEMI and FA, respectively. DA copolymers were then made by blending the prepolymers in the melt followed by copolymerisation at ambient temperature. Prepolymers **PPHA1** and **PPFA1** were used to

synthesise **DAA1**, all comprising the more polar **Capa 8025** backbone. Prepolymers **PPHA2** and **PPFA2** were used to synthesise **DAA2** comprising the hydrophobic backbone **Priplast 1838** (*Table 4.14*).

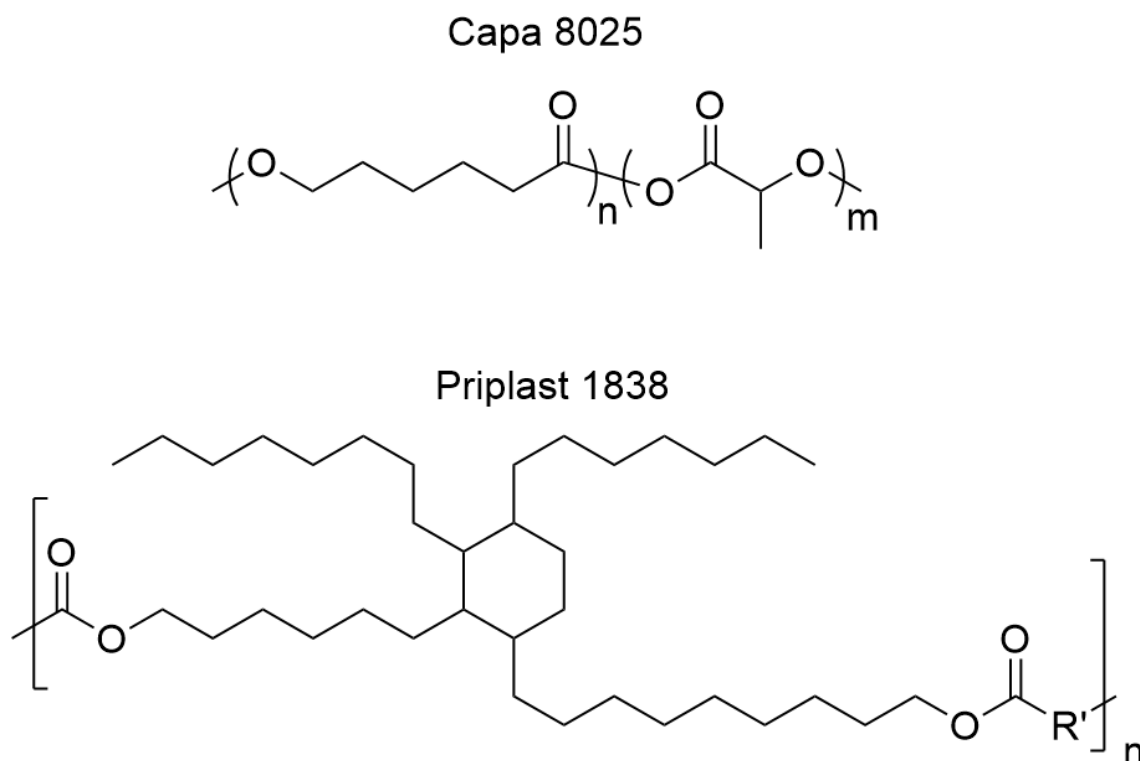


Figure 4.21 Composition of **Capa 8025** (copolymer of ϵ -caprolactone and lactic acid) and approximate structure of **Priplast 1838**. R represents undefined diacid copolymerised.

Table 4.14 Composition of amorphous TPU copolymers synthesised with corresponding SEC data.

Copolymer	Molar Ratio ^a			Comonomer	M_n^c (kDa)	M_w^c (kDa)	\bar{D}_M^c
	PCL	MDI	CE				
PPFA1	1.0	2.0	1.1	FA	6.3	11.7	1.85
PPHA1	1.0	2.0	1.1	HEMI	6.0	11.1	1.85
DAA1	_b	_b	_b	DA	11.0	28.2	2.56
PPFA2	1.0	2.0	1.1	FA	6.0	14.2	2.36
PPHA2	1.0	2.0	1.1	HEMI	6.0	13.8	2.28
DAA2	_b	_b	_b	DA	_d	_d	_d

^a Molar ratio of functional groups

^b Not measured, made from copolymerisation of prepolymers

^c Determined by SEC in $CHCl_3$ against PMMA standards

^d Insoluble so not measured

Synthesis of the prepolymers and copolymers were proven by ^1H NMR and FTIR spectroscopies. In the ^1H spectrum of **PPHA1**, it displayed a resonance at $\delta = 4.32$ ppm ($\text{CH}_2\text{O}(\text{C}=\text{O})\text{NH}$) which signifies the covalent incorporation of HEMI. **PPFA1** showed a resonance at $\delta = 5.15$ ppm ($\text{CH}_2\text{O}(\text{C}=\text{O})\text{NH}$) which suggests incorporation of FA into the polymer. Similar resonances at $\delta = 4.33$ and 5.17 ppm were recorded for **PPHA2** and **PPFA2**, respectively. The spectrum of **DAA1** showed a resonance at $\delta = 5.31$ ppm which corresponds to $\text{CH}(\text{O})(\text{CH})(\text{CH})$ in the DA cycloadduct and two resonances at $\delta = 3.02$ and 2.92 ppm which relate to two protons $\text{CH}(\text{CH})\text{C}=\text{O}$ either side of the N atom in the DA cycloadduct as discussed previously for **DA1** (*Figure 4.1*). However, **DAA2** was insoluble in CHCl_3 , so no NMR spectra were obtained.³⁷

SEC results of **DAA1** revealed an increase in molecular weight relative to its component prepolymers **PPHA1** and **PPFA1**. However, the M_n of **DAA1** (11.0 kDa) is much lower than expected compared to the increases in molecular weight for previous materials. Additionally, it was not possible to obtain molecular weight values of **DAA2** as a consequence of poor solubility. As previously, FTIR spectra of **DAA1** and **DAA2** display a disappearance of the absorbance at $\nu_{\text{max}} = 696 \text{ cm}^{-1}$ over time which signifies the consumption of free maleimide. Both SEC and FTIR spectroscopy results imply the formation the DA cycloadduct.

Further FTIR spectroscopic analysis of the carbonyl region of the two **DAX** copolymers and four prepolymers reveals details on the type of intermolecular interactions present. Materials based on **Capa 8025** show a large absorbance at $\nu_{\text{max}} = 1728 \text{ cm}^{-1}$ which corresponds to ester within the polyol backbone (*Figure 4.22(a)*). **PPFA1** displays a slight shoulder at lower wavenumbers which is representative of urethane carbonyl groups. **PPHA1** shows two peaks, the lower at $\nu_{\text{max}} = 1711 \text{ cm}^{-1}$ which is caused by the imide carbonyl functionality as described

previously. The resulting copolymer **DAA1** shows a spectrum with a main absorbance at $\nu_{\max} = 1728 \text{ cm}^{-1}$ and a significant shoulder at 1711 cm^{-1} . Interestingly, all materials based on the hydrophobic backbone **Priplast 1838** show two overlapping absorbances (**Figure 4.22(b)**). One absorbance at $\nu_{\max} = 1733 \text{ cm}^{-1}$ which relates to the ester within the polyol backbone is present in all spectra. The second for **PPFA2** appears at $\nu_{\max} = 1700 \text{ cm}^{-1}$ on account of urethane carbonyl groups. **PPHA2** displays its second high intensity absorbance at $\nu_{\max} = 1705 \text{ cm}^{-1}$ corresponding to imide carbonyl groups. Finally, **DAA2** has a broad absorbance at $\nu_{\max} = 1703 \text{ cm}^{-1}$ which is a combination of imide and urethane carbonyls. The higher relative absorbance for the peak at lower wavenumber are likely to result from the lower concentration of ester groups in the backbone. This analysis aligns with the data previously discussed for the semi-crystalline TPU copolymers which suggests crystallinity does not prevent formation of intermolecular interactions. In fact, absorbances in the amorphous materials tend to appear at higher wavenumbers which suggests these interactions are weaker.

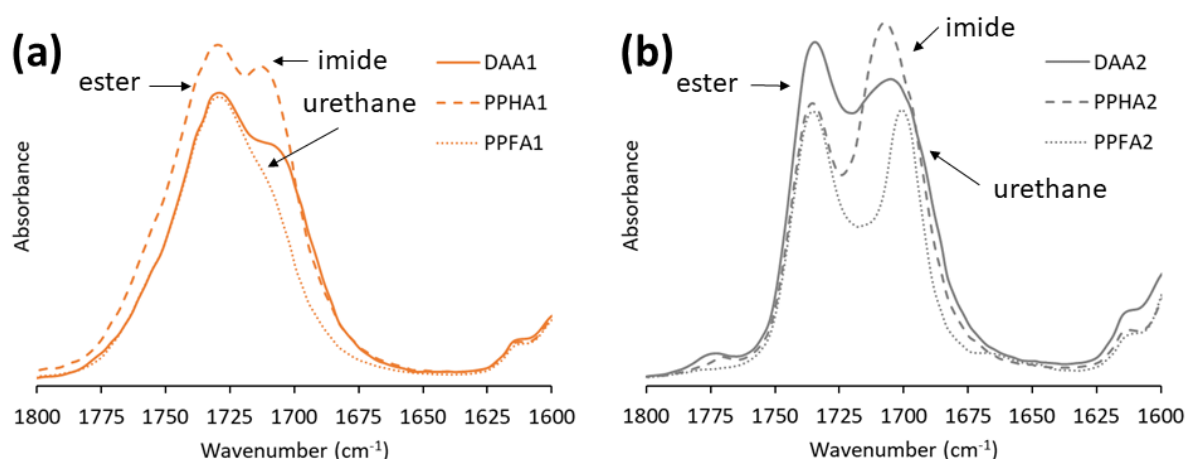


Figure 4.22 FTIR spectra showing carbonyl regions of (a) **DAA1**, **PPHA1** and **PPFA1** and (b) **DAA2**, **PPHA2** and **PPFA2**.

Thermal analysis was performed on the amorphous materials *via* DSC with the same method as all previous materials. Heating cycles of the **Capa 8025** polyol displayed a clear T_g which increased on copolymerisation with MDI and reaction with HEMI or FA to make the prepolymers (**Table 4.15**). Copolymerisation of **PPHA1** and **PPFA1** to form **DAA1** showed an additional increase in T_g . This trend reveals that there is restriction to rotation around main chain bonds upon copolymerisation. The T_g also becomes a little broader with copolymerisation which indicates a decrease in material homogeneity (**Figure 4.23(a)**). The data suggests that formation of the DA cycloadducts significantly hinders chain mobility. **PPHA1** displays a shallow undefined thermal transition at 98 °C which could be a sign of end group association, as seen for the previous materials **PPH1**, **PPH3** and **PPH4**. There are no other thermal transitions observed for the pure polyol **Capa 8025**, **PPHA1** or **PPFA1**. However, as expected, **DAA1** displays two endotherms at 117 & 145 °C corresponding to the rDA reaction. It is notable that the enthalpy change due to the dissociation of cycloadducts (ΔH_{rDA}) of the amorphous **DAA1** (11.9 J.g⁻¹) is only slightly higher than the poly(ϵ -caprolactone) copolymer **DA1** (8.9 J.g⁻¹) which indicates that the presence of crystallinity within the latter has a small effect on hindering DA cycloadduct formation.

The thermogram of **Priplast 1838** displays a T_g at -62 °C which is very low due to the aliphatic and flexible nature of the material. The T_g increases upon copolymerisation with MDI and reaction with HEMI or FA as a consequence of increased restriction of chain mobility, but remains relatively low which is promising for low temperature applications. Just above the T_g , there is second feature that is not observed after copolymerisation of **Priplast 1838** (**Figure 4.23(b)**).

Table 4.15 Thermal analysis data of the two copolymers, two prepolymers and polyols for materials based on **Capa 8025** and **Priplast 1838**, obtained via DSC.

Material	T_g (°C)	T_{alt}^a (°C)	ΔH_{alt}^a (J.g ⁻¹)	T_{rDA} (°C)	ΔH_{rDA} (J.g ⁻¹)
8025	-55	- ^b	- ^b	- ^c	- ^c
PPFA1	-25	- ^b	- ^b	- ^c	- ^c
PPHA1	-24	98	- ^b	- ^c	- ^c
DAA1	-12	- ^b	- ^b	117 & 145	11.9
1838	-62	-35	3.7	- ^c	- ^c
PPFA2	-45	76	7.7	- ^c	- ^c
PPHA2	-47	86 & 137	9.6 & 4.7	- ^c	- ^c
DAA2	-45	55	- ^b	116 & 145	6.7

^a Alternative (unconfirmed) thermal transitions

^b Non detected

^c No rDA detected

The pure **Priplast 1838** polyol does not display any other thermal transitions at higher temperatures which shows it is amorphous at ambient temperature. **PPFA2** and **PPHA2** show endotherms at 76 and 86 °C, respectively, suggesting some order or phase separation which could be driven by the difference in polarity between the hydrophobic polyol backbone (nonpolar) and the end groups comprising FA or HEMI (polar) which leads to thermodynamic incompatibility. While **PPFA2** does not show any further thermal transitions, **PPHA2** displays an additional endotherm at 137 °C which potentially represents polar end group association. The disparity between **PPFA2** and **PPHA2** could be explained by the presence of imide carbonyl groups in **PPHA2** which allows for favourable intermolecular H-bonding and therefore association, which is enhanced in such a hydrophobic matrix. **DAA2** also shows a slight thermal transition at 55 °C which could also be due to phase separation. Importantly, the double endotherm is once again present at 116 and 145 °C in this copolymer which confirms the presence of *exo* and *endo* DA cycloadducts. The recorded ΔH_{rDA} of **DAA2** is 6.9

$\text{J}\cdot\text{g}^{-1}$, which is somewhat lower than for **DAA1** ($11.9 \text{ J}\cdot\text{g}^{-1}$). The decrease in ΔH_{rDA} might feasibly be linked to the additional phase separation but further detailed studies would be required for confirmation.

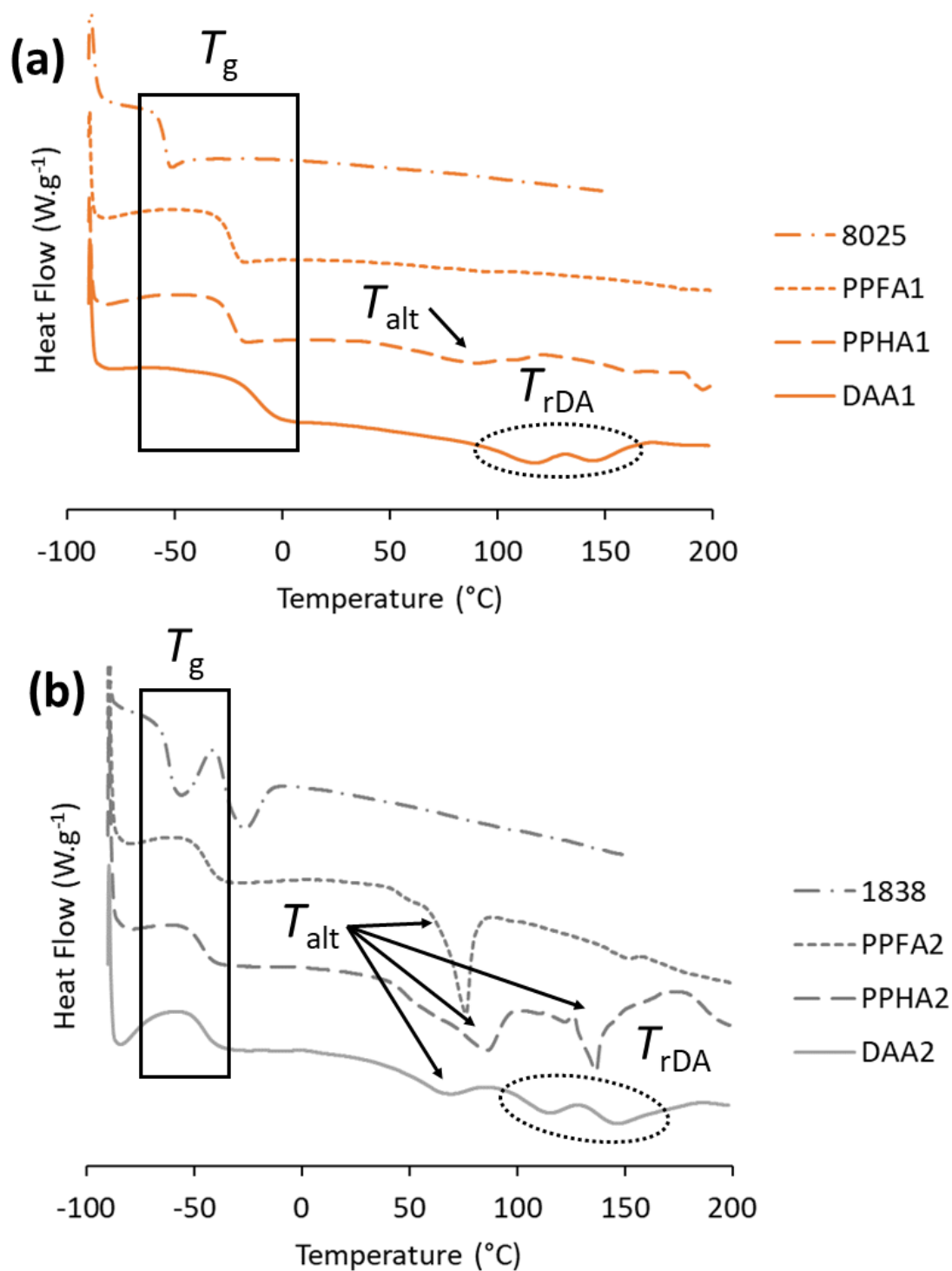


Figure 4.23 DSC thermograms of the four materials, thermal transitions are highlighted and labelled. (a) **DAA1**, **PPHA1**, **PPFA1** and **Capa 8025**. (b) **DAA2**, **PPHA2**, **PPFA2** and **Priplast 1838**. First heating cycles used at a heating rate of $10 \text{ }^{\circ}\text{C}\cdot\text{min}^{-1}$. Exo up.

DMA was used to improve understanding of thermal properties of the two amorphous **DAX** copolymers (**Figure 4.24**). The T_g of **DAA1** appears at a higher temperature than **DAA2**, confirming results obtained *via* DSC. **DAA2** has an impressively low T_g , the lowest of all materials measured *via* DMA in this chapter which indicates favourable low temperature properties (**Table 4.16**). Above T_g , **DAA1** displays a region where the modulus has a moderate dependence on temperature. However, **DAA2** has a significantly more stable rubbery plateau above T_g that occurs over a wide temperature range, which could be evidence of the additional strength offered by phase separation. Such a stable E' would allow for good mechanical properties over a wide temperature range which is industrially useful in applications. Values of E' above T_g for both amorphous copolymers are significantly lower than the semi-crystalline analogues (up to over 250 times lower) which demonstrates the reinforcement gained from crystallinity (**Table 4.16** vs **Table 4.3** and **Table 4.10**).

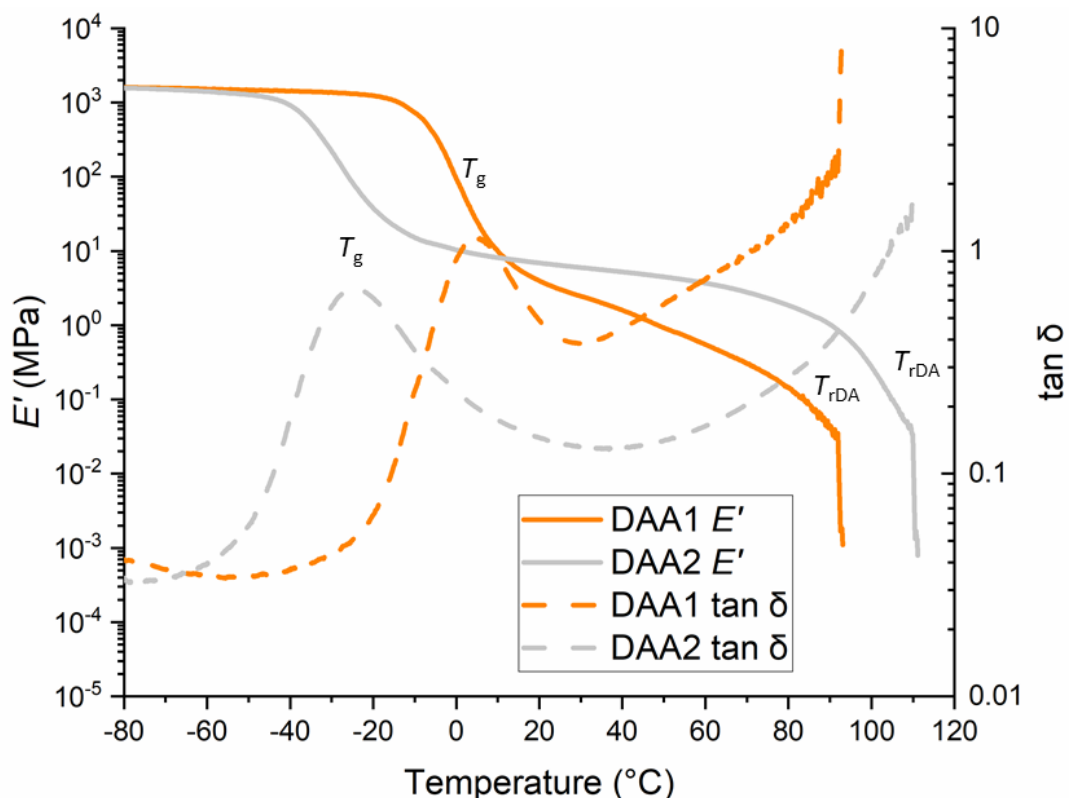


Figure 4.24 DMA of **DAA1** and **DAA2** with a heating rate of $3\text{ }^{\circ}\text{C}\cdot\text{min}^{-1}$. Storage modulus (E') (left y-axis) and $\tan \delta$ (right y-axis) as a function of temperature.

At 92 and 110 °C, the E' of **DAA1** and **DAA2**, respectively, rapidly decrease which shows loss of cohesion, however neither sample broke in testing. This sudden decrease is caused by the onset of the rDA, where the cycloadducts are broken and molecular weight begins to decrease which has a negative influence on the mechanical properties of the copolymer. Overall, there is a large difference between T_g and T_{rDA} for **DAA2** (approximately 120 °C) where the modulus is relatively consistent which presents an impressive service temperature range. T_{rDA} is also substantially higher for **DAA2**, a likely consequence of phase separation.

Table 4.16 Thermal data of **DAA1-2** obtained via DMA at a heating rate of 3 °C.min⁻¹.

Copolymer	$E' (T > T_g)^a$ (MPa)	T_g^b (°C)	$E' (T > T_g)^c$ (MPa)	T_{rDA}^d (°C)
DAA1	1480	5	4	92
DAA2	1270	-24	7	110

^a Modulus measured at -50 °C

^b Measured as peak in $\tan \delta$

^c Modulus measured at 20 °C

^d Estimated from the final sudden drop in modulus

It is interesting to observe that the amorphous materials show enough cohesion to reach T_{rDA} via DMA testing, unlike the semi-crystalline copolymers. Two theories were proposed earlier regarding the lack of strength in the semi-crystalline materials above $T_{m(pol)}$: DA cycloadducts concentration is too low or the internal copolymer arrangement lacks order. DSC revealed that the enthalpy of rDA for semi-crystalline **DA1** (8.9 J.g⁻¹) is only slightly lower than amorphous **DAA1** (11.9 J.g⁻¹) and higher than **DAA2** (6.7 J.g⁻¹) which discounts the initial theory associated with DA cycloadduct concentration. With respect to the semi-crystalline materials, crystal formation precedes DA cycloaddition. According to the solidification model, the arrangement in the molten state resembles that of the crystalline state, thereby suggesting few entanglements are present above $T_{m(pol)}$.³⁸ Therefore, it is reasonable to presume there is insufficient chain interactions and entanglement above $T_{m(pol)}$ to maintain a

cohesive material in the molten semi-crystalline copolymers. Purely amorphous materials do not contain crystalline regions hindering chain movement and entanglement. Therefore, the second hypothesis regarding internal arrangement appears a more likely cause.

The flow properties were determined as a function of temperature for **DAA1** and **DAA2**. Both display a temperature dependent η^* with a significant decrease at approximately 100 °C (**Figure 4.25**). It is important to note that both materials achieve the predetermined target η^* (10 Pa.s⁻¹) below 150 °C.

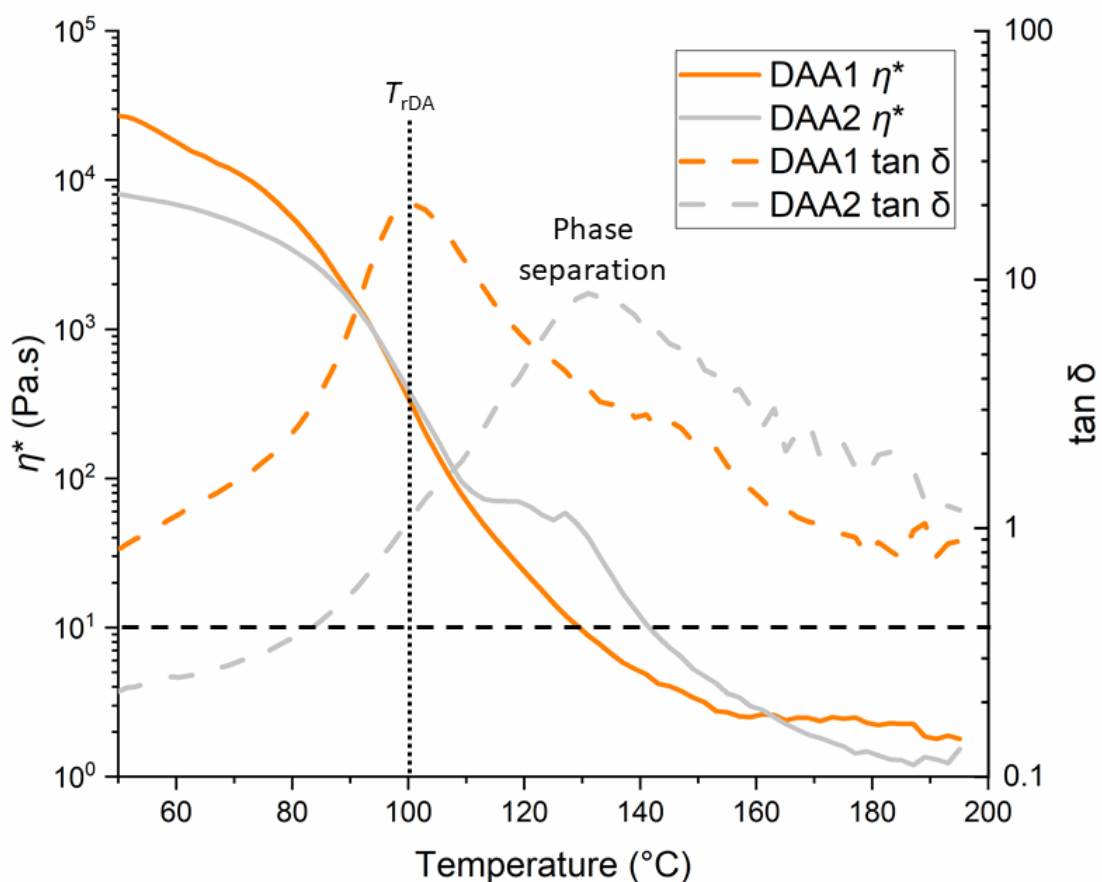


Figure 4.25 Rheological analysis of **DAA1** and **DAA2**. Complex viscosity (η^*) (left y-axis) and $\tan \delta$ (right y-axis) as a function of temperature. The horizontal short dashed black line represents the target η^* of 10 Pa.s⁻¹. The vertical dotted line represents the T_{rDA} for both materials.

This drop is evidence of the rDA reaction and thereby a decrease in molecular weight as the copolymer cleaves at the DA cycloadduct sites to reform the lower molecular weight prepolymers. **DAA1** shows a significant peak in $\tan \delta$ at 100 °C which signifies the T_{rDA} , however in the temperature sweep of **DAA2** this feature only appears as a shoulder in a larger peak. The dominant peak in **DAA2** appears at approximately 130 °C, which could be indicative of phase separation.

The stress-strain curves from tensile testing of **DAA1** and **DAA2** are typical for elastomeric materials (**Figure 4.26**).³⁹ Both materials display very low modulus compared to the previous semi-crystalline materials, as a consequence of having an amorphous backbone (**Table 4.17**). **DAA1** is very weak and loses strength with elongation (it continues to stretch with strain to the maximum dimensions of the tensometer used so the true ϵ_{max} is unknown).

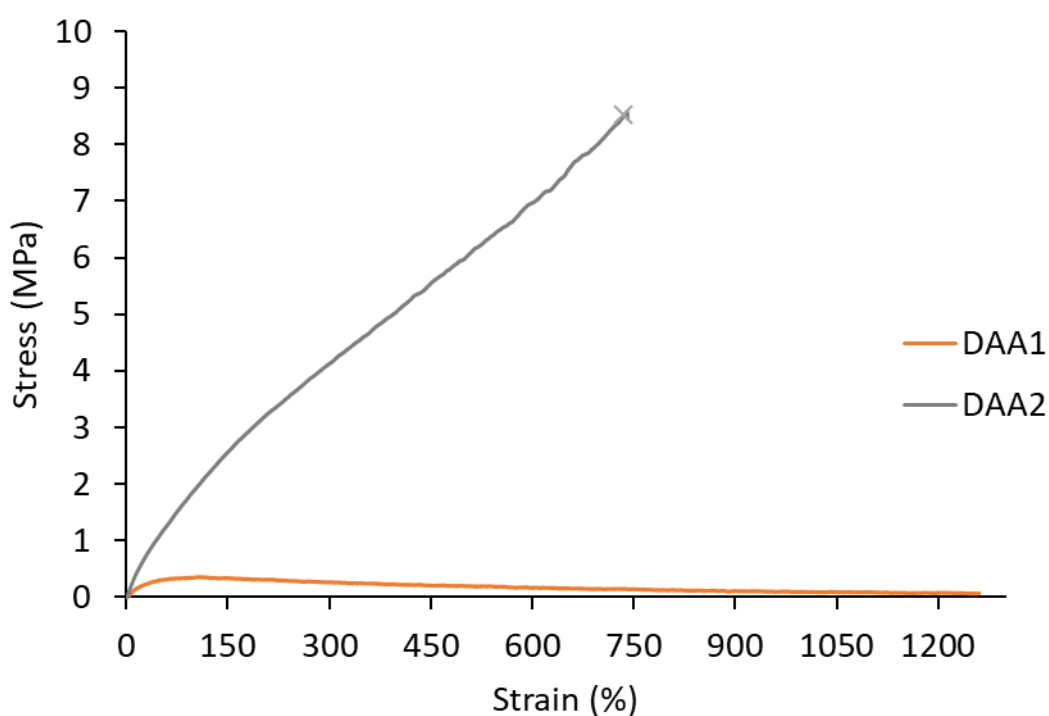


Figure 4.26 Stress-strain curves of **DAA1** and **DAA2**. **DAA1** did not break within the measured strain. Rate of 10 mm.min⁻¹.

However, **DAA2** exhibits increasing stress as a function of strain (strain-hardening). The material records its maximum stress (8.5 ± 0.7 MPa) at its highest elongation (740 ± 40 %) which is classic behaviour of elastomeric materials. On account of high stress and strain, **DAA2** exhibits impressive toughness (3465 ± 420 MPa) which is the highest value of U_T for any material measured in this chapter. This high performance is also a likely consequence of phase separation and highlights **DAA2** as an interesting material for flexible applications.

Table 4.17 Summary of mechanical data obtained from tensile stress-strain measurements for **DAA1** and **DAA2** at a rate of $10 \text{ mm}\cdot\text{min}^{-1}$.

Copolymer	E^a (MPa)	σ_{\max}^b (MPa)	U_T^c (MPa)	ϵ_{\max}^d (%)
DAA1	1.4 ± 0.2	$0.3 \pm < 0.1$	230 ± 10^e	1270 ± 10^e
DAA2	3.6 ± 0.2	8.5 ± 0.7	3465 ± 420	740 ± 40

^a Young's modulus is calculated from the initial gradient before the Yield point.

^b Ultimate tensile strength is the maximum recorded stress the sample can withstand before failure.

^c Modulus of toughness is measured as the area under the curve and represents the total energy a material can withstand without breaking.

^d Elongation at break is the strain (%) at which the sample breaks.

^e Maximum elongation of tensometer reached (sample not broken) so value unknown.

Lap shear adhesion tests were performed on **DAA1** and **DAA2** with beechwood substrates. **DAA1** and **DAA2** record bond strengths of 1.5 ± 0.2 and 4.4 ± 0.4 MPa, respectively, which are significantly lower than the semi-crystalline **DAX** copolymers as a consequence of the lack of crystallinity within the **DAAX** copolymers. The higher bond strength of **DAA2** relative to **DAA1** is likely caused by phase separation present in **DAA2** and is comparable to irreversibly crosslinked PU (approx. 5 MPa). Therefore, **DAA1** appears as a likely poor choice for adhesive applications, whereas **DAA2** shows potential as a flexible adhesive.

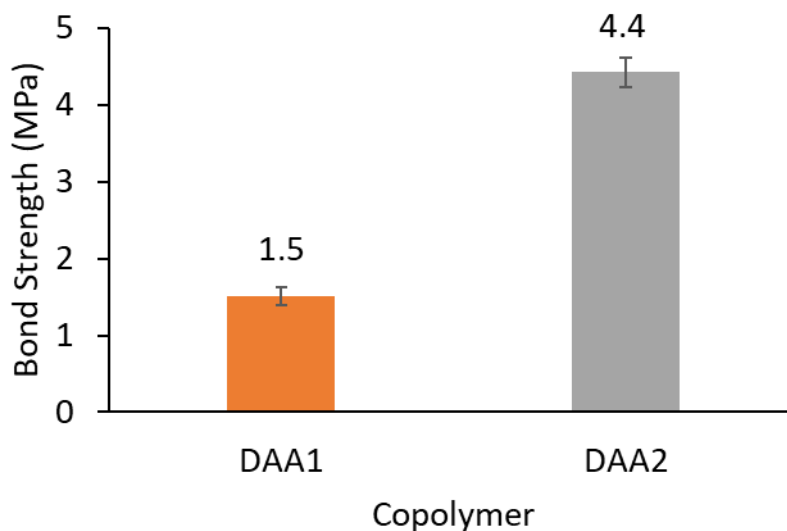


Figure 4.27 Bond strengths for **DAA1** and **DAA2** with beechwood substrates.

As with previous materials, the copolymers **DAA1** and **DAA2** were also investigated to determine the reversibility of the DA cycloadduct by measuring several properties of film samples as a function of time at ambient temperature after application from a homogenous molten blend of the two prepolymers. SEC results of **DAA1** showed the familiar trend of low molecular weight immediately after melt application (prepolymers reformed) followed by an increase in molecular weight with time (**Figure 4.28**). Like with all other materials, a plateau establishes after approximately 7 days due to the equilibration of the forward and reverse DA reactions. This qualitative match in trend with the semi-crystalline materials suggests polyol crystallinity does not influence the rate of cycloaddition. While **DAA2** was soluble for one day after melting, it became insoluble in CHCl_3 after two days so is not included in this analysis. The change in solubility is a likely consequence of increasing molecular weight.

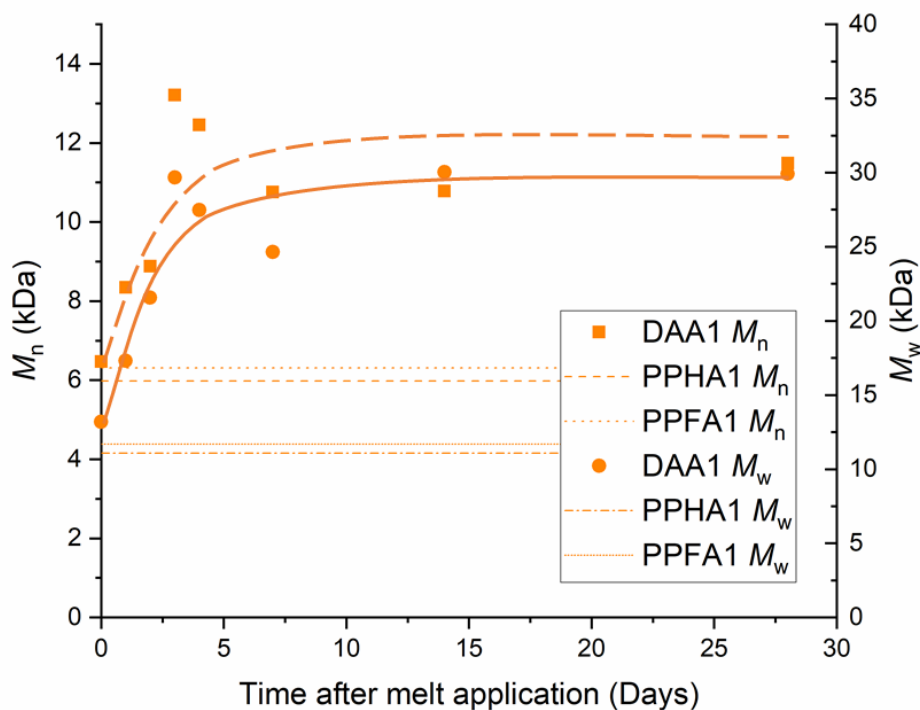


Figure 4.28 M_n (left y-axis) and M_w (right y-axis) as a function of time at ambient temperature after melt application for **DAA1**. The prepolymer molecular weights are marked with horizontal dashed lines. Determined by SEC in CHCl_3 against PMMA standards.

FTIR spectra of **DAA1** and **DAA2** was used to measure the consumption of free maleimide over time by monitoring the intensity of the absorbance at $\nu_{\text{max}} = 696 \text{ cm}^{-1}$. They also show the same trend as observed for **DA1-4**, *i.e.* an initial rapid decrease in intensity, followed by a slower decrease as an equilibrium is reached between the DA and rDA reactions (**Figure 4.29**). A very similar amount of free maleimide remains for both materials which is also very similar to that obtained for the semi-crystalline **DA1** which suggests that the crystallinity present in this material has minimal influence of DA cycloaddition (**Figure 4.10**).

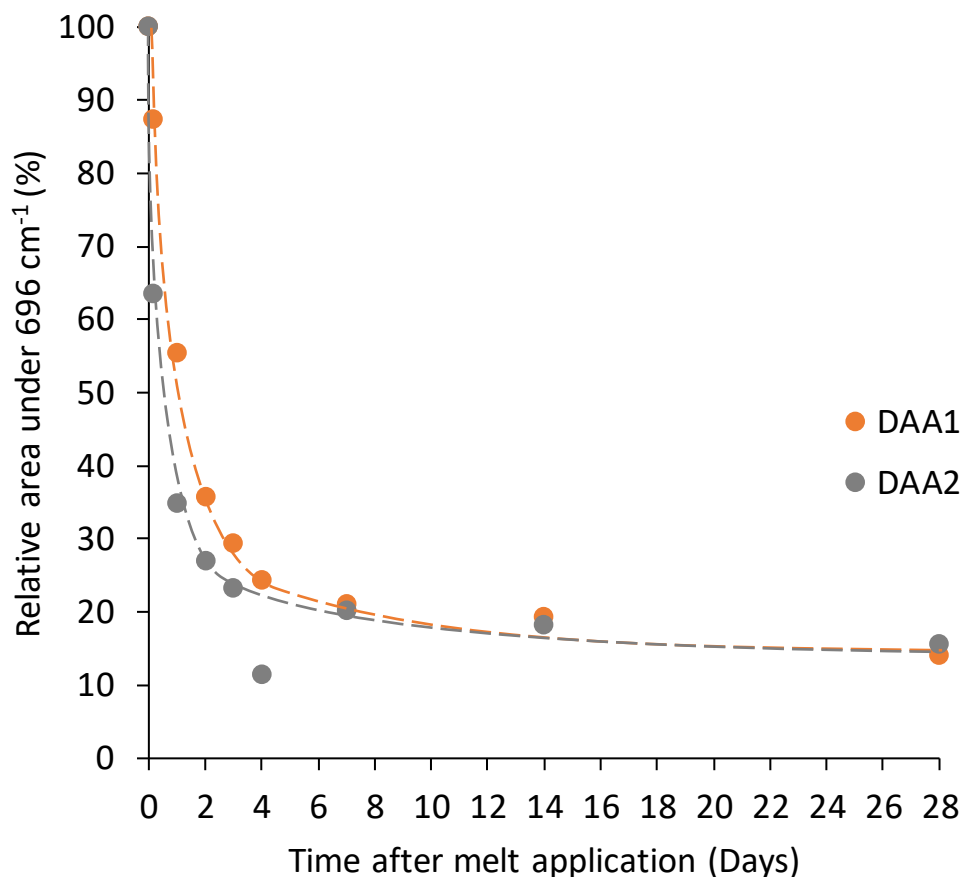


Figure 4.29 Relative intensities of FTIR absorbance at $\nu_{max} = 696 \text{ cm}^{-1}$ with time at ambient temperature after melt application for **DAA1** and **DAA2**.

Finally, DSC analysis revealed an increase in the amount of DA cycloadducts formed with time for both **DAA1** and **DAA2** (**Figure 4.30(a) & (b)**, respectively). Qualitatively, ΔH_{rDA} increases initially and then levels off due the establishment of an equilibrium (**Figure 4.30(c)**). However, it seems that less bonds are broken in the initial melting for **DAA2**.

DAA1 displays the same T_g throughout the 28 days and does not gain any new thermal features. However, while the T_g of **DAA2** also remains constant, the undefined transition at $55 \text{ }^\circ\text{C}$ (labelled as T_{alt}) appears slightly after 0.5 days and becomes more apparent after 7 days (**Figure 4.31**). This change might be the result of phase separation which becomes more

extreme with an increase in molecular weight and which could then inhibit the formation of further cycloadducts (ΔH_{rDA} lower for **DAA2**).

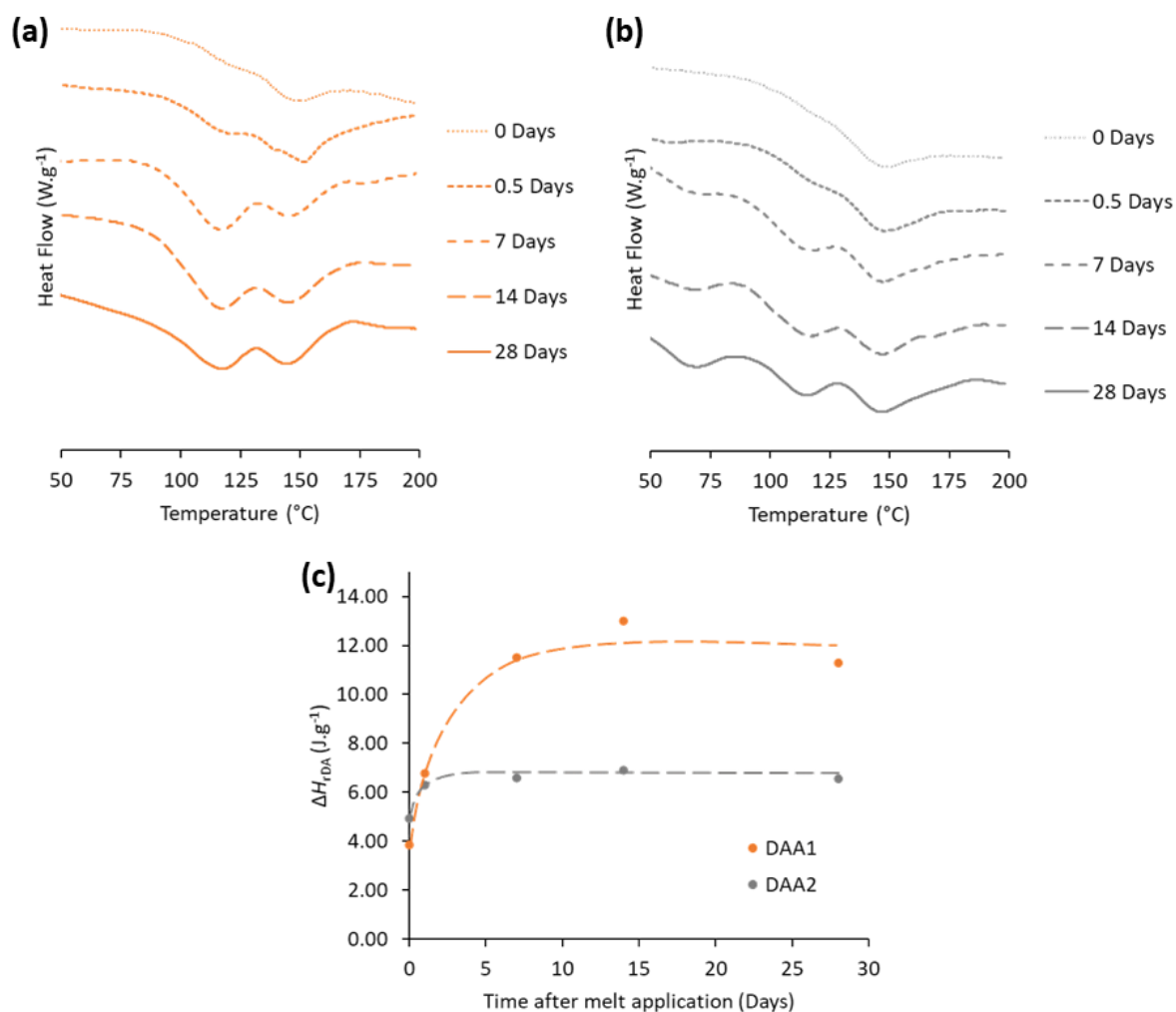


Figure 4.30 Increase in ΔH_{rDA} with time for **(a) DAA1** and **(b) DAA2**. First heating run used at a rate of $10\text{ }^{\circ}\text{C}\cdot\text{min}^{-1}$. Exo up. **(c)** Plot of ΔH_{rDA} as a function of time.

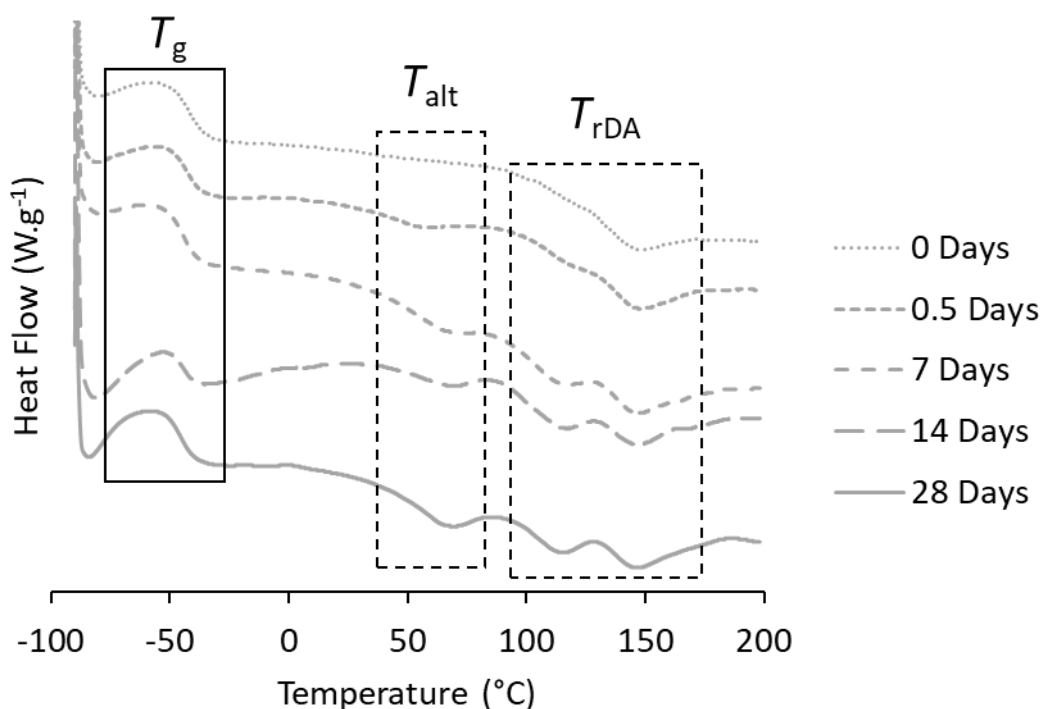


Figure 4.31 DSC thermograms of **DAA2** as a function of time. Thermal features are highlighted and labelled. First heating cycles used at a heating rate of $10\text{ }^{\circ}\text{C}\cdot\text{min}^{-1}$. Exo up.

4.3 Conclusions

The effects of incorporating reversible covalent bonds *via* DA cycloadducts within linear TPU copolymers were investigated with comparison to a traditional linear TPU copolymer containing 1,4-butanediol as a chain extender (**D1**). The potential for reversible adhesive applications was also assessed. The DA-containing copolymer (**DA1**) was successfully synthesised by the copolymerisation of HEMI- and FA-terminated prepolymers which was proven *via* ^1H NMR and FTIR spectroscopies and SEC analysis. DA cycloadducts required up to 7 days at ambient temperature to equilibrate after melt application. In comparison to the traditional TPU, the DA cycloadducts increased the variety of physical interactions on account of the introduction of imide carbonyls. Cycloadducts also increased the amount and homogeneity of PCL SS crystallinity. DSC analysis showed a double endotherm at 117 and 145 $^{\circ}\text{C}$, characteristic of the *endo* and *exo* DA cycloadducts, whereas the traditional TPU

displayed a single melt correlating to melting of HS crystallinity. While **D1** remained cohesive above $T_{m(\text{pol})}$, the DA cycloadducts did not offer enough internal strength for DMA measurement above this temperature. The cohesion of **D1** is granted by the extensive H-bonding present. However, these physical interactions displayed lower sensitivity to thermal stimulus *via* rheological temperature sweeps than the covalent DA cycloadducts which dissociated to allow for the reformation of the low molecular weight prepolymers. The impressively low melt viscosity recorded at 140 °C for **DA1** (14 times lower than **D1**) combined with enhanced mechanical and adhesive properties highlights using DA cycloadducts in linear TPUs as a viable route for thermally reversible adhesives.

Further studies on TPUs including DA cycloadducts within more highly crystalline backbones with higher T_m (**DA2**, **3** & **4**) were conducted to determine the interplay between DA cycloadduct and polyol crystallinity. Most trends observed *via* analytical techniques are qualitatively comparable to those observed with the lower T_m copolymer (**DA1**), such as increase in molecular weight with time and time taken to reach equilibrium after melt application (7 days) *via* SEC, decrease in free maleimide and increase in variety of carbonyl groups *via* FTIR spectroscopy. Copolymerisation incorporating the highly crystalline polyesters did not completely remove all crystallinity, therefore **DA2**, **3** & **4** maintain a substantial degree of crystallinity. The DA cycloadducts were determined to have minimal influence of the crystallisation kinetics of these polyester segments. Additionally, copolymerisation of these highly crystalline prepolymers still shows the dual endotherm associated with the DA cycloadducts in each case. The enthalpy of rDA is similar for **DA2**, **3** & **4**, but significantly smaller than **DA1**, which suggests DA cycloaddition appears to be a function of comprising polyol molecular weight (**DA1** = 2.0 kDA, **DA2**, **3** & **4** = 3.5 kDA). DMA

and rheological temperature sweeps reveal the importance of the comprising polyol. The melting temperature dictates the upper service temperature limit of the material, above which the copolymer loses strength and melts. Additionally, the melting temperatures also appears to control the mechanical and adhesive properties, with performance increasing in line with T_m (**DA2** < **DA3** < **DA4**). As a result of high stiffness, **DA4** recorded a bond strength on aluminium substrates of 20.3 ± 0.9 MPa, remarkable for a thermoplastic material and double that previously reported for a thermally reversible amorphous crosslinked network. Importantly, all three highly crystalline copolymers achieve the target viscosity ($10 \text{ Pa}\cdot\text{s}^{-1}$) below $150 \text{ }^\circ\text{C}$, which shows a dynamic relationship between low and high molecular weight exists. However, the highly crystalline segments appeared to decrease the percent of DA cycloadduct formation (*via* FTIR spectroscopy), possibly due to hinderance of mobility. Therefore, further work should explore promotion of DA cycloadducts with heat treatment to achieve higher molecular weight copolymers and potentially enhanced material performance.

Two further copolymers containing DA cycloadducts were synthesised based on amorphous backbones to act as 'zero crystallinity' references. Again, an increase in molecular weight (except for **DAA2** comprising **Priplast 1838** which displayed poor solubility), a decrease in the absorbance at $\nu_{\text{max}} = 696 \text{ cm}^{-1}$ and dual endotherms above $100 \text{ }^\circ\text{C}$ signified successful DA cycloaddition. The presence of DA cycloadducts appeared to increase chain stiffness and promote phase separation in the case of copolymer containing the relatively nonpolar **Priplast 1838**. This phase separation coupled with a low T_g afforded the material to have an impressively wide service temperature range which would be useful in industrial applications. Purely amorphous materials display inferior mechanical and adhesive properties (with the

exception of flexibility) relative to semi-crystalline analogues as a consequence of an amorphous backbone. This decrease in performance suggests crystallinity is required within a linear TPU copolymer to achieve good bond strengths. The separate amorphous and semi-crystalline copolymers (containing polyols of equal molecular weight) display similar percentages of free maleimide consumed 28 days after melt application, DA cycloadduct concentration and rate of DA cycloaddition (7 days). Therefore, it appears that crystalline segments with similar composition have minimal influence of the DA cycloadducts which is most probably because cycloadduct association occurs in the amorphous chain ends of the prepolymers.

All copolymers containing DA cycloadducts display a highly dynamic physical response to temperature, which suggests cycloadduct dissociation is not a function of concentration or copolymer composition. In all cases, independent of composition, the TPU copolymers dissociate to low molecular weights similar to the constituent prepolymers on heating and then increase in molecular weight by simply reacting at ambient temperature. This finding is very exciting as it opens potential for targeted properties by careful selection and design of the prepolymers to determine the subsequent copolymer mechanical performance.

4.4 Experimental

4.4.1 Materials

Capa™ 2200J and Capa™ 8025D were provided by Ingevity. Dynacoll® 7360, Dynacoll® 7380 and Dynacoll® 7490 were provided by Evonik Industries. Priplast™ 1838 was provided by Croda International. 4,4'-methylene bis(phenyl isocyanate) (98 %), 1,4-butanediol *ReagentPlus*® (99 %), furfuryl alcohol and chloroform-*d* (99.8 atom % D) were purchased from

Sigma-Aldrich. 2-Hydroxyl ethyl maleimide was provided by Henkel Corporation. All reagents were used as received.

4.4.2 Instrumental methods

Proton (^1H) nuclear magnetic resonance (NMR) spectra were recorded using a Bruker Avance 400 spectrometer (400 MHz). Spectra were analysed on MestReNova v6.0.2. Samples were prepared in CDCl_3 as the solvent. All chemical shifts were recorded in parts per million (ppm) relative to a reference peak of chloroform solvent at $\delta = 7.26$ ppm. **Molecular weights and dispersities** were determined *via* size-exclusion chromatography (SEC) using an Agilent 1260 Infinity GPC system equipped with a refractive index detector. Two Agilent PL-gel $5\ \mu\text{m}$ Mixed-C columns and a guard column were connected in series and maintained at $35\ ^\circ\text{C}$. HPLC grade chloroform containing $0.25\ \%$ v/v NEt_3 was used as the eluent and the flow rate was set at $1.0\ \text{mL}\cdot\text{min}^{-1}$. The refractive index detector was used for calculation of molecular weights and dispersities by calibration using a series of near-monodisperse poly(methyl methacrylate) standards. Analysis was performed on Agilent SEC software. **Attenuated Total Reflectance Fourier Transform Infrared (ATR-FTIR)** spectra was collected on a PerkinElmer Spectrum Two instrument with a UATR Two accessory. Analysis was performed on PerkinElmer Spectrum software. **Differential scanning calorimetry (DSC)**) was performed on a Discovery DSC 25 TA instrument. All experiments were carried out under a nitrogen atmosphere and with a heating rate of $10\ ^\circ\text{C}\cdot\text{min}^{-1}$. Pre-weighed samples of $2 \pm 1\ \text{mg}$ were loaded at $25\ ^\circ\text{C}$, cooled to $-90\ ^\circ\text{C}$ and heated to $200\ ^\circ\text{C}$. T_g was taken as the midpoint of inflexion and T_m and T_{rDA} were measured as the temperature at the minimum heat flow of the appropriate endotherms. For time dependent measurements, samples for 0 Days measurements were loaded at $25\ ^\circ\text{C}$, heated to $150\ ^\circ\text{C}$, held for 1 hour, cooled to $-90\ ^\circ\text{C}$ then heated to $200\ ^\circ\text{C}$ at a rate of $10\ ^\circ\text{C}\cdot\text{min}^{-1}$.

Analysis was performed on TRIOS v5.1.1 software. **Dynamic Mechanical Analysis (DMA)** was performed on TA Instruments Q800 Dynamic Mechanical Analyser with an ACS-3 (Refrigerated Chiller System). Samples of approximately 40 × 5 × 1 mm were loaded at room temperature and clamped lightly (finger tight). A sample length of 10 mm was used for all measurements. For each measurement, the sample was first cooled to -80 °C and held at this temperature for a minimum of 5 minutes to fully equilibrate. The furnace was then opened and the sample clamped to a pressure of 4.5 psi using a small torque wrench. After clamping, the furnace was then immediately closed and temperature re-equilibration established at -80 °C. The method was then started. The thermal method used is: Motor Drive Off, Data Storage Off, equilibrate at -80 °C, isotherm 5 minutes, Motor Drive ON, Data Storage ON, ramp 3 °C.min⁻¹ to 100 °C. The measurement parameters used were as follows: strain applied (0.05 %), force track (110 %), initial sample length (10 mm) with deformation frequency (1 Hz) fixed. Sample dimensions were calculated as follows: width was measured using digital callipers at three positions along the sample (End 1, Middle, End 2). Thickness was measured using digital callipers at three positions along the sample (End 1, Middle, End 2). Average values calculated and used. The software used was TA Instruments Advantage Control Software and data analysis was performed on TA Instruments Universal Analysis Data Analysis Program.

Rheological temperature sweeps were performed on an Anton Paar MCR502 with a 25 mm disposable geometry and a disposable bottom plate fixture. Tests were run in oscillatory mode at a fixed amplitude (1 %) and angular frequency (1 rad.s⁻¹) from 50 – 200 °C. Sample sizes were approximately 25.0 mm diameter discs of 0.8 mm height. **Tensile tests** were run on films approximately 300 µm thick, according to ISO 527-2 type 5B on a Zwickline tensometer. The general procedure is as follows: dimensions of dog bone measured with digital calliper and noted on the system. The zero gap is set within Zwick software so the

gauge length is known. The sample is then securely clamped and the absolute cross head length is reset. The force is then zeroed. The test is run at a speed of $10 \text{ mm}\cdot\text{min}^{-1}$ until the sample fails. Results analysed on TestXpert II software. **Adhesion lap shear tests with beechwood substrates** were performed on films $250 \text{ }\mu\text{m}$ thick that were cut to $25 \times 25 \text{ mm}$. Lap shear joints were assembled by carefully applying the film between beechwood test pieces using an overlap of 25 mm and a width of 25 mm , applying light pressure. The materials were placed in an oven for 20 minutes at $150 \text{ }^\circ\text{C}$ to melt the copolymers. Bonded samples were then allowed to cure for 14 days at ambient conditions before measurement. The lap shear strength was determined from an average of four bonded samples using an Instron tensiometer with a load cell of 30 kN and a displacement speed of $1.27 \text{ mm}\cdot\text{min}^{-1}$. **Adhesion lap shear tests with aluminium substrates.** Aluminium test pieces were grit blasted and cleaned with acetone. Films $250 \text{ }\mu\text{m}$ thick were cut to $12.5 \times 25 \text{ mm}$. Lap shear joints were assembled by carefully applying the film between aluminium test pieces using 0.1 mm glass spacer beads, an overlap of 15 mm and a width of 25 mm , applying light pressure with a Hoffman clamp. The materials were placed in an oven for 20 minutes at $150 \text{ }^\circ\text{C}$ to thermally reverse the networks into a melt. Bonded samples were then allowed to cure for 14 days at $23 \text{ }^\circ\text{C} / 50 \text{ \%RH}$ before measurement. The lap shear strength was determined from an average of four bonded samples using an Instron tensiometer with a load cell of 30 kN and a displacement speed of $1.27 \text{ mm}\cdot\text{min}^{-1}$.

4.4.3 Sample preparation

Rheology discs of $25.0 \times 0.8 \text{ mm}$ were prepared with a MeltPrep® vacuum compression mould. Copolymers (approx. 0.40 g) were separately melted in the chamber at 70 , 120 and $150 \text{ }^\circ\text{C}$, respectively. Melting was followed by approximately 10 seconds of pressure (0.1

mbar). Vacuum was removed and materials were then cooled with compressed air and allowed to solidify before being removed from the chamber. **DMA bars** were prepared in a similar way as the rheology discs. However, a 10 x 40 mm insert and chamber were used instead of cylindrical versions. Once solidified, samples were cut down the middle lengthwise to give two bars of 0.5 x 40 mm. **Tensile testing dog bones** were prepared as follows. First, film samples (300 μm) were made by coating out molten material (1 hour at 150 °C) with a 500 μm coating block on release paper. After films were allowed to solidify, dog bone shapes were cut out using a ZwickRoell® knee manual cutting press ZCP 020 with cutting device for ISO 527-2 type 5B die attachment. **Adhesion films** were prepared by heating some material in an oven at 150 °C for approximately 20 minutes, after which a film was drawn with a coating block with an approximate thickness of 250 μm . Once solid enough, squares of 25 x 25 mm were then cut out of the film for use in the lap shear sample preparation.

4.4.4 *Synthesis of furfuryl-terminated prepolymers (PPFX)*

All furfuryl-terminated prepolymers were synthesised using a similar method, a typical procedure is as follows: **Capa 2200** (77.96 g, 0.039 mol) was loaded into a 250 mL flange flask, equipped with an overhead mechanical stirrer, gas inlet and digital thermometer. Vacuum was applied for 1 hour at 87 °C and a stirring rate of 90 rpm. Vacuum was removed and **MDI** (19.69 g, 0.079 mol) was added at 110 °C which decreased the mixture temperature to 90 °C with a subsequent exotherm to 111 °C. Immediately after **MDI** addition, the stirring rate was increased to 180 rpm and the vacuum was reapplied after 15 minutes. Vacuum was again removed after 1 hour, **FA** (8.52 g, 0.087 mol) was added at 111 °C which decreased the reaction temperature to 105 °C. A reflux condenser was added and the vacuum was not reapplied (exotherm to 110 °C). After a further 1 hour 26 minutes, more **FA** (0.82 g, 0.008

mol) was added at 111 °C. After another 2 hours, there was minimal NCO absorbance detected *via* FTIR spectroscopy so the reaction was switched off and the mixture was decanted while hot. The product was put under vacuum at 40 °C for a total of 48 hours to remove and residual free **FA** (determined *via* ¹H NMR spectroscopy).

PPF1: SEC (CHCl₃): $M_n = 6.3$ kDa, $M_w = 12.6$ kDa, $D_M = 1.94$.

¹H NMR (400 MHz, 298 K, CDCl₃): $\delta = 7.46$ (s, CH=CHO (FA)), 7.30 (m, Ar), 7.12 (d, $J = 7.8$ Hz, Ar), 6.69 (s, NH), 6.60 (s, NH), 6.47 (d, $J = 2.9$ Hz, CHCH=CHO (FA)), 6.40 (s, CCHCH (FA)), 5.16 (s, OCHC (FA)), 4.17 (t, $^3J_{H-H} = 6.4$ Hz, CH₂OC=O), 4.08 (t, $^3J_{H-H} = 6.7$ Hz, CH₂OC=O), 4.00 (s, MDI CH₂Ar), 3.90 (s, NPG CH₂O), 2.33 (t, $^3J_{H-H} = 7.5$ Hz, CH₂C=OO), 1.00 (d, $J = 9.4$ Hz, NPG CH₃), 1.68 and 1.41 (all remaining protons) ppm.

ATR-FTIR: $\nu_{MAX} = 3338$ (N-H), 2944 – 2865 (C-H), 1722 (C=O), 1597 (C-N), 1531 (Ar C=C), 1295 and 1163 (C-O) cm⁻¹.

PPF2: SEC (CHCl₃): $M_n = 12.8$ kDa, $M_w = 24.3$ kDa, $D_M = 2.18$.

¹H NMR (400 MHz, 298 K, CDCl₃): $\delta = 7.45$ (s, CH=CHO (FA)), 7.30 (d, $J = 3.7$ Hz Ar), 7.10 (d, $J = 1.8$ Hz, Ar), 6.73 (s, NH), 6.67 (s, NH), 6.47 (d, $J = 3.2$ Hz, CHCH=CHO (FA)), 6.39 (m, CCHCH (FA)), 5.16 (s, OCHC (FA)), 4.16, 4.08, 3.89, 2.34 1.67, 1.40 (DynaColl 7360) ppm.

ATR-FTIR: $\nu_{MAX} = 3343$ (N-H), 2936 – 2867 (C-H), 1726 (C=O), 1597 (C-N), 1532 (Ar C=C), 1163 (C-O) cm⁻¹.

PPF3: SEC (CHCl₃): $M_n = 12.5$ kDa, $M_w = 26.2$ kDa, $D_M = 1.90$.

^1H NMR (400 MHz, 298 K, CDCl_3): δ = 7.45 (s, $\text{CH}=\text{CHO}$ (FA)), 7.31 (m, Ar), 7.12 (m, Ar), 6.68 (s, NH), 6.63 (s, NH), 6.47 (d, J = 3.1 Hz, $\text{CHCH}=\text{CHO}$ (FA)), 6.39 (m, CCHCH (FA)), 5.16 (s, OCHC (FA)), 4.16, 4.09, 3.90, 2.31, 1.64, 1.40, 1.30 (DynaColl 7380) ppm.

ATR-FTIR: ν_{MAX} = 3339 (N-H), 2916 – 2850 (C-H), 1728 (C=O), 1597 (C-N), 1532 (Ar C=C), 1169 (C-O) cm^{-1} .

PPF4: SEC (CHCl_3): M_n = 15.2 kDa, M_w = 29.4 kDa, D_M = 1.93.

^1H NMR (400 MHz, 298 K, CDCl_3): δ = 7.45 (s, $\text{CH}=\text{CHO}$ (FA)), 7.30 (m, Ar), 7.12 (m, Ar), 6.70 (m, NH), 6.63 (s, NH), 6.47 (d, J = 3.2 Hz, $\text{CHCH}=\text{CHO}$ (FA)), 6.39 (m, CCHCH (FA)), 5.16 (s, OCHC (FA)), 4.37, 4.33, 4.31, 4.29, 4.08, 3.90, 2.34, 1.63 and 1.29 (DynaColl 7490) ppm.

ATR-FTIR: ν_{MAX} = 3343 (N-H), 2917 – 2849 (C-H), 1735 (C=O), 1598 (C-N), 1534 (Ar C=C), 1308 and 1166 (C-O) cm^{-1} .

PPFA1: SEC (CHCl_3): M_n = 6.3 kDa, M_w = 11.7 kDa, D_M = 1.85.

^1H NMR (400 MHz, 298 K, CDCl_3): δ = 7.45 (s, $\text{CH}=\text{CHO}$ (FA)), 7.30 (m, Ar), 7.11 (d, J = 8.3 Hz Ar), 6.76 (s, NH), 6.69 (s, NH), 6.46 (d, J = 3.2 Hz, $\text{CHCH}=\text{CHO}$ (FA-CL)), 6.38 (m, CCHCH (FA-CL)), 6.36 (m, $\text{CHCH}=\text{CHO}$ (FA-LA)), 6.31 (d, J = 3.1 Hz, CCHCH (FA-LA)), 5.15 (s, OCHC (FA)), 5.19, 5.10, 4.16, 4.08, 3.89, 2.41, 2.31, 1.64, 1.58, 1.51, 1.40 and 0.99 (Capa 8025) ppm.

ATR-FTIR: ν_{MAX} = 3343 (N-H), 2942 – 2866 (C-H), 1729 (C=O), 1598 (C-N), 1532 (Ar C=C), 1309 and 1160 (C-O) cm^{-1} .

PPFA2: SEC (CHCl_3): M_n = 6.0 kDa, M_w = 14.2 kDa, D_M = 2.36.

^1H NMR (400 MHz, 298 K, CDCl_3): δ = 7.46 (s, CH=CHO (FA)), 7.30 (m, Ar), 7.12 (d, J = 8.3 Hz, Ar), 6.59 (m, NH), 6.48 (d, J = 3.1 Hz, CHCH=CHO (FA)), 6.40 (m, CCHCH (FA)), 5.17 (s, OCHC (FA)), 4.17, 4.08, 3.91, 2.31, 1.65, 1.40, 1.28 and 0.91 (Priplast 1838) ppm.

ATR-FTIR: ν_{MAX} = 3334 (N-H), 2922 – 2853 (C-H), 1735 and 1701 (C=O), 1596 (C-N), 1534 (Ar C=C), 1312 and 1171 (C-O) cm^{-1} .

4.4.5 Synthesis of hydroxyethyl maleimide-terminated prepolymers (PPHX)

All hydroxyethyl maleimide-terminated prepolymers were synthesised using a similar method, a typical procedure is as follows: **Capa 2200** (81.86 g, 0.04 mol) was loaded into a 250 mL flange flask, equipped with an overhead mechanical stirrer, gas inlet and digital thermometer. Vacuum was applied for 1 hour at 110 °C and a stirring rate of 90 rpm. Vacuum was removed and **MDI** (20.67 g, 0.08 mol) was added at 110 °C which decreased the mixture temperature to 95 °C with a subsequent exotherm to 110 °C. Immediately after **MDI** addition, the stirring rate was increased to 180 rpm and the vacuum was reapplied after 15 minutes. Vacuum was again removed after 1 hour, **HEMI** (12.81 g, 0.09 mol) was added at 110 °C which decreased the reaction temperature to 95 °C. A reflux condenser was added and the vacuum was not reapplied. Exotherm to 105 °C. After a further 2 hours 19 minutes, more **HEMI** (1.19 g, 0.008 mol) was added at 110 °C. After another 32 minutes, there was minimal NCO absorbance detected *via* FTIR spectroscopy so the reaction was switched off and the mixture was decanted while hot.

PPH1: SEC (CHCl_3): M_n = 6.5 kDa, M_w = 12.6 kDa, D_M = 2.02.

^1H NMR (400 MHz, 298 K, CDCl_3): δ = 7.31 (d, J = 8.0 Hz, Ar), 7.11 (d, J = 8.3 Hz, Ar), 6.75 (s, C=OCHCH (HEMI)), 6.73 (s, C=OCHCH (HEMI)), 6.65 (s, NH), 6.61 (s, NH), 4.32 (t, $^3J_{\text{H-H}}$ = 5.2 Hz,

$\text{NCH}_2\text{CH}_2\text{O}$ (HEMI)), 3.85 (t, $^3J_{\text{H-H}} = 5.2$ Hz, $\text{NCH}_2\text{CH}_2\text{O}$ (HEMI)), 4.16, 4.08, 3.99, 3.92, 3.90, 3.80, 3.76, 2.32, 1.67, 1.40, 0.99 (Capa 2200) ppm.

ATR-FTIR: $\nu_{\text{MAX}} = 3341$ (N-H), 2944 – 2865 (C-H), 1722 and 1709 (C=O), 1597 (C-N), 1532 (Ar C=C), 1295 and 1164 (C-O) cm^{-1} .

PPH2: SEC (CHCl_3): $M_n = 9.4$ kDa, $M_w = 20.3$ kDa, $\mathcal{D}_M = 2.15$.

^1H NMR (400 MHz, 298 K, CDCl_3): $\delta = 7.31$ (d, $J = 7.8$ Hz, Ar), 7.11 (d, $J = 8.2$ Hz, Ar), 6.76 (s, C=OCHCH (HEMI)), 6.74 (s, C=OCHCH (HEMI)), 6.63 (s, NH), 6.57 (s, NH), 4.32 (t, $^3J_{\text{H-H}} = 5.1$ Hz, $\text{NCH}_2\text{CH}_2\text{O}$ (HEMI)), 3.86 (t, $^3J_{\text{H-H}} = 5.2$ Hz, $\text{NCH}_2\text{CH}_2\text{O}$ (HEMI)), 4.16, 4.08, 3.90, 3.86, 3.81, 3.77, 2.33, 1.67, 1.40, 1.27 (DynaColl 7360) ppm.

ATR-FTIR: $\nu_{\text{MAX}} = 3343$ (N-H), 2950 – 2866 (C-H), 1726 (C=O), 1597 (C-N), 1532 (Ar C=C), 1163 (C-O) cm^{-1} .

PPH3: SEC (CHCl_3): $M_n = 9.6$ kDa, $M_w = 20.9$ kDa, $\mathcal{D}_M = 2.10$.

^1H NMR (400 MHz, 298 K, CDCl_3): $\delta = 7.31$ (d, $J = 8.0$ Hz, Ar), 7.11 (d, $J = 8.3$ Hz, Ar), 6.76 (d, $J = 2.2$ Hz, C=OCHCH (HEMI)), 6.74 (s, C=OCHCH (HEMI)), 6.69 (d, $J = 8.0$ Hz, NH), 6.59 (d, $J = 13.9$ Hz, NH), 4.32 (t, $^3J_{\text{H-H}} = 5.2$ Hz, $\text{NCH}_2\text{CH}_2\text{O}$ (HEMI)), 3.85 (m, $\text{NCH}_2\text{CH}_2\text{O}$ (HEMI)), 4.16, 4.08, 3.90, 3.81, 3.76, 2.30, 1.63, 1.40, 1.30 (DynaColl 7380) ppm.

ATR-FTIR: $\nu_{\text{MAX}} = 3326$ (N-H), 2916 – 2850 (C-H), 1728 and 1702 (C=O), 1596 (C-N), 1533 (Ar C=C), 1169 (C-O) cm^{-1} .

PPH4: SEC (CHCl_3): $M_n = 11.4$ kDa, $M_w = 25.3$ kDa, $\mathcal{D}_M = 2.22$.

^1H NMR (400 MHz, 298 K, CDCl_3): $\delta = 7.30$ (d, $J = 9.0$ Hz, Ar), 7.12 (m, Ar), 6.76 (s, C=OCHCH (HEMI)), 6.74 (s, C=OCHCH (HEMI)), 6.71, 6.68, 6.60, 6.54 (NH), 4.37 (m, $\text{NCH}_2\text{CH}_2\text{O}$ (HEMI)),

3.86 (m, NCH₂CH₂O (HEMI)), 4.33, 4.29, 4.08, 3.91, 3.81, 3.76, 2.34, 1.63, 1.29 (Dynacoll 7490) ppm.

ATR-FTIR: $\nu_{\text{MAX}} = 3325$ (N-H), 2916 – 2849 (C-H), 1736 and 1706 (C=O), 1597 (C-N), 1533 (Ar C=C), 1167 (C-O) cm⁻¹.

PPHA1: SEC (CHCl₃): $M_n = 6.0$ kDa, $M_w = 11.1$ kDa, $D_M = 1.85$.

¹H NMR (400 MHz, 298 K, CDCl₃): $\delta = 7.31$ (d, $J = 7.3$ Hz, Ar), 7.11 (d, $J = 6.7$ Hz, Ar), 6.76 (d, $J = 2.7$ Hz, C=OCHCH (HEMI)), 6.73 (s, C=OCHCH (HEMI)), 6.64 (s, NH), 6.59 (s, NH), 4.32 (t, ³J_{H-H} = 5.0 Hz, NCH₂CH₂O (HEMI)), 3.85 (t, ³J_{H-H} = 5.1 Hz, NCH₂CH₂O (HEMI)), 5.12, 4.17, 4.08, 3.97, 3.88, 3.81, 3.76, 2.41, 2.32, 1.65, 1.58, 1.53, 1.49, 1.40, 0.99 (Capa 8025) ppm.

ATR-FTIR: $\nu_{\text{MAX}} = 3344$ (N-H), 2942 – 2866 (C-H), 1729 and 1713 (C=O), 1598 (C-N), 1532 (Ar C=C), 1310 and 1160 (C-O) cm⁻¹.

PPHA2: SEC (CHCl₃): $M_n = 6.0$ kDa, $M_w = 13.8$ kDa, $D_M = 2.28$.

¹H NMR (400 MHz, 298 K, CDCl₃): $\delta = 7.31$ (d, $J = 8.1$ Hz, Ar), 7.11 (d, $J = 7.0$ Hz, Ar), 6.76 (s, C=OCHCH (HEMI)), 6.74 (s, C=OCHCH (HEMI)), 6.63 (s, NH), 6.55 (s, NH), 4.33 (t, ³J_{H-H} = 5.2 Hz, NCH₂CH₂O (HEMI)), 3.86 (t, ³J_{H-H} = 5.2 Hz, NCH₂CH₂O (HEMI)), 4.17, 4.09, 3.90, 2.31, 1.64, 1.41, 1.29 and 0.89 (Priplast 1838) ppm.

ATR-FTIR: $\nu_{\text{MAX}} = 3348$ (N-H), 2922 – 2853 (C-H), 1735 and 1707 (C=O), 1596 (C-N), 1533 (Ar C=C), 1312 and 1171 (C-O) cm⁻¹.

4.4.6 Synthesis of final linear TPU copolymers (**DAX**)

All **DAX** copolymers were synthesised using a similar method, a typical procedure is as follows:

PPF1 (30.17 g, 0.011 mol) and **PPH1** (31.37 g, 0.011 mol) were loaded into a 250 mL flange

flask, equipped with an overhead stirrer and gas inlet. The formulation was stirred at 120 °C under vacuum for 1 hour to provide sufficient mixing of prepolymers and prevent bubble formation. The mixture was decanted while hot and allowed to copolymerise under ambient conditions in a silicone dish until solid enough to be stored in polyethylene bag.

DA1: SEC (CHCl₃): $M_n = 20.9$ kDa, $M_w = 54.6$ kDa, $\bar{D}_M = 2.63$.

¹H NMR (400 MHz, 298 K, CDCl₃): $\delta = 7.31$ (d, $J = 8.3$ Hz, Ar), 7.12 (d, $J = 7.3$ Hz, Ar), 6.77 (s, C(C)HCH=CH (DA)), 6.74 (s, C(C)HCH=CH (DA)), 6.57 (s, NH), 6.51 (s, NH), 5.32 (s, CH(O)(CH)(CH) (DA)), 3.03 (s, CH(CH)C=O (DA)), 2.90 (s, CH(CH)C=O (DA)), 4.17, 4.08, 3.99, 3.93, 3.90, 2.33, 1.67, 1.40, 1.00 (Capa 2200) ppm.

ATR-FTIR: $\nu_{MAX} = 3339$ (N-H), 2944 – 2865 (C-H), 1721 (C=O), 1598 (C-N), 1531 (Ar C=C) and 1188 (C-O) cm⁻¹.

DA2: SEC (CHCl₃): $M_n = 23.7$ kDa, $M_w = 47.3$ kDa, $\bar{D}_M = 2.00$.

¹H NMR (400 MHz, 298 K, CDCl₃): $\delta = 7.30$ (m, Ar), 7.12 (d, $J = 8.4$ Hz, Ar), 6.76 (s, C(C)HCH=CH (DA)), 6.74 (s, C(C)HCH=CH (DA)), 6.57 (s, NH), 6.52 (m, NH), 5.33 (s, CH(O)(CH)(CH) (DA)), 3.03 (s, CH(CH)C=O (DA)), 2.90 (s, CH(CH)C=O (DA)), 4.17, 4.08, 3.88, 3.76, 3.67, 2.33, 1.67, 1.40, 1.27 (Dynacoll 7360) ppm.

ATR-FTIR: $\nu_{MAX} = 3343$ (N-H), 2949 – 2865 (C-H), 1725 (C=O), 1598 (C-N), 1530 (Ar C=C) and 1166 (C-O) cm⁻¹.

DA3: SEC (CHCl₃): $M_n = 29.2$ kDa, $M_w = 74.0$ kDa, $\bar{D}_M = 2.55$.

¹H NMR (400 MHz, 298 K, CDCl₃): $\delta = 7.29$ (m, Ar), 7.12 (d, $J = 7.2$ Hz, Ar), 6.77 (s, C(C)HCH=CH (DA)), 6.74 (s, C(C)HCH=CH (DA)), 6.58 (s, NH), 6.51 (m, NH), 5.32 (s, CH(O)(CH)(CH) (DA)), 3.03

(s, CH(CH)C=O (DA)), 2.90 (s, CH(CH)C=O (DA)), 4.16, 4.08, 3.88, 3.68, 2.31, 1.63, 1.40, 1.30 (DynaColl 7380) ppm.

ATR-FTIR: $\nu_{\text{MAX}} = 3336$ (N-H), 2916 – 2850 (C-H), 1728 (C=O), 1598 (C-N), 1532 (Ar C=C) and 1170 (C-O) cm^{-1} .

DA4: SEC (CHCl₃): $M_n = 31.5$ kDa, $M_w = 84.3$ kDa, $D_M = 2.68$.

¹H NMR (400 MHz, 298 K, CDCl₃): $\delta = 7.30$ (m, Ar), 7.13 (d, $J = 8.4$ Hz, Ar), 6.77 (s, C(C)HCH=CH (DA)), 6.74 (s, C(C)HCH=CH (DA)), 6.58 (s, NH), 6.53 (m, NH), 5.33 (s, CH(O)(CH)(CH) (DA)), 3.03 (s, CH(CH)C=O (DA)), 2.90 (s, CH(CH)C=O (DA)), 4.37, 4.34, 4.31, 4.29, 4.08, 3.90, 3.81, 3.73, 2.34, 1.62, 1.29 (DynaColl 7490) ppm.

ATR-FTIR: $\nu_{\text{MAX}} = 3344$ (N-H), 2917 – 2849 (C-H), 1733 (C=O), 1599 (C-N), 1532 (Ar C=C) and 1168 (C-O) cm^{-1} .

DAA1: SEC (CHCl₃): $M_n = 11.0$ kDa, $M_w = 28.2$ kDa, $D_M = 2.56$.

¹H NMR (400 MHz, 298 K, CDCl₃): $\delta = 7.30$ (m, Ar), 7.11 (d, $J = 8.0$ Hz, Ar), 6.76 (s, C(C)HCH=CH (DA)), 6.73 (s, C(C)HCH=CH (DA)), 6.56 (s, NH), 6.51 (m, NH), 5.31 (s, CH(O)(CH)(CH) (DA)), 3.02 (s, CH(CH)C=O (DA)), 2.90 (s, CH(CH)C=O (DA)), 5.13, 4.15, 4.08, 3.90, 3.88, 3.67, 2.41, 2.31, 1.65, 1.57, 1.53, 1.50, 1.40, 0.99 (Capa 8025) ppm.

ATR-FTIR: $\nu_{\text{MAX}} = 3341$ (N-H), 2942 – 2866 (C-H), 1729 (C=O), 1599 (C-N), 1532 (Ar C=C), 1310 and 1160 (C-O) cm^{-1} .

DAA2: ATR-FTIR: $\nu_{\text{MAX}} = 3335$ (N-H), 2922 – 2853 (C-H), 1734 and 1705 (C=O), 1598 (CN), 1531 (Ar C=C) and 1310 (C-O) cm^{-1} .

4.5 References

1. H. W. Engels, H. G. Pirkl, R. Albers, R. W. Albach, J. Krause, A. Hoffmann, H. Casselmann and J. Dormish, *Angew. Chem. Int. Ed.*, 2013, **52**, 9422-9441.
2. B. Claeys, A. Vervaeck, X. K. Hillewaere, S. Possemiers, L. Hansen, T. De Beer, J. P. Remon and C. Vervaet, *Eur. J. Pharm. Biopharm.*, 2015, **90**, 44-52.
3. O. Diels and K. Alder, *Liebigs Ann. Chem.*, 1928, **460**, 98-122.
4. K. Inoue, M. Yamashiro and M. Iji, *J. Appl. Polym. Sci.*, 2009, **112**, 876-885.
5. X. Chen, M. A. Dam, K. Ono, A. Mal, H. Shen, S. R. Nutt, K. Sheran and F. Wudl, *Science*, 2002, **295**, 1698-1702.
6. A. Gandini, *Prog. Polym. Sci.*, 2013, **38**, 1-29.
7. C. Zeng, H. Seino, J. Ren, K. Hatanaka and N. Yoshie, *Macromolecules*, 2013, **46**, 1794-1802.
8. S. Chen, F. Wang, Y. Peng, T. Chen, Q. Wu and P. Sun, *Macromol. Rapid Comm.*, 2015, **36**, 1687-1692.
9. A. Amalin Kavitha and N. K. Singha, *J. Polym. Sci. A1*, 2007, **45**, 4441-4449.
10. J. A. Mikroyannidis, *J. Polym. Sci. A1*, 1990, **28**, 669-677.
11. M. Yamashiro, K. Inoue and M. Iji, *Polym. J.*, 2008, **40**, 657-662.
12. S. Yu, R. Zhang, Q. Wu, T. Chen and P. Sun, *Adv. Mater.*, 2013, **25**, 4912-4917.
13. U. W. Gedde, *Polymer Physics*, Springer Netherlands, 2013.
14. X. Kuang, G. Liu, L. Zheng, C. Li and D. Wang, *Polymer*, 2015, **65**, 202-209.
15. P. Wu, H. Cheng, X. Wang, R. Shi, C. Zhang, M. Arai and F. Zhao, *Green Chem.*, 2021, **23**, 552-560.
16. K. Ishida, Y. Nishiyama, Y. Michimura, N. Oya and N. Yoshie, *Macromolecules*, 2010, **43**, 1011-1015.

17. Y. Zhang, Z. Dai, J. Han, T. Li, J. Xu and B. Guo, *Polym. Chem.*, 2017, **8**, 4280-4289.
18. J. Stille and L. Plummer, *J. Org. Chem.*, 1961, **26**, 4026-4029.
19. M. Watanabe and N. Yoshie, *Polymer*, 2006, **47**, 4946-4952.
20. T. Brand and M. Klapper, *Des. Monomers Polym.*, 1999, **2**, 287-309.
21. M. Wu, Y. Liu, P. Du, X. Wang and B. Yang, *Int. J. Adhes. Adhes.*, 2020, **100**, 102597.
22. J. D. Mayo and A. Adronov, *J. Polym. Sci. A1*, 2013, **51**, 5056-5066.
23. X. Liu, P. Du, L. Liu, Z. Zheng, X. Wang, T. Joncheray and Y. Zhang, *Polym. Bull.*, 2013, **70**, 2319-2335.
24. C. Lakatos, K. Czifrák, R. Papp, J. Karger-Kocsis, M. Zsuga and S. Kéki, *Express Polym. Lett.*, 2016, **10**, 324-336.
25. P. Du, X. Liu, Z. Zheng, X. Wang, T. Joncheray and Y. Zhang, *RSC Adv.*, 2013, **3**, 15475-15482.
26. X. Du, L. Jin, S. Deng, M. Zhou, Z. Du, X. Cheng and H. Wang, *ACS Appl. Mater. Inter.*, 2021, **13**, 42991-43001.
27. O. W. J. Zhai, W. Zhao, X. Tao, S. L. Hsu and A. Slark, *J. Polym. Sci. Pol. Phys.*, 2018, **56**, 1265-1270.
28. G. Song, Y. Zhang, D. Wang, C. Chen, H. Zhou, X. Zhao and G. Dang, *Polymer*, 2013, **54**, 2335-2340.
29. S. Lee, P. H. Hong, J. Kim, K. Choi, G. Moon, J. Kang, S. Lee, J. B. Ahn, W. Eom and M. J. Ko, *Macromolecules*, 2020, **53**, 2279-2286.
30. D. H. Turkenburg, H. van Bracht, B. Funke, M. Schmider, D. Janke and H. R. Fischer, *J. Appl. Polym. Sci.*, 2017, **134**.
31. J. Canadell, H. Fischer, G. De With and R. A. Van Benthem, *J. Polym. Sci. A1*, 2010, **48**, 3456-3467.

32. J. E. Báez, Á. Marcos-Fernández, A. Martínez-Richa and P. Galindo-Iranzo, *Polym.-Plast. Technol.*, 2017, **56**, 889-898.
33. M. A. Gorbunova, E. V. Komov, L. Y. Grunin, M. S. Ivanova, A. F. Abukaev, A. M. Imamutdinova, D. A. Ivanov and D. V. Anokhin, *Phys. Chem. Chem. Phys.*, 2022, **24**, 902-913.
34. L. M. Sridhar, M. O. Oster, D. E. Herr, J. B. Gregg, J. A. Wilson and A. T. Slark, *Green Chem.*, 2020, **22**, 8669-8679.
35. S. A. Canary and M. P. Stevens, *J. Polym. Sci. A1*, 1992, **30**, 1755-1760.
36. J. Aizpurua, L. Martin, E. Formoso, A. Gonzalez and L. Irusta, *Prog. Org. Coat.*, 2019, **130**, 31-43.
37. C. Goussé and A. Gandini, *Polym. Int.*, 1999, **48**, 723-731.
38. M. Dettenmaier, E. Fischer and M. Stamm, *Colloid Polym. Sci.*, 1980, **258**, 343-349.
39. W. Panwiriyarat, V. Tanrattanakul, J. F. Pilard, P. Pasetto and C. Khaokong, *J. Appl. Polym. Sci.*, 2013, **130**, 453-462.

5 Designing linear TPU copolymers containing semi-crystalline and amorphous polyols covalently bonded *via* Diels-Alder chemistry

5.1 Introduction

Thermoplastic polyurethanes (TPUs) are commonplace materials on account of their diverse thermal and mechanical properties.¹ A large factor in determining TPU properties is the choice of polyol the copolymer is based on which can be either semi-crystalline or amorphous. Semi-crystalline polyols typically afford materials with higher strength and toughness.² Korley *et al.* demonstrated how crystallinity acts as a load-bearing component by enhancing material toughness within poly(ethylene oxide)-*block*-poly(propylene oxide)-*block*-poly(ethylene oxide) (PEO-PPO-PEO) based TPUs.³ However, very high crystallinity can often result in brittle materials with low elongation.⁴ On the other hand, amorphous polyols typically produce TPU copolymers with high flexibility which can often come at the cost of low strength as a consequence of lack of regular chain conformation.⁵

To overcome issues faced by both semi-crystalline and amorphous polymers, it is possible to blend multiple polyols together to produce hybrid materials that include benefits from both parent polyols. Nijenhuis *et al.* showed how pure poly(lactic acid) (PLA) is extremely brittle, but when it is blended with PEO, elongation was reported as greater than 500 %.⁶ With respect to PU copolymers, Dou *et al.* demonstrated a range of thermal and mechanical properties are achievable by altering the ratio between PLA and poly(ϵ -caprolactone) (PCL) diols.⁵ When blending polyols, it is important to have a degree of compatibility, otherwise resulting materials will be extremely heterogenous and mechanically inferior. Previous studies have shown that covalent linkage *via* copolymerisation of two polyols with connecting MDI units increases compatibility.⁷

While phase separation and a well-ordered hard segment (HS) gives TPU copolymers with favourable mechanical properties, it can also limit their ease of processing and application.

Strong HS association can persist while in the melt phase to result in a highly viscous melt which requires high temperature and expensive specialist equipment to overcome.⁸ High viscosity also restricts applications for reversible adhesion where a low viscosity is required for simple removal of adhesive.

Therefore, by using a blend of semi-crystalline and amorphous polyols, it might be possible to form phase separated TPUs without chain extension. In this case, the amorphous polyol would act as the flexible soft segment (SS) and the semi-crystalline polyol would act as the reinforcing HS. In this way, the HS could be more easily dissociated at lower temperatures than traditional HS, which would ease processing and mitigate the need for expensive high shear equipment.

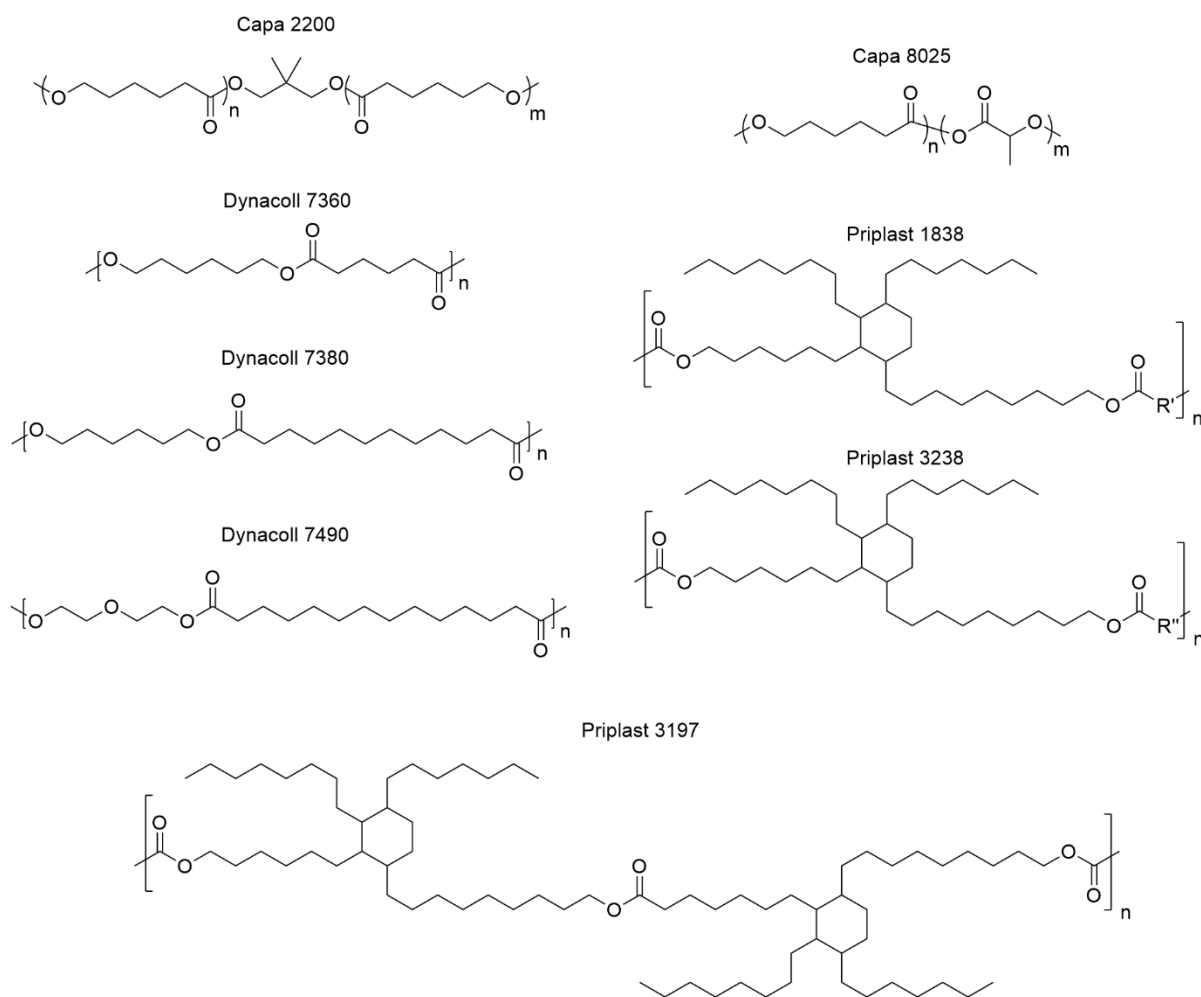
These tuneable materials could be used in tandem with reversible Diels-Alder (DA) chemistry. The DA reaction is a clean and atom efficient [4+2] cycloaddition with no side reactions and can be easily incorporated within linear TPUs to afford copolymers with dynamic molecular weights which change as a function of stimulus.^{9,10} This switchable molecular weight is a consequence of the reversibility of the DA cycloadduct which can form *via* the DA reaction at ambient temperatures and then revert to its precursors *via* the retro-Diels-Alder (rDA) reaction at elevated temperatures.¹¹ The combination of both techniques could afford materials that are high mechanically performing solids at room temperatures and low viscosity melts above 100 °C.^{12,13}

Therefore, the aim of this work is to investigate DA-active linear TPUs based on copolymerising semi-crystalline and amorphous prepolymers which have dynamic properties, controllable *via* changes in temperature.

5.2 Results and discussion

5.2.1 Determination of polyol compatibility

An initial study was conducted on the compatibility of polyols with one another for use in blended DA-active TPU copolymers. The polyols investigated are grouped as semi-crystalline or amorphous (**Scheme 5.1**). The semi-crystalline polyols are **Capa 2200** ((PCL), $T_m = 53\text{ }^\circ\text{C}$, 2.0 kDa), **Dynacoll 7360** (hexanediol and adipic acid copolymer, $T_m = 58\text{ }^\circ\text{C}$, 3.5 kDa), **Dynacoll 7380** (hexanediol and dodecanedioic acid copolymer, $T_m = 74\text{ }^\circ\text{C}$, 3.5 kDa) and **Dynacoll 7490** (diethylene glycol and tetradecanoic acid copolymer, $T_m = 91\text{ }^\circ\text{C}$, 3.5 kDa). The amorphous polyols are **Capa 8025** (random copolymer of ϵ -caprolactone (CL) 75 % and lactic acid (LA) 25, 2.0 kDa), **Priplast 1838** (C_{36} diol copolymerised with an undefined diacid, 2.0 kDa), **Priplast 3238** (C_{36} diol copolymerised with an undefined diacid, 2.0 kDa) and **Priplast 3197** (copolymer of C_{36} diol and C_{36} diacid, 2.0 kDa).



Scheme 5.1 Structures of polyols investigated. Semi-crystalline (left) and amorphous (right and bottom). R' and R'' represent different undefined diacids.

The compatibility of each semi-crystalline polyol with each amorphous polyol was determined by mixing in turn 33 wt% semi-crystalline polyol with 67 wt% amorphous polyol. The first method used was to heat two polyols in the same glass jar so that the semi-crystalline material was fluid, stir manually once an hour and after 3 hours determine solubility by visual inspection (**Figure 5.1**). While in the liquid state, miscible polyols would appear as one phase, whereas immiscible polyols would have a visible horizontal line signifying two separate fluids.

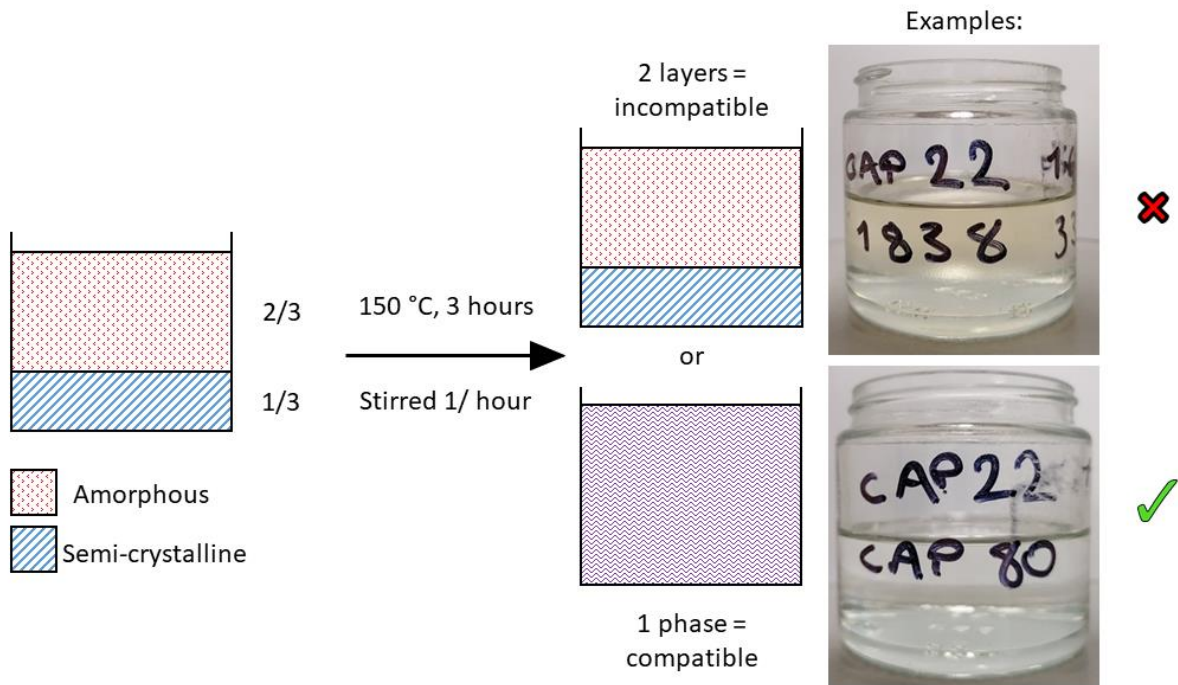


Figure 5.1 Method for basic testing of compatibility of polyols by visual inspection.

Most semi-crystalline polyols are only compatible with **Capa 8025**, a result of similarities in polarity (**Table 5.1**). The **Priplast** polyols are relatively nonpolar as a consequence of long aliphatic chains. **Dynacoll 7380** is not compatible with **Capa 8025**, but is compatible with both **Priplast 1838** and **Priplast 3238**. This miscibility is due to the similarly low polarities of these materials, **Dynacoll 7380** contains hexanediol and dodecanedioic acid which means ester group concentration is low compared to other **Dynacoll** polyols. **Priplast 3197** appears not miscible with any of the semi-crystalline polyols as it is very nonpolar with the lowest concentration of ester groups.

Table 5.1 Results from visual inspection of basic mixing of molten polyols to determine compatibility.

		Amorphous			
		Capa 8025	Priplast 1838	Priplast 3238	Priplast 3197
Semi-crystalline	Capa 2200	Yes	No	No	No
	Dynacoll 7360	Yes	No	No	No
	Dynacoll 7380	No	Yes	Yes	No
	Dynacoll 7490	Yes	No	No	No

DSC heating cycles were conducted on the pure polyols and the blended materials. The first heating cycles were analysed as a consequence of slow recrystallisation kinetics. For combinations that showed immiscibility, a sample was taken from the semi-crystalline phase. Compatibility of polyols is considered by observing differences in the enthalpy of melting of polyol crystallinity (ΔH_m) as this feature is affected by the presence of other polyols (**Table 5.2**).⁷

The unblended amorphous polyols all display clear glass transitions temperatures (T_g) (**Figure 5.2(a)**). No other thermal transitions are observed above 0 °C.

The DSC thermograms of **Capa 2200** mixed with the three **Priplast** polyols are comparable to that of unblended **Capa 2200**, which shows that **Capa 2200** crystallinity is not diluted, thereby indicating immiscibility (**Figure 5.2(c)**). However, when mixed with **Capa 8025**, there is a

significant decrease in both T_m and ΔH_m . This reduction implies **Capa 2200** crystallinity has been diluted by the presence of **Capa 8025** and therefore suggests the two polyols are compatible.⁶ This conclusion agrees with results from visual inspection. Results for the **Dynacoll 7360** are very similar to **Capa 2200** which implies **Dynacoll 7360** is only compatible with **Capa 8025** (*Figure 5.2(d)*).

Table 5.2 Key thermal data obtained via DSC for determining compatibility of semi-crystalline polyols with amorphous polyols. Compatible mixtures are purple. Blends highlighted in yellow fulfil criteria for further investigation.

Semi-Crystalline	Unblended ^a		Capa 8025		Priplast 1838		Priplast 3238		Priplast 3197	
	T_m (°C)	ΔH_m (J.g ⁻¹)	T_m (°C)	ΔH_m (J.g ⁻¹)	T_m (°C)	ΔH_m (J.g ⁻¹)	T_m (°C)	ΔH_m (J.g ⁻¹)	T_m (°C)	ΔH_m (J.g ⁻¹)
Capa 2200	53	83	36 & 46	23	34 & 52	76	35 & 50	72	34 & 52	75
Dynacoll 7360	58	108	51	23	58	88	57	89	58	94
Dynacoll 7380	70	119	72	109	69	43	69	45	72	109
Dynacoll 7490	91	127	89	65	88	64	88	75	90	97

^a Greyed out for clarity

The pure unblended semi-crystalline polyols have clear endotherms associated with the melting of crystalline regions (*Figure 5.2(b)*). T_m and ΔH_m increase in the order **Capa 2200** < **Dynacoll 7360** < **Dynacoll 7380** < **Dynacoll 7490**.

Dynacoll 7380 displays different behaviour, ΔH_m is significantly reduced when mixed with **Priplast 1838** and **Priplast 3238**, indicating compatibility (*Figure 5.2(e)*). In contrast, **Dynacoll 7490** records a reasonable decrease in ΔH_m when mixed with all four amorphous polyols (*Figure 5.2(f)*). This interesting behaviour is likely a consequence of **Dynacoll 7490** containing both a relatively polar component (diethylene glycol) and a nonpolar component

(tetradecanoic acid) which allows for at least partial miscibility with both polar polyols (**Capa 8025**) and nonpolar polyols (**Priplast 3197**).

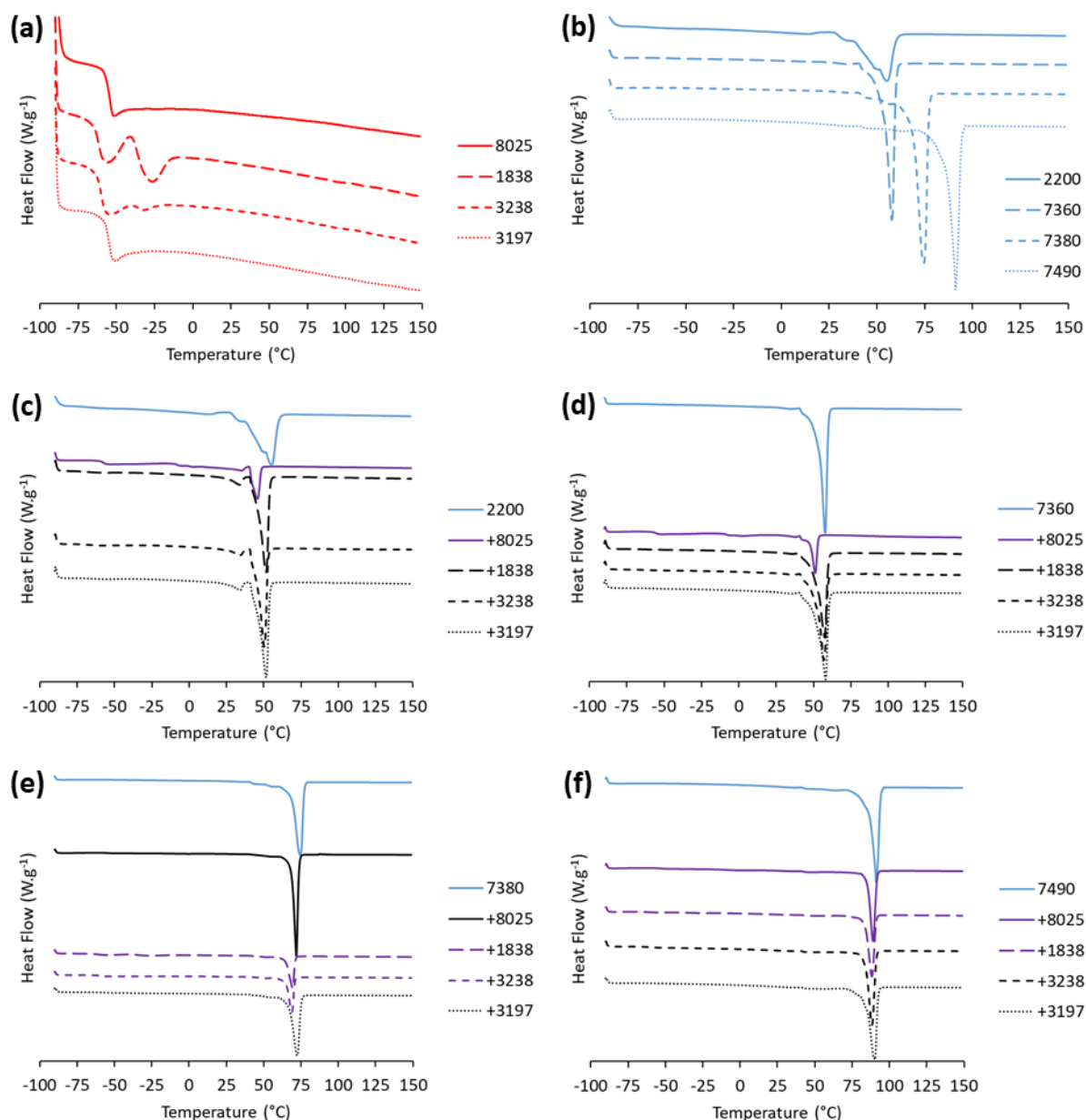


Figure 5.2 DSC thermograms of **(a)** pure amorphous polyols. **(b)** pure semi-crystalline polyols. Amorphous polyols are mixed in turn with **(c)** **Capa 2200**, **(d)** **Dynacoll 7360**, **(e)** **Dynacoll 7380** and **(f)** **Dynacoll 7490**. Red = unblended amorphous polyols, blue = unblended semi-crystalline polyols, black = immiscible mixtures and purple = miscible mixtures. First heat cycle used at a heating rate of $10\text{ }^{\circ}\text{C}\cdot\text{min}^{-1}$. Exo up.

To determine which blends should be explored further, two factors were considered to ensure the material could be industrially relevant as an adhesive. Firstly, desirable blended polyols should have a $T_m > 70$ °C to afford a reasonable maximum service temperature. Secondly, the blends should have a significant reduction in ΔH_m (approximately ≥ 50 %) relative to the respective unblended semi-crystalline polyol to highlight combinations with greatest compatibility. Only two blends fulfil both criteria, **Dynacoll 7490** with **Capa 8025** and **Dynacoll 7490** with **Priplast 1838** (*Table 5.2*). Additionally, it was decided that **Capa 2200** with **Capa 8025** and **Capa 2200** with **Priplast 1838** would also be investigated as reference materials.

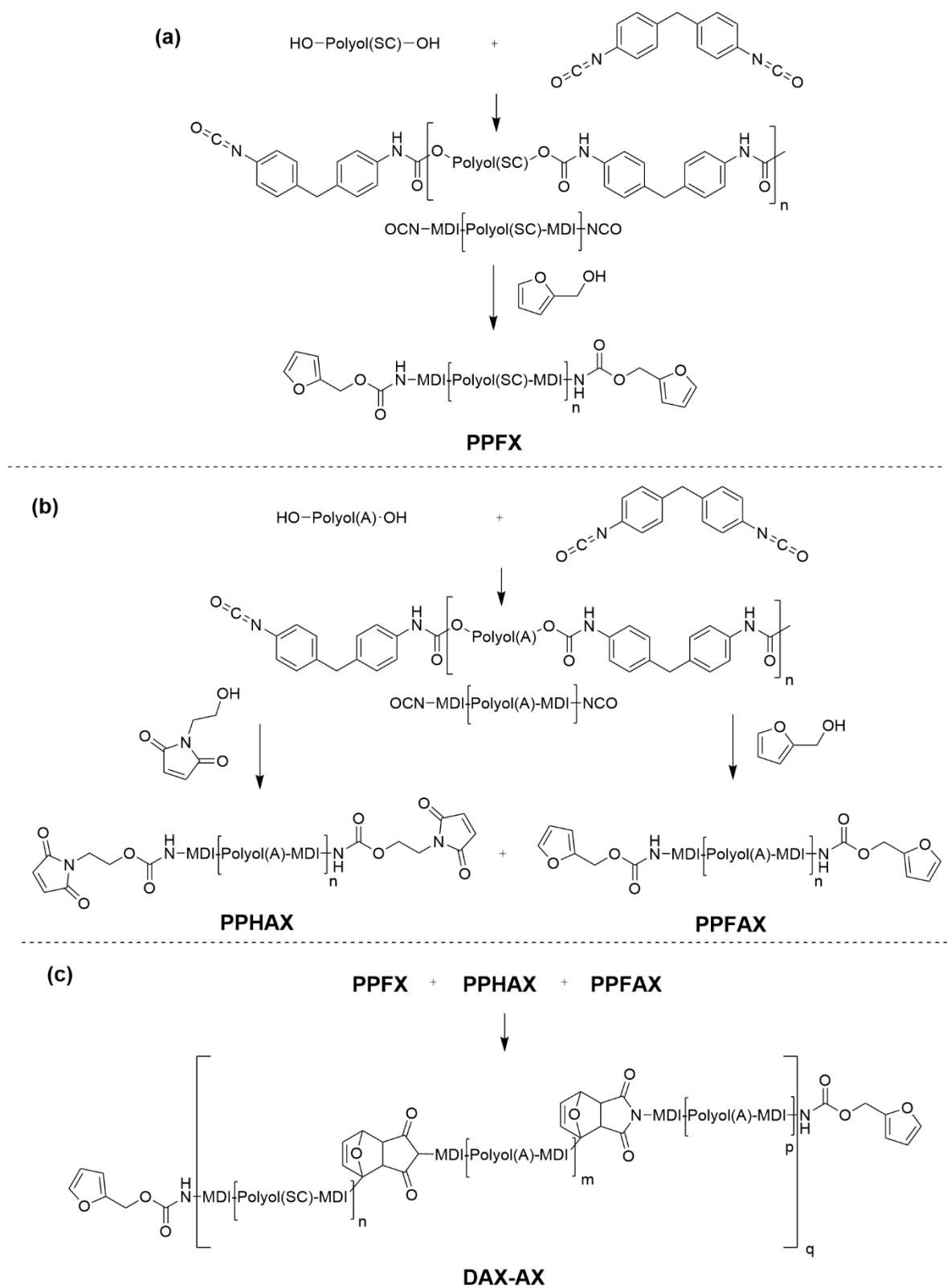
5.2.2 *Synthesis of linear TPUs containing semi-crystalline and amorphous polyols*

covalently bonded via Diels-Alder chemistry

Linear TPUs including DA cycloadducts and based on copolymers of semi-crystalline and amorphous prepolymers were synthesised in bulk *via* a multistep reaction pathway (*Scheme 5.2*). Synthesis was solvent-free which mitigates risks and hazards associated with organic-based solution polymerisation. The same ratio of semi-crystalline (33 wt%) and amorphous (67 wt%) polyols were used in this synthesis to form the final TPU copolymer as in the previous compatibility tests. Initially, semi-crystalline polyols and MDI were reacted at a stoichiometry of 1.0 : 2.0 to form NCO-terminated prepolymers. These species were then reacted further with monofunctional furfuryl alcohol (FA) to afford furan-terminated prepolymers (**PPFX**) (*Scheme 5.2(a)*). In two separate reaction vessels, the same procedure was repeated with amorphous polyols, MDI and FA and amorphous polyols, MDI and 2-hydroxy ethylmaleimide (HEMI) to afford both FA- (**PPFAX**) and HEMI-terminated (**PPHAX**) amorphous prepolymers (*Scheme 5.2(b)*). These prepolymers are benign and typically solid materials, which allows the

next and final step to be performed at any time. Finally, a predetermined mixture of **PPFX**, **PPFAX** and **PPHAX** were blended in the melt phase and then copolymerised over time under ambient conditions, thereby forming the DA cycloadducts. In this step, one third of the mass was semi-crystalline prepolymer and two thirds were amorphous prepolymer and the stoichiometry of furan : maleimide was 1.0 : 1.0 to produce a final linear TPU copolymer (**DAX-AX**) (*Scheme 5.2(c)*).

Furan-terminated prepolymers based on semi-crystalline **Capa 2200**, **Dynacoll 7490** are denoted **PPF1** and **PPF4**, respectively, and furan-terminated prepolymers based on amorphous **Capa 8025** and **Priplast 1838** are denoted **PPFA1** and **PPFA2**, respectively (as labelled in Chapter 4). HEMI-terminated prepolymers based on **Capa 8025** and **Priplast 1838** are denoted **PPHA1** and **PPHA2**, respectively. Copolymers comprising the different semi-crystalline and amorphous polyols are labelled **DAX-AX**, where the first **X** represents the semi-crystalline prepolymer and the second **X** the amorphous prepolymer. Therefore, copolymer of **Capa 2200** with **Capa 8025** is labelled as **DA1-A1**, **Capa 2200** with **Priplast 1838** is **DA1-A2**, **Dynacoll 7490** with **Capa 8025** is **DA4-A1** and **Dynacoll 7490** with **Priplast 1838** is **DA4-A2** (*Table 5.3*).



Scheme 5.2 (a) Synthesis of furan-terminated prepolymer containing semi-crystalline polyol (**PPFX**). (b) Synthesis of furan- and maleimide-terminated prepolymers containing amorphous polyol (**PPFAX** and **PPHAX**, respectively). (c) Synthesis of **DAX-AX** from a mixture of semi-crystalline and amorphous based prepolymers. **X = 1, 2 or 4**)

Table 5.3 Composition of the TPU copolymers and prepolymers synthesised with various polyols with correlating SEC data.

Material	Molar Ratio ^a			Polyol (SC)	Polyol (A)	Comonomer	M_n^d (kDa)	M_w^d (kDa)	\bar{D}_M^d
	Polyol	MDI	FA/HEMI						
PPF1	1.0	2.0	1.1	Capa 2200	- ^c	FA	6.3	12.6	1.94
PPF4	1.0	2.0	1.1	Dynacoll 7490	- ^c	FA	15.2	29.4	1.93
PPHA1	1.0	2.0	1.1	- ^c	Capa 8025	HEMI	6.0	11.1	1.85
PPFA1	1.0	2.0	1.1	- ^c	Capa 8025	FA	6.3	11.7	1.85
PPHA2	1.0	2.0	1.1	- ^c	Priplast 1838	HEMI	6.0	13.8	2.28
PPFA2	1.0	2.0	1.1	- ^c	Priplast 1838	FA	6.0	14.2	2.36
DA1-A1	- ^b	- ^b	- ^b	Capa 2200	Capa 8025	DA	13.5	34.4	2.52
DA1-A2	- ^b	- ^b	- ^b	Capa 2200	Priplast 1838	DA	13.3	51.2	3.42
DA4-A1	- ^b	- ^b	- ^b	Dynacoll 7490	Capa 8025	DA	15.1	34.7	2.61
DA4-A2	- ^b	- ^b	- ^b	Dynacoll 7490	Priplast 1838	DA	23.3	56.5	2.53

^a Molar ratio of functional group

^b Not measured as made via melt blending multiple prepolymers

^c Not present

^d Determined by SEC in $CHCl_3$ against PMMA standards

Successful synthesis of **DAX-AX** was proven *via* 1H NMR and FTIR spectroscopies and size exclusion chromatography (SEC). In the 1H NMR spectra of all **DAX-AX** there is a resonance at $\delta = 5.32$ ppm which corresponds to $CH(O)(CH)(CH)$ of the DA cycloadduct. There are also two resonances at $\delta = 3.02$ and 2.90 ppm which relate to two protons $CH(CH)C=O$ either side of the N atom in the DA cycloadduct.

In the FTIR spectra of all the prepolymers there is no absorbance at $\nu_{max} = 2260$ cm^{-1} , corresponding to the NCO of NCO-terminated polyol. This absence demonstrates successful reaction of the NCO-terminated prepolymer with FA or HEMI to form **PPFX** or **PPHX**,

respectively. Melt blending of **PPFX**, **PPFAX** and **PPHAX** followed by copolymerisation at ambient temperatures decreases the absorbance at $\nu_{\max} = 696 \text{ cm}^{-1}$ which relates to free maleimide, inferring that the maleimide end groups are consumed to form the DA cycloadduct by reaction with furan end groups.¹⁴

Results from SEC show there is an increase in weight average molecular weight (M_w) for **DA1-A1**, **DA1-A2**, **DA4-A1** and **DA4-A2** with respect to their constituent prepolymers. This increase suggests successful DA cycloadduct formation which leads to an increase in chain length.¹⁵ However, the number average molecular weight (M_n) increases for all **DAX-AX** but **DA4-A1**. The reason for this discrepancy is undetermined and requires further investigation.

5.2.3 Structural characterisation of DAX-AX copolymers

Inspection of the carbonyl regions of FTIR spectra gives information about the type of molecular interactions present within the linear TPU copolymers. The carbonyl region of **DA1-A1** is dominated by the absorbance of backbone ester at approximately $\nu_{\max} = 1725 \text{ cm}^{-1}$, but also shows a shoulder at lower wavenumbers associated with H-bonded urethane and imide carbonyls (**Figure 5.3**).^{16, 17} The copolymer **DA1-A2** shows a broad maximum absorbance at $\nu_{\max} = 1731 \text{ cm}^{-1}$ as it encompasses different polyester backbones from **Capa 2200** and **Priplast 1838**. A secondary broad maximum is observed at $\nu_{\max} = 1709 \text{ cm}^{-1}$ in the spectrum of **DA1-A2**, corresponding to urethane and imide carbonyl groups. The spectra for **DA4-A1** and **DA4-A2** also display absorbances for the different backbones present and shoulders at lower wavenumbers corresponding to H-bonding carbonyl groups. Overall, the spectrum of all **DAX-AX** appear to contain a range of carbonyl types, which opens up the potential for a substantial number of physical interactions.

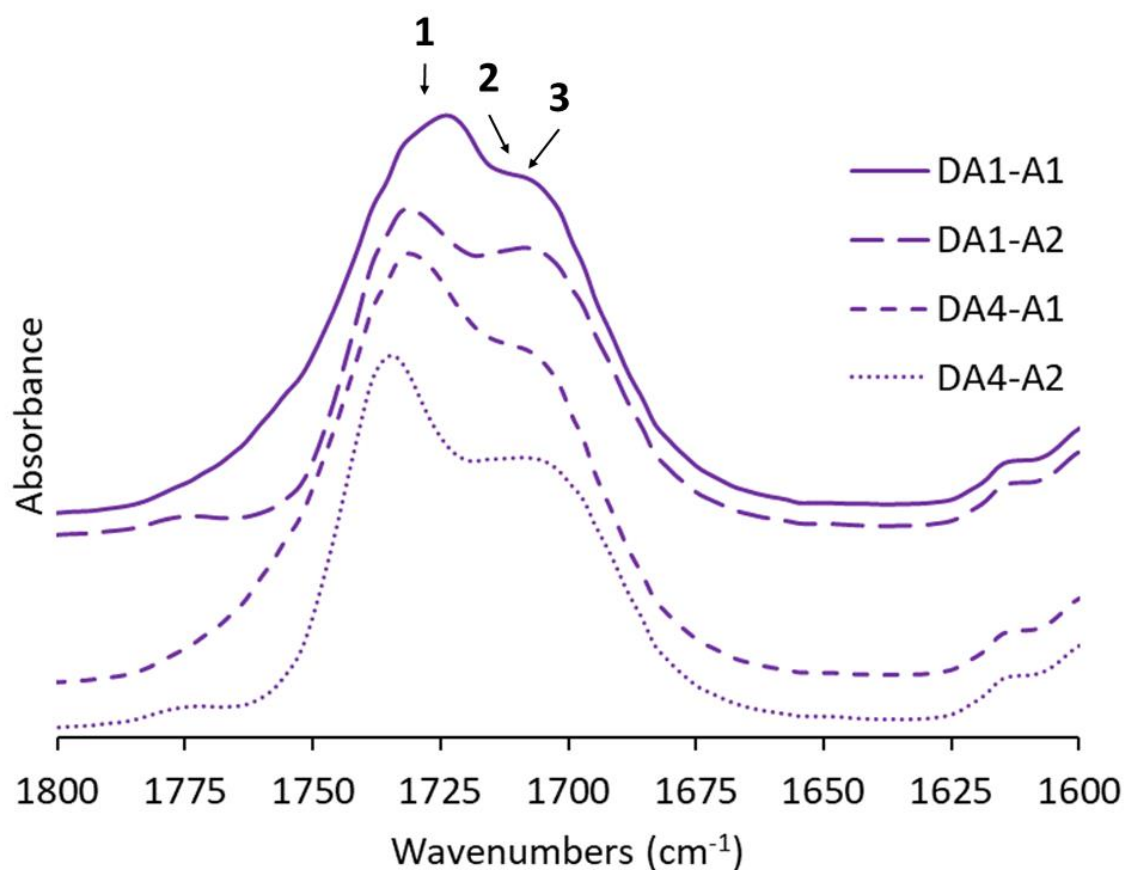


Figure 5.3 Carbonyl regions of FTIR spectra for **DAX-AX** copolymers. 1 = polyol backbone ester. 2 = H-bonded urethane. 3 = imide carbonyl.

The thermal properties of **DAX-AX** were determined with reference to blended polyols without covalent linkage from the initial compatibility studies (**X-AX**, where **X** = **1**, **2** or **4**) (**Table 5.4**). The first heating cycles were analysed to account for slow crystallisation and DA cycloaddition. In the thermogram of **DA1-A1**, there is a clear T_g at -17 °C. Interestingly, the non-covalently attached blend of **Capa 2200** and **Capa 8025 (1-A1)** displays two distinct and well separated T_g at -58 and -8 °C which suggests partial incompatibility of the two polyols. Yet after copolymerisation, only one T_g is observed as a consequence of improved miscibility when covalently bound as the two backbones are forced into close proximity.⁷ A melting endotherm is observed at 43 °C for **DA1-A1** which corresponds to the melting of crystalline PCL from **Capa 2200 (Figure 5.4(a))**. The ΔH_m (5 J.g^{-1}) is significantly reduced with comparison

to the DA copolymer comprising only **Capa 2200 (DA1)**, discussed in Chapter 4) which recorded a value of 27 J.g⁻¹. This decrease is mostly due to the lower content of **Capa 2200** with respect to polyol content in **DA1-A1 (DA1-A1 = 33 %, DA1 = 100 %)**. At higher temperatures, **DA1-A1** shows a double peaked endotherm at 116 and 148 °C characteristic of the rDA reaction (which is also present in unblended **DA1** and **DAA1** in Chapter 4).¹⁸ No temperature of rDA (T_{rDA}) is detected for **1-A1** as there are no DA cycloadducts present in the material. In **DA1-A1**, the enthalpy of rDA (ΔH_{rDA}) (10.2 J.g⁻¹) is similar to that of **DA1** (8.9 J.g⁻¹) and **DAA1** (11.9 J.g⁻¹), previously described, which proves that using a blend of polyols does not prevent DA cycloadduct formation.

Table 5.4 Thermal data collected from DSC analysis for copolymers **DAX-AX** and blends without covalent attachment **X-AX**. First heating cycle used at a heating rate of 10 °C.min⁻¹.

Material	T_g (°C)	T_{alt} (°C)	T_m (°C)	ΔH_m (J.g ⁻¹)	T_{rDA} (°C)	ΔH_{rDA} (J.g ⁻¹)
DA1-A1	-17	- ^b	43	5	116 & 148	10.2
DA1-A2	-45	- ^b	44	7	116 & 146	8.8
DA4-A1	-11	49	78 & 82	22	117 & 144	6.5
DA4-A2	-45	50	81	24	118 & 143	5.8
1-A1	-58 & -8	- ^b	36 & 46	23	- ^c	- ^c
1-A2	-67	- ^b	34 & 52	76	- ^c	- ^c
4-A1	-53 & -8	43	89	65	- ^c	- ^c
4-A2	-61 & -35	42	88	64	- ^c	- ^c

^a No T_g detected

^b No T_{alt} present

^c No DA cycloadduct present

The thermogram of **DA1-A2** displays a T_g at -45 °C attributed to the amorphous component and an endotherm at 44 °C corresponding to melting of PCL crystallinity (**Figure 5.4(b)**). This melt shows how PCL crystallinity is consistent with multiple amorphous copolymers. Interestingly, the initial compatibility studies suggested **Capa 2200** and **Priplast 1838** to be incompatible. This change in solubility proves the effect covalent attachment has on

miscibility of polyols. An endotherm corresponding to rDA is also present in **DA1-A2** at 116 and 146 °C.

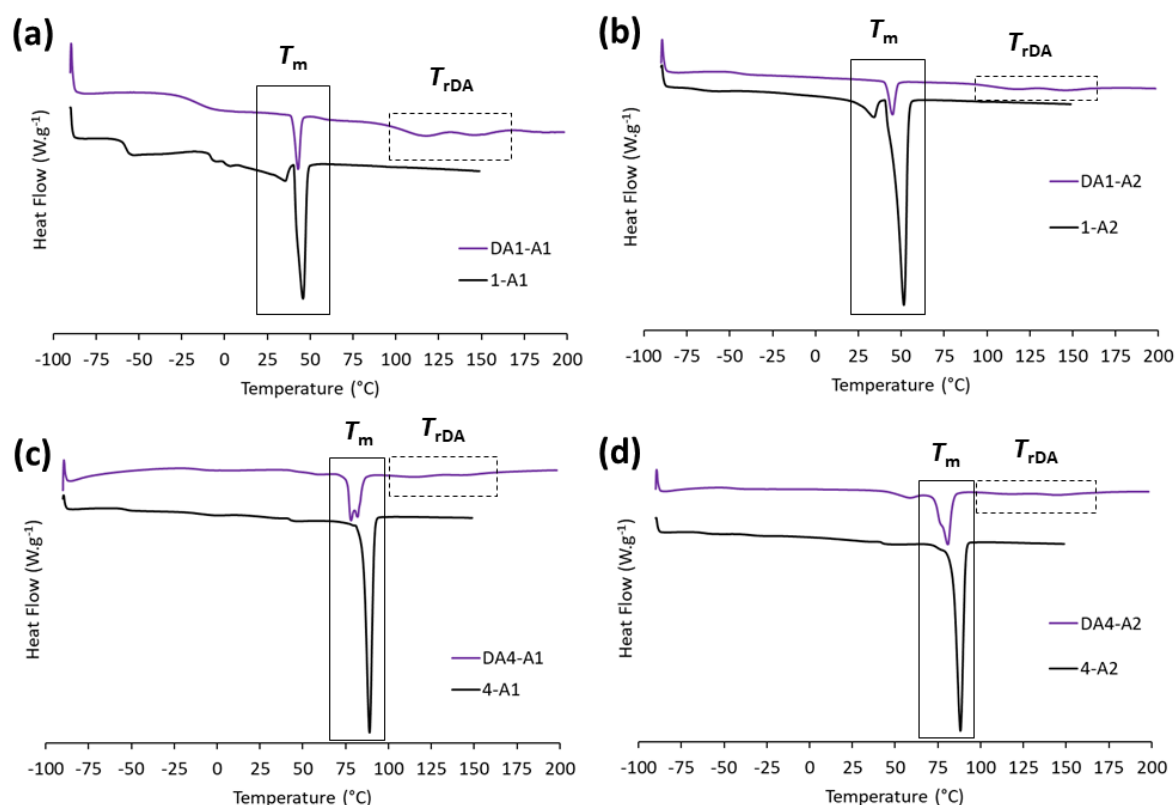


Figure 5.4 DSC heating thermograms of copolymers and physical blends. **(a) DA1-A1 and 1-A1, (b) DA1-A2 and 1-A2, (c) DA4-A1 and 4-A1 and (d) DA4-A2 and 4-A2.** First heating cycle used at a heating rate of 10 °C.min⁻¹. Exo up.

In the thermogram of **DA4-A1** a T_g is observed at -11 °C but the non-covalently attached blend **4-A1** displays two T_g which reinforces the notion that covalent attachment improves compatibility of polyols. There is a large endotherm with peaks at 78 and 82 °C which relates to the crystallinity of **Dynacoll 7490** (**Figure 5.4(c)**). The ΔH_m (22 J.g⁻¹) is significantly larger than that of the two **Capa 2200** based copolymers (**DA1-A1** & **-A2** = 5 & 7 J.g⁻¹, respectively). The physical blend **4-A1** shows a higher ΔH_m than **DA4-A1**, again proving a lower degree of compatibility without covalent linkage. The endotherm correlating to T_{rDA} is detected in **DA4-A1** at 117 and 144 °C. **DA4-A1** shows a lower ΔH_{rDA} (6.5 J.g⁻¹) than **DA1-A1** (different semi-

crystalline polyol, same amorphous polyol) as a consequence of the higher molecular weight of the semi-crystalline polyol used which decreases functional group concentration.

The thermogram of **DA4-A2** displays a T_g of $-45\text{ }^\circ\text{C}$ which matches the T_g of **DA1-A2** exactly which contains the same amorphous component (**Priplast 1838**). An endotherm is present at $88\text{ }^\circ\text{C}$ with a similar ΔH_m as **DA4-A1**, indicating similar compatibilities of **Dynacoll 7490** prepolymer with both **Capa 8025** and **Priplast 1838** based prepolymers (**Figure 5.4(d)**). As in every other case, noncovalently attached **4-A2** displays a higher ΔH_m than **DA4-A2** on account of poorer compatibility of the two polyols without copolymerisation. Finally, **DA4-A2** shows an endotherm corresponding to T_{rDA} at 118 and $143\text{ }^\circ\text{C}$.

Overall, there are some clear trends in the analysis of DSC data. The T_g tends to be dictated by the amorphous component and therefore it suggests so are the low temperature properties. Crystallinity still persists from the semi-crystalline component, but is somewhat decreased by copolymerisation with the amorphous prepolymer. As crystallinity is still present, it shows the aim of making a phase separated linear TPU without chain extender has been achieved. Finally, T_{rDA} is present in all **DAX-AX** materials which shows copolymerisation of prepolymers based on different polyols does not prevent DA cycloadduct formation.

DMA was performed on the four **DAX-AX** copolymers comprising both semi-crystalline and amorphous prepolymers and the four reference copolymers containing only semi-crystalline (**DAX**) and amorphous (**DAAX**) prepolymers. **DA1-A1** displays a peak in $\tan \delta$ at $6\text{ }^\circ\text{C}$ corresponding to a T_g which matches that of the amorphous based reference copolymer **DAA1**, recorded at $5\text{ }^\circ\text{C}$ (**Figure 5.5(a) & (d)**). This transition is followed by a slight plateau in storage modulus (E') which then decreases significantly at $41\text{ }^\circ\text{C}$ as a consequence of PCL crystals melting in **Capa 2200** (**Figure 5.5(a) & (c)**). The E' (52 MPa) is significantly lower than

that of the relevant reference semi-crystalline **DA1** (390 MPa), as a consequence of lower crystallinity and high amorphous polyol content (**DAA1** = 4 MPa) (**Table 5.5**). Therefore, the strength of **DA1-A1** is an intermediate of **DA1** and **DAA1**, as it is an order of magnitude lower and higher than **DA1** and **DAA1**, respectively, a useful feature for targeted properties. Above T_m , **DA1-A1** displays a highly temperature dependent E' until 82 °C where all material strength is lost, although the sample did not break. This final decrease in E' is caused by the rDA reaction, as the cycloadduct returns to the two precursors, it causes a decrease in molecular weight and therefore a decrease in cohesion which is reflected in a drop in E' . Interestingly, the purely semi-crystalline **DA1** does not have enough cohesion to reach T_{rDA} via DMA whereas **DAA1** does, which implies the added cohesion seen in **DA1-A1** is a contribution of the amorphous prepolymer.

DA1-A2 displays a T_g at -25 °C which is a much lower temperature than **DA1-A1**, recorded at 6 °C (**Figure 5.5(a)**). This reduction in T_g reflects the amorphous component present in **DA1-A2**, **Priplast 1838**. E' above T_g is lower for **DA1-A2** than **DA1-A1** which is another observed difference between **DAA1** and **DAA2** reference copolymers. E' of **DA1-A2** is again an intermediate between **DA1** and **DAA2**. A slight decrease in E' at 44 °C signifies the melting of the small amount of crystallinity within **DA1-A2** (**Figure 5.5(a)**). Above T_m , **DA1-A2** displays a region of relatively constant E' not observed in **DA1-A1**. By analysing the two amorphous reference materials, it is clear the **Priplast 1838** based copolymer (**DAA2**) has a E' with significantly less dependence on temperature than the **Capa 8025** based copolymer (**DAA1**). This difference is likely on account of potential phase separation present in **DAA2**, but not **DAA1**, therefore offering greater stability to **DAA2** as discussed previously (Chapter 4). The difference between these two amorphous polyols is therefore observed in **DA1-A1** and **DA1-**

A2 which contain **Capa 8025** and **Priplast 1838**, respectively. **DA1-A2** also displays a higher T_{rDA} than **DA1-A1** which is also observed when comparing the amorphous copolymers **DAA1** and **DAA2**.

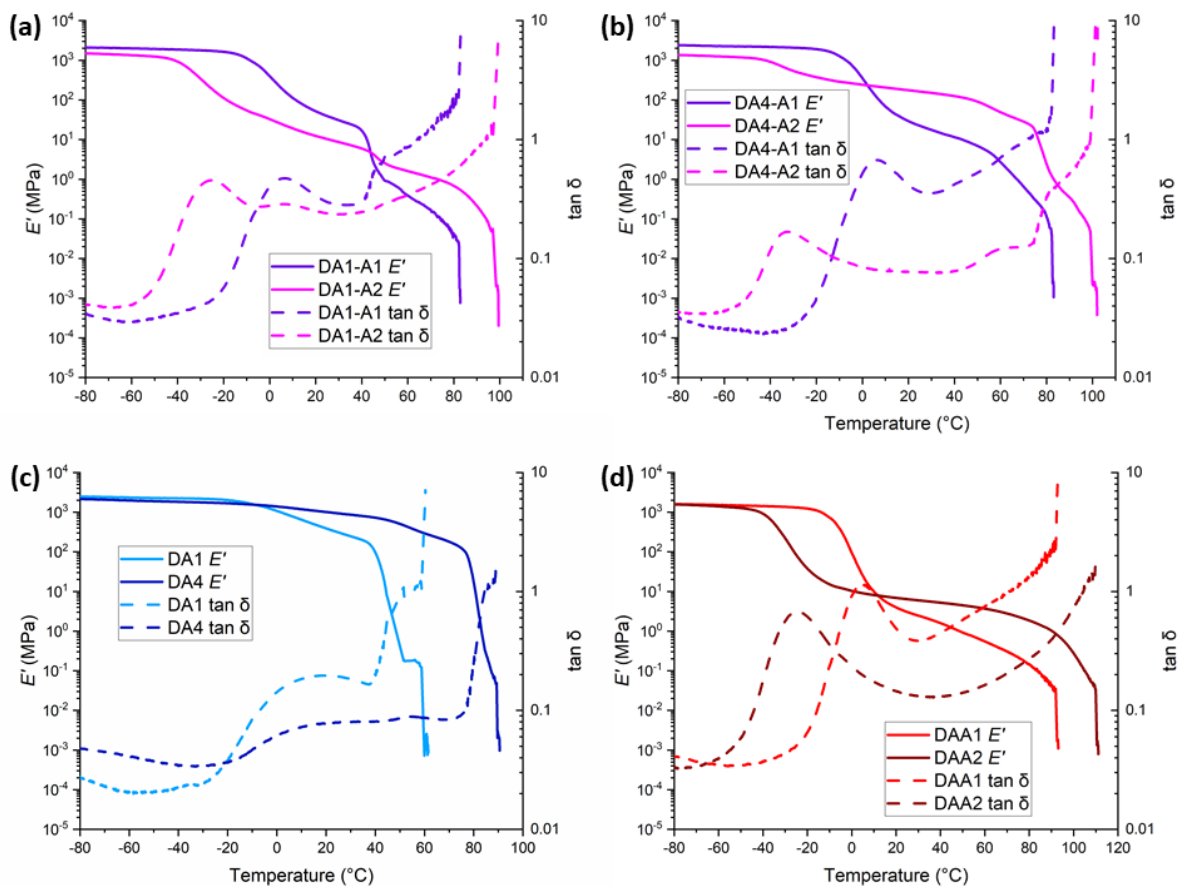


Figure 5.5 DMA results of (a) **DA1-A1** and **DA1-A2**, (b) **DA4-A1** and **DA4-A2** which are compared to reference copolymers (c) **DA1** and **DA4** (semi-crystalline) and (d) **DAA1** and **DAA2** (amorphous). Heating rate of $3\text{ }^{\circ}\text{C}\cdot\text{min}^{-1}$.

DA4-A1 shows similar low temperature properties to **DA1-A1** on account of the presence of **Capa 8025** in both copolymers (**Figure 5.5(a) & (b)**). However, the T_m of **DA4-A1** ($80\text{ }^{\circ}\text{C}$) is almost double that of **DA1-A1** ($41\text{ }^{\circ}\text{C}$) due to copolymerisation of prepolymers comprising **Dynacoll 7490** which has a higher T_m than **Capa 2200**. The final drop in E' at $82\text{ }^{\circ}\text{C}$ signifies the onset of T_{rDA} within **DA4-A1**. As this transition is very close to the T_m of **Dynacoll 7490** it results in a significant loss of material strength within a short temperature range.

Table 5.5 Thermal data obtained for the four copolymers (**DAX-AX**) compared to semi-crystalline (**DAX**) and amorphous (**DAAX**) reference copolymers via DMA with a heating rate of 3 °C.min⁻¹.

Copolymer	E' (T < T_g) ^a (MPa)	T_g ^b (°C)	E' (T > T_g) ^c (MPa)	T_m ^d (°C)	T_{rDA} ^e (°C)
DA1-A1	1940	6	52	41	82
DA1-A2	1240	-25	12	44	97
DA4-A1	2230	6	29	80	82
DA4-A2	1150	-33	176	75	95
DA1	2280	18	390	40	-
DA4	1890	17	1015	78	-
DAA1	1480	5	4	-	92
DAA2	1270	-24	7	-	110

^a Modulus at -50 °C

^b Measured from the peak in $\tan \delta$

^c Modulus at 20 °C

^d Measured as the onset of modulus slope

^e Estimated from the final drop in modulus

As in the previous case, **DA4-A2** displays low temperature thermal properties comparable to **DA1-A2** due to the common presence of the same amorphous segment **Priplast 1838** (**Figure 5.5(a) & (b)**). **DA4-A2** records the highest E' above T_g of 176 MPa due to the high T_m of the crystalline phase and relatively low dependence of E' on temperature. The combination of low T_g and high T_m provides **DA4-A2** with an impressively large service temperature range of approximately 100 °C allowing for potentially a wide variety of applications. The decrease in E' at 75 °C corresponds to the melting of **Dynacoll 7490** crystalline regions and the decrease at 95 °C relates to T_{rDA} .

DMA data generally shows that the amorphous component determines both the low (≤ 5 °C) and very high temperature (≥ 80 °C) thermal properties of the **DAX-AX** copolymers which

would allow for synthesis of materials with specific properties or use in applications at certain temperatures. Therefore, temperatures below 5 °C and above 80 °C in the DMA thermograms of **DA1-A1** and **DA4-A1** resemble **DAA1**, and the same can be said for **DA1-A2** and **DA4-A2** with **DAA2**. Whereas in the intermediate temperature range (5 – 80 °C) thermal properties are largely determined by the semi-crystalline polyol, again allowing for desired properties for specific applications. Typically, at ambient temperatures the E' of **DAX-AX** is decreased by an order of magnitude relative to the reference semi-crystalline **DAX** but it is also increased by an order of magnitude relative to the reference amorphous **DAAX** to afford an intermediate strength. Copolymerising semi-crystalline prepolymers with amorphous prepolymers, to give DA-active copolymers, affords materials that remain cohesive up to T_{rDA} , unlike purely semi-crystalline analogues. This added cohesion is likely due to increased amorphous component which allows for greater entanglements which persist above $T_{m(pol)}$. Results suggest there is the possibility of finely tuning the thermal properties of a desired DA-active material with the prepolymers acting as ‘building blocks’.

5.2.4 Melt phase properties

Rheological temperature sweeps were performed on the four blended copolymers **DAX-AX** to determine their melt phase flow properties. A melt complex viscosity (η^*) of 10 Pa.s⁻¹ was chosen as a suitable target for good surface wetting and simple application and removal in applications as a reversible adhesive.

Both **DA1-A1** and **DA1-A2** display a melt η^* with temperature dependence (**Figure 5.6(a)**). **DA1-A1** shows a rapid decrease in η^* at approximately 100 °C, whereas **DA1-A2** shows a more gradual decrease. The drop in η^* coincides with a peak in $\tan \delta$ and relates to the T_{rDA} . As the rDA reaction occurs, the cycloadducts dissociate to liberate the respective FA- and HEMI-

terminated prepolymers which results in a decrease in molecular weight and therefore a subsequent decrease in η^* . While **DA1-A1** reaches the target η^* of $10 \text{ Pa}\cdot\text{s}^{-1}$ at $163 \text{ }^\circ\text{C}$, **DA1-A2** does not, but does at least obtain a reasonable minimum η^* of $17.5 \text{ Pa}\cdot\text{s}^{-1}$ within the temperature range measured.

DA4-A1 and **DA4-A2** also display a temperature dependent melt η^* (**Figure 5.6(b)**). The initial decrease in η^* at approximately $80 \text{ }^\circ\text{C}$ is on account of the melting of **Dynacoll 7490** crystals. Above this temperature, both copolymers show a dramatic decrease in η^* due to the onset of T_{rDA} . Importantly, both **DA4-A1** and **DA4-A2** achieve very low melt η^* within the temperature range studied and reach the target η^* at $143 \text{ }^\circ\text{C}$. Therefore, all copolymers display a good physical response to thermal stimulus which is extremely encouraging for the application and removal of an adhesive at material end-of-life.

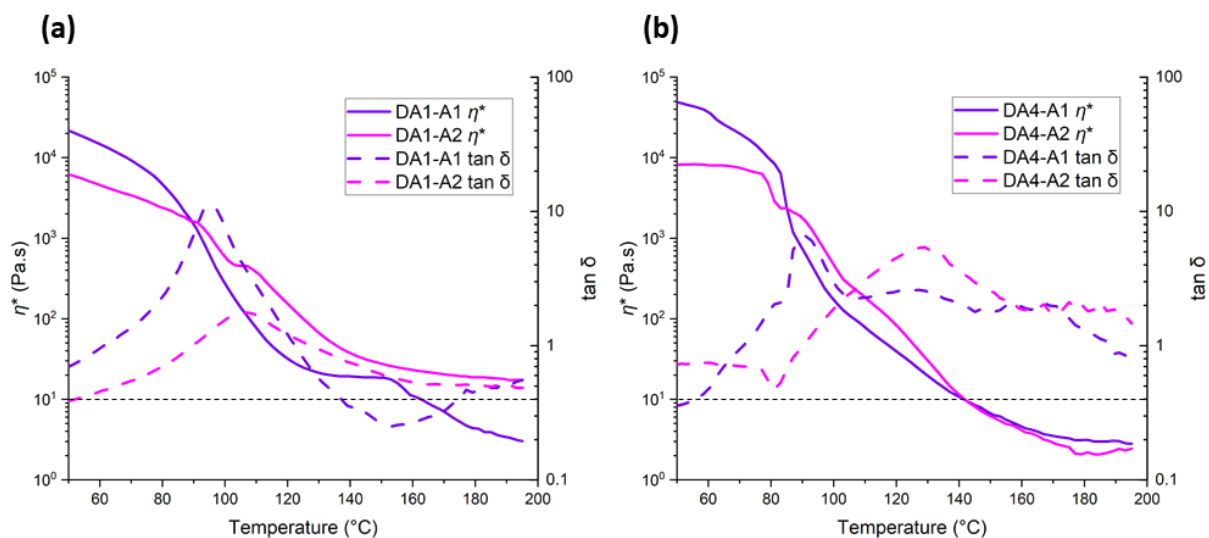


Figure 5.6 Rheological temperature sweeps of (a) **DA1-A1** and **DA1-A2** and (b) **DA4-A1** and **DA4-A2**. Dashed black horizontal line marks the target viscosity.

5.2.5 Mechanical properties

The mechanical properties of **DAX-AX** were determined by performing tensile tests on 300 μm film dog bone samples with comparison to the reference copolymer analogues **DAX** and **DAAX** from the previous chapter, comprising either semi-crystalline or amorphous polyols.

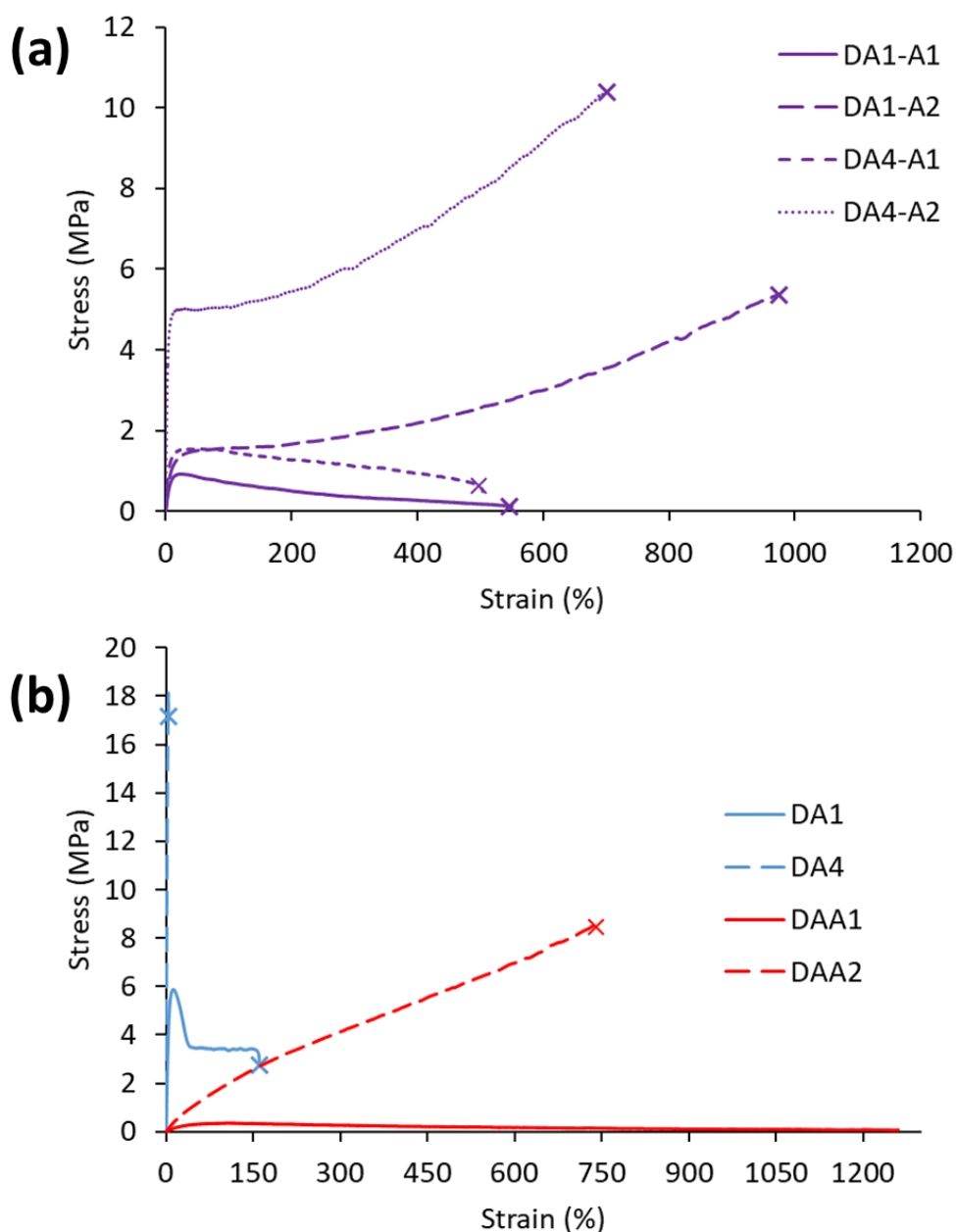


Figure 5.7 Stress-strain curves from tensile testing on (a) four **DAX-AX** copolymers comprising both semi-crystalline and amorphous segments and (b) four reference copolymers **DAX** and **DAAX** from the previous chapter comprising either semi-crystalline or amorphous segments. X marks sample failure by breaking.

The stress-strain curve of **DA1-A1** initially displays a positive linear relationship between stress and strain with small amounts of strain ($\leq 10\%$) (**Figure 5.7(a)**). This relationship is observed in the semi-crystalline reference **DA1**, but not the amorphous **DAA1**, which demonstrates how crystallinity grants strength to the material (**Figure 5.7(b)**). At strains $\leq 10\%$, stress gradually decreases with increasing strain, displaying a ϵ_{\max} of 590 ± 90 MPa which is gifted by the amorphous component, seen in the curve of **DAA1**. Therefore, the combination of semi-crystalline and amorphous polyols produces a TPU material with enhanced flexibility and strength relative to the separate semi-crystalline and amorphous copolymers, respectively. However, both E (11 ± 2 MPa) and σ_{\max} (0.9 ± 0.1 MPa) for **DA1-A1** are an order of magnitude lower than recorded for **DA1** itself (121 ± 12 MPa and 5.9 ± 0.1 MPa, respectively) (**Table 5.6**). Therefore, dilution of the semi-crystalline polyol with an amorphous polyol clearly reduces the strength of the material. Likewise, ϵ_{\max} of **DA1-A1** ($590 \pm 90\%$) is significantly reduced relative to the amorphous reference **DAA1** ($1270 \pm 10\%$) which in fact did not break within the experiment. Considering these results, it can be deduced that **DA1-A1** is a relatively soft material with impressive elongation and moderate toughness (255 ± 55 MPa). With these results in mind, the mechanical properties of the copolymer **DA1-A1** are clearly a hybrid of the respective separate semi-crystalline and amorphous copolymers. **DA4-A1** displays a similar stress-strain curve to **DA1-A1**, but with some differences due to the type of semi-crystalline polyol.

The stress-strain curve of **DA1-A2** also displays a linear positive relationship between stress and strain at low levels of strain (**Figure 5.7(a)**). However, with increasing strain, stress gradually increases on account of strain-hardening.¹⁹ The stress-strain curve of the reference amorphous copolymer **DAA2** displays strain-hardening so this behaviour is known to be a

contribution of the specific material **Priplast 1838 (Figure 5.7(b))**. The combination of strain-hardening, moderate stress and high elongation at break makes **DA1-A2** a very tough material (2655 ± 455 MPa).

Table 5.6 Mechanical properties data of **DAX-AX** from tensile testing compared to reference **DAX** and **DAAX** reported in the previous chapter.

Copolymer	E^a (MPa)	σ_{\max}^b (MPa)	U_T^c (MPa)	ϵ_{\max}^d (%)
DA1-A1	11 ± 2	0.9 ± 0.1	255 ± 55	590 ± 90
DA1-A2	16 ± 4	5.1 ± 0.6	2655 ± 455	980 ± 110
DA4-A1	31 ± 8	1.6 ± 0.4	580 ± 220	505 ± 85
DA4-A2	116 ± 6	10.7 ± 0.5	4595 ± 370	700 ± 35
DA1	121 ± 12	$5.9 \pm \leq 0.1$	640 ± 55	165 ± 5
DA4	588 ± 35	17.9 ± 1.0	50 ± 5	$5 \pm \leq 1$
DAA1	$1 \pm \leq 1$	$0.3 \pm \leq 0.1$	230 ± 10	1270 ± 10^e
DAA2	$4 \pm \leq 1$	8.5 ± 0.7	3465 ± 420	740 ± 40

^a Young's modulus is calculated from the initial gradient before the Yield point.

^b Ultimate tensile strength is the maximum recorded stress the sample can withstand before failure.

^c Modulus of toughness is measured as the area under the curve and represents the total energy a material can withstand without breaking.

^d Elongation at break is the strain (%) at which the sample breaks.

^e Sample did not break

Finally, the stress-strain curve of **DA4-A2** is qualitatively similar to that of **DA1-A2 (Figure 5.7(a))**. However, **DA4-A2** records extremely impressive and consistent mechanical performance in all aspects measured. In fact, **DA4-A2** has the highest E (116 ± 6 MPa) of all **DAX-AX** and displays strength comparable to semi-crystalline **DA1** (121 ± 12 MPa). Interestingly, the U_T of **DA4-A2** is higher than any other copolymer measured in this work at value of 4595 ± 370 MPa, arising from the synergy of the copolymerisation of very stiff semi-crystalline segments and the very flexible amorphous segments. These results indicate that **DA4-A2** is an outstanding material with very diverse and promising mechanical properties and its morphology should be investigated further in the future.

The range of mechanical properties achieved with these eight copolymers indicates a way of achieving a wide library of mechanical performance through fine tuning TPU composition.

The adhesive properties were determined by performing lap shear testing on beechwood substrates adhered to one another with 250 μm films of each copolymer. Samples were prepared by heating for a short time to allow for surface wetting, followed by copolymerisation at ambient temperatures for at least two weeks. Bond strengths for **DA1-A1**, **DA1-A2** and **DA4-A1** are relatively low, recording 1.5 ± 0.2 , 2.1 ± 1.4 and 1.2 ± 0.2 MPa, respectively. These bond strengths are either equal to or lower than the reference amorphous **DAAX** copolymers and all lower than the semi-crystalline **DAX** copolymers (**Figure 5.8**). In contrast, **DA4-A2** provides high bond strength on beechwood (5.6 ± 0.3 MPa) which is an intermediate bond strength of the reference semi-crystalline **DA4** and amorphous **DAA2** copolymers. Again, these results present **DA4-A2** as a very promising material, one that is flexible, strong and shows good adhesion.

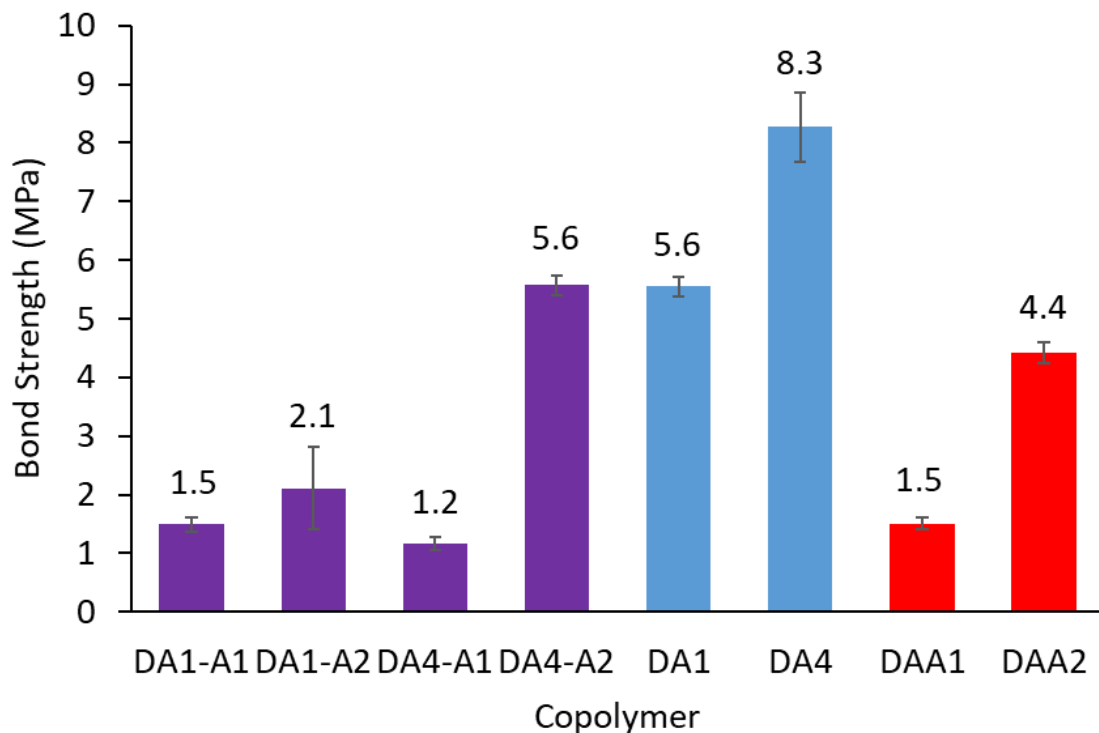


Figure 5.8 Adhesion testing on beechwood substrates for **DAX-AX** comprising both semi-crystalline and amorphous segments with reference to semi-crystalline **DAX** and amorphous **DAAX** copolymers.

5.2.6 Determination of reversibility via Diels-Alder chemistry

The ability to form DA cycloadducts within linear TPU copolymers along with reversal of the cycloadducts back to its respective precursors has been proven *via* various techniques and discussed in detail above. The ability to then reform the cycloadducts proving these **DAX-AX** materials comprising both semi-crystalline and amorphous segments are fully dynamic is now investigated.

Each fully cured copolymer was heated at 150 °C for 1 hour to dissociate the DA cycloadducts and reform the FA- and HEMI-terminated prepolymers. A film was then coated and left under ambient conditions to allow the prepolymers to copolymerise with time. Samples were taken from each material at set intervals and analysed to determine whether reformation of the DA cycloadducts had been successful.

The change in molecular weight was monitored over 28 days after application from the melt *via* SEC (**Table 4.5**). The molecular weight of the prepolymers for each **DAX-AX** was also measured. The average of these prepolymer molecular weights is taken as the theoretical molecular weight for a copolymer that has fully dissociated *via* the rDA reaction and is labelled as **PPX**. When taken straight from the melt, all **DAX-AX** copolymers record a M_n comparable to each respective **PPX** which indicates successful reversal of the DA cycloadducts to the prepolymer stage to cause a decrease in molecular weight. Within 7 days at ambient temperatures there is an increase in molecular weight of **DAX-AX** as copolymerisation occurs *via* DA cycloadduct formation (**Figure 5.9**). After more than 7 days under ambient conditions, molecular weight plateaus as an equilibrium is established between the associative and dissociative DA reactions which occur at the same rate. It is worth noting that **DA4-A2** records

the highest M_n after 28 days after melt application, which could contribute towards the superior mechanical properties displayed by this copolymer.

Table 5.7 Time dependent M_n values for **DAX-AX** at ambient temperature. **PPX** were only measured once and not as a function of time.

Material	M_n with days after melt application (kDa) ^{a, b}								Equilibrated M_n (kDa)
	0	1	2	3	4	7	14	28	
DA1-A1	6.5	8.3	10.5	11.1	12.1	12.5	13.9	14.2	13.5
PP1	6.2 ^c	-	-	-	-	-	-	-	-
DA1-A2	7.1	9.3	12.0	12.1	12.3	12.5	13.6	13.8	13.3
PP2	9.0 ^c	-	-	-	-	-	-	-	-
DA4-A1	6.5	8.7	12.5	13.2	13.8	13.9	17.7	13.7	15.1
PP3	9.2	-	-	-	-	-	-	-	-
DA4-A2	7.7	10.4	16.1	18.9	20.9	20.6	23.0	23.3	22.3
PP4	12.0	-	-	-	-	-	-	-	-

^a Average M_n of **PPHX** and **PPFX** prepolymers

^b Determined by SEC in $CHCl_3$ against PMMA standards

^c Measured as the average of 7, 14 and 28 days

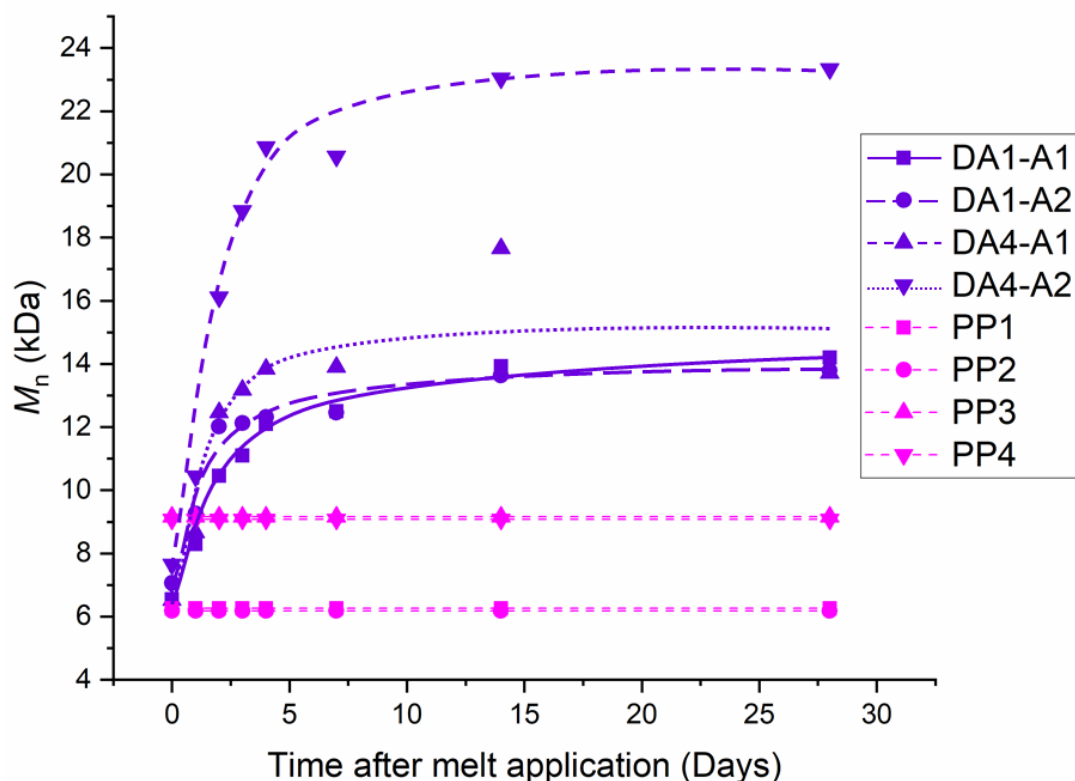


Figure 5.9 Variation of M_n with time after melt application of **DAX-AX**. Average prepolymer M_n are labelled as **PPX**. Determined by SEC in $CHCl_3$ against PMMA standards.

FTIR spectroscopy was used to monitor the reformation of DA cycloadduct. The intensity of the absorbance at $\nu_{\text{max}} = 696 \text{ cm}^{-1}$ which corresponds to free maleimide was measured with time. All copolymers display a dramatic decrease in intensity within the first seven days (**Figure 5.10(a) & (b)**). This reduction shows consumption of the free maleimide and therefore infers formation of the DA cycloadducts. Similar to results observed *via* SEC, after the first 7 days a plateau is reached which indicates an equilibrium has been established between cycloadduct and FA- and HEMI-terminated precursors with association and dissociation occurring at the same rate. Copolymers containing **Capa 2200 (DA1-AX)** show greater consumption of free maleimide than those containing **Dynacoll 7490 (DAB4-AX)**. This difference implies **Dynacoll 7490** segments somewhat hinder the formation of the DA cycloadducts which could be a result of the higher degree of crystallinity restricting chain movement and therefore potential cycloadduct association.²⁰ Additionally, copolymers containing **Dynacoll 7490** have a significantly higher T_m which is much higher than ambient temperature used for cycloadduct formation. Interestingly, **DA4-AX** records approximately 25 % free maleimide after 28 days, whereas the semi-crystalline reference material **DA4** (reported in Chapter 4) records approximately 45 % free maleimide. This increase in free maleimide consumption suggests that the presence of the amorphous component is assisting cycloaddition in **DA4-AX** copolymers, likely a consequence of lower crystalline **Dynacoll 7490** content.

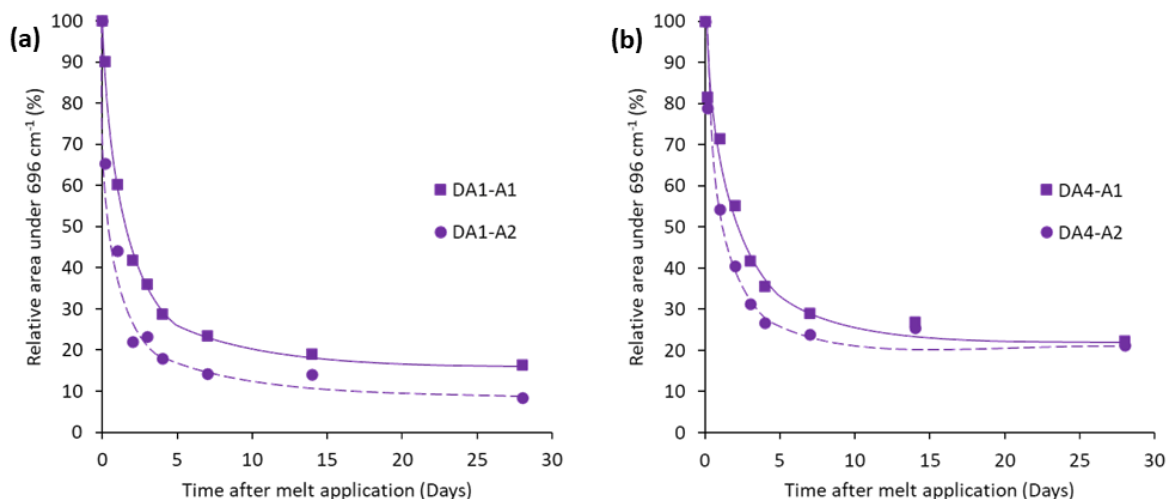


Figure 5.10 Change in intensity of absorbance at $\nu_{max} = 696 \text{ cm}^{-1}$ with time after melt application for (a) DA1-A1 and DA1-A2 and (b) DA4-A1 and DA4-A2 copolymers.

The reformation of DA cycloadducts after melt application was also determined *via* DSC (Table 5.8). Initially after melting, ΔH_{rDA} is low which shows there is little DA cycloadduct present. As the material is left with time, the ΔH_{rDA} increases due to copolymerisation, which reaches a plateau after 7 days (Figure 5.11). Copolymers containing Capa 2200 (DA1-AX) show a greater amount of DA cycloadduct than those made with Dynacoll 7490 (DA4-AX) as a consequence of the higher molecular weight of Dynacoll 7490 (Dynacoll 7490 = 3.5 kDa, Capa 2200 = 2.0 kDa) which decreases functional group concentration.

Table 5.8 Thermal data of **DA1-A1**, **DA1-A2**, **DA4-A1** & **DA4-A2** obtained via DSC over 28 days.

Copolymer	Time after melt application (days)	T_g (°C)	$T_{m(pol)}$ (°C)	$\Delta H_{m(pol)}$ (J.g ⁻¹)	T_{rDA} (°C)	ΔH_{rDA} (J.g ⁻¹)
DA1-A1	0	-19	-	-	146	3.7
	0.5	-23	-	-	147	4.3
	7	-19	43	0.7	116 & 146	9.7
	14	-16	43	5.4	116 & 149	9.8
	28	-17	43	5.0	116 & 147	11.7
DA1-A2	0	-44	-	-	146	4.3
	0.5	-44	-	-	117 & 146	7.6
	7	-45	43	0.1	115 & 146	9.0
	14	-46	43	0.7	115 & 147	8.3
	28	-45	45	7.2	117 & 146	9.1
DA4-A1	0	-11	78 & 83	24.4	147	1.7
	0.5	-14	77 & 82	23.6	145	4.6
	7	-10	78 & 82	21.4	117 & 145	6.5
	14	-12	78 & 82	22.8	117 & 146	6.6
	28	-11	78 & 82	22.4	116 & 142	6.5
DA4-A2	0	-43	74 & 77	23.2	146	3.1
	0.5	-44	81	26.5	146	5.3
	7	-44	81	23.4	119 & 145	5.5
	14	-46	80	26.3	117 & 142	6.2
	28	-45	81	23.4	118 & 144	5.7

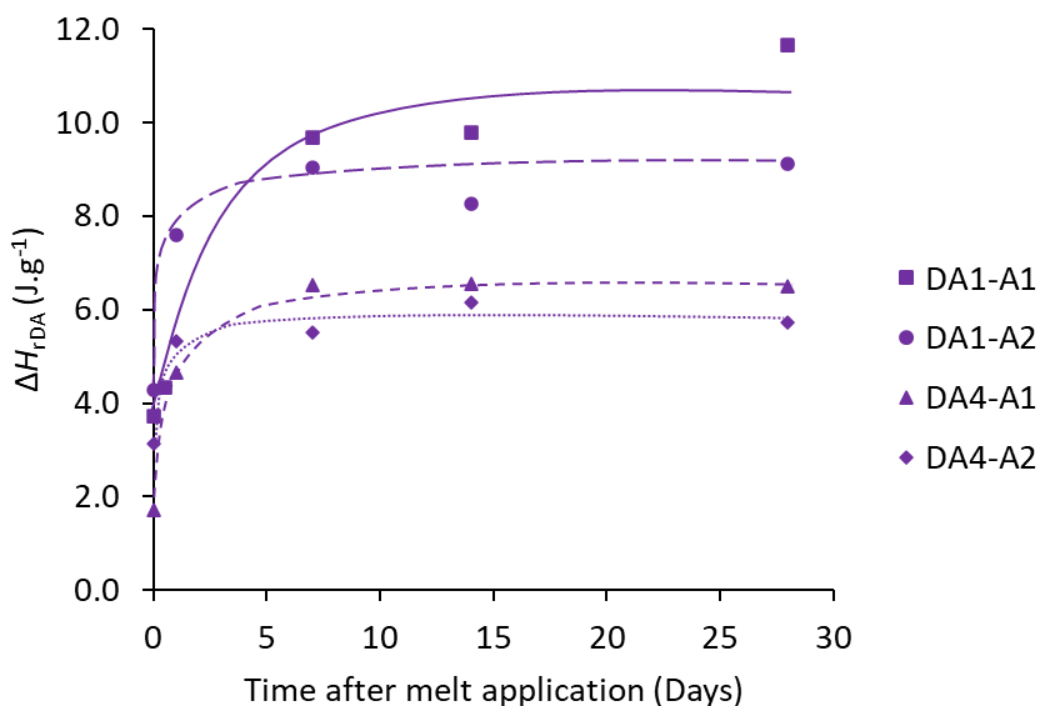


Figure 5.11 Change in ΔH_{rDA} with time after melt application for **DAX-AX** measured via DSC at a heating rate of 10 °C.min⁻¹.

Finally, the effect of time on copolymer crystallinity was monitored over 28 days. **DA1-A1** appears completely amorphous immediately after melting (*Figure 5.12(a)*). A very small melting endotherm (0.7 J.g^{-1}) is detected at $43 \text{ }^\circ\text{C}$ after 7 days and a more substantial melting transition is recorded after 14 days (5.4 J.g^{-1}) which remains constant after 28 days. The delayed crystallisation kinetics indicates that crystallisation of **Capa 2200** segments is greatly suppressed and up to 14 days are required to establish an equilibrium for crystal formation.

Remarkably, the thermograms of **DA1-A2** show an almost amorphous material until 28 days, which indicates the crystallinity of **Capa 2200** is extremely suppressed by covalent attachment with the amorphous **Priplast 1838** polyol segments (*Figure 5.12(b)*). Very small levels of crystallinity are detected after 7 and 14 days, but the $\Delta H_{m(\text{pol})}$ does not exceed 0.7 J.g^{-1} . The melting endotherms of both **DA1-A1** and **DA1-A2** are narrow for all recorded melting endotherms which indicates homogeneous crystals are formed directly.

DA4-A1 displays a significant melting endotherm (24.4 J.g^{-1}) at 78 and $83 \text{ }^\circ\text{C}$, immediately after melt application as a result of the rapid crystallisation kinetics of **Dynacoll 7490**. The ΔH_m remains constant with time, which demonstrates that crystallinity occurs instantaneously within the copolymer. As the endotherm is dual-peaked, it suggests multiple degrees of crystallinity. Initially, the higher temperature peak at $83 \text{ }^\circ\text{C}$ is the dominant melt, but with time, the lower temperature peak at $78 \text{ }^\circ\text{C}$ increases in intensity. As the enthalpy remains constant, rather than a build in amount of crystallinity, it suggests a change in arrangement of crystallinity occurs with time.

Thermograms of **DA4-A2** also display melting endotherms associated with polyol crystallinity instantly from melt application, remaining constant throughout the duration of the experiment. This result presents **DA4-A2** as a potentially fast setting adhesive. As with **DA4-**

A1, DA4-A2 shows a dual-peaked melt endotherm where initially the higher temperature peak at 77 °C dominates. Again, with increasing time after melt application, the lower temperature peak melt at 74 °C seems to grow in intensity so that after 28 days, **DA4-A2** displays a slightly broader melting endotherm. This change indicates a gradual rearrangement of **Dynacoll 7490** crystal formation.

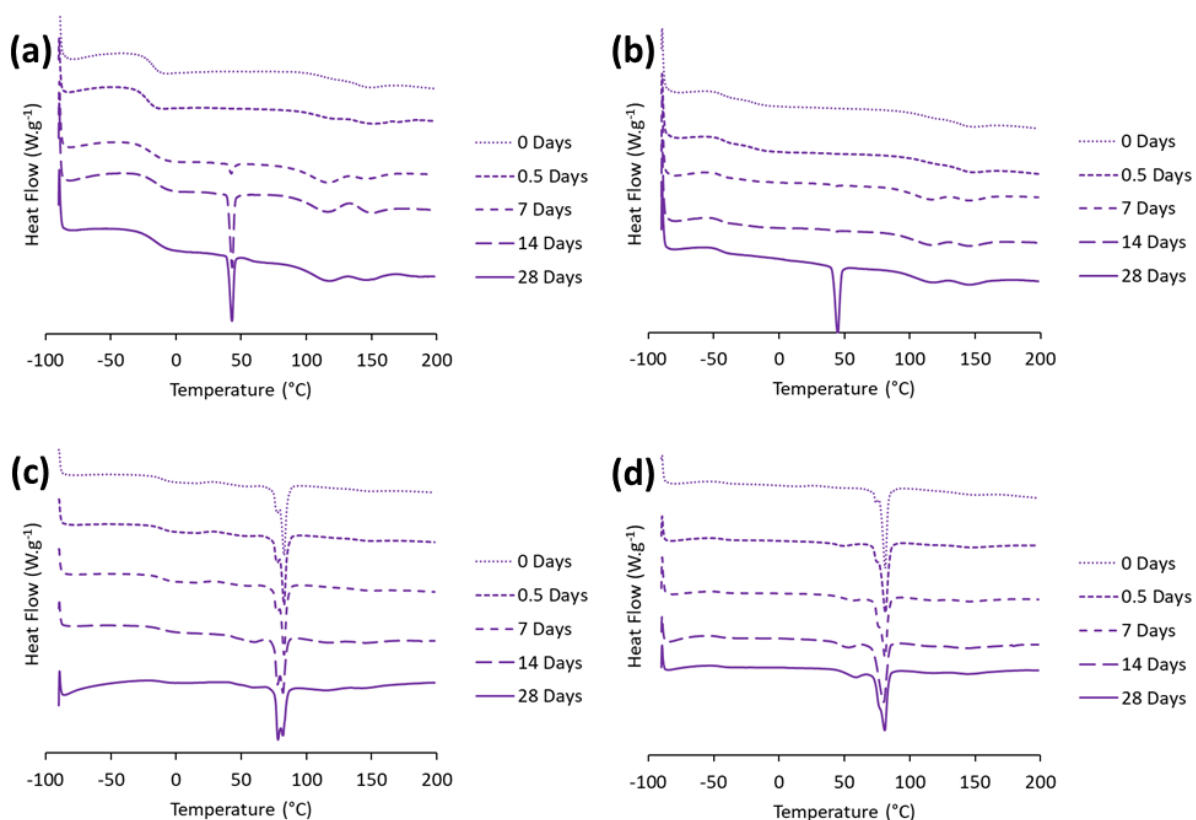


Figure 5.12 DSC thermograms showing crystallinity of (a) DA1-A1, (b) DA1-A2, (c) DA4-A1 and (d) DA4-A2 as a function of time after melt application. First heat cycle used at a heating rate of 10 °C.min⁻¹. Exo up.

The data above shows how the crystallisation of the backbone in **Capa 2200** is greatly influenced by the covalent attachment with an amorphous segment, whereas **Dynacoll 7490** is not. Perhaps this difference is a consequence of greater interactions between the lower molecular weight **Capa 2200** with the amorphous segments than the higher molecular weight

Dynacoll 7490 segments which possibly associate together. However, further studies of the microstructure of each material are required for confirmation.

5.3 Conclusions

The aim of this work was to design a phase separated linear TPU without chain extender by blending semi-crystalline and amorphous polyols together to afford a copolymer with distinct HS (crystalline) and SS (amorphous). The reason for this aim is to overcome the issue of high melt viscosity associated with HS formation in traditional linear TPUs containing chain extender. Reversible DA chemistry was incorporated to improve disparity between solid and molten states.

An initial study was conducted to determine the compatibility of four semi-crystalline polyols with four different amorphous polyols *via* visual inspection and DSC analysis. Criteria were defined to identify pairs of semi-crystalline and amorphous polyols that would have potential for further study as phase separated TPUs without chain extender. The blend must have a $T_m \geq 70$ °C and $\Delta H_m \leq 50$ % of undiluted semi-crystalline polyol, to have a reasonable upper service temperature range and compatibility. Only two combinations fulfilled these criteria: **Dynacoll 7490** with **Capa 8025** and **Dynacoll 7490** with **Priplast 1838**. It was also decided that **Capa 2200** combined with **Capa 8025** and **Priplast 1838** would be analysed as reference copolymers.

Linear TPU copolymers comprising of a blend of semi-crystalline and amorphous polyols were synthesised *via* a stepwise reaction pathway. In the final step, three FA- and HEMI-terminated prepolymers were blended in the melt then copolymerised at ambient temperatures to afford a final TPU copolymer containing DA chemistry (**DAX-AX**). Properties of **DAX-AX** were compared to that of unblended analogues based on semi-crystalline (**DA1** & **4**) and

amorphous polyols (**DAA1 & 2**). FTIR analysis of the carbonyl group regions revealed that **DAX-AX** contained ester, urethane and imide carbonyl groups. DSC analysis of both **DAX-AX** and the non-covalently attached polyol blends (**X-AX**) showed how covalent attachment improves polyol compatibility. All **DAX-AX** contain crystallinity which fulfils the aim of forming phase separated TPUs without chain extension. **DAX-AX** containing **Dynacoll 7490** display larger amounts of crystallinity relative to those containing **Capa 2200** suggesting greater stiffness and strength. A T_{rDA} is also detected as a double peaked endotherm in all **DAX-AX** materials. ΔH_{rDA} is an intermediate of reference copolymers **DAX** (semi-crystalline) and **DAAX** (amorphous), therefore **DA1-A1** and **DA4-A2** reported the highest and lowest ΔH_{rDA} , respectively. DMA presents how the amorphous component dictates both low (≤ 5 °C) and very high (≥ 80 °C) temperature properties of **DAX-AX** with those containing **Priplast 1838** likely to have favourable low temperature properties. On the other hand, the semi-crystalline component controls properties in the intermediate temperature range (5 – 80 °C). In most cases, E' of **DAX-AX** is higher and lower by an order of magnitude relative to reference **DAAX** and **DAX**, respectively, to give intermediate physical properties at ambient temperature. Due to the combination of several factors, **DA4-A2** displays very impressive properties over a wide service temperature range. As properties are a contribution of both the parent polyols, it implies that it is possible to design **DAX-AX** with specific thermal properties by fine tuning constituent polyols. Rheological temperature sweeps showed that copolymers decrease significantly in η^* at approximately 100 °C as a consequence of the drop in molecular weight triggered by the onset of the rDA reaction. **DA1-A1**, **DA4-A1** and **DA4-A2** all reach the target η^* (10 Pa.s⁻¹) within the temperature range measured, whereas **DA1-A2** does not, but still does manage to achieve a reasonable η^* by 200 °C. These results showing good sensitivity of

physical state to temperature are very promising with respect to application and removal of adhesives at end-of-life.

Tensile testing was used to determine the mechanical properties of the copolymers. At low strains (< 10 %), **DAX-AX** parallels properties of **DAX**, whereas as strain increases, the stress-strain curves resemble that of **DAAX**. Again, intermediate properties are observed which opens up potential of fine tuning for desired mechanical performance. While **DAX-AX** containing **Capa 8025 (DA1-A1 & DA4-A1)** are relatively weak materials, those containing **Priplast 1838 (DA1-A2 & DA4-A2)** display impressive mechanical properties due to strain-hardening. **DA4-A2** shows remarkable mechanical performance, both strong (high E and σ_{\max}) and flexible (high ϵ_{\max}) to result in a very tough material ($U_T = 4595 \pm 370$ MPa). The adhesive properties of **DAX-AX** were generally worse than both **DAX** and **DAAX** reference materials. However, **DA4-A2** recorded good bond strength with beechwood substrates and so has the greatest potential for adhesive applications, potentially where both strength and flexibility are important.

The DA cycloadducts were proven to be fully reversible and able to not only reform the FA- and HEMI-terminated prepolymers with heating, but also reassociate back to the cycloadduct with time under ambient conditions. **DAX-AX** display dynamic molecular weights *via* SEC, being able to return to prepolymer molecular weight with heating and then rebuild after time at ambient temperatures. Reformation of DA cycloadducts was also observed *via* FTIR spectroscopy and DSC analysis and was determined to occur within 7 days since melt application, independent of polyol combinations. DSC was also used to highlight the influence of time on polyol crystallinity. The crystallinity of **Capa 2200** was heavily suppressed by covalent attachment of **Capa 8025** and **Priplast 1838**, requiring up to 14 and 28 days for the crystallinity

to equilibrate, respectively. On the other hand, **Dynacoll 7490** demonstrated instantaneous crystal formation from melt application, which presents **DA4-A2** as a potentially fast curing adhesive.

Overall, the results observed indicate the potential to form linear TPUs including DA chemistry with highly tuned thermal and mechanical properties by careful selection of polyols blends. In the future, choices could be made from a library of benign prepolymers for specific applications.

5.4 Experimental

5.4.1 Materials

Capa™ 2200J and Capa™ 8025 were provided from Ingevity. Dynacoll® 7360, Dynacoll® 7380 and Dynacoll® 7490 were provided from Evonik Industries. Priplast™ 1838, Priplast™ 3197 and Priplast™ 3238 were provided by Croda International. 4,4'-methylenebis (phenyl isocyanate) (98 %), furfuryl alcohol and chloroform-d (99.8 atom % D) were purchased from Sigma-Aldrich. 2-Hydroxyl ethyl maleimide was provided by Henkel Corporation. All reagents were used as received.

5.4.2 Instrumental methods

Proton (¹H) nuclear magnetic resonance (NMR) spectra were recorded using a Bruker Avance 400 spectrometer (400 MHz). Spectra were analysed on MestReNova v6.0.2. Samples were prepared in CDCl₃ as the solvent. All chemical shifts were recorded in parts per million (ppm) relative to a reference peak of chloroform solvent at $\delta = 7.26$ ppm. **Molecular weights and dispersities** were determined *via* size-exclusion chromatography (SEC) using an Agilent 1260 Infinity GPC system equipped with a refractive index detector. Two Agilent PL-gel 5 μ m Mixed-C columns and a guard column were connected in series and maintained at 35 °C. HPLC grade

chloroform containing 0.25 % v/v NEt_3 was used as the eluent and the flow rate was set at 1.0 mL.min⁻¹. The refractive index detector was used for calculation of molecular weights and dispersities by calibration using a series of near-monodisperse poly(methyl methacrylate) standards. Analysis was performed on Agilent SEC software. **Attenuated Total Reflectance Fourier Transform Infrared (ATR-FTIR)** spectra was collected on a PerkinElmer Spectrum Two instrument with a UATR Two accessory. Analysis was performed on PerkinElmer Spectrum software. **Differential scanning calorimetry (DSC)** was performed on a Discovery DSC 25 TA instrument. All experiments were carried out under a nitrogen atmosphere and with a heating rate of 10 °C.min⁻¹. Pre-weighed samples of 2 ± 1 mg were loaded at 25 °C, cooled to -90 °C and heated to 200 °C. T_g was taken as the midpoint of inflexion and T_m and T_{rDA} were measured as the temperature at the minimum heat flow of the appropriate endotherms. For time dependent measurements, samples for 0 Days measurements were loaded at 25 °C, heated to 150 °C, held for 1 hour, cooled to -90 °C then heated to 200 °C at a rate of 10 °C.min⁻¹. Analysis was performed on TRIOS v5.1.1 software. **Dynamic Mechanical Analysis (DMA)** was performed on TA Instruments Q800 Dynamic Mechanical Analyser with an ACS-3 (Refrigerated Chiller System). Samples of approximately 40 × 5 × 1 mm were loaded at room temperature and clamped lightly (finger tight). A sample length of 10 mm was used for all measurements. For each measurement, the sample was first cooled to -80 °C and held at this temperature for a minimum of 5 minutes to fully equilibrate. The furnace was then opened and the sample clamped to a pressure of 4.5 psi using a small torque wrench. After clamping, the furnace was then immediately closed and temperature re-equilibration established at -80 °C. The method was then started. The thermal method used is: Motor Drive Off, Data Storage Off, equilibrate at -80 °C, isotherm 5 minutes, Motor Drive ON, Data Storage ON, ramp 3 °C.min⁻¹ to 100 °C. The measurement parameters used were as follows: strain applied (0.05

%), force track (110 %), initial sample length (10 mm) with deformation frequency (1 Hz) fixed. Sample dimensions were calculated as follows: width was measured using digital callipers at three positions along the sample (End 1, Middle, End 2). Thickness was measured using digital callipers at three positions along the sample (End 1, Middle, End 2). Average values calculated and used. The software used was TA Instruments Advantage Control Software and data analysis was performed on TA Instruments Universal Analysis Data Analysis Program.

Rheological temperature sweeps were performed on an Anton Paar MCR502 with a 25 mm disposable geometry and a disposable bottom plate fixture. Tests were run in oscillatory mode at a fixed amplitude (1 %) and angular frequency (1 rad.s^{-1}) from 50 – 200 °C. Sample sizes were approximately 25.0 mm diameter discs of 0.8 mm height. **Tensile tests** were run on films approximately 300 μm thick, according to ISO 527-2 type 5B on a Zwickline tensometer. The general procedure is as follows: dimensions of dog bone measured with digital calliper and noted on the system. The zero gap is set within Zwick software so the gauge length is known. The sample is then securely clamped and the absolute cross head length is reset. The force is then zeroed. The test is run at a speed of 10 mm.min^{-1} until the sample fails. Results analysed on TestXpert II software. **Adhesion lap shear tests** were performed on cured films 250 μm thick that were cut to 25 × 25 mm. Lap shear joints were assembled by carefully applying the film between beechwood test pieces using an overlap of 25 mm and a width of 25 mm, applying light pressure. The materials were placed in an oven for 20 minutes at 150 °C to melt the copolymers. Bonded samples were then allowed to cure for 14 days at ambient conditions before measurement. The lap shear strength was determined from an average of four bonded samples using an Instron tensiometer with a load cell of 30 kN and a displacement speed of 1.27 mm.min^{-1} .

5.4.3 *Sample preparation*

Rheology discs of 25.0 × 0.8 mm were prepared with a MeltPrep vacuum compression mould. Copolymers (approx. 0.40 mg) were separately melted in the chamber at 70, 120 and 150 °C, respectively. Melting was followed by approximately 10 seconds of pressure (0.1 mbar). Vacuum was removed and materials were then cooled with compressed air and allowed to solidify before being removed from the chamber. **DMA bars** were prepared in a similar way as the rheology discs. However, a 10 x 40 mm insert and chamber were used instead of cylindrical versions. Once solidified, samples were cut down the middle lengthwise to give two bars of 0.5 x 40 mm. **Tensile testing dog bones** were prepared as follows. First, film samples (300 µm) were made by coating out molten material (1 hour at 150 °C) with a 500 µm coating block on release paper. After films were allowed to solidify, dog bone shapes were cut out using a ZwickRoell knee manual cutting press ZCP 020 with cutting device for ISO 527-2 type 5B die attachment. **Adhesion films** were prepared by heating some material in an oven at 150 °C for approximately 20 minutes, after which a film was drawn with a coating block with an approximate thickness of 250 µm. Once solid enough, squares of 25 x 25 mm were then cut out of the film for use in the lap shear sample preparation.

5.4.4 *Preparation of blended polyols without covalent attachment (X-AX)*

All blends of polyols were prepared by the same method, a typical procedure is as follows: **Capa 2200** (16.67 g) was added to a jar containing **Capa 8025** (33.33 g) and placed in an oven for 3 hours at 120 °C. The mixture was stirred manually after 1 and 2 hours. Visual inspection of polyol compatibility was carried out immediately after 3 hours while both polyols were in the molten phase.

5.4.5 Synthesis of furfuryl-terminated prepolymers (PPFX)

All furfuryl-terminated prepolymers were synthesised in a similar method, a typical procedure is as follows: **Capa 2200** (77.96 g, 0.039 mol) was loaded into a 250 mL flange flask, equipped with an overhead mechanical stirrer, gas inlet and digital thermometer. Vacuum was applied for 1 hour at 87 °C and a stirring rate of 90 rpm. Vacuum was removed and **MDI** (19.69 g, 0.079 mol) was added at 110 °C which initially decreased the mixture temperature to 90 °C followed by a subsequent exotherm to 111 °C. Immediately after **MDI** addition, the stirring rate was increased to 180 rpm and the vacuum was reapplied after 15 minutes. Vacuum was again removed after 1 hour, **FA** (8.52 g, 0.087 mol) was added at 111 °C which decreased the reaction temperature to 105 °C. A reflux condenser was added and the vacuum was not reapplied (exotherm to 110 °C). After a further 1 hour 30 minutes, further **FA** (0.82 g, 0.008 mol) was added at 111 °C. After another 2 hours, there was minimal NCO absorbance detected *via* FTIR spectroscopy so the reaction was switched off and the mixture was decanted while hot. The resulting material was put under vacuum at 40 °C for a total of 48 hours to remove any residual free **FA** (determined *via* ¹H NMR spectroscopy).

PPF1: SEC (CHCl₃): $M_n = 6.3$ kDa, $M_w = 12.6$ kDa, $D_M = 1.94$.

¹H NMR (400 MHz, 298 K, CDCl₃): $\delta = 7.46$ (s, CH=CHO (FA)), 7.30 (m, Ar), 7.12 (d, $J = 7.8$ Hz, Ar), 6.69 (s, NH), 6.60 (s, NH), 6.47 (d, $J = 2.9$ Hz, CHCH=CHO (FA)), 6.40 (s, CCHCH (FA)), 5.16 (s, OCHC (FA)), 4.17 (t, $^3J_{H-H} = 6.4$ Hz, CH₂OC=O), 4.08 (t, $^3J_{H-H} = 6.7$ Hz, CH₂OC=O), 4.00 (s, MDI CH₂Ar), 3.90 (s, NPG CH₂O), 2.33 (t, $^3J_{H-H} = 7.5$ Hz, CH₂C=OO), 1.00 (d, $J = 9.4$ Hz, NPG CH₃), 1.68 and 1.41 (all remaining hydrogens) ppm.

ATR-FTIR: $\nu_{MAX} = 3338$ (N-H), 2944 – 2865 (C-H), 1722 (C=O), 1597 (C-N), 1531 (Ar C=C), 1295 and 1163 (C-O) cm⁻¹.

PPF4: SEC (CHCl₃): $M_n = 15.2$ kDa, $M_w = 29.4$ kDa, $D_M = 1.93$.

¹H NMR (400 MHz, 298 K, CDCl₃): $\delta = 7.45$ (s, CH=CHO (FA)), 7.30 (m, Ar), 7.12 (m, Ar), 6.70 (m, NH), 6.63 (s, NH), 6.47 (d, $J = 3.2$ Hz, CHCH=CHO (FA)), 6.39 (m, CCHCH (FA)), 5.16 (s, OCHC (FA)), 4.37, 4.33, 4.31, 4.29, 4.08, 3.90, 2.34, 1.63 and 1.29 (DynaColl 7490) ppm.

ATR-FTIR: $\nu_{MAX} = 3343$ (N-H), 2917 – 2849 (C-H), 1735 (C=O), 1598 (C-N), 1534 (Ar C=C), 1308 and 1166 (C-O) cm⁻¹.

PPFA1: SEC (CHCl₃): $M_n = 6.3$ kDa, $M_w = 11.7$ kDa, $D_M = 1.85$.

¹H NMR (400 MHz, 298 K, CDCl₃): $\delta = 7.45$ (s, CH=CHO (FA)), 7.30 (m, Ar), 7.11 (d, $J = 8.3$ Hz Ar), 6.76 (s, NH), 6.69 (s, NH), 6.46 (d, $J = 3.2$ Hz, CHCH=CHO (FA-CL)), 6.38 (m, CCHCH (FA-CL)), 6.36 (m, CHCH=CHO (FA-LA)), 6.31 (d, $J = 3.1$ Hz, CCHCH (FA-LA)), 5.15 (s, OCHC (FA)), 5.19, 5.10, 4.16, 4.08, 3.89, 2.41, 2.31, 1.64, 1.58, 1.51, 1.40 and 0.99 (Capa 8025) ppm.

ATR-FTIR: $\nu_{MAX} = 3343$ (N-H), 2942 – 2866 (C-H), 1729 (C=O), 1598 (C-N), 1532 (Ar C=C), 1309 and 1160 (C-O) cm⁻¹.

PPFA2: SEC (CHCl₃): $M_n = 6.0$ kDa, $M_w = 14.2$ kDa, $D_M = 2.36$.

¹H NMR (400 MHz, 298 K, CDCl₃): $\delta = 7.46$ (s, CH=CHO (FA)), 7.30 (m, Ar), 7.12 (d, $J = 8.3$ Hz, Ar), 6.59 (m, NH), 6.48 (d, $J = 3.1$ Hz, CHCH=CHO (FA)), 6.40 (m, CCHCH (FA)), 5.17 (s, OCHC (FA)), 4.17, 4.08, 3.91, 2.31, 1.65, 1.40, 1.28 and 0.91 (Priplast 1838) ppm.

ATR-FTIR: $\nu_{MAX} = 3334$ (N-H), 2922 – 2853 (C-H), 1735 and 1701 (C=O), 1596 (C-N), 1534 (Ar C=C), 1312 and 1171 (C-O) cm⁻¹.

5.4.6 Synthesis of hydroxyethyl maleimide terminated prepolymers (**PPHX**)

All hydroxyethyl maleimide-terminated prepolymers were synthesised in a similar method, a typical procedure is as follows: **Capa 2200** (208.15 g, 0.11 mol) was loaded into a 500 mL flange flask, equipped with an overhead mechanical stirrer, gas inlet and digital thermometer. Vacuum was applied for 1 hour at 110 °C using a stirring rate of 90 rpm. Vacuum was removed and **MDI** (52.89 g, 0.21 mol) was added at 107 °C which decreased the mixture temperature to 100 °C with a subsequent exotherm to 110 °C. Immediately after **MDI** addition, the stirring rate was increased to 180 rpm and the vacuum was reapplied after 15 minutes. Vacuum was again removed after 1 hour, **HEMI** (33.18 g, 0.24 mol) was added at 110 °C which decreased the reaction temperature to 100 °C. A reflux condenser was added and the vacuum was not reapplied. Exotherm to 114 °C. After a further 1 hours 45 minutes, there was no NCO absorbance detected *via* FTIR spectroscopy so the reaction was switched off and the mixture was decanted while hot.

PPHA1: SEC (CHCl₃): $M_n = 6.0$ kDa, $M_w = 11.1$ kDa, $D_M = 1.85$.

¹H NMR (400 MHz, 298 K, CDCl₃): $\delta = 7.31$ (d, $J = 7.3$ Hz, Ar), 7.11 (d, $J = 6.7$ Hz, Ar), 6.76 (d, $J = 2.7$ Hz, C=OCHCH (HEMI)), 6.73 (s, C=OCHCH (HEMI)), 6.64 (s, NH), 6.59 (s, NH), 4.32 (t, ³J_{H-H} = 5.0 Hz, NCH₂CH₂O (HEMI)), 3.85 (t, ³J_{H-H} = 5.1 Hz, NCH₂CH₂O (HEMI)), 5.12, 4.17, 4.08, 3.97, 3.88, 3.81, 3.76, 2.41, 2.32, 1.65, 1.58, 1.53, 1.49, 1.40, 0.99 (Capa 8025) ppm.

ATR-FTIR: $\nu_{MAX} = 3344$ (N-H), 2942 – 2866 (C-H), 1729 and 1713 (C=O), 1598 (C-N), 1532 (Ar C=C), 1310 and 1160 (C-O) cm⁻¹.

PPHA2: SEC (CHCl₃): $M_n = 6.0$ kDa, $M_w = 13.8$ kDa, $D_M = 2.28$.

^1H NMR (400 MHz, 298 K, CDCl_3): δ = 7.31 (d, J = 8.1 Hz, Ar), 7.11 (d, J = 7.0 Hz, Ar), 6.76 (s, C=OCHCH (HEMI)), 6.74 (s, C=OCHCH (HEMI)), 6.63 (s, NH), 6.55 (s, NH), 4.33 (t, $^3J_{\text{H-H}}$ = 5.2 Hz, $\text{NCH}_2\text{CH}_2\text{O}$ (HEMI)), 3.86 (t, $^3J_{\text{H-H}}$ = 5.2 Hz, $\text{NCH}_2\text{CH}_2\text{O}$ (HEMI)), 4.17, 4.09, 3.90, 2.31, 1.64, 1.41, 1.29 and 0.89 (Priplast 1838) ppm.

ATR-FTIR: ν_{MAX} = 3348 (N-H), 2922 – 2853 (C-H), 1735 and 1707 (C=O), 1596 (C-N), 1533 (Ar C=C), 1312 and 1171 (C-O) cm^{-1} .

5.4.7 Synthesis of final linear TPU copolymers comprising a blend of semi-crystalline and amorphous polyols (**DAX-AX**)

All **DAX-AX** copolymers were synthesised in a similar method, a typical procedure is as follows: **PPF1** (20.10 g, 0.008 mol), **PPFA1** (30.68 g, 0.012 mol) and **PPHA1** (9.52 g, 0.007 mol) were loaded into a 250 mL flange flask, equipped with an overhead stirrer and gas inlet. The formulation was stirred under vacuum for 60 minutes to provide sufficient mixing of prepolymers and prevent the formation of bubbles. The mixture was decanted while hot and allowed to copolymerise under ambient conditions in a silicone dish until solid enough to be stored in polyethylene bag.

DA1-A1: SEC (CHCl_3): M_n = 13.5 kDa, M_w = 34.4 kDa, D_M = 2.52.

^1H NMR (400 MHz, 298 K, CDCl_3): δ = 7.30 (m, Ar), 7.11 (d, J = 7.7 Hz, Ar), 6.76 (d, J = 1.9 Hz, C(C)HCH=CH (DA)), 6.73 (s, C(C)HCH=CH (DA)), 6.56 (s, NH), 6.51 (s, NH), 5.31 (s, CH(O)(CH)(CH) (DA)), 3.02 (s, CH(CH)C=O (DA)), 2.90 (s, CH(CH)C=O (DA)), 5.12, 4.14, 4.08, 3.88, 3.81, 3.71, 2.41, 2.33, 1.66, 1.57, 1.53, 1.49, 1.40, 0.99 (Capa 2200 and Capa 8025) ppm.

ATR-FTIR: ν_{MAX} = 3341 (N-H), 2943 – 2867 (C-H), 1724 (C=O), 1598 (C-N), 1532 (Ar C=C), 1309 and 1161 (C-O) cm^{-1} .

DA1-A2: SEC (CHCl₃): $M_n = 13.3$ kDa, $M_w = 51.2$ kDa, $\bar{D}_M = 3.42$.

¹H NMR (400 MHz, 298 K, CDCl₃): $\delta = 7.29$ (m, Ar), 7.12 (d, $J = 8.0$ Hz, Ar), 6.74 (s, C(C)HCH=CH (DA)), 6.57 (s, NH), 6.51 (s, NH), 5.32 (s, CH(O)(CH)(CH) (DA)), 3.02 (s, CH(CH)C=O (DA)), 2.90 (s, CH(CH)C=O (DA)), 4.17, 4.08, 4.00, 3.92, 3.90, 3.84, 2.33, 1.67, 1.40, 1.28, 1.00 and 0.88 (Capa 2200 and Priplast 1838) ppm.

ATR-FTIR: $\nu_{MAX} = 3338$ (N-H), 2923 – 2854 (C-H), 1732 and 1709 (C=O), 1598 (C-N), 1532 (Ar C=C), 1310 and 1164 (C-O) cm⁻¹.

DA4-A1: SEC (CHCl₃): $M_n = 15.1$ kDa, $M_w = 34.7$ kDa, $\bar{D}_M = 2.61$.

¹H NMR (400 MHz, 298 K, CDCl₃): $\delta = 7.30$ (m, Ar), 7.11 (d, $J = 6.2$ Hz, Ar), 6.76 (s, C(C)HCH=CH (DA)), 6.74 (s, C(C)HCH=CH (DA)), 6.56 (s, NH), 6.51 (s, NH), 5.32 (s, CH(O)(CH)(CH) (DA)), 3.02 (s, CH(CH)C=O (DA)), 2.90 (s, CH(CH)C=O (DA)), 5.12, 4.36, 4.33, 4.29, 4.16, 4.08, 3.90, 2.42, 2.32, 1.65, 1.57, 1.53, 1.49, 1.40, 1.29 and 0.99 (Dynacoll 7490 and Capa 8025) ppm.

ATR-FTIR: $\nu_{MAX} = 3341$ (N-H), 2917 – 2850 (C-H), 1731 (C=O), 1598 (C-N), 1532 (Ar C=C), 1309 and 1162 (C-O) cm⁻¹.

DA4-A2: SEC (CHCl₃): $M_n = 23.3$ kDa, $M_w = 56.5$ kDa, $\bar{D}_M = 2.53$.

¹H NMR (400 MHz, 298 K, CDCl₃): $\delta = 7.30$ (m, Ar), 7.10 (m, Ar), 6.74 (s, C(C)HCH=CH (DA)), 6.51 (s, NH), 6.47 (s, NH), 5.32 (s, CH(O)(CH)(CH) (DA)), 3.02 (s, CH(CH)C=O (DA)), 2.90 (s, CH(CH)C=O (DA)), 4.34, 4.29, 4.16, 4.08, 3.90, 2.32, 1.63, 1.40, 1.29 and 0.88 (Dynacoll 7490 and Priplast 1838) ppm.

ATR-FTIR: $\nu_{MAX} = 3336$ (N-H), 2918 – 2851 (C-H), 1735 (C=O), 1598 (C-N), 1532 (Ar C=C), 1310 and 1172 (C-O) cm⁻¹.

5.5 References

1. H. W. Engels, H. G. Pirkl, R. Albers, R. W. Albach, J. Krause, A. Hoffmann, H. Casselmann and J. Dormish, *Angew. Chem. Int. Ed.*, 2013, **52**, 9422-9441.
2. G. Perego, G. D. Cella and C. Bastioli, *J. Appl. Polym. Sci.*, 1996, **59**, 37-43.
3. L. T. J. Korley, B. D. Pate, E. L. Thomas and P. T. Hammond, *Polymer*, 2006, **47**, 3073-3082.
4. L. H. Innocentini - Mei, J. R. Bartoli and R. C. Baltieri, 2003.
5. H.-M. Dou, J.-H. Ding, H. Chen, Z. Wang, A.-F. Zhang and H.-B. Yu, *RSC Adv.*, 2019, **9**, 13104-13111.
6. A. Nijenhuis, E. Colstee, D. Grijpma and A. Pennings, *Polymer*, 1996, **37**, 5849-5857.
7. T. Gurunathan, S. Mohanty and S. K. Nayak, *J. Mater. Sci.*, 2014, **49**, 8016-8030.
8. W. Lei, C. Fang, X. Zhou, Y. Cheng, R. Yang and D. Liu, *Thermochim. Acta*, 2017, **653**, 116-125.
9. O. Diels and K. Alder, *Liebigs Ann. Chem.*, 1928, **460**, 98-122.
10. A. Gandini, *Prog. Polym. Sci.*, 2013, **38**, 1-29.
11. M. Watanabe and N. Yoshie, *Polymer*, 2006, **47**, 4946-4952.
12. T. Brand and M. Klapper, *Des. Monomers Polym.*, 1999, **2**, 287-309.
13. M. Wu, Y. Liu, P. Du, X. Wang and B. Yang, *Int. J. Adhes. Adhes.*, 2020, **100**, 102597.
14. C. Zeng, H. Seino, J. Ren, K. Hatanaka and N. Yoshie, *Macromolecules*, 2013, **46**, 1794-1802.
15. X. Liu, P. Du, L. Liu, Z. Zheng, X. Wang, T. Joncheray and Y. Zhang, *Polym. Bull.*, 2013, **70**, 2319-2335.
16. O. W. J. Zhai, W. Zhao, X. Tao, S. L. Hsu and A. Slark, *J. Polym. Sci. Pol. Phys.*, 2018, **56**, 1265-1270.

17. G. Song, Y. Zhang, D. Wang, C. Chen, H. Zhou, X. Zhao and G. Dang, *Polymer*, 2013, **54**, 2335-2340.
18. J. Canadell, H. Fischer, G. De With and R. A. Van Benthem, *J. Polym. Sci. A1*, 2010, **48**, 3456-3467.
19. Y. Miao, H. He and Z. Li, *Polym. Eng. Sci.*, 2020, **60**, 1083-1092.
20. X. Kuang, G. Liu, L. Zheng, C. Li and D. Wang, *Polymer*, 2015, **65**, 202-209.

6 Conclusions and future work

6.1 Conclusions

Initially, a series of model TPU copolymers were synthesised from PCL and MDI without chain extender. Copolymerisation of PCL with MDI increased the degree of H-bonding interactions and T_g , but decreased T_m and ΔH_m of the crystalline phase. Bulk and solution polymerisation methods were compared to determine the effects each technique has on linear TPU products. While solution polymerisation allowed for synthesis of higher molecular weight copolymers, it required more resources, time and safety concerns as a consequence of the use and removal of organic solvents. Linear TPUs of the same molecular weight displayed structural and thermal properties which were identical, independent of synthesis method. By studying the effect of polyol molecular weight, it was observed that it influences H-bonding interactions and thermal properties of copolymers without chain extender. Lower molecular weight PCL ($M_n = 1.0$ kDa) showed a large increase in T_g after copolymerisation with MDI. Copolymers comprising higher molecular weight PCL ($M_n = 2.0$ kDa) recorded greater amounts of crystallinity, whereas those containing lower molecular weight PCL displayed crystallinity which was completely suppressed by the presence of MDI above TPU copolymer $M_n = 8.0$ kDa.

Three different chain extended copolymers with similar molecular weights were synthesised and compared to a non-chain extended PCL-MDI copolymer as a reference. The influence of CE branching, symmetry and urea functionality were examined. The copolymer comprising the branched chain extender did not display any thermal transitions above the $T_{m(SS)}$, implying it consist of a phase mixed morphology. Therefore, above this temperature, the material loses all strength and exhibits a steady decrease in viscosity with temperature. At ambient temperature, this copolymer has poor mechanical and adhesion properties as it is too brittle.

Copolymerisation including the symmetrical 1,4-butanediol (BD) as a chain extender displayed a melting endotherm above $T_{m(SS)}$ correlating to HS crystallinity as a consequence of substantial urethane H-bonding, which allowed for material cohesion between $T_{m(SS)}$ and $T_{m(HS)}$. These results are indicative of phase separation. The material displayed a reasonable physical response (reduction in viscosity) to an increase in temperature. The mechanical properties of this material comprising BD were unremarkable, expected for a copolymer of low molecular weight. The copolymer containing the bisurea diol also appeared to be phase separated, displaying a second glass transition temperature signifying partial HS order ($T_{g(HS)}$) above $T_{m(SS)}$ and remaining cohesive until approximately 140 °C. Copolymerisation with the bisurea diol vastly improved mechanical properties, displaying performance comparable to classic high molecular weight TPU copolymers. The adhesive properties were also double that of the reference TPU copolymer comprising BD. However, the urea interactions displayed minimal sensitivity to heat (maintaining a high viscosity throughout the rheological temperature sweep) which would prevent simple application of this material as an adhesive. Overall changing the nature of the chain extender and resulting TPU copolymer does not produce the desirable combination of high mechanical performance and low melt viscosity.

A linear TPU copolymer based on PCL, containing reversible DA cycloadducts in the backbone was synthesised (**DA1**) from prepolymers comprising maleimide and furan end groups. This material was compared to a traditional chain extended copolymer of PCL, MDI and BD (**D1**) as a reference. FTIR analysis revealed that the presence of DA cycloadducts allows for more intermolecular interactions due to the introduction of imide carbonyl groups. Cycloadducts also promote more homogenous PCL SS crystallinity *via* DSC analysis. Two endotherms at 117 and 145 °C were detected corresponding to stereoisomers of the DA cycloadduct.

Cycloadduct formation was measured as requiring 7 days to reach an equilibrium *via* SEC, FTIR spectroscopy and DSC analysis. The TPU molecular weight obtained *via* copolymerisation at ambient temperature was $M_n = 21$ kDa. The copolymer depolymerised back to the prepolymer molecular weight ($M_n = 6$ kDa) on heating. Rheological temperature sweeps showed that **DA1** reaches a lower η^* than **D1**, thanks to the decrease in molecular weight triggered by the rDA reaction. This result shows that the DA cycloadducts are more sensitive to thermal stimulus than the physical interactions in the traditional TPU. **DA1** also recorded enhanced mechanical and adhesive performance compared to **D1**. Three further TPU copolymers containing thermally reversible DA cycloadducts along the backbone were synthesised from prepolymers comprising polyols with high T_m and high crystallinity (**DA2, 3 & 4**). Analysis of these materials was qualitatively very similar to **DA1** which revealed that it is still possible to form and dissociate DA cycloadducts despite the high T_m and crystallinity in the backbones. ΔH_{rDA} was very similar for **DA2, 3 & 4**, but was significantly lower compared to **DA1** because of the lower DA cycloadduct concentration (resulting from the higher molecular weight of the high T_m polyols). Mechanical performance was highly dependent on backbone composition, varying in strength, flexibility and toughness. The highly crystalline copolymers displayed remarkable adhesive properties, with **DA4** recording a bond strength of 20.3 ± 0.9 MPa on aluminium substrates which is significantly higher than reported values for related systems which are crosslinked and not thermoplastic. After copolymerisation, the molecular weight of TPU **DA4** was $M_n = 32$ kDa, after 7 days. The copolymer depolymerised back to the prepolymer molecular weight ($M_n = 11$ kDa) on heating. This dynamic change of molecular weight as a function of temperature enabled not only very high mechanical properties, but also low melt viscosity above 120 °C. Two other copolymers containing reversible DA cycloadducts along the backbone were synthesised comprising amorphous

polyols (**DAA1** & **2**). Analysis again proved successful incorporation of the reversible DA cycloadducts that allowed for dynamic molecular weights and mechanical properties as a function of temperature. While both were very flexible materials, **DAA2** displayed enhanced properties compared to **DAA1**, likely on account of phase separation caused by the difference between relatively nonpolar soft segments and polar DA cycloadduct-MDI units.

Finally, phase separated linear TPUs without chain extender and containing DA cycloadducts along the backbone were synthesised by copolymerising both semi-crystalline and amorphous prepolymers to afford copolymers with distinct HS (crystalline) and SS (amorphous). Following initial compatibility studies between semi-crystalline and amorphous polyols, four suitable combinations were selected for further study, **Capa 2200** with **Capa 8025** or **Priplast 1838 (DA1-A1 & -A2)** and **Dynacoll 7490** with **Capa 8025** or **Priplast 1838 (DA4-A1 & -A2)**. DSC analysis of **DAX-AX** and the noncovalently attached polyol blends (**X-AX**) showed how covalent attachment improves polyol compatibility. All **DAX-AX** contain crystallinity which fulfils the aim of forming phase separated TPUs without chain extension. A T_{rDA} is also detected as a double peaked endotherm in all **DAX-AX** materials. DMA revealed that the amorphous component dictates both low (≤ 5 °C) and very high (≥ 80 °C) temperature properties while the semi-crystalline component controls the intermediate temperature range (5 – 80 °C), which would allow for tailored mechanical properties. **DA4-A2** displays very impressive properties over a wide service temperature range. In rheological temperature sweeps, copolymers displayed a significant decrease in η^* at approximately 100 °C due to the T_{rDA} causing depolymerisation to the prepolymers. While **DAX-AX** containing **Capa 8025 (DA1-A1 & DA4-A1)** are relatively weak materials, those containing **Priplast 1838 (DA1-A2 & DA4-A2)** display impressive mechanical properties due to strain-hardening. **DA4-A2** shows

remarkable mechanical performance, both strong (high E and σ_{\max}) and flexible (high ϵ_{\max}) to result in a very tough material ($U_T = 4595 \pm 370$ MPa) and offering good bond strength with beechwood substrates. The enhanced properties of this copolymer are due to the synergy of highly stiff and highly flexible prepolymers. Overall, there is potential to form linear TPUs including DA chemistry with highly tuned thermal and mechanical properties by careful design or selection of component polyols. In the future, choices could be made from a library of benign prepolymers for specific applications.

6.2 Future work

In the future, it would be beneficial to conduct x-ray scattering techniques (SAXS and WAXS) and atomic force microscopy (AFM) analysis on the copolymers containing different chain extenders (**D1**, **P1** and **U1**) to determine the influence of chain extender on copolymer morphology. These techniques could provide more detail and confirmation of observations *via* DSC, DMA and optical microscopy. Further self-healing studies on **D1** and particularly **U1** would be interesting. Reprocessing tests would also be useful to examine the potential to reuse these materials, particularly the high mechanically performing copolymer containing bisurea diol as the chain extender.

Analysis of dissociation of DA cycloadducts as a function of temperature and time *via* FTIR spectroscopy would be interesting to determine the rate of dissociation (*i.e.* how quickly can the prepolymers be reformed). Post synthesis heat treatment of copolymers containing DA cycloadducts could promote DA cycloadduct formation. Heating to 60 °C is known to increase the rate and conversion of cycloaddition by reducing the energy barrier of the reaction pathway. Additionally, this temperature would still be below $T_{m(\text{pol})}$ of some materials so potentially could lead to higher molecular weights without loss of crystallinity. Determination

of the subsequent effects on thermal and mechanical properties would be performed with the hope that an increase in molecular weight would correlate to an increase in mechanical performance. Annealing would be partially useful for the high T_m **DA2, 3 & 4** which contain the lowest amount of DA cycloadduct. Furthermore, it would be important to investigate whether materials are able to maintain high properties over multiple lifetimes and display thermal stability under reprocessing conditions or whether degradation occurs (thermogravimetric analysis) to determine potential circularity as reversible adhesives. Studies on whether the morphology and mechanical properties are affected by repeated processing cycles would therefore be important, conducted by repeating measurements (*e.g.* lap shear, DSC *etc.*) between reprocessing of materials. Aging, durability and creep studies would be interesting to determine to which potential environments and applications certain copolymers would be best suited. Copolymers would be subjected to various extreme conditions (*e.g.* heat, water, acid *etc.*).

The range of copolymers containing DA cycloadduct which comprise a blend of semi-crystalline and amorphous polyols could be expanded. The potential of MDI to increase compatibility could be explored further by inspecting combinations of polyols that showed lower degrees of compatibility in the initial physical blending studies. Combinations that could potentially lead to a large service temperature range and good thermal stability would be industrially useful. By investigating more combinations of polyols, a library of benign prepolymers could be created to allow for copolymers with targeted thermal and mechanical properties.

The information learned in these studies could be applied to different classes of polymers. For example, non-isocyanate polyurethanes would be interesting to investigate as potentially

environmentally friendly materials, as the mitigation of hazard isocyanates (and hazardous precursors *i.e.* phosgene) used to form traditional TPUs would be more in line with the circular economy approach. In a similar way, polyesters derived from natural resources would also be interesting to explore.